

Multi-app of Heparin Mimetics Derived from L-Idose

विद्या वाचस्पति की
उपाधि की अपेक्षाओं की आंशिक पूर्ति में प्रस्तुत शोध
प्रबंध

A thesis submitted in partial fulfilment of the requirements of the degree
of Doctor of Philosophy

द्वारा / By

शरत एस वी / Sharath S V

पंजीकरण सं. / Registration No.:
20193663

शोध प्रबंध पर्यवेक्षक / Thesis Supervisor:

प्रोफेसर राघवेंद्र किक्केरी / Prof. Raghavendra Kikkeri



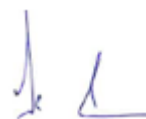
भारतीय विज्ञान शिक्षा एवं अनुसंधान संस्थान पुणे
INDIAN INSTITUTE OF SCIENCE EDUCATION AND RESEARCH PUNE

2024

I would like to dedicate my thesis to my beloved family

CERTIFICATE

This is to certify that the work incorporated in this thesis entitled “*Multi-app of heparin mimetics derived from L-Idose*” submitted by **Sharath S V** was carried out by candidate at Indian Institute of Science Education and Research, Pune under my supervision. The work presented here or any part of it has not been included in any other thesis submitted previously for the award of any degree or diploma from any other university or institution.



Date: 29-7-2024

Prof. Raghavendra Kikkeri
IISER, Pune

Declaration by Student

Name of Student: Sharath S V

Reg. No.: 20193663

Thesis Supervisor(s): Prof. Raghavendra Kikkeri

Department: Chemistry

Date of joining program: August 1st 2019

Date of Pre-Synopsis Seminar : Feb 28th 2024

Title of Thesis : *Multi-app of heparin mimetics derived from L-Idose*

I declare that this written submission represents my idea in my own words and where others' ideas have been included; I have adequately cited and referenced the original sources. I declare that I have acknowledged collaborative work and discussions wherever such work has been included. I also declare that I have adhered to all principles of academic honesty and integrity and have not misrepresented or fabricated or falsified any idea/data/fact/source in my submission. I understand that violation of the above will be cause for disciplinary action by the Institute and can also evoke penal action from the sources which have thus not been properly cited or from whom proper permission has not been taken when needed.

The work reported in this thesis is the original work done by me under the guidance of Dr./Prof. Raghavendra Kikkeri

Date: 29-7-2024



Signature of the student

Acknowledgements

I extend my deepest gratitude to Prof. Raghavendra Kikkeri, whose relentless efforts, dedication, and patience have been crucial to the success of this thesis. His unwavering support, passion, and creativity have not only inspired excellence but also fostered significant personal growth and confidence.

I would like to thank my collaborators, Dr. Vered and Shani, from Tel-Aviv University, Israel, Prof. Jesús Jiménez-Barbero (CIC bioGUNE), Dr. Vito Ferro (University of Queensland, Australia) for their time and efforts. Collaborating with them has immensely enriched my research work. I would also like to thank my RAC members, Prof. Ramkrishna. G. Bhat (IISER, Pune), Prof. C. V. Ramana (NCL, Pune) for their valuable suggestions during my course of research.

I would like to thank Prof. Subbaiah (Govt Degree college, Tumkur) who inculcated in me the interest towards chemistry in the initial days. I would express my gratitude to my uncle Prof. K. R. Prabhu (Senior Scientist, IISc, Bangalore) without whom I would have not be in IISER, Pune.

My friends from college handheld me throughout my journey right from clearing the CSIR exam to making up my mind to join Ph. D in IISER, Pune. I am indebted to Dr. Krishnaswamy, Suresh, Ranganath. They all stood by me and believed in me which gave confidence to move towards goal. Without their selfless support this would have not been possible. Words are falling short to express my gratitude for them.

I would like to thank IISER Pune for providing me financial support. My heartfelt thanks to our previous IISER director Prof. Jayant Udgaonkar, and previous Chair chemistry Prof. H.N. Gopi, also I would like to thank our present IISER director Prof. Sunil S. Bhagwat and present Chair Chemistry Prof. Nirmalya Ballav for providing excellent research facilities. A big thanks to all the chemistry technical team and instrument operators, especially Dr. Sandeep Kanade (for mass spectrometry, Dr Sandeep Mishra and Mr. Nitin (for NMR) and, Mr. Saurav (for FACS) for making the Ph.D. process much more valuable.

I would like to thank my lab mates for their unlimited support throughout my Ph.D. Special thanks to my senior's, Dr. Chethan D. Shanthamurthy, Dr. Prashant Jain, Dr. Balamurugan S., Dr. Sandhya Mardhekar for making me do the chemistry the right way. It is their contribution and hard work in my initial days that made things easy for me. A big thanks to Dr. Preeti Bhoge madam who helped me for biological studies. A big thanks to lab mates Dr. Vijendra, Dr. Trimbak, Dr. Deepak, Haritha, Dipti and Mohini for keeping the lab atmosphere alive and joyful.

This thesis remains incomplete without mentioning the blessings and love of my family. My heartfelt gratitude to my father S. B. Vishweshwara, my mother T. N. Rajeshwari, my father-in-law V. K. Somashekhar and my mother-in-law H. R. Venkatalakshamma. There are no better words to express my gratitude for their unconditional love, gracious understanding and life time support.

Last but not the least I express my appreciation to my wife Deepashree for her persistent support for being with me right from the initial days. Being my better half, she has stood by me throughout all the ups and downs. It is because of her motivation which made me to pursue Ph. D work.

Finally, I pray to almighty Lord 'Shree Guru RaghavendraSwamy' whose blessings made me able to complete the research work and submit this thesis for Ph. D degree.

Sharath S V

Contents

Abbreviations.....	xi
Abstract of the Thesis	xv

Chapter-1: Introduction

1.1 Introduction.....	2
1.2 Heparan Sulfate (HS) binding proteins.....	4
1.2.1 Conformational Plasticity of L-Iduronic acid.....	5
1.2.2 Growth Factors.	5
1.2.3 Anti-Heparan Sulfate Antibody.....	7
1.2.4 Amyloid- β Interaction with Heparan Sulfate	8
1.2.5 Viral Spike Proteins.....	10
1.2.6 Non-Glucosamino glycans like molecules as Heparan Sulfate mimics	11
1.3 References	13

Chapter-2: Immunogenic Sulfate L-Idose Homo Oligosaccharide Elicit Neutralizing Antibody Against Native Heparan Sulfate with Biomarker and Therapeutic Applications

Abstract.....	27
2.1 Introduction.....	28
2.2 Results and Discussion	30
2.2.1 General Procedure	32
2.2.2 Antibody response for ID49@CRM ₁₉₇ and cross reactivity against Serum-Antibody.....	34
2.2.3 FACS Assay	36
2.2.4 Immunohistochemistry.....	37
2.2.5 Ex-Vivo assay	38

2.3 Conclusions.....	40
2.4 Experimental Section	41
2.4.1 General information	41
2.4.2 RDKit Analysis	51
2.4.3 Synthesis and characterization of ID49@CRM ₁₉₇	51
2.4.4 Immunization Studies.....	52
2.4.5 General Protocol to synthesis HS-Thio derivatives	52
2.4.6 General Protocol for BSA Conjugation.	52
2.4.7 Characterization of ID49@CRM ₁₉₇ and BSA Conjugates.....	53
2.4.8 Evaluation of Serum Antibody titer using ELISA	53
2.4.9 FACS Analysis.....	53
2.4.10 Immunohistochemistry of Tissue sections.	53
2.4.11 Ex-Vivo Blood coagulation assay.....	54
2.5 References.....	54
2.6 Similarity Index of Heparin Mimics	58
2.7 SDS-PAGE and MALDI-TOF Spectras of BSA Conjugates	60
2.8 NMR	72

Chapter-3: Heparan Sulfate Neoproteoglycan Promotes Lysosome Targeting Chimeras of Amyloid- β Protein.

Abstract.....	86
3.1 Introduction.....	87
3.2 Results and Discussion	89
3.3 conclusion.....	94
3.4 Experimental Part.....	94
3.4.1 General Information	94
3.4.2 Isothermal calorimetric Titrations(ITC).....	95
3.4.3 Synthesis of PG@ID49 and PG@HH26S	96
3.4.3.1 General Procedure for conjugation of sugar molecules.....	96

3.4.4 Cell surface Engineering studies	97
3.4.5 Co-localization studies	97
3.4.6 MTT assay.....	98
3.4.7 Confocal imaging of lysosomal degradation chimera of A β (1-42)	98
3.4.8 FACS Study	99
3.4.9 Synthesis of ID49	99
3.5 References.....	104
3.6 NMR.....	109

Chapter-4: Amphiphilic Heparinoids as potent antiviral agents against SARS-CoV-2

Abstract	119
4.1 Introduction.....	120
4.2 Results and Discussion	122
4.2.1 Synthesis of L-Idose and L-Iduronic acid based amphiphiles	123
4.2.2 Biological Evaluation.....	124
4.2.3 Molecular Docking Studies	127
4.3 Conclusions.....	132
4.4 Experimental Section	132
4.4.1 General information	132
4.4.2 Synthesis of IAC and IDC series.....	133
4.4.3 Plaque Reduction Neutralization Test (PRNT).....	135
4.4.4 Cytotoxicity Assay	136
4.4.5 Heparanase Inhibition assay.....	136
4.4.6 Isothermal titration Calorimetry(ITC).....	136
4.4.7 Molecular Docking.....	137
4.5 References.....	138
4.9 NMR.....	145

Chapter-5: Modulation of the Growth Factors and Chemokines Specificity of Heparan Sulfate Through Charge Diversity

Abstract	153
5.1 Introduction.....	154
5.2 Results and Discussion	155
5.3 Conclusions.....	160
5.4 Experimental Part.....	160
5.4.1 General Information.....	160
5.5 References.....	178
5.6 NMR	180
List of Publications.....	216

Abbreviations

Ac = acetyl	Et ₃ N = Triethylamine
AcOH = Acetic acid	EtOAc = Ethylacetate
Ac ₂ O = Acetic anhydride	EtOH = Ethanol
Aβ ₄₂ = Amyloid beta 42	FGF = Fibroblast Growth Factor
BMP-2 = Bone Morphogenetic Protein-2	FGFR = Fibroblast Growth Factor Receptor
BF ₃ .Et ₂ O = Boron trifluoride diethyl etherate	GAGs = Glycosaminoglycans
BnBr = Benzylbromide	GDF = Growth Differentiation Factor
BSA = Bovine Serum Albumin	GlcA = Glucuronic Acid
CD ₃ OD = Deuterated methanol	GlcNAc = <i>N</i> -acetylglucosamine
CDCl ₃ = Deuterated chloroform	GPC = Glypican
CH ₃ = methyl	GPI = Glycosylphosphatidylinositol
CH ₃ CN = Acetonitrile	H = Hydrogen
CHCl ₃ = Chloroform	HB-EGF = Heparin Binding EGF like Growth Factor
CLR = C-type lectin receptor	HCl = Hydrochloric Acid
CRM ₁₉₇ = Cross reacting material 197	HRP = Horseradish Peroxidase
CS = Chondroitin Sulfate	H ₂ SO ₄ = Sulfuric Acid
D ₂ O = Deuterium oxide	HPLC = High-Performance Liquid Chromatography
DCM = Dichloromethane	HP = Heparin
DCC = <i>N,N</i> -Dicyclohexylcarbodiimide	HRMS = High resolution mass spectroscopy
DMF = <i>N,N</i> -Dimethylformamide	HS = Heparan Sulfate
DMAP = 4-Dimethylaminopyridine	HMBC = Heteronuclear Multiple Quantum Coherence
ECM = Extracellular Matrix	HRMS = High Resolution Mass Spectroscopy
EGF = Epidermal Growth Factor	

HSPG = Heparan Sulfate Proteoglycan
HSQC = Heteronuclear Single Quantum Coherence
IC₅₀ = Inhibitory concentration
IgG = Immunoglobulins G
J = Coupling constant
IdoA = Iduronic Acid
LMWH = Low Molecular Weight Heparin
m/z = Mass to charge ratio
MALDI = Matrix-Assisted Laser Desorption Ionization
MeOH = Methanol

NMR = Nuclear magnetic resonance
Py = Pyridine
PBS = Phosphate-buffered saline
P-TsOH = *Para*-toluenesulfonic acid
RFU = Relative Fluorescence Unit
R.T = Room temperature
SO₃.Et₃N = Sulfur trioxide triethylamine
SPR = Surface Plasmon resonance
TBAI = Tetrabutylammonium iodide
TEMPO = (2,2,6,6-Tetramethylpiperidin-1-yl) oxy

MHz = Mega Hertz
mL = Mille Liter
mM = Millimolar
M.S = Molecular Sieves
M_w = Molecular weight
NaCl = Sodium chloride
NAP-Br = Naphthyl Bromide
NIS = *N*-Iodosuccinimide
NaOH = Sodium hydroxide
NaOMe = Sodium methoxide
NDST = *N*-deacetylase/*N*-sulfotransferase
NIS=*N*-Iodosuccinimide
THF = Tetrahydrofuran
TLC = Thin Layer Chromatography
TMSOTf= Trimethylsilyltrifluoromethanesulfonate
TMSSPh = Trimethyl(thiophenol)silane
UFH = Unfractionated Heparin
VEGF = Vascular Endothelial Growth Factor
ZnI₂ = Zinc Iodide
 δ = chemical shift
 μ M = Micromolar

Abstract

Chapter 1 introduces the structure-activity relationship of Heparan Sulfate (HS) and its mimetics. HS is a negatively charged polysaccharide, widely present on the surface of all mammalian cells and in the extracellular matrix. Depending on the sulfation patterns and uronic acid compositions, the HS sequence binds to various proteins, including growth factors, chemokines, and bacterial and viral spike proteins. These interactions play a crucial role in viral and bacterial infections, as well as cancer progression. Despite rapid progress in the synthesis of structurally defined HS oligosaccharides, the direct contribution of uronic acid residues to HS biological functions remains largely unclear. Hence, HS mimetics such as PG545 and PI88 were synthesized to develop drug molecules.

Chapter 2 discusses the potential application of HS mimetics in the development of anti-HS antibodies. To this end, we synthesized sulfated Oligo-L-idose (ID49), which represents 70% similarity to native heparin structures. When ID49 was conjugated to CRM₁₉₇ and used for immunisation, the serum collected at different time intervals resulted in a high-titre IgG antibody response against ID49, also directed against the *N*-unsubstituted and *N*-sulfated HS ligands. Further screening for specificity towards sulfation patterns confirmed that the antibody targets 6-*O*-sulfated and 2-*O*-sulfated HS *N*-sulfated ligands. The pharmaceutical potential of these antibodies was demonstrated by selectively staining cancer cells and tissue sections.

Chapter 3 explores another potential application of heparan sulfate and its mimetics in regulating lysosomal-targeting chimera (LYTAC) of amyloid- β . We have demonstrated that native HS ligands carrying proteoglycan mimetics (**PG@HH26S**) have a greater potential to be expressed on the cell membrane compared to their mimetics (**PG@ID49**). Further, we explored successful application of proteoglycan mimetic in A β peptide-targeted degradation. HS serves as a ligand for more than 500 proteins, playing a role in numerous pathological conditions. The targeted degradation of HS-binding proteins using a synthetic neoproteoglycan backbone is critically needed.

Chapter 4 discusses the synthesis of amphiphilic carbohydrates to block viral entry. We synthesized a library of amphiphilic heparin mimetics carrying sulfated Oligo-L-idose and Oligo-L-iduronic acid. Among them, sulfated higher oligosaccharides of L-idose with lipophilic aglycones displayed potent anti-SARS-CoV-2 and antiheparanase activity, similar to or better than pixatimod (PG545), and were more potent than their isosteric L-iduronic acid congeners. The findings confirm that fine-tuning higher oligosaccharides, the degree of sulfation, and lipophilic groups can yield compounds with potent anti-SARS-CoV-2 activity.

Chapter 5 reports on a library of novel L-idose (Ido)-based HS mimics with a wide range of sulfation patterns designed to replicate many of the functions of native HS oligosaccharides. We employed a linear synthesis strategy to obtain a rare oligo-Idose precursor, utilizing anhydrous β -L-idopyranosyl and Idose thiophenol building blocks. HS mimic microarray binding studies with different growth factors and chemokines showed that selectivity and avidity are greatly modulated by the oligosaccharide length, sulfation code, and Idose conformation. Notably, we have identified highly sulfated HS mimetics as potential ligands for inflammatory chemokines and growth factors. Further investigation into their therapeutic value is ongoing.

CHAPTER – 1

Introduction

1.1 Introduction

Glycans, often referred to as the "dark matter" of the biological system, pose significant challenges in elucidating their structure and functions¹⁻⁴. Their structural complexity arises from the unique template-independent biosynthetic pathway, leading to highly heterogeneous structures with numerous modifications on core structures. Recent advancements in chemical and enzymatic glycans synthesis have sparked increased scientific interest in evaluating the structure-functional relationship of glycans⁵⁻⁹. Among the diverse array of cell surface glycans, glycosaminoglycans (GAGs) stand out as linear polysaccharide structures that regulate a wide range of biological activities. GAGs encompass heparan sulfate (HS), heparin (HP), chondroitin sulfate (CS), dermatan sulfate (DS), and hyaluronic acid (HA) among their repertoire. Heparan sulfate (HS), in particular, assumes prominence as a vital macromolecular constituent of cellular surfaces, serving as a ubiquitous receptor/coreceptor for an expansive repertoire of over 500 proteins (Figure. 1)¹⁰⁻¹⁵.

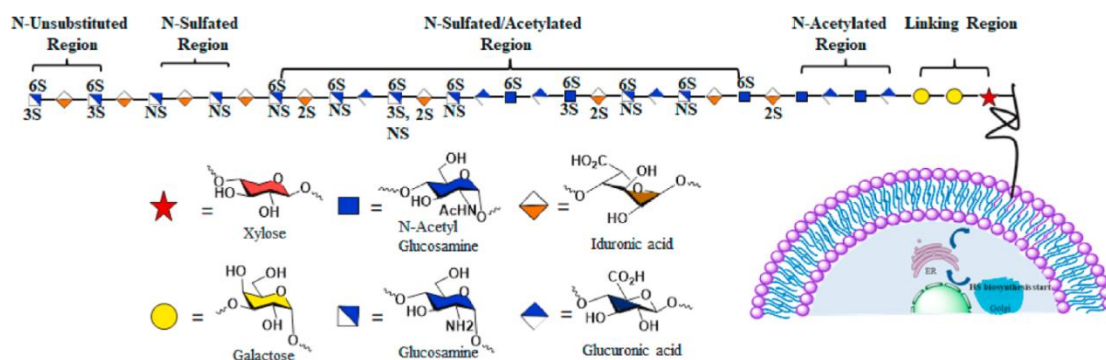


Figure 1. Representative general structure of heparan sulfate proteoglycan with different domains and detail sugar composition.

In that HS engages with a diverse array of growth factors including fibroblast growth factors (FGF), vascular endothelial growth factors (VEGF), and epidermal growth factors (EGF), are instigating intricate downstream signaling cascades that intricately regulate fundamental cellular processes such as proliferation, angiogenesis, and differentiation¹⁶. Additionally, heparan sulfate (HS) assumes a pivotal role in modulating immune responses, orchestrating leukocyte trafficking dynamics including rolling, adhesion, and migration at sites of inflammation through its interaction with selectins and chemokine release¹⁷⁻²³. Furthermore, the dysregulation of heparanase enzyme activity at tumor foci signifies structural modifications in HS within the cellular membrane and extracellular matrix, thereby fostering tumor growth, immune evasion mechanisms, and metastatic dissemination²⁴⁻²⁶. Moreover, heparan sulfate (HS) functions as a pivotal receptor facilitating the adhesion of

various viruses and bacteria to the cellular surface, thus promoting infection^{27–30}. Notably, in the context of SARS-CoV-2, the spike protein interacts with both cellular HS and angiotensin-converting enzyme 2 (ACE2) via its receptor-binding domain (RBD)^{31,32}. This intricate binding event induces a conformational alteration in the spike protein, leading to its transition into a trimeric state, thereby activating the ACE2 receptor (Figure. 2).

Heparan sulfate (HS) is composed of repeating disaccharide units linked via $\alpha(1-4)$ glycosidic bonds, comprising glucosamine and uronic acid moieties. The remarkable structural diversity of HS emanates from variations in sulfation patterns and uronic acid composition (Figure. 1)³³. Noteworthy sulfation patterns encompass *O*-sulfation at positions C-6 and C-3 of glucosamine, as well as at position C-2 of the uronic acid unit, with additional N-sulfation occurring at glucosamine residues^{34–36}.

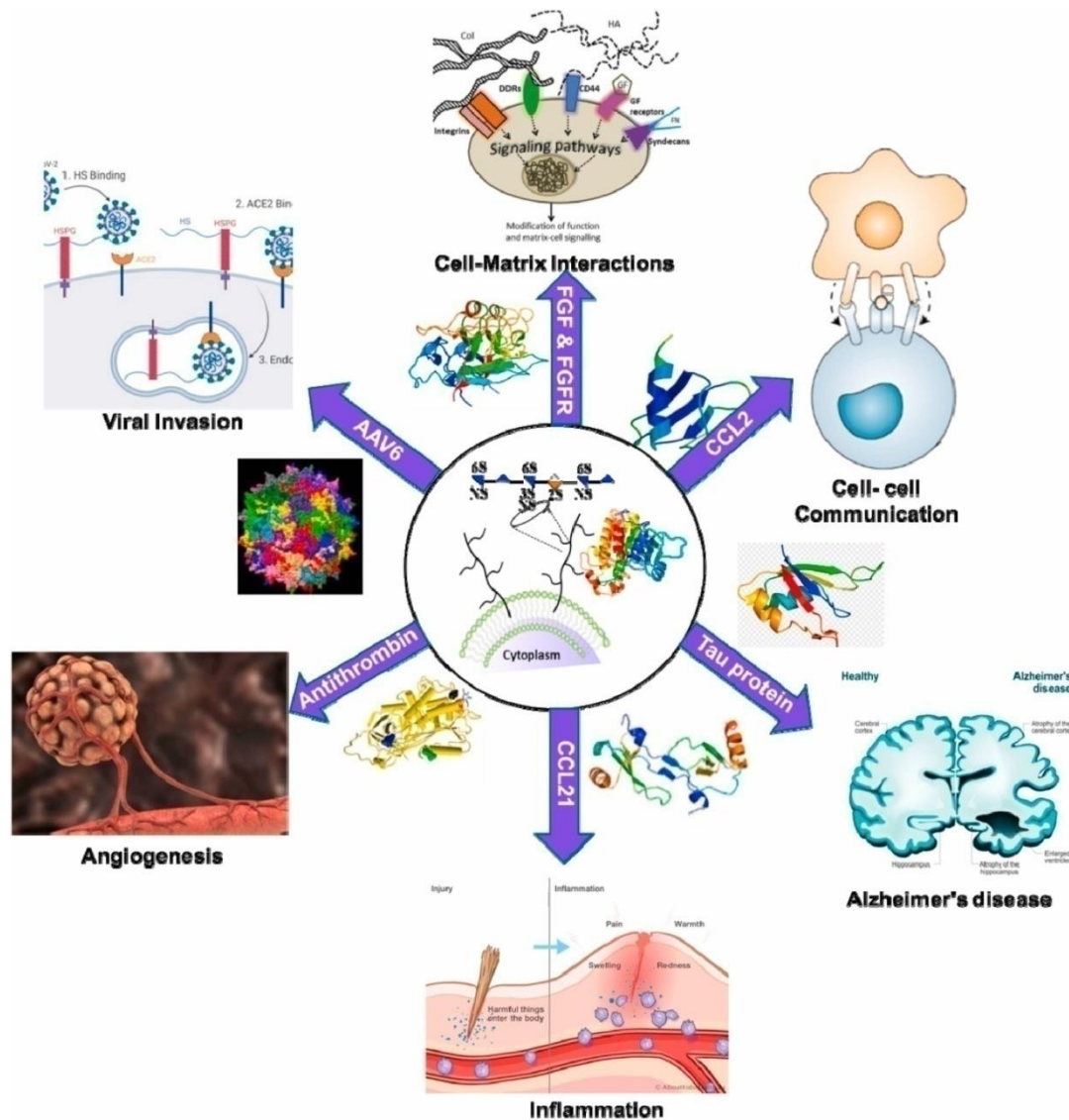


Figure 2. Importance of Heparan sulfate-protein interactions in various physiological and pathophysiological process.

Moreover, modifications at the uronic acid moiety, which may manifest as either D-glucuronic acid (GlcA) or L-iduronic acid (IdoA), afford 48 theoretical disaccharide configurations, among which 21 are naturally observed. However, the precise biological functions of these modifications remain incompletely understood, and the extensive heterogeneity of HS presents challenges in predicting specific structural alterations and rationalizing their functional implications.

To address this challenge, researchers are venturing into the exploration of unconventional modifications, employing bioisosteric groups to enhance both the selectivity and sensitivity of heparan sulfate proteoglycan interactions (HSPI)^{37–40}. Furthermore, the inherent flexibility in the conformation of L-iduronic acid (IdoA) introduces an additional layer of complexity, known to intricately fine-tune HSPI^{41–44}. Recent advancements in NMR spectroscopy have unveiled a novel ²S₀-conformation of IdoA, promising to unravel a new dimension of microheterogeneity and provide unparalleled insights into the differentiation of HSPI⁴⁵.

1.2 Heparan sulfate binding proteins

Heparan sulfate binding proteins (HSBPs) are categorized across diverse functional classes, including chemokines, cytokines, growth factors, morphogens, extracellular structural proteins, complement pathway components, single-transmembrane signaling receptors, and cell adhesion molecules. Furthermore, HSBPs encompass specialized groups such as proteases residing within intracellular hematopoietic cell granules, lipid-binding proteins implicated in lipoprotein metabolism, and amyloid and tau proteins associated with Alzheimer's disease¹⁶. Pathogens exploit the interaction between HSBPs and heparan sulfate (HS) to facilitate infection, often through evolutionary adaptation or acquisition of specific HSBPs. The wide-ranging repertoire of HSBPs underscores their indispensable roles in numerous biological processes. The interplay between HSBPs and HS chains, HS plays a pivotal role in mediating these functions. For example, growth factors and morphogens are crucial for orchestrating developmental processes and tissue regeneration, while extracellular structural proteins provide essential scaffolding for tissue integrity. Proteins involved in complement pathways contribute significantly to immune defense, whereas single-transmembrane signaling receptors and cell adhesion molecules govern intercellular communication and adhesion events. A comprehensive understanding of the intricate structure-function relationships governing HS in these biological processes holds immense promise for informing the design and development of next-generation therapeutics.

1.2.1 Conformation plasticity of L-iduronic acid

L-Iduronic acid (L-IdoA) predominantly adopts the 1C_4 -boat and 2S_0 -skew boat conformations, with the 1C_4 -boat conformation being relatively rare (Figure. 3). In contrast, D-glucuronic acid (D-GlcA) typically favors the 4C_1 -chair conformation^{48,49}. The inherent flexibility of L-IdoA allows for the repositioning of sulfate and carboxylic acid residues, which is pivotal in certain protein binding interactions. Nieto and colleagues synthesized a trisaccharide heparin library incorporating an L-IdoA residue flanked by various sulfated GlcN residues. Through extensive 2D-NMR and molecular dynamics studies, they demonstrated that compounds featuring a 6-*O*-sulfate group on the reducing end glucosamine (GlcN) exhibited a consistent population level of approximately 40% in the 2S_0 conformation^{50,51}. Moreover, *N*-sulfation and 6-*O*-sulfation of GlcN significantly augmented the prevalence of the 2S_0 conformation compared to *N*-acetylation. Similarly, Jian and colleagues investigated the conformational preferences of a fondaparinux mimic using 2D-NMR studies, revealing that 6-*O*-, 3-*O*-sulfated, and *N*-sulfated GlcN residues substantially shifted the conformational equilibrium of IdoA from the 1C_4 to the 2S_0 geometry, reaching a population of 75%⁵².

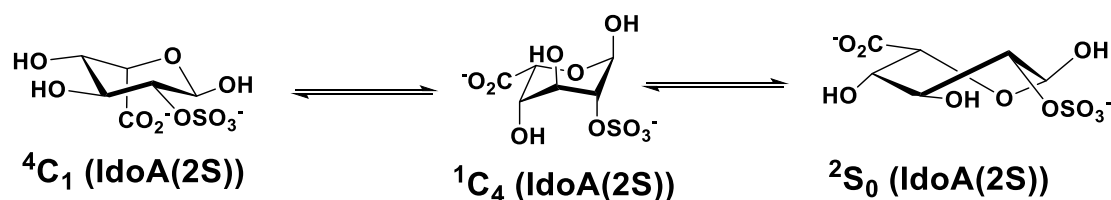


Figure 3. conformational dynamics of L-IdoA.

Recently, our lab group reported the synthesis of L-IdoA-based heparan sulfate (HS) mimics with varied sulfation patterns. NMR analysis of these HS mimics confirmed that 4-*O*-sulfation increased the prevalence of the 1C_4 geometry. Intriguingly, the 1C_4 conformer became exclusive upon additional 2-*O*-sulfation. Overall, the sulfation patterns on the GlcN residue, particularly 2-*O*-sulfation of L-IdoA, significantly influence the conformational dynamics of L-IdoA⁵³.

1.2.2 Growth factors

VEGF is a highly significant HS binding protein that regulates vascular development and function. Therefore, understanding the specific structural features required for VEGF binding is crucial for developing oligosaccharide-based anti-angiogenesis drugs. Linhardt and coworkers⁵⁴ systematically investigated the heparin-specific structural features required for VEGF binding. The study showed that octasaccharide unit is minimum length required to bind to both VEGF165 and VEGF55 efficiently. Interestingly, the degree of sulfation at different positions in HS affects the strength of protein binding, with N- and 6-*O*-sulfated groups contributing more than 2-*O*-sulfation. The study also highlights the important role of the IdoA residue in VEGF binding. Notably, the study revealed that the 3-*O*-sulfation found within the antithrombin binding site of heparin is not required for VEGF165 binding. These findings demonstrate the pivotal role of uronic acid in VEGF binding and provide new insight into the inherent kinetics and affinities for VEGF association with HS. Recently, we investigated the binding of VEGF165 with N-unsubstituted (NU) domain and N-acetate (NAc) domain ligands⁵⁵. Our group confirmed that 3-*O*-sulfation is not essential for VEGF165 binding, and both NU and NAc domain ligands showed similar binding preferences. All these studies revealed that L-IdoA is pivotal for VEGF and FGF binding. To delineate the conformation plasticity of L-IdoA oligomers, Our group have synthesized HS biomimetics analogs using pure IdoA components with different sulfation and oligosaccharide chain length patterns. We hypothesized that these HS biomimetics may expose IdoA residues at the reducing and non-reducing end of the oligosaccharides, giving a unique scaffold to study the conformation plasticity of IdoA at different positions. 1D and 2D NMR studies have permitted assessing that sulfation at position *O*-4 enhances the population of the ¹C₄ geometry at the corresponding ring. The ¹C₄ conformer becomes almost exclusive upon additional sulfation at *O*-2⁵³. Microarray and SPR analysis of HS biomimetic analogs with different growth factors have also established that optimal oligosaccharide length, sulfation code and exclusive IdoA conformation synergistically modulate growth factors activity. Finally, our group identified unique mono and disaccharide-IdoA ligands with unusual conformation plasticity and sulfation pattern that can selectively interact with VEGF165. This opened new avenues for generating drug molecules for cancer therapy.

Inspired by these findings, we undertook investigations into the binding of growth factors with oligo-idose mimetics. Our research involves the synthesis of oligo-idose and

encompasses various biological studies, specifically focusing on growth factors binding studies and developing antibody against HS.

1.2.3 Anti-HS Antibody

The intricate structural microheterogeneity of HS is evidenced by the staggering potential arrangements of a tetrasaccharide HS into 2,304 combinations, as documented by research⁵⁶. This complexity underscores the imperative of pinpointing specific HS epitopes implicated in biological processes and the subsequent development of targeted antibodies or small molecule inhibitors, which holds immense potential for advancing drug and vaccine development⁵⁶⁻⁵⁹.

For instance, prior investigations have elucidated the indispensable role of 3-*O*-sulfation of HS in facilitating the entry of Herpes simplex virus type 1 (HSV-1) into HeLa cells⁶⁰⁻⁶¹. Conversely, Adeno-Associated Virus (AAV) serotypes exploit HS sequences containing N-sulfated glucosamine and 2-*O*-sulfated iduronic acid residues to elicit virulence⁶². Additionally, HS microarray analysis with SAR-Cov-2 spike proteins has pinpointed highly N-sulfated patterns and iduronic acid composition as potential ligands for viral infection⁶³⁻⁶⁴, underscoring the critical need for antibodies targeting these HS ligands in the fight against viral diseases.

To date, various approaches have been explored for the development and commercialization of anti-heparan sulfate/heparin antibodies. However, in many cases, purified HS proteoglycans have been utilized as antigens.⁶⁵⁻⁶⁷ Antibodies generated against these antigens have shown to exhibit broad reactivity with different sulfation patterns, predominantly resulting in the production of IgM class antibodies. For example, the F58-10E4 antibody, produced using HS proteoglycan from human fetal lung fibroblast displayed reactivity with mixed HS domains containing both *N*-acetylated and *N*-sulfated disaccharide units, including *N*-unsulfated glycosamines.⁶⁸ On the other hand, the HepSS-1 mouse IgM antibody exhibited a strong binding preference to *N*-sulfated HS domains,^{69,70} but failed to differentiate the 3-*O*- or 6-*O*-sulfation code. The JM403 antibody displayed a preference for glucuronate over iduronate and exhibited strong binding to *N*-nonsulfated glucosamine.^{67,69} The NAH46 antibody bound to sulfated HS disaccharide units, but lacked specificity for sulfation patterns. Lastly, the FG69-3G10 anti-HS antibody demonstrated strong binding to unsaturated

uronated at the nonreducing end.⁷⁰ Overall, all these antibodies failed to demonstrate specificity to the sulfation codes and uronic acid compositions. Here, we employed an innovative immunization strategy that exploits molecular mimicry of HS to generate antibodies against HS sequences.

1.2.4 Amyloid beta (A β)

HS-protein interactions demonstrate dual effects: they enhance receptor activity, particularly in growth factors and chemokines, and inhibit protein aggregation in various neurological disorders⁷¹. Heparan sulfate (HS) can play important roles in the biology and pathology of amyloid β (A β), a hallmark of Alzheimer's disease. An illustrative example includes HS binding to β -secretase (BACE-1), which mitigates amyloid plaque formation linked to Alzheimer's disease⁷². Turnbull and colleagues extensively explored the structure-activity relationships (SARs) of BACE-1, highlighting that 6-*O*-sulfated and *N*-acetylated derivatives exhibit promising anti-BACE-1 activity over anti-Xa agents. Notably, variations in uronic acid composition showed no significant impact on their activity, while 2-*O*-sulfation of uronic acid marginally enhanced anti-BACE-1 efficacy^{73,74}.

Beta-amyloid and tau proteins are prominent HS-binding neural proteins. Liu et al., in their investigation to identify potential HS ligands, utilized a combinatorial HS library and microarray analysis. Their findings revealed that higher oligosaccharides (6–8 mers) with 3-*O*-sulfation at glucosamine and a mixed uronic acid residue combination on HS exhibit strong binding affinity to tau protein⁷⁵. In contrast, highly sulfated *N*-sulfated ligands exhibited robust adhesion to A β -protein. Additionally, higher oligosaccharides carrying 3-*O*-sulfated mixed uronic acid-containing HS ligands demonstrated significant binding affinity to neprilysin-1, a neural growth factor.

In the previous report by Xuefei Huang and coworkers have shown the structure–activity relationship of HS/A β interactions, synthetic HS oligosaccharides ranging from tetrasaccharides to decasaccharides have been utilized to study A β interactions. Surface plasmon resonance experiments showed that the highly sulfated HS tetrasaccharides bearing full 2-*O*, 6-*O*, and *N*-sulfations exhibited the strongest binding with A β among the tetrasaccharides investigated. Elongating the glycan length to hexa- and deca-saccharides significantly enhanced A β affinity compared to the corresponding HS tetrasaccharide. The strong binding HS oligosaccharides could reduce the cellular toxicities induced by A β ⁸⁵.

These discoveries offer valuable insights into the potential therapeutic applications of HS and its derivatives for treating neurological disorders linked to interactions involving beta-amyloid and tau proteins.

In Alzheimer's disease, impaired processing of amyloid precursor protein (APP) by γ -secretase results in the accumulation of amyloid beta ($A\beta$) oligomers and plaques. Syndecan (SDC) heparan sulfate proteoglycans (HSPGs) on cell surfaces and in the extracellular matrix facilitate $A\beta$ internalization, potentially contributing to disease progression. The presence of these $A\beta$ aggregates causes shrinkage of brain regions critical for memory, decision-making, and personality, such as the cerebral cortex, and the hippocampus, important for learning and memory.¹¹⁶ (Figure 4)

Further, Heparan sulfate (HS) significantly influences the metabolism of amyloid beta ($A\beta$) in Alzheimer's disease through direct and indirect mechanisms. The sulfation patterns and modifications of HS, as well as the conformational state of $A\beta$, dictate their binding interactions. Direct binding of HS accelerates $A\beta$ aggregation and deposition in the brain. Indirectly, HS interacts with key proteins such as sAPP, BACE1, and ApoE, which collectively modulate $A\beta$ production, uptake, and clearance pathways. This dual role underscores HS's pivotal involvement in the pathophysiology of Alzheimer's disease⁷².

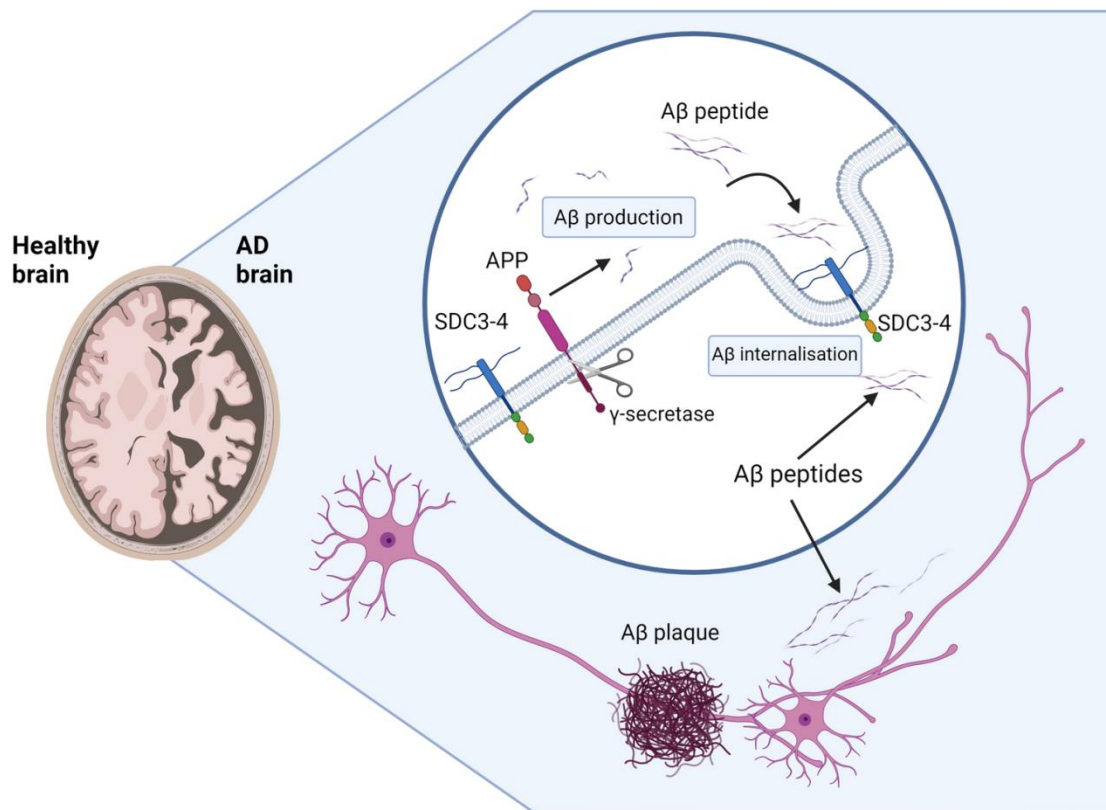


Figure 4. Heparan Sulfate plays a key role in internalization of amyloid beta (A β) oligomers and plaques.

1.2.5 Viral spike proteins

Pathogens such as viruses, bacteria, and parasites exploit heparan sulfate (HS) to invade the human immune system ⁷⁶. For example, Herpes simplex virus type 1 (HSV-1) initiates infection by binding to HS proteoglycans through viral envelope glycoproteins gB and gC ⁷⁷. Previous studies indicate that 3-*O*-sulfation of HS is crucial for blocking HSV-1 entry into cells like HeLa, and variations in uronic acid composition also influence the inhibition of HSV-1 infection ^{78,79}.

Similarly, uronic acid composition plays a critical role in recognizing Adeno-Associated Virus (AAV) serotypes. Specifically, AAV3 preferentially binds to HS sequences featuring N-sulfated glucosamine alternating with 2-*O*-sulfated iduronic acid (IdoA), while AAV6 binds to sequences containing sulfated glucosamine with non-sulfated IdoA ⁸⁰.

Studies on COVID-19 viral pathogenesis have revealed that the interaction between the virus spike protein and the angiotensin-converting enzyme-2 (ACE2) cell surface receptor, facilitated by HS, is crucial for its pathogenicity ^{31,32}. (Figure 5) Consequently, significant

efforts have been made to identify HS and its mimetics' binding sequences to the active sites of SARS-CoV-2 and inhibit viral replication. Researchers such as Boons et al. ^{32,81}, Tan et al. ⁸², Desai et al. ⁸³, and Skidmore et al. ⁸⁴ used limited HS libraries to identify active HS ligands for the spike receptor binding domain (RBD) through microarray and surface plasmon resonance (SPR) analyses.

These studies suggest that sulfation patterns and IdoA composition, specifically 2-*O* or 6-*O*-sulfated groups and *N*-sulfation, are potential ligands that modulate SARS-CoV-2 activity. These findings underscore the importance of uronic acid composition in viral infection and highlight the potential of HS mimetics as a therapeutic strategy against various diseases.

1.2.6 Non-Glucosamino glycan like molecules as Heparin Mimetic

Viruses often bind to cell surface carbohydrate residues like sialic acid or sulfated glycosaminoglycan (GAG) chains to initiate infection, making these carbohydrates promising antiviral targets. For instance, approved treatments for influenza utilize specific sialic acid mimetics⁸⁶. Similarly, GAG chain mimetics, such as sulfated polysaccharides, have been shown to effectively inhibit various GAG-binding viruses like HIV, HSV, and RSV in cultured cells ⁸⁷⁻⁸⁹. However, these compounds have failed to provide protection against HIV in human trials ^{90,91}.

The failure of these compounds in human trials may be due to the nature of GAGs and their mimetics. These long, anionic chains bind to viral proteins through weak and reversible electrostatic interactions ⁹². For example, in the case of HSV, the presence of a GAG mimetic must be constant during virus attachment, as dilution can release infectious virus ⁹³.

Human RSV targets ciliated cells in the bronchial epithelium and type 1 pneumocytes in the alveoli, leading to acute bronchiolitis and pneumonia in infants, the elderly, and immunocompromised individuals ⁹⁴⁻⁹⁶. In cultured cells, RSV initially binds to cell surface sulfated GAGs via its attachment protein G ⁹⁷, specifically targeting iduronic acid-containing GAGs like heparan sulfate or chondroitin sulfate B ⁹⁸.

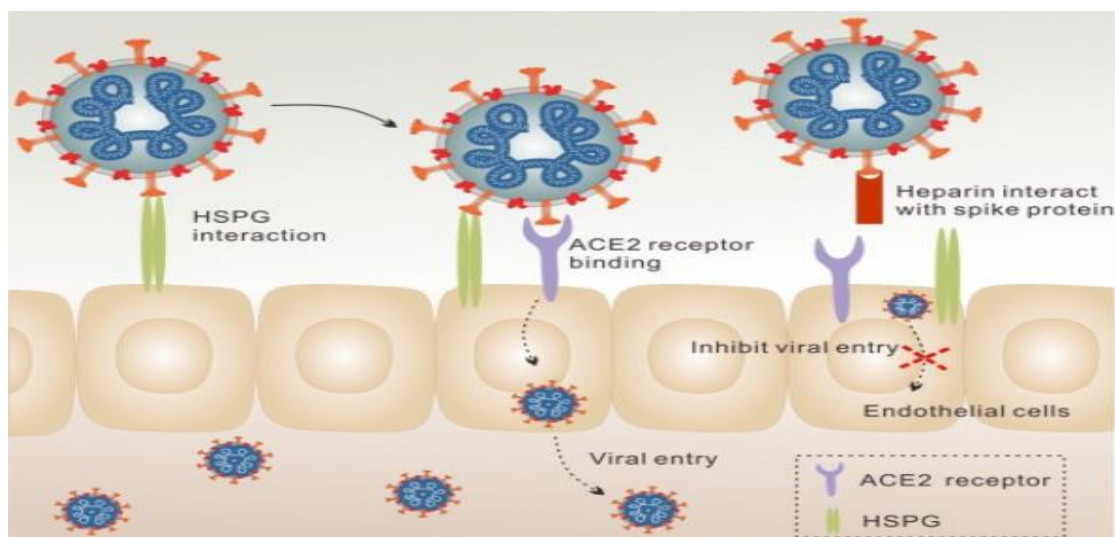


Figure 5. HSPG role in SARS-CoV-2 viral entry.

However, heparan and chondroitin sulfate chains are not significantly expressed on human airway epithelial surfaces ⁹⁹. Instead, keratan sulfate, abundantly found on the apical surface of ciliated cells in the bronchial epithelium ¹⁰⁰, might facilitate RSV infection, suggesting that GAG-mimicking compounds could protect against RSV.

Muparfostat (formerly PI-88), an anti-cancer drug candidate ¹⁰¹ consists of highly sulfated mannose-containing oligosaccharides and shows antiviral activities against various viruses, including HIV ¹⁰², HSV ¹⁰³, dengue, and encephalitic flaviviruses ¹⁰⁴, as well as malaria ¹⁰⁵. Inspired by the virucidal activity of certain polysulfonated compounds like PRO2000, which contains aromatic/lipophilic chains ^{106,107}, and the enhanced antiviral activity of peptide-based inhibitors conjugated with cholesterol ^{108,109}, efforts were made to enhance muparfostat's antiviral properties.

In oncology, PG545 has demonstrated anti-angiogenic properties, inhibiting pathways involved in tumor-associated blood vessel formation ¹¹⁰. Preclinical studies show its effectiveness in reducing tumor growth and metastasis in cancers such as melanoma and pancreatic cancer ^{110,111}. Beyond its anti-cancer properties, PG545 exhibits anti-inflammatory effects and has shown efficacy in models of fibrosis and autoimmune diseases ¹¹².

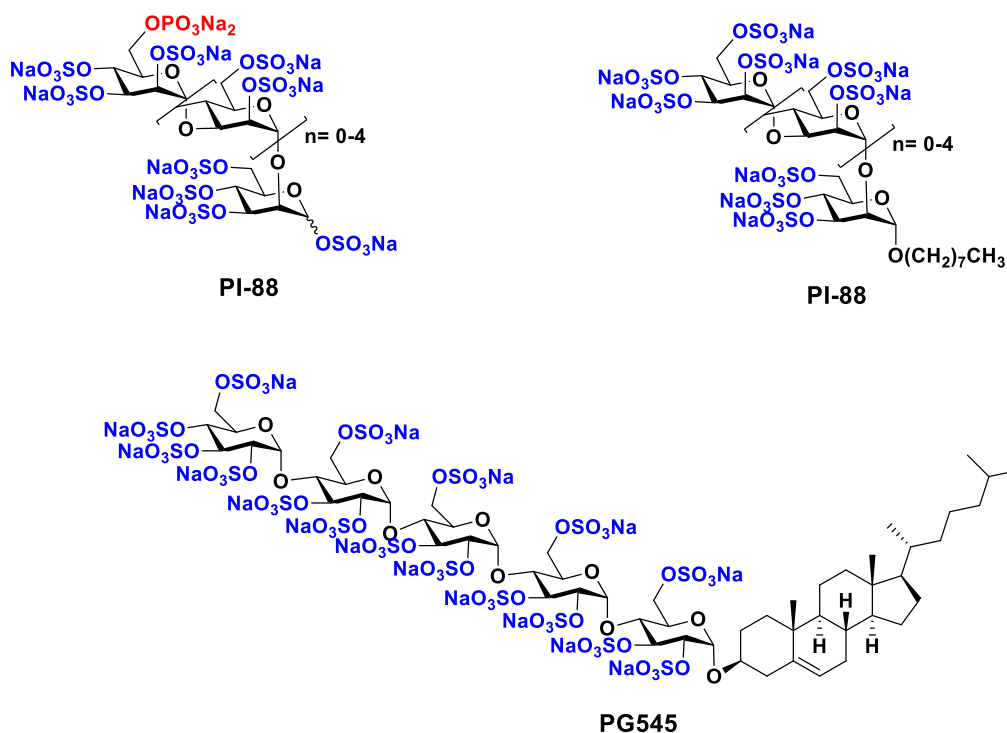


Figure 6. Structures of some of Non-glycosamino glycans like molecules, PG545 and PI-88.

In addition to its applications in oncology and inflammatory diseases, PG545 targets heparan sulfate proteoglycans (HSPGs), key receptors for various viruses, to inhibit viral entry. PG545, works as a novel RSV inhibitor, by mimicking the structure of HS, PG545 can competitively inhibit virus attachment to cell surface HSPGs, preventing viral entry into host cells¹¹³.

Additionally, PG545 and related glycosides exhibit potent virucidal activities against HSV¹¹⁴ and HIV¹¹⁵, making cholestanyl-conjugated oligosaccharides promising candidates for treating and preventing infections by viruses that utilize GAGs as initial receptors.

1.3 Reference:

1. Krasnova, L.; Wong, C.H.; Understanding the chemistry and biology of glycosylation with glycan synthesis. *Annu. Rev. Biochem.* **2016**, 85, 599–630.
2. Wang, L.X.; Davis, B.G.; Realizing the promise of chemical glycobiology. *Chem. Sci.* **2013**, 4, 3381–3394.
3. Varki, A.; Biological roles of glycans. *Glycobiology.* **2017**, 27, 3–49.
4. Prescher, J.; Bertozzi, C.; Chemistry in living systems, *Nat. Chem. Biol.* **2005**, 1, 13–21.

5. Zhu, X.; Schmidt, R.R.; New principles for glycoside-bond formation. *Angew. Chem. Int. Ed. Engl.* **2009**, 48, 1900–1934.
6. Zhang, X.; Lin, L.; Huang, H.; Linhardt, R.J.; Chemoenzymatic synthesis of Glycosaminoglycans. *Acc. Chem. Res.* **2019**, 53, 333–346.
7. Kulkarni, S.S.; Wang, C.C.; Sabbavarapu, N.M.; Podilapu, A.R.; Liao, P.H.; Hung, S.C.; "One-Pot" protection, glycosylation, and protection-glycosylation strategies of carbohydrates. *Chem. Rev.* **2018**, 118, 8025–8104.
8. Hunter, C.D.; Guo, T.; Daskhan, G.; Richards, R.; Cairo, C.W.; Synthetic strategies for modified glycosphingolipids and their design as probes. *Chem. Rev.* **2018**, 118, 8188–8241.
9. Boltje, T.J.; Buskas, T.; Boons, G.J.; Opportunities and challenges in synthetic oligosaccharide and glycoconjugate research. *Nat. Chem.* **2009**, 1, 611–622.
10. Bishop, J.R.; Schuksz, M.; Esko, J.D.; Heparan sulphate proteoglycans fine-tune mammalian physiology. *Nature.* **2007**, 446, 1030.
11. Lindahl, U.; Kusche-Gullberg, M.; Kjellen, L.; Regulated diversity of heparan sulfate. *J. Biol. Chem.* **1998**, 273, 24979–24982.
12. Weiss, R.J.; Esko, J.D.; Tor, Y.; Targeting heparin and heparan sulfate protein interactions. *Org. Biomol. Chem.* **2017**, 15, 5656–5668.
13. Kreuger, J.; Spillmann, D.; Li, J.; Lindahl, U.; Interactions between heparan sulfate and proteins: the concept of specificity, *J. Cell Biol.* **2006**, 174, 323–327.
14. Capila, R.; Linhardt, R. J.; Heparin-protein interactions, *Angew. Chem. Int. Ed. Engl.* **2002**, 41, 391–412.
15. Xu, D.; Esko, J.D.; Demystifying heparan sulfate-protein interactions, *Annu. Rev. Biochem.* **2014**, 83, 129–157.
16. Forsten-Williams, K.; Chu, C.L.; Fannon, M.; Buczek-Thomas, J.A.; Nugent, M.A.; Control of growth factor networks by heparan sulfate proteoglycans, *Ann. Biomed. Eng.* **2008**, 12, 2134–2148.
17. Duni, A.; Liakopoulos, V.; Koutlas, V.; Pappas, C.; Mitsis, M.; Dounousi, E.; The endothelial glycocalyx as a target of ischemia and reperfusion injury in kidney transplantation-where have we gone so far? *Int. J. Mol. Sci.* **2021**, 22, 2157.
18. Collins, L.E.; Troeberg, L.; Heparan sulfate as a regulator of inflammation and immunity, *J. Leukoc. Biol.* **2019**, 105, 81–92.

19. Lipowsky, H.H.; Role of the glycocalyx as a barrier to leukocyte-endothelium adhesion. *Adv. Exp. Med. Biol.* **2018**, 1097, 51–68.
20. Rajarathnam, K.; Sepuru, K.M.; Joseph, P.R.B.; Sawant, K.V.; Brown, A.J.; Glycosaminoglycan interactions fine-tune chemokine-mediated neutrophil trafficking: structural insights and molecular mechanisms, *J. Histochem. Cytochem.* **2018**, 66, 229–239.
21. Papy-Garcia, D.; Albanese, P.; Heparan sulfate proteoglycans as key regulators of the mesenchymal niche of hematopoietic stem cells, *Glycoconj. J.* **2017**, 34, 377–391.
22. A.V. Kumar, S.K. Katakam, A.K. Urbanowitz, M. Gotte, Heparan sulphate as a regulator of leukocyte recruitment in inflammation, *Curr. Protein Pept. Sci.* 2015, 16, 77–86.
23. Reijmers, R.M.; Spaargaren, M.; Pals, S.T.; Heparan sulfate proteoglycans in the control of B cell development and the pathogenesis of multiple myeloma, *FEBS J.* **2013**, 280, 2180–2193,
24. Hammond, E.; Khurana, A.; Shridhar, V.; Dredge, K.; The role of heparanase and sulfatases in the modification of heparan sulfate proteoglycans within the tumor microenvironment and opportunities for novel cancer therapeutics. *Front. Oncol.* **2014**, 4, 195.
25. Yang, Y.; Yuan, F.; Zhou, H.; Quan, J.; Liu, C.; Wang, Y.; Xiao, F.; Liu, Q.; Liu, J.; Zhang, Y.; Yu, X.; Potential roles of heparanase in cancer therapy: current trends and future direction. *J. Cell. Physiol.* **2023**, 1–22.
26. Vlodavsky, P.; Beckhove, I.; Lerner, C.; Pisano, A.; Meirovitz, N.; Ilan, M.; Elkin.; Significance of heparanase in cancer and inflammation, *Cancer Microenviron* **2012**, 2, 115–132.
27. V. Cagno, E.D. Tseligka, S.T. Jones, C. Tapparel, Heparan sulfate proteoglycans and viral attachment: true receptors or adaptation bias? *Viruses.* **2019**, 11, 596.
28. De Pasquale, V.; Quiccione, M.S.; Tafuri, S.; Avallone, L.; Pavone, L.M.; Heparan sulfate proteoglycans in viral infection and treatment: a special focus on SARSCoV-2. *Int. J. Mol. Sci.* **2021**, 22, 6574.
29. García, B.; Fernández-Vega, I.; García-Suárez, O.; Castañón, S.; Quirós, L.M.; The role of heparan sulfate proteoglycans in bacterial infections. *J. Med. Microbiol. Diagn.* **2014**, 3, 1000157.
30. Aquino, R.S.; Hayashida, K.; Hayashida, A.; Role of HSPGs in systemic bacterial infections, *Methods Mol. Biol.* **2022**, 2303, 605–625
31. Clausen, T.M.; Sandoval, D.R.; Spliid, C.B.; Pihl, J.; Perrett, H.R.; Painter C.D.; Narayanan, A.; Majowicz, S.A.; Kwong, E.M.; McVicar, R.N.; Thacker, B.E.;

- Glass, C.A.; Yang, Z.; Torres, J.L.; Golden, G.J.; Bartels, P.L.; Porell, R.N.; Garretson, A.F.; Laubach, L.; Feldman, J.; Yin, X.; Pu, Y.; Hauser, B.M.; Caradonna, T.M.; Kellman, B.P.; Martino, C.; Gordts, P.L.S.M.; Chanda, S.K.; Schmidt, A.G.; Godula, K.; Leibel, S.L.; Jose, J.; Corbett, K.D.; Ward, A.B.; Carlin, A.F.; Esko, J.D.; SARS-CoV-2 infection depends on cellular heparan sulfate and ACE2. *Cell***2020**, *183*, 1043–1057.
32. Liu, L.; Chopra, P.; Li, Bouwman, X.K.M.; Tompkins, S.M.; Wolfert, M.A.; de Vries, R.P.; Boons, G.J.; Heparan sulfate proteoglycans as attachment factor for SARSCoV-2. *ACS Cent. Sci.***2021**, *7*, 1009–1018.
 33. Marques, C.; Reis, C.A.; Viv`es, R.R.; Magalhães, A.; Heparan sulfate biosynthesis and sulfation profiles as modulators of cancer signalling and progression, *Front. Oncol.***2021**, *11*, 778752.
 34. El Masri, R.; Seffouh, A.; Lortat-Jacob, H.; Viv`es, R.R.; The "in and out" of glucosamine 6-O-sulfation: the 6th sense of heparan sulfate. *Glycoconj. J.***2017**, *34*, 285–298.
 35. Chen, J.; Duncan, M.B.; Carrick, K.; Pope, R.M.; Liu, J.; Biosynthesis of 3-O-sulfated heparan sulfate: unique substrate specificity of heparan sulfate 3-O-sulfotransferase isoform 5. *Glycobiology.***2003**, *13*, 785–794.
 36. Marques, C.; Reis, C.A.; Viv`es, R.R.; Magalhães, A.; Heparan sulfate biosynthesis and sulfation profiles as modulators of cancer signalling and progression. *Front. Oncol.***2021**, *11*, 778752.
 37. Hu, Y.P.; Zhong, Y.Q.; Chen, Z.G.; Chen, C.Y.; Shi, Z.; Zulueta, M.M.; Ku, C.C.; Lee, P. Y.; Wang, C.C.; Hung, S. C; Divergent synthesis of 48 heparan sulfate-based disaccharides and probing the specific sugar-fibroblast growth factor-1 interaction. *J. Am. Chem. Soc.* **2012**, *134*, 20722–20727.
 38. Mende, M.; Bednarek, C.; Wawryszyn, M.; Sauter, P.; Biskup, M.B.; Schepers, U.; Br`ase, S.; Chemical synthesis of glycosaminoglycans, *Chem. Rev.* **2016**, *116*, 8193–8255.
 39. Tsai, C.T.; Zulueta, M.; Hung, S.C.; Synthetic heparin and heparan sulfate: probes in defining biological functions. *Curr. Opin. Chem. Biol.***2017**, *40*, 152–159.
 40. Xu, D.; Arnold, K.; Liu, J.; Using structurally defined oligosaccharides to understand the interactions between proteins and heparan sulfate. *Curr. Opin. Chem. Biol.* **2018**, *50*, 155–161.
 41. S.K. Das, J.M. Mallet, J. Esnault, P.A. Driguez, P. Duchaussoy, P. Sizun, J. P. Herault, J.M. Herbert, M. Petitou, P. Sinaÿ, Synthesis of conformationally locked L-iduronic acid derivatives: direct evidence for a critical role of the skew-boat 2S0 conformer in the activation of antithrombin by heparin. *Chemistry.* **2001**, *7*, 4821–4834.

42. Nieto, L.; Canales, A.; Fernández, I.S.; Santillana, E.; González-Corrochano, R.; Redondo-Horcajo, M.; Cañada, F.J.; Nieto, P.; Martín-Lomas, M.; Giménez-Gallego, G.; Jiménez-Barbero, J. Heparin modulates the mitogenic activity of fibroblast growth factor by inducing dimerization of its receptor. a 3D view by using NMR. *Chembiochem.* **2013**, *14*, 1732–1744.
43. Muñoz-García, J.C.; Corzana, F.; de Paz, J.L.; Angulo, J.; Nieto, P.M.; Conformations of the iduronate ring in short heparin fragments described by time-averaged distance restrained molecular dynamics, *Glycobiology.* **2013**, *23*, 1220–1229.
44. Muñoz-García, C.; López-Prados, J.; Angulo, J.; Díaz-Contreras, I.; Reichardt, N.; de Paz, J.L.; Martín-Lomas, M.; Nieto, P.M.; Effect of the substituents of the neighboring ring in the conformational equilibrium of iduronate in heparin-like trisaccharides. *Chemistry.* **2012**, *18*, 16319–16331.
45. Hsieh, P.H.; Thieker, D.F.; Guerrini, M.; Woods, R.J.; Liu, J.; Hsieh, P.H.; Thieker, D.F.; Guerrini, M.; Woods, R.J.; Liu, J.; Uncovering the relationship between sulphation patterns and conformation of iduronic acid in heparan sulphate. *Sci. Rep.* **2016**, *6*, 29602.
46. Kim, Y.; Hyun, J.Y.; Shin, I.; Glycan microarrays from construction to applications, *Chem. Soc. Rev.* **2022**, *51*, 8276–8299.
47. Pomin, V.H.; Wang, X.; Synthetic oligosaccharide libraries and microarray technology: a powerful combination for the success of current glycosaminoglycan interactomics, *ChemMedChem.* **2018**, *13*, 648–661.
48. Casu, B.; Choay, J.; Ferro, D.R.; Gatti, G.; Jacquinet, J.C.; Petitou, M.; Provasoli, A.; Ragazzi, M.; Sinay, P.; Torri, G.; Controversial glycosaminoglycan conformations. *Nature.* **1986**, *322*, 215–216.
49. Ferro, D.R.; Provasoli, A.; Ragazzi, M.; Torri, G.; Casu, B.; Gatti, G.; Jacquinet, J.-C.; Sinay, P.; Petitou, M.; Choay, J.; Evidence for conformational equilibrium of the sulfated L-iduronate residue in heparin and in synthetic heparin mono- and oligosaccharides: NMR and force-field studies. *J. Am. Chem. Soc.* **1986**, *108*.
50. Muñoz-García, J.C.; Corzana, F.; de Paz, J.L.; Angulo, J.; Nieto, P.M.; Conformations of the iduronate ring in short heparin fragments described by time-averaged distance restrained molecular dynamics, *Glycobiology* **2013**, *23*, 1220–1229.
51. Muñoz-García, J.C.; López-Prados, J.; Angulo, J.; Díaz-Contreras, I.; Reichardt, N.; de Paz, J. L.; Martín-Lomas, M.; Nieto, P.M.; Effect of the substituents of the neighboring ring in the conformational equilibrium of iduronate in heparin-like trisaccharides. *Chemistry.* **2012**, *18*, 16319–16331.
52. Hsieh, P.-H.; Thieker, D.F.; Guerrini, M.; Woods, R.J.; Liu, J.; Uncovering the relationship between sulphation patterns and conformation of iduronic acid in heparan sulphate. *Sci. Rep.* **2016**, *6*, 29602.

53. Shanthamurthy, C.D.; Gimeno, A.; Ben-Arye, Leviatan S.; Kumar, N.V.; Jain, P.; Padler-Karavani, V.; Jiméenez-Barbero, J.; Kikkeri, R.; Sulfation code and conformational plasticity of l-iduronic acid homo-oligosaccharides mimic the biological functions of heparan sulfat, *ACS Chem. Biol.***2021**, 16, 2481–2489.
54. Zhao, W.; McCallum, S.A.; Xiao, Z.; Zhang, F.; Linhardt, R.J.; Binding affinities ofvascular endothelial growth factor (VEGF) for heparin-derived oligosaccharides. *Biosci. Rep.***2012**, 32, 71–81.
55. Jain, P.; C.D. Shanthamurthy, S. Leviatan Ben-Arye, S. Yehuda, S.S. Nandikol, H.V. Thulasiram, V. Padler-Karavani, R. Kikkeri, Synthetic heparan sulfate ligands forvascular endothelial growth factor to modulate angiogenesis.*Chem. Commun. (Camb).***2021**, 57,3516–3519.
56. Hu, Y. P.; Lin. S. Y.; Huang, C. Y.; Zulueta, M. M.; Liu, J. Y.; Chang, W.; Hung, S. C. Synthesis of 3-O-sulfonated heparan sulfate octasaccharides that inhibit the herpes simplex virus type 1 host–cell interaction. *Nat. Chem.* **2011**, 3, 557–563.
57. Zong, C.; Venot, A.; Li, X.; Lu, W.; Xiao, W.; Wilkes, J. S. L.; Salanga, C. L.; Handel, T. M.; Wang, L.; Wolfert, M. A.; Boons, G. J. Heparan sulfate microarray reveals that heparan sulfate–protein binding exhibits different ligand requirements *J. Am. Chem. Soc.***2017**, 139, 9534 – 9543.
58. Jain. P.; Shanthamurthy, C. D.; Leviatan Ben-Arye, S.; Woods, R. J.; Kikkeri, R.; Padler-Karavani, V. Discovery of rare sulfated N-unsubstituted glucosamine based heparan sulfate analogs selectively activating chemokines. *Chem. Sci.* **2021**, 12, 3674-3681.
59. Chopra, P.; Joshi, A.; Wu, J.; Lu, W.; Yadavalli, T.; Wolfert, M. A.; Shukla, D.; Zaia, J.; Boons, G. J. The 3-O-sulfation of heparan sulfate modulates protein binding and lyase degradation. *PNAS*, **2021**, 118, e2012935118. O'Donnell andShukla, 2008; Copeland et al., 2008.
60. O'Donnell, C. D.; Shukla,D. The Importance of Heparan Sulfate in Herpesvirus Infection. *Virol. Sin.* 2008,23, 383-393.
61. Copeland, R.; Balasubramaniam, A.; Tiwari, V.; Zhang, F.; Bridges, A.; Linhardt, R. J.; Shukla, D.; Liu,J. Using a 3-O-sulfated heparin octasaccharide to inhibit the entry of herpes simplex virus type 1. *Biochemistry.***2008**,47, 5774-83,
62. Mietzsch, M.; Broecker, F.; Reinhardt, A.; Seeberger, P. H.; Heilbronn,R. Differential adeno-associated virus serotype-specific interaction patterns with synthetic heparins and other glycans. *J. Virol.* **2014**, 88, 2991-3003.

63. Clausen, T. M.; Sandoval, D. R.; Spliid, C. B.; Pihl, J.; Perrett, H. R.; Painter, C. D.; Narayanan, A.; Majowicz, S. A.; Kwong, E. M.; McVicar, R. N.; Thacker, B. E.; Glass, C. A.; Yang, Z.; Torres, J. L.; Golden, G. J.; Bartels, P. L.; Porell, R. N.; Garretson, A. F.; Laubach, L.; Feldman, J.; Yin, X.; Pu, Y.; Hauser, B. M.; Caradonna, T. M.; Kellman, B. P.; Martino, C.; Gordts, P. L. S. M.; Chanda, S. K.; Schmidt, A. G.; Godula, K.; Leibel, S. L.; Jose, J.; Corbett, K. D.; Ward, A. B.; Carlin, A. F.; Esko, J. D. SARS-CoV-2 Infection depends on cellular heparan sulfate and ACE2. *Cell*.**2020**,183,1043-1057.e15.
64. Liu, L.; Chopra, P.; Li, X.; Bouwman, K. M.; Tompkins, S. M.; Wolfert, M. A.; de Vries, R. P.; Boons, G. J. Heparan Sulfate Proteoglycans as Attachment Factor for SARS-CoV-2. *ACS Cent. Sci.***2021**, 7, 1009-1018,
65. David, G.; Bai, X. M.; Van der Schueren, B.; Cassiman, J. J.; Van den Berghe. H. Developmental changes in heparan sulfate expression: in situ detection with mAbs. *J. Cell. Biol.***1992**, 119, 961–75.
66. van den Born, J.; Salmivirta, K.; Henttinen, T.; Ostman, N.; Ishimaru, T.; Miyaura, S.; Yoshida, K.; Salmivirta. M. Novel heparan sulfate structures revealed by monoclonal antibodies. *J. Biol. Chem.* **2005**, 280, 20516-20523.
67. Leteux, C.; Chai, W.; Nagai, K.; Herbert, C. G.; Lawson, A. M.; Feizi. T. 10E4 antigen of Scrapie lesions contains an unusual nonsulfated heparan motif. *J Biol Chem.* **2001**, 276, 12539–12545.
68. Kure, S.; Yoshie, O. A syngeneic monoclonal antibody to murine meth-A sarcoma (HepSS-1) recognizes heparan sulfate glycosaminoglycan (HS-GAG): Cell density and transformation dependent alteration in cell surface HS-GAG defined by HepSS-1. *J Immunol.***1986**137, 3900—3908.
69. van den Born, J.; van den Heuvel, L. P.; Bakker, M. A.; Veerkamp, J. H.; Assmann, K. J.; Berden, J. H. A monoclonal antibody against GBM heparan sulfate induces an acute selective proteinuria in rats. *Kidney Int.***1992**, 41, 115-23.
70. Suzuki, K.; Yamamoto, K., Kariya, Y.; Maeda, H.; Ishimaru, T.; Miyaura, S.; Fujii, M.; Yusa, A.; Joo, E. J.; Kimata, K.; Kannagi, R.; Kim, Y. S.; Kyogashima, M. Generation and characterization of a series of monoclonal antibodies that specifically recognize [HexA(+/-2S)-GlcNAc]_n epitopes in heparan sulfate. *Glycoconj. J.* **2008**, 25, 703-712.
71. Maïza, A.; Chantepie, S.; Vera, C.; Fifre, A.; Huynh, M.B.; Stettler, O.; Ouidja, M.O.; Papy-Garcia, D.; The role of heparan sulfates in protein aggregation and their potential impact on neurodegeneration, *FEBS Lett.* **2018**, 592, 3806–3818.

72. Ozsan I.; McMillan, Li, J.P.; Wang, L.; Heparan sulfate proteoglycan in Alzheimer's disease: aberrant expression and functions in molecular pathways related to amyloid- β metabolism. *Am. J. Physiol. Cell Physiol.***2023**, *324*, C893-C909.
73. Patey, S.J.; Edwards, E.A.; Yates, E.A.; Turnbull, J.E.; Heparin derivatives as inhibitors of BACE-1, the Alzheimer's beta-secretase, with reduced activity against factor Xa and other proteases. *J. Med. Chem.***2006**, *49*, 6129-6132.
74. Li, J.; Su, G.; Xu, Y.; Arnold, K.; Pagadala, V.; Wang, C.; Liu, J. Synthesis of 3-O-sulfated heparan sulfate oligosaccharides using 3-O-sulfotransferase isoform 4. *ACS Chem. Biol.***2021**, *16*, 2026–2035.
75. Chen, Y.; Götze, M.; Liu, J.; Park, P. W. Microbial subversion of heparan sulfate proteoglycans. *Mol. Cells***2008**, *26*, 415–426.
76. Schwörer, R.; Zubkova, O.V.; Turnbull, J.E.; Tyler, P.C.; Synthesis of a targeted library of heparan sulfate hexa- to dodecasaccharides as inhibitors of β -secretase: potential therapeutics for Alzheimer's disease. *Chemistry***2013**, *19*, 6817-6823.
77. O'Donnell, C.D.; Shukla, D.; The importance of heparan sulfate in herpesvirus infection, *Viol. Sin.***2008**, *23*, 383-393.
78. Copeland R.,; Balasubramaniam, A.; Tiwari, V.; Zhang, F.; Bridges, A.; Linhardt, R. J.; Shukla, D.; Liu, J.; Using a 3-O-sulfated heparin octasaccharide to inhibit the entry of herpes simplex virus type 1. *Biochemistry***2008**, *47*, 5774–5783.
79. Hu, Y. P.; Lin, S. Y.; Huang, C. Y.; Zulueta, M. M.; Liu, J. Y.; Chang, W.; Hung, S. C. Synthesis of 3-O-sulfonated heparan sulfate octasaccharides that inhibit the herpes simplex virus type 1 host-cell interaction. *Nat. Chem.***2011**, *3*, 557–563.
80. Mietzsch, M.; Broecker, F.; Reinhardt, A.; Seeberger, P. H.; Heilbronn, R. Differential adeno-associated virus serotype-specific interaction patterns with synthetic heparins and other glycans. *J. Virol.***2014**, *88*, 2991–3003.

81. Chopra, P.; Joshi, A.; Wu, J.; Lu, W.; Yadavalli, T.; Wolfert, M. A.; Shukla, D.; Zaia, J.; Boons, G. J. The 3-O-sulfation of heparan sulfate modulates protein binding and lyase degradation. *Proc. Natl. Acad. Sci. U S A*.**2021**, *118*, e2012935118.

82. Hao, W.; Ma, B.; Li, Z.; Wang, X.; Gao, X.; Li, Y.; Qin, B.; Shang, S.; Cui, S.; Tan, Z. Binding of the SARS-CoV-2 spike protein to glycans. *Sci. Bull.***2021**, *66*, 1205–1214.

83. Chittum, J. E.; Sankaranarayanan, N. V.; O’Hara, C. P.; Desai, U. R. On the selectivity of heparan sulfate recognition by SARS-CoV-2 spike glycoprotein. *ACS Med. Chem. Lett.***2021**, *12*, 1710–1717.

84. Guimond, S. E.; Mycroft-West, C. J.; Gandhi, N. S.; Tree, J. A.; Le, T. T.; Spalluto, C. M.; Humbert, M. V.; Buttigieg, K. R.; Coombes, N.; Elmore, M. J.; Wand, M.; Nyström, K.; Said, J.; Setoh, Y. X.; Amarilla, A. A.; Modhiran, N.; Sng, J. D. J.; Chhabra, M.; Young, P. R.; Rawle, D. J.; Lima, M. A.; Yates, E. A.; Karlsson, R.; Miller, R. L.; Chen, Y.-H.; Bagdonaite, I.; Yang, Z.; Stewart, J.; Nguyen, D.; Laidlaw, S.; Hammond, E.; Dredge, K.; Wilkinson, T. M. A.; Watterson, D.; Khromykh, A. A.; Suhrbier, A.; Carroll, M. W.; Trybala, E.; Bergström, T.; Ferro, V.; Skidmore, M. A.; Turnbull, J. E. Synthetic heparan sulfate mimetic pixatimod (PG545) potently inhibits SARS-CoV-2 by disrupting the Spike-ACE2 interaction. *ACS Cent. Sci.***2022**, *8*, 527–545.

85. Wang, P.; Zhao, J.; Hossaini Nasr, S.; Otieno, S. A.; Zhang, F.; Qiang, W.; Linhardt, R. J.; Huang, X. Probing Amyloid β Interactions with Synthetic Heparan Sulfate Oligosaccharides. *ACS Chem. Biol.***2021**, *16* (10), 1894-1899.

86. Holzer, C. T.; Von Itzstein, M.; Jin, B.; et al. Inhibition of sialidases from viral, bacterial and mammalian sources by analogues of 2-deoxy-2,3-didehydro-N-acetylneuraminic acid modified at the C-4 position. *Glycoconjugate J.***1993**, *10*, 40–44.

87. Vaheri, A. Heparin and Related Polyonic Substances as Virus Inhibitors.**1964**, 98

88. Witvrouw, M.; De Clercq, E. Sulfated polysaccharides extracted from sea algae as potential antiviral drugs. *Gen. Pharmacol.: Vasc. Syst.***1997**, *29*, 497-511.

89. McCarthy, J.J. Optimal paradigms. *Linguist. Dep. Fac. Publ. Ser.***2005**, Jan 1:55.

90. Abrams, G.; Adolphsen, C.E.; Akerlof, C.; Alexander, J.P.; Alvarez, M.; Averill, D.; Baden, A.R.; Ballam, J.; Barish, B.C.; Barklow, T.; Barnett, B.A. The Mark II detector for the SLC. *Nucl. Instrum. Methods Phys. Res., Sect. A***1989**, *281*, 55-80.
91. Van de Wijgert, J.H.; Shattock, R.J. Vaginal microbicides: moving ahead after an unexpected setback. *AIDS***2007**, *21*(18), 2369-2376.
92. Neyts, J.; Reymen, D.; Letourneur, D.; Jozefonvicz, J.; Schols, D.; Este, J.; Andrei, G.; McKenna, P.; Witvrouw, M.; Ikeda, S.; Clement, J. Differential antiviral activity of derivatized dextrans. *Biochem. Pharmacol.***1995**, *50*(6), 743-751.
93. Vaheri, A. *Heparin and Related Polyonic Substances as Virus Inhibitors*.**1964**, 98 .
94. Beasley, C.L.; Zhang, Z.J.; Patten, I.; Reynolds, G.P. Selective deficits in prefrontal cortical GABAergic neurons in schizophrenia defined by the presence of calcium-binding proteins. *Biol. Psychiatry***2002**, *52*(7), 708-715.
95. Welliver, T.P.; Garofalo, R.P.; Hosakote, Y.; Hintz, K.H.; Avendano, L.; Sanchez, K.; Velozo, L.; Jafri, H.; Chavez-Bueno, S.; Ogra, P.L.; McKinney, L. Severe human lower respiratory tract illness caused by respiratory syncytial virus and influenza virus is characterized by the absence of pulmonary cytotoxic lymphocyte responses. *J. Infect. Dis.***2007**, *195*(8), 1126-1136.
96. Collins, P.L.; Graham, B.S. Viral and host factors in human respiratory syncytial virus pathogenesis. *J. Virol.***2008**, *82*(5), 2040-2055.
97. Krusat, T.H.; Streckert, H.J. Heparin-dependent attachment of respiratory syncytial virus (RSV) to host cells. *Arch. Virol.***1997**, *142*, 1247-1254.
98. Hallak, L.K.; Collins, P.L.; Knudson, W.; Peeples, M.E. Iduronic acid-containing glycosaminoglycans on target cells are required for efficient respiratory syncytial virus infection. *Virology***2000**, *271*(2), 264-275.
99. Li, W.; Shi, Z.; Yu, M.; Ren, W.; Smith, C.; Epstein, J.H.; Wang, H.; Crameri, G.; Hu, Z.; Zhang, H.; Zhang, J. Bats are natural reservoirs of SARS-like coronaviruses. *Science***2005**, *310*(5748), 676-679.
100. Beasley, C.L.; Zhang, Z.J.; Patten, I.; Reynolds, G.P. Selective deficits in prefrontal cortical GABAergic neurons in schizophrenia defined by the presence of calcium-binding proteins. *Biol. Psychiatry***2002**, *52*(7), 708-715.

101. Parish, C.R.; Freeman, C.; Brown, K.J.; Francis, D.J.; Cowden, W.B. Identification of sulfated oligosaccharide-based inhibitors of tumor growth and metastasis using novel in vitro assays for angiogenesis and heparanase activity. *Cancer Res.***1999**, *59*(14), 3433-3441.
102. Said, E.A.; Dupuy, F.P.; Trautmann, L.; Zhang, Y.; Shi, Y.; El-Far, M.; Hill, B.J.; Noto, A.; Ancuta, P.; Peretz, Y.; Fonseca, S.G. Programmed death-1–induced interleukin-10 production by monocytes impairs CD4+ T cell activation during HIV infection. *Nat. Med.***2010**, *16*(4), 452-459.
103. Nyberg, L.; Salami, A.; Andersson, M.; Eriksson, J.; Kalpouzos, G.; Kauppi, K.; Lind, J.; Pudas, S.; Persson, J.; Nilsson, L.G. Longitudinal evidence for diminished frontal cortex function in aging. *Proc. Natl. Acad. Sci. U.S.A.***2010**, *107*(52), 22682-22686.
104. Lee, J.C.; Vivanco, I.; Beroukhi, R.; Huang, J.H.; Feng, W.L.; DeBiasi, R.M.; Yoshimoto, K.; King, J.C.; Nghiemphu, P.; Yuza, Y.; Xu, Q. Epidermal growth factor receptor activation in glioblastoma through novel missense mutations in the extracellular domain. *PLoS Med.***2006**, *3*(12), e485.
105. Carlton, J.M.; Adams, J.H.; Silva, J.C.; Bidwell, S.L.; Lorenzi, H.; Caler, E.; Crabtree, J.; Angiuoli, S.V.; Merino, E.F.; Amedeo, P.; Cheng, Q. Comparative genomics of the neglected human malaria parasite *Plasmodium vivax*. *Nature***2008**, *455*(7214), 757-763.
106. Cheshenko, N.; Keller, M.J.; MasCasullo, V.; Jarvis, G.A.; Cheng, H.; John, M.; Li, J.H.; Hogarty, K.; Anderson, R.A.; Waller, D.P.; Zaneveld, L.J. Candidate topical microbicides bind herpes simplex virus glycoprotein B and prevent viral entry and cell-to-cell spread. *Antimicrob. Agents Chemother.***2004**, *48*(6), 2025-2036.
107. Cohen, J.I.; Kimura, H.; Nakamura, S.; Ko, Y.H.; Jaffe, E.S. Epstein–Barr virus-associated lymphoproliferative disease in non-immunocompromised hosts: a status

report and summary of an international meeting, 8–9 September 2008. *Ann. Oncol.***2009**, *20*(9), 1472-1482.

108. Ingallinella, P.; Bianchi, E.; Ladwa, N.A.; Wang, Y.J.; Hrin, R.; Veneziano, M.; Bonelli, F.; Ketas, T.J.; Moore, J.P.; Miller, M.D.; Pessi, A. Addition of a cholesterol group to an HIV-1 peptide fusion inhibitor dramatically increases its antiviral potency. *Proc. Natl. Acad. Sci. U.S.A.***2009**, *106*(14), 5801-5806.
109. Wolf, M.C.; Freiberg, A.N.; Zhang, T.; Akyol-Ataman, Z.; Grock, A.; Hong, P.W.; Li, J.; Watson, N.F.; Fang, A.Q.; Aguilar, H.C.; Porotto, M. A broad-spectrum antiviral targeting entry of enveloped viruses. *Proc. Natl. Acad. Sci. U.S.A.***2010**, *107*(7), 3157-3162.
110. Zhou, T.; Georgiev, I.; Wu, X.; Yang, Z.Y.; Dai, K.; Finzi, A.; Do Kwon, Y.; Scheid, J.F.; Shi, W.; Xu, L.; Yang, Y. Structural basis for broad and potent neutralization of HIV-1 by antibody VRC01. *Science***2010**, *329*(5993), 811-817.
111. Ferro, F.; Elefante, E.; Puxeddu, I.; Baldini, C.; Bartoloni, E.; Baratè, C.; Galimberti, S.; Talarico, R.; Mosca, M.; Bombardieri, S. COVID-19: the new challenge for rheumatologists. First update. *Clin. Exp. Rheumatol.***2020**, *38*(3), 373-382.
112. Guan, W.J.; Ni, Z.Y.; Hu, Y.; Liang, W.H.; Ou, C.Q.; He, J.X.; Liu, L.; Shan, H.; Lei, C.L.; Hui, D.S.; Du, B. Clinical characteristics of coronavirus disease 2019 in China. *N. Engl. J. Med.***2020**, *382*(18), 1708-1720.
113. won, H.I.; Kim, Y.I.; Park, S.J.; Kim, E.H.; Kim, S.; Si, Y.J.; Song, M.S.; Pascua, P.N.; Govorkova, E.A.; Webster, R.G.; Webby, R.J. A novel neuraminidase-dependent hemagglutinin cleavage mechanism enables the systemic spread of an H7N6 avian influenza virus. *mBio***2019**, *10*(6), e02810-19.
114. Ekblad, M.; Adamiak, B.; Bergstrom, T.; Johnstone, K.D.; Karoli, T.; Liu, L.; Ferro, V.; Trybala, E. A highly lipophilic sulfated tetrasaccharide glycoside related to

muparfostat (PI-88) exhibits virucidal activity against herpes simplex virus. *Antiviral Res.***2010**, 86(2), 196-203.

115. Said, E.A.; Dupuy, F.P.; Trautmann, L.; Zhang, Y.; Shi, Y.; El-Far, M.; Hill, B.J.; Noto, A.; Ancuta, P.; Peretz, Y.; Fonseca, S.G. Programmed death-1–induced interleukin-10 production by monocytes impairs CD4⁺ T cell activation during HIV infection. *Nat. Med.***2010**, 16(4), 452-459.
116. Petersen, S. I.; Okolicsanyi, R. K.; Haupt, L. M. Exploring Heparan Sulfate Proteoglycans as Mediators of Human Mesenchymal Stem Cell Neurogenesis. *Cell. Mol. Neurobiol.***2024**, 44 (1), 30.

CHAPTER- 2

**Immunogenic Sulfate L-Idose Homo
Oligosaccharide Elicit Neutralizing Antibody
Against Native Heparan Sulfate with
Biomarker and Therapeutic Applications**

Abstract

Heparan sulphate (HS) sequences facilitate numerous growth factor signals, as well as in the adhesion and infection processes of viruses and pathogens. Identifying these HS sequences and obstructing their recognition with antibodies holds promise for advancing pharmacological agent development. Nevertheless, HS is non-immunogenic antigen and developing antibodies against specific sulfated patterns in HS poses significant challenges. Herein, we employed an innovative immunization strategy that exploits molecular mimicry of HS to generate antibodies against HS sequences. Cheminformatics structural similarity analysis of heparin mimetics against native HS ligands confirmed that sulfated oligo-L-idose (**ID49**) has maximum of ~67% of the conserved structure compared other sulfate homo oligosaccharide analogs. Mice were immunized with **ID49@CRM₁₉₇** conjugate resulted in the production of robust IgG antibody responses targeting **ID49**, and cross-reactivity with the highly sulfated *N*-sulfated HS ligands and induce the complement-dependent cell cytotoxicity against tumor cells. Such pharmacological agent exhibited distinct staining of tissues sections and inhibited heparin mediated anticoagulation activity similar to protamine. These finding highlight the biomarker and therapeutic capability of the antibodies.

2.1 Introduction

Heparan sulfate (HS) is a major component of the glycocalyx and extracellular matrix, binding to growth factors, chemokines, viral and bacterial proteins, as well as toxins. These interactions play critical roles in regulating processes such as angiogenesis, viral infection, and tumor progression.¹⁻⁶ Structurally, HS comprises repeating units of D-glucosamine and uronic acid disaccharide units. The uronic acid composition can be either D-glucuronic acid or L-iduronic acid. The structural diversity of HS primarily arises from sulfation patterns, encompassing *O*-sulfation and *N*-sulfation. *O*-sulfation occurs particularly on glucosamine at the 6th, 3rd position, along with 2-*O*-sulfation of uronic acid residues. Additionally, amine residues of glucosamine are either *N*-sulfation (NS), *N*-acetylated (NAc) and *N*-unsubstituted (NU).⁷⁻¹⁰ Overall, a tetrasaccharide HS can be arranged in 2,304 combinations, highlighting the structural microheterogeneity of HS.¹² Identifying the specific HS epitopes involved in particular biological recognitions and developing antibodies or small molecule inhibitors against them represent a promising target for drug and vaccine development.¹²⁻¹⁵ For instance, previous research has shown that the 3-*O*-sulfation of HS is essential for facilitating the entry of Herpes simplex virus type 1 (HSV-1) into HeLa cells.¹⁶⁻¹⁷ Whereas, Adeno-Associated Virus (AAV) serotypes bind to HS sequences containing *N*-sulfated glucosamine and 2-*O*-sulfated iduronic acid residues to induce virulence.¹⁸ HS microarray analysis with SAR-Cov-2 spike proteins has revealed that highly *N*-sulfated patterns and iduronic acid composition serve as potential ligands for viral infection.¹⁹⁻²⁰ Therefore, antibodies targeting these HS ligands is crucial for combating viral diseases.

To date, various approaches have been explored for the development and commercialization of anti-heparan sulfate/heparin antibodies, including phage display Technology using purified HS proteoglycans as antigens.²¹⁻²³ Antibodies generated *via* phage display technology offer a promising tactic for generating anti-heparin specific V_H germinal segments. These anti-HSFv antibodies exhibited positive binding to specific HS sulfation patterns, with potential applications in inhibiting the anticoagulant activity of fondaparinux, staining HS epitopes at the tissue level and block viral infection at cellular level. However, these antibodies are fragments rather than full length antibodies, which limit its suitability to produce antibody-dependent cellular cytotoxicity (ADCC) and complement-dependent cytotoxicity (CDC), which is essential for therapeutic purpose. Further half-life and stability of these antibodies are poor due to the absence of Fc region and posttranslational modification. Hence,

traditional immunization strategy to produce antibody is highly recommended. However, antibodies generated by the immunization of HS proteoglycan showed broad reactivity with different sulfation patterns, predominantly resulting in the production of IgM class antibodies. For example, the F58-10E4 antibody, produced using HS proteoglycan from human fetal lung fibroblast displayed reactivity with mixed HS domains containing both *N*-acetylated and *N*-sulfated disaccharide units, including *N*-unsulfated glycosamines.²³ On the other hand, the HepSS-1 mouse IgM antibody exhibited a strong binding preference to *N*-sulfated HS domains,^{24,22} but failed to differentiate the 3-*O*- or 6-*O*-sulfation code. The JM403 antibody displayed a preference for glucuronate over iduronate and exhibited strong binding to *N*-nonsulfated glucosamine.^{23,25} The NAH46 antibody bound to sulfated HS disaccharide units, but lacked specificity for sulfation patterns. While, the FG69-3G10 anti-HS antibody demonstrated strong binding to unsaturated uronated at the nonreducing end.²⁶ Overall, we need a better antigenic substrate to produce robust IgG antibody with specificity to the sulfation patterns and uronic acid composition.

To address these limitations, we employed an innovative immunization strategy leveraging aspects of molecular mimicry²⁷ to generate antibodies demonstrating cross-reactivity with native HS ligands. Specifically, mice were immunized with sulfated oligo-L-idose (ID49) ligand, which shares a more than 70% similarity index with highly sulfated *N*-unsubstituted and *N*-sulfated HS tetrasaccharide ligands. This immunization elicited in a high-titer IgG antibody response against ID49, which is also directed against the highly *N*-sulfated HS oligosaccharides. Subsequent screening for specificity towards synthetic HS sulfation patterns confirmed that the antibodies are directed against 6-*O*-sulfated and 2-*O*-sulfated HS *N*-sulfated HS ligands and least binding to *N*-unsubstituted and *N*-acetate HS ligands. The biomarker potential of these antibodies has been demonstrated by selectively staining of fixed tissue sections. Additionally, their therapeutic potential was evidenced by their ability to neutralization of heparin-mediated anticoagulation activity.

2.2 Result and Discussion

To identify potential heparin mimetics with structural resembling native HS sequences, we initiated our investigation by assessing the similarity scores using native sequences. The heparin mimetics library was derived from PG545 and sulfated oligo-iduronic acid, both recognized as potential ligands for targeting and modulating HS binding proteins.²⁸⁻²⁹ Specifically, we utilized tetrasaccharides as the minimum glycan length and evaluated sulfated hexoses such as L-idose, L-iduronic acid, D-glucose, and D-glucuronic acid based heparinoids to determine their similarity scores. RDKit, a cheminformatics toolkit, was employed to generate these similarity scores. RDKit decode the structural similarity by creating a custom representation of the partial charges of atoms in the molecules and use similarity matrix to develop similarity index. Previously, RDKit was extensively used graphic neural networks (GNN) to generate molecular modeling and prediction. Here, we generated SMILES structures for all 2,304 HS tetrasaccharides (<https://github.com/rkikkeri/HS-similarity-index>. File name: chemdraw 1-2304.pdf) and compared their similarity scores with **I45**, **I49**, **ID49**, **ID413**, **G413**, **GA49**, **G49** and **GA45** (Figure 1a). As anticipated, all heparin mimetics exhibited varying degree of structural similarity score to native sequences (0 to 1) (Figure 1b & 1c Figure S1). **ID49** and **I45** showed optimal similarity indices of ~ 67% and 66% respectively, to native HS ligands when compared to other heparin mimetics. Notably, all analogues demonstrated strong binding to *N*-unsubstituted (NU) domains, followed by *N*-acetate (NAc) mixed domain ligands. **I45** showed a preference for 6-*O*-sulfated or 3-*O*-sulfated NU domain ligands containing 2-*O*-sulfated uronic acid residues (Compound numbers: 1, 34, 50, 83, 1585, 1634, and 1667). Conversely, **I49** displayed 56% similarity with the same ligands (Compound numbers: 1, 34, 50, 83, and 1585), indicating that increased sulfation on uronic acid composition decreases structural similarity with native heparin structures. Whereas, **ID49** exhibited a strong preference for 6-*O*-sulfated NU domain ligands carrying 2-*O*-uronic acid residues (Compound numbers: 99, 124, 1251, 1275, 1276), indicating that heparin mimetics with L-iduronic acid and L-idose can cause differences in molecular-level interactions. **ID413** and **GL413**, on the other hand, showed identical similarity indices, with 58% preference for 3,6-*O*-sulfated NU domain ligands (Compound numbers: 148, 180, 1684, 1716). Similarly, **G49** and **GA45** showed similarity to **ID49** and **I45** respectively. Overall, these results demonstrated that RDKit was unable to differentiate uronic acid compositions of heparin mimetics when evaluating structural similarity. Overall,

ID49 and **G49** stands out as a potential heparin mimetic to target native heparin structures. Here, we choose **ID49** for further studies, as their structure is not existing in the mammalian glyocalyx. The detailed similarity index Excel sheet, RDKit code with smile structures, and the chemical structures of all 2304 native heparin structures are freely available for download on a GitHub repository (<https://github.com/rkikkeri/HS-similarity-index>).

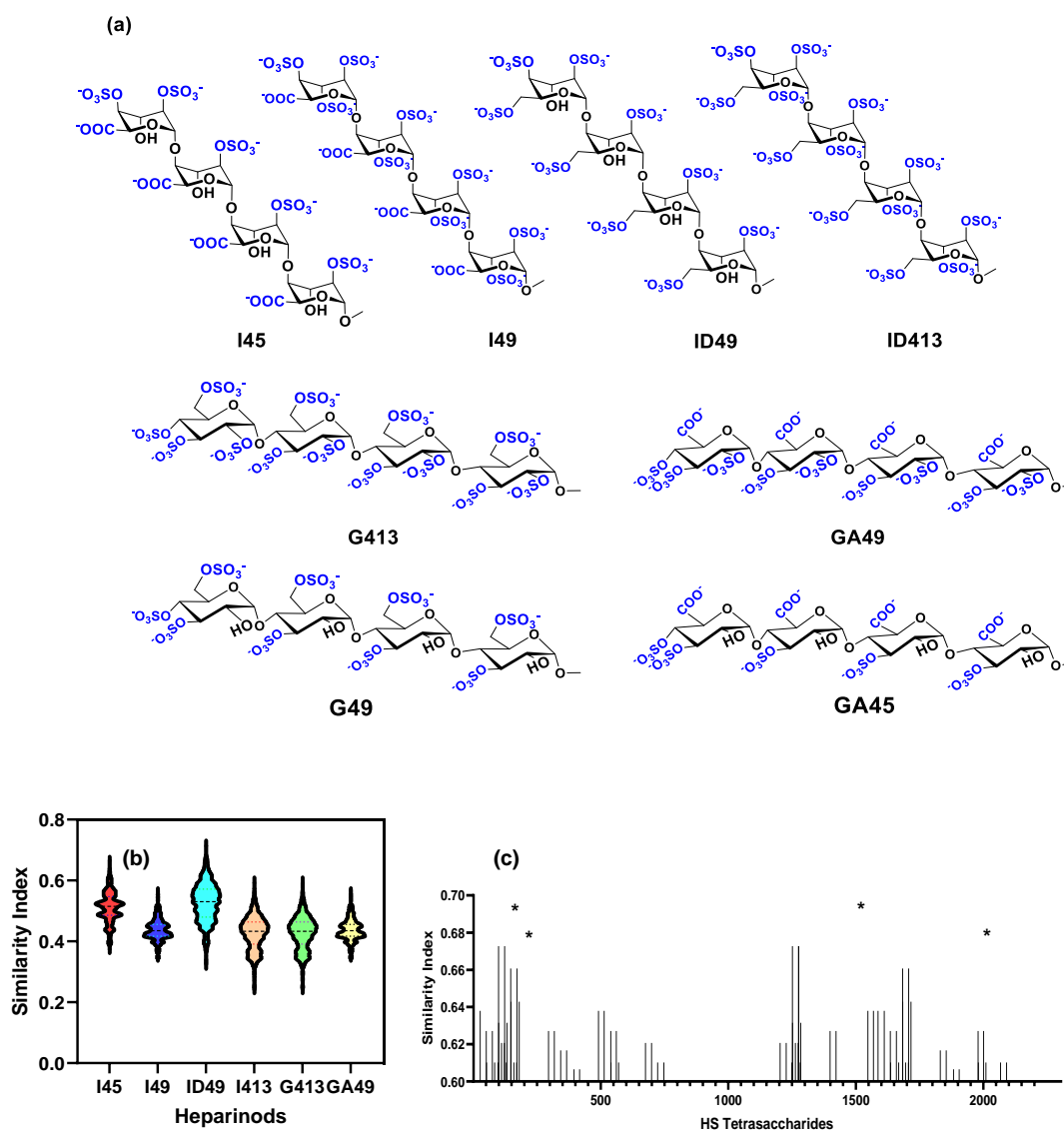


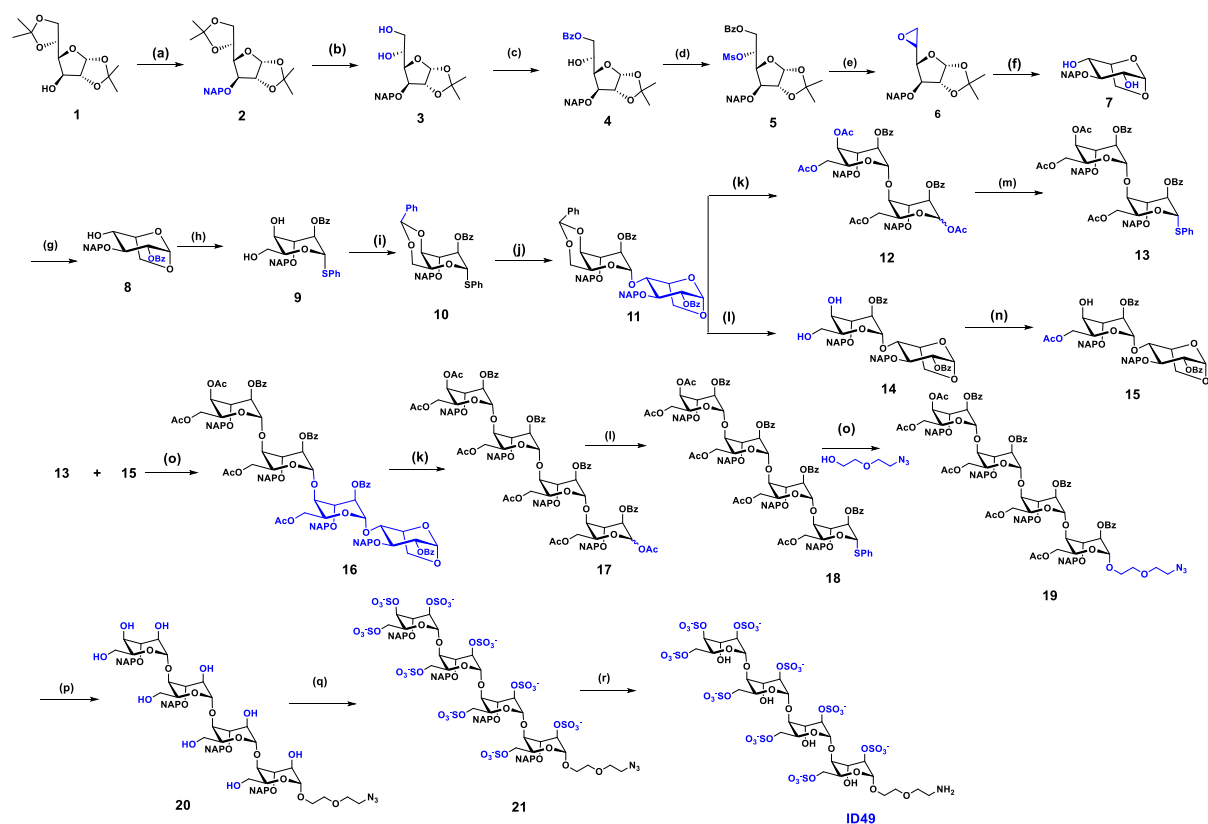
Figure 1. (a) Structures of heparinoids and (b) graphical representation of similarity index analysis with 2,304 native HS tetrasaccharides vs heparinods; (c) Similarity index of ID49: *Comp no 99: GlcNH₂(6S)-IdoA(2S)-GlcNH₂(6S)-IdoA(2S), 124: GlcNH₂(6S)-IdoA(2S)-GlcNHAc-GlcA(2S), 1251: GlcNH₂(6S)-IdoA(2S)-GlcNHAc(6S)-IdoA(2S), 1275: GlcNH₂(6S)-GlcA(2S)-GlcNH₂(6S)-GlcA(2S), 1276: GlcNH₂(6S)-GlcA(2S)-GlcNHAc-GlcA(2S) (Chemical <https://github.com/rkikkeri/HS-similarity-index>)

2.2.1 General Procedure

ID49 was synthesized from idose disaccharide **11** (Scheme 1), which were derived from 1,6-anhydro- β -L-idopyranosyl, 4-alcohol **7** and idose-thiophenoldonor **10** precursor. Compound **7** was synthesized with a total yield of 27% from 1,2:5,6-di-*O*-isopropylidene- α -D-glucofuranose through a six-step reaction. Selective 2-*O*-benzoylation, followed by regioselective ring opening with trimethyl(phenylthio)silane in the presence of ZnI₂ at room temperature, resulted in thioglycoside **9**. Compound **9** was then treated with benzaldehyde dimethyl acetal and a catalytic amount of *p*-toluenesulfonic acid (*p*-TSA) at room temperature, leading to **10**. Glycosylation of compound **10** and **8** in the presence of *N*-Idosuccinimide (NIS) and a catalytic amount of trimethylsilyltrifluoromethanesulfonate (TMSOTf) in DCM at -10°C yielded 55% of **11**. Compound **11** was divided into two portions; for one part, it was converted to acetate derivative by using Copper(II) trifluoromethanesulfonate (Cu(OTf)₂) in the presence of acetic anhydride under 0°C stirred overnight to obtain **12**. Another part was treated with *p*-TSA in MeOH/DCM (2/1) to obtain benzylidene-protected disaccharide **14**. Compound **12** was treated with trimethyl(phenylthio)silane in the presence of ZnI₂ in DCM at room temperature to obtain disaccharide donor **13**. Meanwhile, compound **14** underwent selective acetylation in the presence of acetic anhydride and a catalytic amount of triethylamine (TEA) to get disaccharide acceptor **15** with a 65% yield (Scheme1). The glycosylation of donor **13** with acceptor **15** in the presence of NIS and a catalytic amount of TMSOTf in DCM at -10°C yielded **16**. Later, **16** was converted to acetylated and thiophenol donor **18**. Tetrasaccharide donor **18** was glycosylated with linker, followed by deprotection of acetate, benzoyl group with lithium hydroxide (LiOH) yielded **20**. Sulfation of **20** was carried out with sulfur trioxide trimethylamine complex in DMF at 60°C to obtain compound **21**, which was subjected to hydrogenation in the presence of a catalytic amount of palladium hydroxide (Pd(OH)₂) in water for 24 h to obtain 65% yield of **ID49** ligand. The structure of **ID49** was confirmed by nuclear magnetic resonance (NMR) spectroscopy and high-resolution mass spectrometry (HRMS) for further use.

ID49 was conjugated to carrier protein CRM₁₉₇ to immunize the mice. The conjugation process involved activating **ID49** with disuccinimidyl suberate ester, followed by cross-linking to CRM₁₉₇ in the subsequent step.³⁰ The **ID49@CRM₁₉₇** glycoconjugate was

characterized through gel electrophoresis and MALDI-TOF mass spectrometry (Figure 7 & 8).



Scheme 1. Synthesis of **ID49**. Reagents and Conditions: (a) NAP-Br, NaH, DMF, 0 °C 92%; (b) 64% AcOH, 40 °C, 85%; (c) BzCl, DCM/Py (3/1), 0 °C 76%; (d) MsCl, Py, 0 °C 60%; (e) ^tBuOK, ^tBuOH/DCM (1/1) 88%; (f) 2N H₂SO₄, 1,4-Dioxane, reflux 75%; (g) BzCl, DCM/Py (4:1), 0 °C, 60%; (h) ZnI₂/TMSSPh, DCM, 93%; (i) Benzaldehyde dimethyl acetal, p-TSA, ACN, 86%; (j) NIS TMSOTf, 4 Å M.S., -10 °C, 90%; (k) Cu(OTf)₂, Ac₂O, 0 °C, 90% (**13**), 70% (**17**); (l) ZnI₂, TMSSPh, DCM, 85% (**14**); 85% (**18**); (m) p-TSA, MeOH/DCM (2/1) 77% ; (n) Ac₂O, TEA, DCM, 12h, 65%; (o) NIS, TMSOTf, 4 Å M.S., -10 °C 55% (**16**); 63% (**19**); (p) LiOH, THF/MeOH/H₂O (4/2/1), 0 °C, 70%; (q) SO₃.NMe₃, DMF, 60 °C, 55%; (r) H₂/Pd(OH)₂, H₂O, 65%.

2.2.2 Antibody response for ID49@CRM₁₉₇ and Cross reactivity against Serum antibody

To assess the immunogenicity of **ID49@CRM₁₉₇**, a group of four female C57BL/6 mice received subcutaneous immunizations with **ID49** (6 µg per dose) along with aluminum hydroxide and Freund's adjuvant at biweekly intervals. Controls included immunizations

with CRM₁₉₇, PBS, and adjuvants alone. Sera were collected biweekly, as well as on the 37th and 60th days (Figure 2a). The **ID49**-specific antibody response in post-immune sera was evaluated by ELISA, using **ID49@BSA** conjugate (Figure 7 and 8) as the antigen. Analysis of the 37th day sera at different dilutions revealed a strong IgG antibody response compared to IgM by **ID49@CRM₁₉₇** with both adjuvants (Figure 2b & 3c). In contrast, CRM₁₉₇, PBS alone, alum, and Freund's alone showed nominal responses, indicating the immunogenic nature of **ID49** (Figure 2b). Subsequent screening indicated that antibody production against **ID49** commenced after the 15th day and continued for an extended period. Even at a 1/100,000 dilution, a robust antibody response was observed, suggesting that **ID49** can induce strong immune responses (Fig2d). Among adjuvants, Freund's exhibited a better antibody response compared to alum. Further screening of IgG subclasses revealed that both adjuvants exhibited a preferential IgG2b antibody response over IgG3, with Freund's adjuvant again showing a superior IgG subclass response compared to alum conjugation (Figure 2e and 2f).

Upon confirming the immunogenicity of the serum of **ID49@CRM₁₉₇**, we started to investigate cross-reactivity of the antibodies with native HS sequences. To achieve this, we synthesized a panel of BSA-conjugated-HS ligands, ranging from disaccharide, tetra to hexasaccharide with various sulfation patterns from NAc, NU, NS-domain and conducted ELISA plate analysis (Figure 2g Table 6). Surprisingly, serum from **ID49@CRM₁₉₇-freund's/alum** immunization exhibited cross-reactivity specific to heparin, *N*-sulfate HS ligands (Figure 2g). Contrasting with the RDkit analysis, *N*-unsubstituted, *N*-acetate, and HS tetrasaccharide ligands showed poor binding, implying that the structural processing of the ID49 ligand during immunization differed from that predicted by cheminformatics toolkit. The negatively charged biomacromolecules such as hyaluronic acid (HA), collagen-I, oligonucleotide (DNA), and BSA exhibited poor binding, confirming the specificity of the antibodies to sulphated heparin structures (Figure 2g).

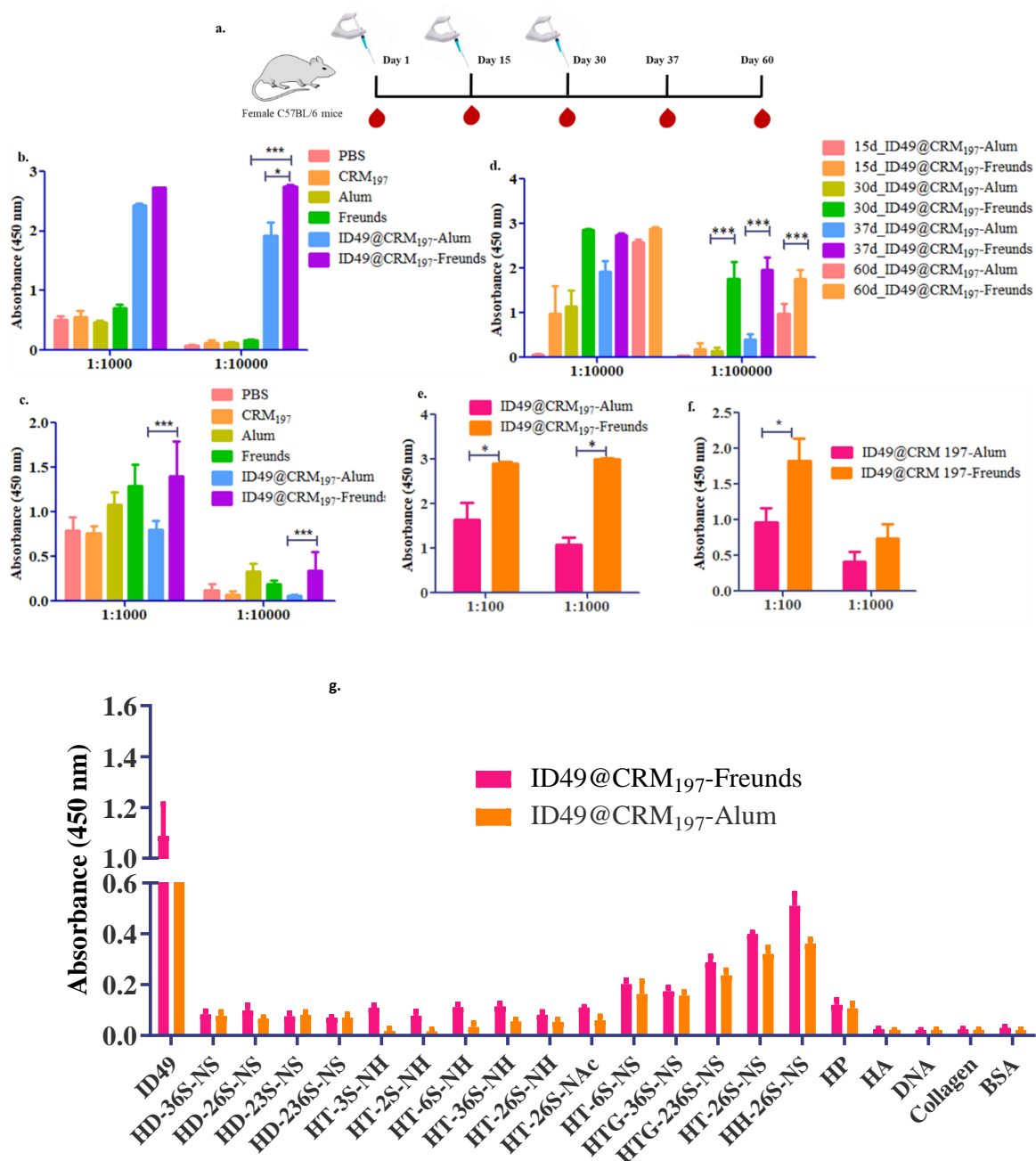


Figure 2. (a) Immunization regime for C57B/L female mice (4 mice/group); (b) ELISA of the antisera induced by vaccines preparation **ID49@CRM₁₉₇** mixed with alum hydroxide and Freund's adjuvant Total IgG antibody titer on 37th Day; (c) Total IgM antibody titer on 37th day; (d) Total IgG antibody titer at different days; (e) IgG2b antibody titer on 37th day; (f) IgG3 antibody titer on 37th day; (g) ELISA plate cross reactivity analysis of **ID49@CRM₁₉₇** against HS di, tetra and hexasaccharides and biomolecules: **HD-36S-NS**: GlcNS(36S) α (1-4)GlcA α -Pro-NH₂; **HD-26S-NS**: GlcNS(6S) α (1-4)IdoA(2S) α -Pro-NH₂; **HD-236S-NS**: GlcNS(36S) α (1-4)GlcA(2S) α -Pro-NH₂; **HD-236S-NS**: GlcNS(36S) α (1-4)IdoA(2S) α -Pro-NH₂; **HT-3S-NH**: GlcNH(3S) α (1-4)IdoA α (1-4)GlcNH(3S) α (1-4)IdoA α -Pro-NH₂; **HT-2S-**

NH: GlcNH α (1-4)IdoA(2S) α (1-4)GlcNH α (1-4)IdoA(2S) α -Pro-NH₂; **HT-6S-NH:**
 GlcNH(6S) α (1-4)IdoA α (1-4)GlcNH(6S) α (1-4)IdoA α -Pro-NH₂; **HT-36S-NH:**
 GlcNH(36S) α (1-4)IdoA α (1-4)GlcNH(36S) α (1-4)IdoA α -Pro-NH₂; **HT-26S-NH:**
 GlcNH(6S) α (1-4)IdoA(2S) α (1-4)GlcNH(6S) α (1-4)IdoA(2S) α -Pro-NH₂; **HT-26S-NAc:**
 GlcNAc(6S) α (1-4)IdoA(2S) α (1-4)GlcNAc(6S) α (1-4)IdoA(2S) α -Pro-NH₂; **HT-6S-NS:**
 GlcNS(6S) α (1-4)IdoA α (1-4)GlcNS(6S) α (1-4)IdoA α -Pro-NH₂; **HTG-36S-NS:**
 GlcNS(36S) α (1-4)GlcA α (1-4)GlcNS(36S) α (1-4)GlcA α -Pro-NH₂; **HTG-236S-NS:**
 GlcNS(36S) α (1-4)GlcA(2S) α (1-4)GlcNS(36S) α (1-4)GlcA(2S) α -Pro-NH₂; **HT-36S-NS:**
 GlcNS(36S) α (1-4)IdoA α (1-4)GlcNS(36S) α (1-4)IdoA α -Pro-NH₂; **HH-26S-NS:**
 GlcNS(6S) α (1-4)IdoA(2S) α (1-4) GlcNS(6S) α (1-4)IdoA(2S) α (1-4)GlcNS(6S) α (1-4)IdoA(2S) α -Pro-NH₂; **HP:** Heparin; **HA:** hyaluronic acid; **DNA:** plasmid deoxyribonucleotide.

Interestingly, the **ID49@CRM197** antibody bound to highly *N*-sulfated HS tetrasaccharides and hexasaccharide ligands. The serum antibody showed a slight preference for L-iduronic acid-based (**HT-26S-NS** and **HH-26S-NS**) ligands over D-glucuronic acid-based (**HTG-36S-NS** and **HTG-236S-NS**). Further, the binding preference increased from **HT-6S-NS** to **HT-26S-NS**, demonstrating stronger binding with increased sulfation. Overall, these results suggest that the **ID49@CRM197** antibody is specific to *N*-sulphated higher oligosaccharide domain HS ligands with a structural similarity to **ID49** ligands ranging between 59-63%.

2.2.3 FACS assay

To demonstrate the biomarker proficiency of the antibody, we performed immunostaining assay of **ID49@CRM197** on cancer cells exhibiting varying levels of aggression (MDA-MB-468, SK-BR-3 and MCF-7) and normal cells (NIH-3T3). We incubated cells with 60th day **ID49@CRM197** serum (1:100 dilution) for 1 h and treated them with goat anti-mouse IgG secondary antibody conjugated with Alexa Fluor 488 and quantified the amount of fluorescent staining by flow cytometry. Our findings revealed that cancer cells which are aggressive and metastasis in nature like MDA-MB-468 and SK-BR-3 exhibited nearly 1.3-fold higher fluorescence staining compared to MCF-7 (milder cancer cells) and normal cells (Figure 3). This indicates that as the aggression level of the cancer cells increases there is corresponding increase in *N*-sulfated HS ligands. This also correlates to the literature findings that triple negative breast cancer cell lines expressed higher amount of HS compared to normal cells.³¹

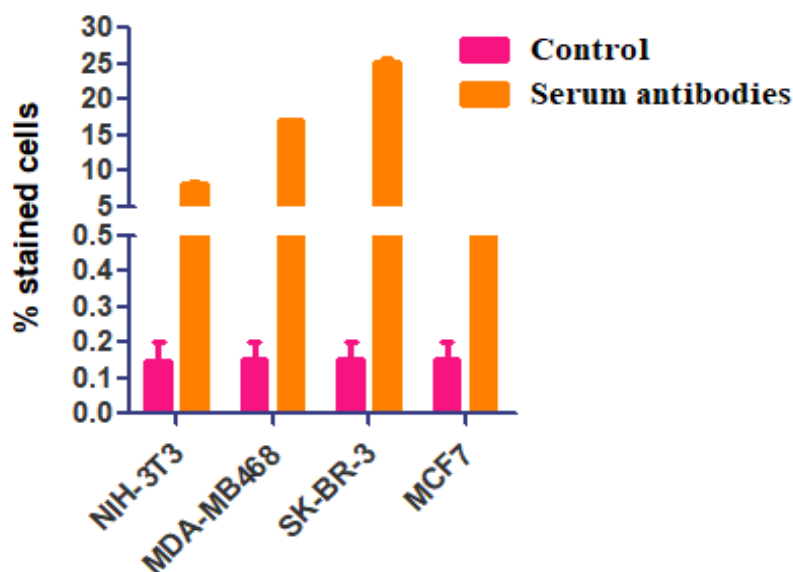


Figure 3. FACS quantification data of **ID49@CRM197** serum staining of different cancer and normal cells using and Goat anti-mouse IgG secondary antibody Alexa Fluor 568

2.2.4 Immunohistochemistry

We next performed immunostaining of the antibody with different tissue section of mice. For this purpose, we prepared 1mm thickness slices of mouse liver, kidney, heart, lung and brain and treated them with **ID49@CRM197** serum (1:100 dilution), followed by secondary antibody (Goat anti-mouse IgG secondary antibody Alexa Fluor 568) (Figure 9). Previous studies have been shown that HS epitopes are not evenly distributed in these tissue sections. Immunofluorescence studies of kidney sections with anti-K5 mAb 865 and 3G10 showed disparity in the staining of the tubular basement membrane, extracellular matrix compared to the glomerulus region and vice versa with mAb 865 antibody, indicating the presence of highly sulfated HS region in the basement membrane compared to glomerulus region.²⁵ Similarly, MP3B2'20 b.k anti-HS antibodies generated by phage display methods showed strong staining of kidney glomerulus but not Bowman's capsule, whereas MDPA11 antibody stained Bowman's capsule, but not the glomeruli.³² These results showed there is a significant difference in the HS composition in the kidney regions and ideal tissue slice for differentiating anti-HS antibodies. As hypothesized, **ID49@CRM197** antibodies strongly stained distal and proximal tubules (Figure 4a & 4b). When observed at a higher resolution, the staining was observed mainly at the proximal tubular epithelial cell membrane and tight junction region rather than the tubular basement membrane, clearly indicating that there is a

significant difference in the HS sequence in the basement membrane over the epithelial cells, which was not observed in the other anti-HS antibodies. Unlike kidney section, the heart and lung section showed staining of cell membrane as well as internal organoids of the cardiac muscle cells, as well as resident cells and transient cells in the alveoli, alveolar sac and duct region of the lung slices (Figure 4c & 4d). Whereas, liver sections showed staining of cell membrane, extracellular matrix and internal part of the hepatocytes cells and differentiate the sinusoids (Figure 4e). To our surprise, **ID49@CRM197** antibody failed to stain brain cerebellum sections (Figure 4f). Previously, anti-HS antibodies such as 10E4, NAH46, AS25, ACH55 and 3G10 antibodies showed selective binding of Purkinje, endothelial and granular cells in cerebellum.²⁶ However, non-staining of **ID49@CRM197** antibodies, indicate that highly sulfated *N*-sulfate HS composition is absent in the brain cerebellum part, but abundant in lung, heart and liver sections, and selectively expressed in kidney. In order to confirm whether the **ID49@CRM197** antibody binding to these tissue slides is through heparin mediated interaction. We performed several control experiment, including treating the tissue sections without serum (Figure 4g-4i) and we pretreated the kidney and liver specimen with heparinase-I for 1 h before performing immunostaining. Our results showed that the pretreatment with heparinase-I strongly inhibited **ID49@CRM197** antibody staining, suggesting that HS epitopes on this specimen are the key recognition site for **ID49@CRM197** antibody (Figure 10).

2.2.5 Ex-Vivo assay

The effect of this antibodies on the HS mediated biological activity was examined by anti-coagulation assay using human blood sample. To this end, we incubated human blood (100 μ l) with heparin (130 μ M), followed by **ID49@CRM197** serum. We observed inhibition of heparin mediated anti-coagulation activity at 1:100 dilution (Figure 5a) similar to protamine activity. Consistent with our immunostaining assay, anti-coagulation assay confirmed that the **ID49@CRM197** antibody directly binds to highly sulfated NS-domain HS ligands and lock their biological activities. Finally, complement-dependent cytotoxicity (CDC) was investigated using SK-BR-3 cells (Figure 5b). The antibodies in the sera from day 35 and day 60 exhibited significantly greater cancer cell cytotoxicity compared to those in the sera from day 0 and day 15. These findings indicate that the **ID49** antigen is capable of eliciting antibodies against native heparin sequences and inducing the cytotoxicity necessary for vaccine development.

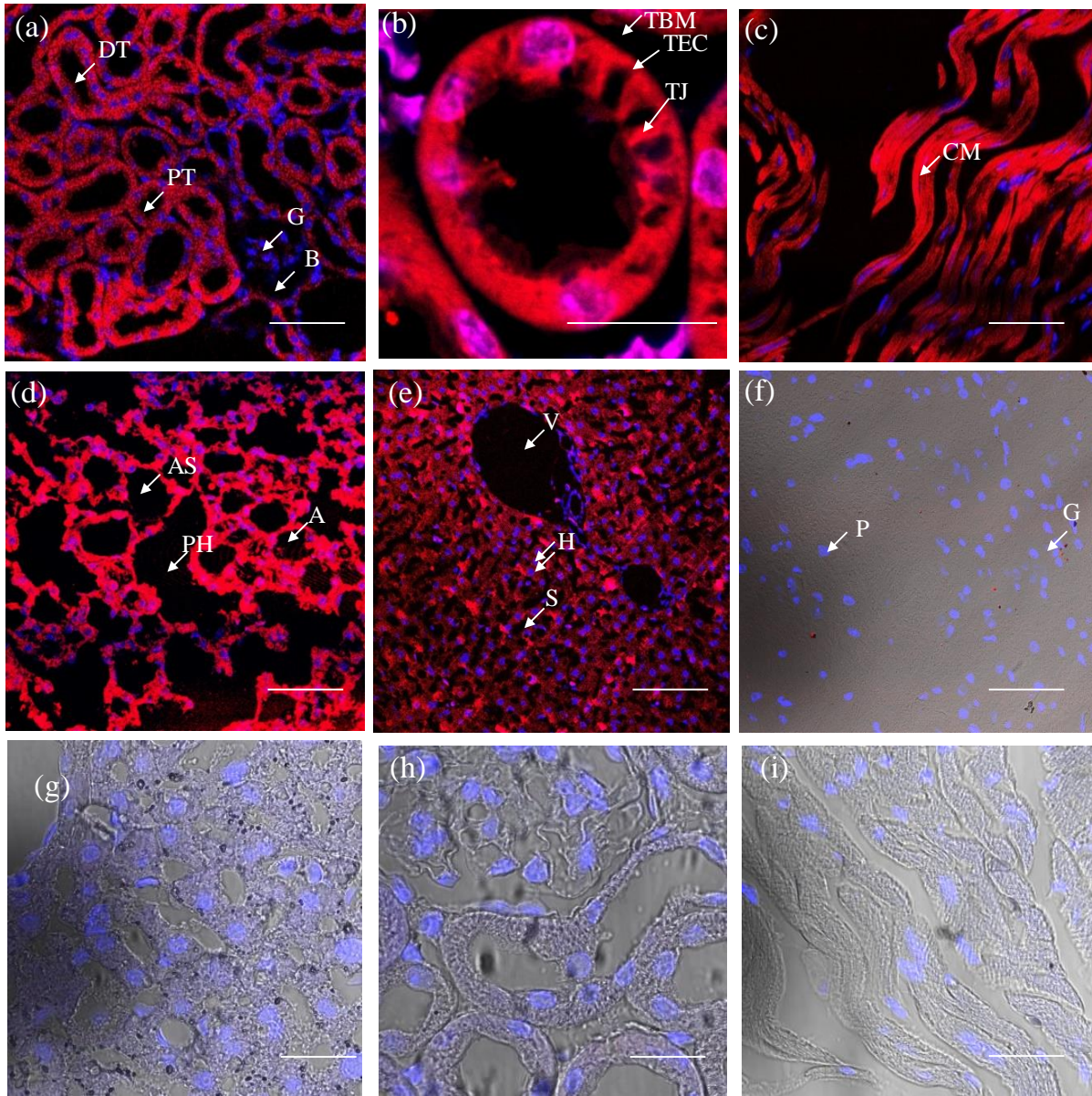


Figure 4. Immunofluorescent images of specimens treated with **ID49** antibody and Goat anti-mouse IgG secondary antibody Alexa Fluor 568 (a) kidney sections showing selective staining of distal (DT) and proximal tubules (PT) compared to glomerulus (G) and Bowman's capsule region; (b) kidney section of proximal tubules epithelial cells (PTE) and claudin tight junctions (TJ) compared to tubular basement membrane (TBM); (c) heart section staining cardiac muscle cells; (d) lung sections staining cells in the alveolar sacs (AS), alveoli (A) region; (e) liver section staining the hepatocyte cells (H) compared to synovial space (S); (f) brain cerebellum region showed no staining of Purkinje (P) or granular cells (G); (g)-

(i) tissue section treated with IgG secondary antibody without **ID49@CRM197**: liver (g); kidney (h) and heart (i). (scale bar 100 μ m).

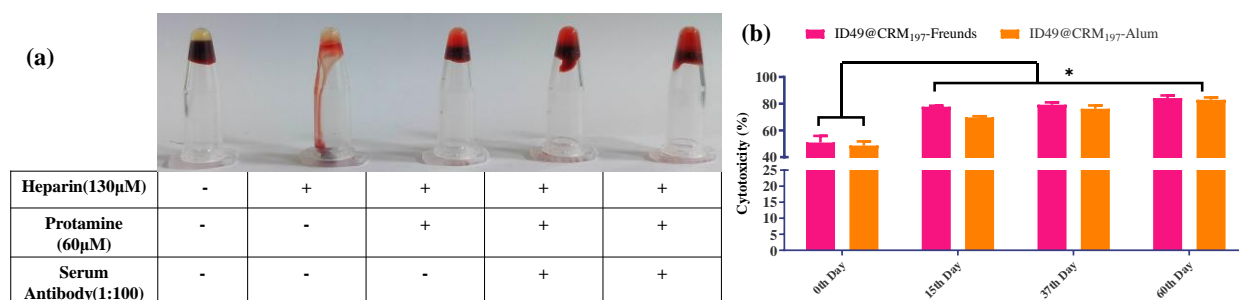


Figure 5. (a) Snap shot images of anticoagulation of mice blood in the presence of **ID49@CRM197** and protamine; (b) Antibodies elicited by **ID49** at different time interval mediate complement dependent cytotoxicity (CDC). SK-BR-3 cells were incubated with serum collected at different time interval at 37 °C for 2 h, the cytotoxicity induced by the serum was then determined using the LDH assay. *P < 0.05.

2.3 CONCLUSIONS

In this work, we have presented an innovative approach to produce antibodies targeting specific heterogeneity within heparan sulfate polysaccharides. Using cheminformatics, we have identified that homo-oligosaccharides carrying sulfated L-idose/L-iduronic acid exhibit greater similarity index to native HS oligosaccharides with specific sulfation patterns. By employing a divergent [2+2] glycosylation method, we successfully synthesized the **ID49** oligosaccharides and thoroughly characterized using NMR and mass spectrometric techniques. The synthetic heparinoids **ID49** were then conjugated to the CRM₁₉₇ carrier protein, with an average of eight to nine glycans per CRM₁₉₇ molecule, as ascertained through mass spectrometric analysis. C57BL/6 mice were immunized with the conjugates formulated with adjuvants such as aluminium hydroxide and Freund's adjuvant respectively. Following three biweekly immunizations, the **ID49** antigen elicited a robust anti-IgG **ID49** antibody response. Further, the IgG antibody titer response can be seen at a dilution of 1/100,000 and showed cross reactivity with native HS sequences. Specifically, they were selective against *N*-sulfated 6-*O* and 2-*O* sulfated higher oligosaccharides, which has been proved to be a vital HS ligand for various biological activities.⁸ This property is a real asset for mapping the HS heterogeneity in cancer and normal cells. Further, these antibodies were able to stain different compartment of tissue sections, which is not stained by other HS

antibodies. Particularly in kidney sections, **ID49@CRM197** antibody was able to stained the plasma membrane of distal (DT) and proximal tubules (PT) compared to glomerulus (G) and Bowman's capsule region. Indicating the HS sequence expression on the plasma membrane of tubules compartment of kidney is different from that of capsule region. Finally, anticoagulation assay and cytotoxicity assay reiterates the therapeutic potential of the antibodies. Isolation of the mAb and atomic level structure-activity studies of **ID49@CRM197** antibody can offer rational approach to design antibodies against HS epitopes to alter physiological and pathological process.

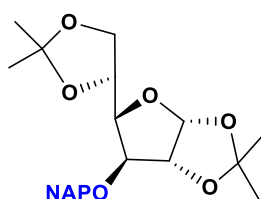
2.4 EXPERIMENTAL SECTION

2.4.1 General Information

All chemicals were reagent grade and used without further purification unless otherwise noted. Reactions were carried out in anhydrous solvents under a nitrogen atmosphere. Reaction progress was monitored by analytical thin-layer chromatography (TLC) on Merck silica gel 60 F₂₅₄. Spots on TLC plate were visualized under UV light or by dipping the TLC plate in CAM/ninhydrin solution followed by heating. Column chromatography was carried out using Fluka kieselgel 60 (230-400 mesh). ¹H and ¹³C NMR spectra of compounds were measured with Bruker 400 MHz, Bruker 600 MHz and Jeol 400 MHz using residual solvents as an internal reference (CDCl₃ δH 7.26 ppm, δC 77.3 ppm, CD₃OD δH 3.31 ppm, δC 49.0 ppm, and D₂O δH 4.79 ppm). The chemical shifts (δ) are reported in ppm and coupling constants (J) in Hz. UV-visible measurements were performed with Evolution 300 UV-visible spectrophotometer (Thermo Fisher Scientific, USA). Fluorescence spectra were measured with FluoroMax-4 spectrofluorometer (Horiba Scientific, U.S.A.). All microscopy images were captured using Leica SP8 confocal microscope and processed using Image J software. Heparin was gifted by Lupin. India. Pune. Diphtheria Toxin, CRM mutant was purchase from Fina biosolutions, Maleimido active BSA was purchased from sigma-Aldrich. Goat anti mouse IgG secondary Antibody HRP conjugated, Goat antimouse IgM secondary Antibody HRP conjugated, Goat anti mouse IgG3 secondary Antibody HRP conjugated, Goat Anti mouse IgG 2b cross absorbed secondary antibody HRP, Goat anti-Mouse IgG (H+L) Cross-Adsorbed Secondary Antibody, Alexa Fluor™ 488, Goat anti-Mouse IgG (H+L) Highly Cross-Adsorbed Secondary Antibody, Alexa Fluor™ 568 were purchased from Invitrogen. All animal studies were performed with the approved protocol from the

institutional animal ethical committee. **ID49** purity was further confirmed by PAMN-HPLC using monopotassium phosphate 1.5 M for 50 min at a flow rate of 0.5 mL/min.

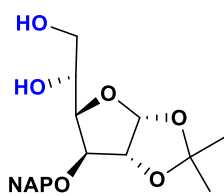
Compound 2.



2

In a 1-lt RB, compound1 (43 g, 0.165 moles) was dissolved in 100 ml of dimethylformamide (DMF). The reaction mixture was cooled to 0°C in an ice bath. Then, sodium hydride (NaH) (8.34 g, 0.334 moles) was added in portions, followed by the dropwise addition of 2-Bromomethyl)naphthalene (55.6 g, 0.2508 moles). The reaction mixture was stirred for 2 hours under a nitrogen atmosphere. The progress of the reaction was monitored by thin-layer chromatography (TLC). After the reaction was complete, the mixture was concentrated under vacuum using a rotary evaporator. Subsequently, an ethyl acetate (EtOAc) extraction was carried out with brine, and the organic layer was dried over anhydrous sodium sulfate (Na₂SO₄). The resulting solution was concentrated under reduced pressure and purified by column chromatography using a dichloromethane (DCM)/hexane solvent system to yield compound **2** in a 92% yield. (400 MHz, Chloroform-*d*) 5.93 (d, *J* = 3.7 Hz, 1H), 4.90 – 4.74 (m, 2H), 4.63 (d, *J* = 3.7 Hz, 1H), 4.42 (dt, *J* = 7.7, 6.0 Hz, 1H), 4.23 – 4.11 (m, 2H), 4.08 (d, *J* = 3.1 Hz, 1H), 4.03 (dd, *J* = 8.5, 5.8 Hz, 1H), 1.49 (s, 3H), 1.43 (s, 3H), 1.39 (s, 3H), 1.31 (s, 3H), 7.87 – 7.72 (m, 4H), 7.56 – 7.36 (m, 3H)¹³C NMR (101 MHz, Chloroform-*d*) δ 135.17, 133.33, 133.16, 128.33, 127.99, 127.82, 126.58, 126.29, 126.11, 125.75, 111.94, 109.15, 105.43, 82.77, 81.70, 81.45, 72.63, 72.52, 67.53, 26.94, 26.36, 25.58. HR-ESI-MS (m/z): [M+Na]⁺, calculated for C₂₃H₂₈O₆Na, 423.1784 ; Found 423.1789.

Compound 3.

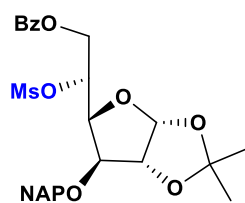


3

In a 1-lt RB, compound2 (48 g, 0.1218 moles) was dissolved in 64% acetic acid (AcOH). The reaction mixture was stirred overnight at 40°C in an oil bath (without reflux). The progress of the reaction was monitored by thin-layer chromatography (TLC). After the reaction was complete, it was quenched with a cold sodium bicarbonate (NaHCO₃) solution. Ethyl acetate (EtOAc) extraction was performed, and the organic layer was dried over anhydrous sodium sulfate (Na₂SO₄). The crude product was further purified by column chromatography

using a dichloromethane (DCM)/ethyl acetate (EtOAc) solvent system to obtain compound **3** in 85% yield. ^1H NMR (400 MHz, Chloroform-*d*) 5.96 (d, $J = 3.8$ Hz, 1H), 4.88 (d, $J = 11.9$ Hz, 1H), 4.71 (d, $J = 11.9$ Hz, 1H), 4.67 (d, $J = 3.8$ Hz, 1H), 4.18 – 4.11 (m, 2H), 4.07 (ddd, $J = 7.2, 5.4, 3.3$ Hz, 1H), 3.82 (dd, $J = 11.5, 3.4$ Hz, 1H), 3.71 (dd, $J = 11.5, 5.4$ Hz, 1H), 1.48 (s, 3H), 1.32 (s, 3H), 8.18 – 7.63 (m, 4H), 7.60 – 7.35 (m, 3H) ^{13}C NMR (101 MHz, Chloroform-*d*) δ 134.60, 133.30, 133.20, 128.77, 128.04, 127.86, 127.00, 126.52, 126.36, 125.60, 111.97, 105.26, 82.26, 82.00, 80.05, 72.35, 69.33, 64.45, 26.82, 26.32. HR-ESI-MS (m/z): $[\text{M}+\text{Na}]^+$, calculated for $\text{C}_{20}\text{H}_{24}\text{O}_6\text{Na}$ 383.1471; Found 383.1473.

Compound 5.



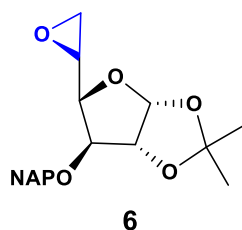
5

In a 500 ml RB, compound **3** (48 g, 0.1331 moles) was dissolved in a dry dichloromethane/pyridine (4:1) solvent mixture under a nitrogen atmosphere. The reaction mixture was cooled to 0°C in an ice bath. Benzoyl chloride (18.5 ml, 0.1598 moles) was then added dropwise using a dropping funnel. The reaction progress was monitored by TLC.

After the reaction was complete, it was quenched with methanol (MeOH), followed by subsequent workup with 10% hydrochloric acid (HCl) and saturated sodium bicarbonate (NaHCO_3) solution. The resulting mixture was dried over anhydrous sodium sulfate (Na_2SO_4). The workup solution was concentrated and dried under reduced pressure using a rotary evaporator, and then taken to the next step without purification. The crude product was dissolved in dry pyridine, and the resulting mixture was cooled to 0°C. Methanesulfonyl chloride (14.5 ml, 0.1884 moles) was added dropwise under an inert nitrogen atmosphere at 0°C. The reaction mixture was stirred overnight. The progress of the reaction was monitored by TLC. After the reaction was complete, the reaction mixture was concentrated under high vacuum. Subsequently, an extraction with dichloromethane (DCM) using 10% HCl and brine solutions was performed. The organic layer was dried over anhydrous sodium sulfate (Na_2SO_4), and the crude product was purified by column chromatography using a hexane/ethyl acetate (EtOAc) solvent system to obtain compound **5** in a 60% yield. ^1H NMR (400 MHz, Chloroform-*d*) 5.95 (d, $J = 3.6$ Hz, 1H), 5.46 (ddd, $J = 8.1, 6.3, 2.0$ Hz, 1H), 4.95 (dd, $J = 12.8, 2.1$ Hz, 1H), 4.92 – 4.73 (m, 2H), 4.67 (d, $J = 3.6$ Hz, 1H), 4.57 – 4.43 (m, 2H), 4.21 (d, $J = 3.1$ Hz, 1H), 2.98 (s, 3H), 1.51 (s, 3H), 1.32 (s, 3H), 8.17 – 7.87 (m, 2H) 7.93 – 7.69 (m, 4H), 7.62 – 7.38 (m, 6H) ^{13}C NMR (101 MHz, Chloroform-*d*) δ 134.69, 133.42, 133.20, 129.85, 128.63, 128.42, 128.14, 127.79, 127.03, 126.27, 126.18, 126.00, 112.44,

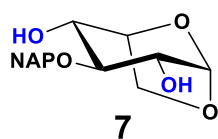
105.51, 81.68, 81.37, 78.45, 75.49, 72.61, 64.20, 39.22, 26.96, 26.41. HR-ESI-MS (m/z): [M+Na]⁺, calculated for C₂₈H₃₀O₉SNa 565.1508; Found 565.1509.

Compound 6.



Compound **5** (34 g, 0.0632 mol) was dissolved in dry DCM/t-BuOH (1/1) ratio in 10 Volume each. Then potassium tertiary butoxide (BuO⁻K⁺) (15.5 g, 0.139 mol) was added at 0°C. Reaction mixture was kept for stirring for overnight. Reaction completion was confirmed by MALDI-TOF-MS. Further, reaction mixture was concentrated under reduced pressure then subsequently did DCM extraction with brine solution and purified by column chromatography in Hexane/EtOAc solvent system to get compound **6** in a 88% yield. ¹H NMR (400 MHz, Chloroform-*d*) 6.03 (d, *J* = 3.8 Hz, 1H), 5.04 – 4.81 (m, 1H), 4.76 – 4.56 (m, 2H), 4.01 (d, *J* = 3.5 Hz, 1H), 3.81 (dd, *J* = 6.1, 3.5 Hz, 1H), 3.32 (ddd, *J* = 6.2, 4.3, 2.7 Hz, 1H), 2.77 (t, *J* = 4.6 Hz, 1H), 2.53 (dd, *J* = 4.9, 2.7 Hz, 1H), 1.44 (s, 3H), 1.33 (s, 3H), 7.93 – 7.70 (m, 4H), 7.59 – 7.35 (m, 3H) ¹³C NMR (101 MHz, Chloroform-*d*) δ 134.73, 127.94, 127.86, 126.81, 126.32, 125.59, 105.59, 82.60, 82.51, 82.14, 72.07, 50.30, 43.34, 26.94, 26.43. HR-ESI-MS (m/z): [M+Na]⁺, calculated for C₂₀H₂₂O₅Na 365.1365; Found 365.1366.

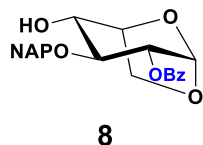
3-*O*-(2-naphthylmethyl)-1,6-anhydro-β-L-idopyranoside (7).



Compound **6** (14.3 g, 0.04187 mol) was dissolved in 1,4-Dioxane/2N H₂SO₄ (1/1) ratio. The reaction mixture kept on reflux at 105°C for overnight. The completion of reaction was monitored by TLC. Further, reaction mixture was extracted with EtOAc against NaHCO₃ Solution and dried over anhydrous Na₂SO₄. Crude was purified by column chromatography in EtOAc/Hexane solvent system to get compound **7** in a 75% yield. ¹H NMR (400 MHz, Methanol-*d*₄) 5.15 (d, *J* = 1.9 Hz, 1H), 4.94 (d, *J* = 4.7 Hz, 2H), 4.29 (t, *J* = 4.7 Hz, 1H), 4.21 (s, 1H), 4.01 (d, *J* = 7.7 Hz, 1H), 3.78 (ddd, *J* = 8.0, 4.4, 1.1 Hz, 1H), 3.62 (ddd, *J* = 7.8, 5.1, 1.1 Hz, 1H), 3.54 – 3.40 (m, 2H), 3.24 (p, *J* = 1.7 Hz, 1H), 7.86 – 7.66 (m, 4H), 7.51 – 7.27 (m, 3H) ¹³C NMR (101 MHz, Methanol-*d*₄) δ 136.24, 127.74, 127.70, 127.43, 126.33, 125.93, 125.79, 125.60, 102.15,

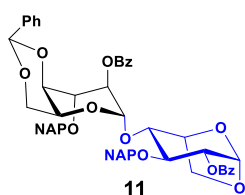
83.48, 77.84, 77.52, 77.20, 75.75, 74.86, 74.80, 71.13, 64.72, 48.40. HR-ESI-MS (m/z): [M+Na]⁺, calculated for C₁₇H₁₈O₅Na 325.1052; Found 325.1055.

2,4-O-Dibenzoyl-3-O-(2-naphthylmethyl)-1,6-anhydro-β-L-idopyranoside (8).



Compound **7** (8 g, 0.0278 mol) was dissolved in DCM/Pyridine (4/1) ratio solvents. The reaction mixture was cooled to 0°C and then benzoyl chloride (3.86 ml, 0.03336 mol) was added dropwise under N₂ atmosphere. The reaction mixture was monitored by using TLC, after completion of reaction, mixture was quenched by MeOH. Further, workup was carried out by 10% HCl and NaHCO₃ and dried over Na₂SO₄. Purification was done by column chromatography in EtOAc/Hexane solvent system to get compound **8** in a 60% yield. ¹H NMR (400 MHz, Chloroform-*d*) 5.53 (d, *J* = 1.7 Hz, 1H), 5.10 (dd, *J* = 8.2, 1.8 Hz, 1H), 4.93 (d, *J* = 11.8 Hz, 1H), 4.83 (d, *J* = 11.8 Hz, 1H), 4.47 (t, *J* = 4.6 Hz, 1H), 4.14 (dd, *J* = 7.7, 0.8 Hz, 1H), 4.09 – 3.97 (m, 1H), 3.91 (t, *J* = 8.2 Hz, 1H), 3.73 (ddd, *J* = 7.9, 5.0, 1.1 Hz, 1H), 8.02 (dd, *J* = 8.3, 1.4 Hz, 2H), 7.87 – 7.65 (m, 4H), 7.62 – 7.49 (m, 1H), 7.51 – 7.33 (m, 5H) ¹³C NMR (101 MHz, Chloroform-*d*) δ 135.46, 133.52, 133.25, 133.10, 129.91, 129.45, 128.60, 128.56, 127.96, 127.80, 126.86, 126.33, 126.16, 125.75, 99.57, 80.31, 76.77, 75.21, 74.82, 71.60, 65.41. HR-ESI-MS (m/z): [M+Na]⁺, calculated for C₂₄H₂₂O₆Na 429.1314; Found 429.1316.

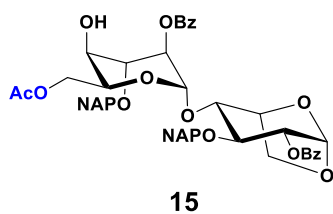
(4,6-benzylidiny-2-benzoyl-3-O-(2-naphthylmethyl))-α-L-idopyranosyl-α-(1→4)(2-O-benzoyl-3-O-(2-naphthylmethyl)-1,6-anhydro)-β-L-idopyranoside (11).



Monosaccharide donor **10** (1 g, 1.664 mmol), acceptor **8** (0.733 g, 1.82 mmol) and freshly dried 4 Å molecular sieves were taken in round bottom flask and was dissolved in dry DCM in 10 volumes, kept for stirring for 2h under N₂ atmosphere. Then reaction mixture was cooled to - 10°C. Further, TMSOTf (62 μl, 0.336 mmol) and NIS (0.486 g, 2.164 mmol) were added and kept for stirring. The reaction completion was monitored by TLC, after completion of reaction, it was neutralized with triethylamine Et₃N and did cilite filtration and subsequently did sodium thiosulfate Na₂S₂O₃ workup and dried over Na₂SO₄. Purification was done by silica column in EtOAc/Hexane solvent system to get compound **11** in a 55% yield. ¹H NMR (400 MHz, Chloroform-*d*) 5.57 (d, *J* = 1.7 Hz, 2H), 5.28 (t, *J* = 15.7 Hz, 3H), 5.14 – 5.03 (m, 2H), 4.91 (d, *J* = 11.4 Hz, 1H), 4.73 – 4.55 (m, 3H), 4.35 – 4.24 (m, 2H), 4.13 – 3.95 (m, 3H), 3.89 (dd, *J* = 19.4, 7.8 Hz,

3H), 3.32 (d, $J = 11.4$ Hz, 1H), 7.96 (d, $J = 7.1$ Hz, 3H), 7.92 – 7.81 (m, 5H), 7.74 – 7.66 (m, 1H), 7.58 (dd, $J = 17.9, 8.3$ Hz, 3H), 7.53 – 7.47 (m, 4H), 7.46 – 7.42 (m, 2H), 7.42 – 7.36 (m, 3H), 7.35 – 7.28 (m, 4H) 7.27 (d, $J = 3.3$ Hz, 1H), 7.23 (d, $J = 8.1$ Hz, 2H), 7.10 (d, $J = 7.0$ Hz, 1H)¹³C NMR (101 MHz, Chloroform-*d*) 165.75, 165.27 δ 133.40, 133.36, 130.14, 129.81, 128.96, 128.47, 128.38, 128.13, 128.00, 127.93, 127.88, 127.82, 127.70, 127.21, 126.49, 126.36, 126.25, 126.18, 125.89, 100.89, 99.50, 95.39, 78.69, 74.35, 73.52, 72.99, 72.00, 65.95, 59.69. HR-ESI-MS (m/z): $[M+Na]^+$, calculated for C₅₅H₄₈O₁₃Na 923.3043; Found 923.3047.

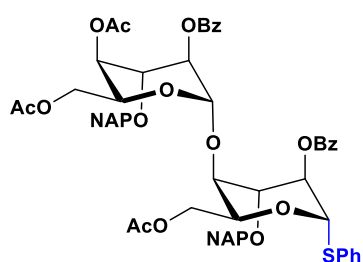
(6-*O*-acetyl-2-*O*-benzoyl-3-*O*-(2-naphthylmethyl))- α -L-idopyranosyl- α (1 \rightarrow 4)(2-*O*-benzoyl-3-*O*-(2-naphthylmethyl)-1,6-anhydro)- β -L-idopyranoside (15**).**



Compound **11** (1.143 g, 1.27 mmol) was dissolved in DCM/MeOH (2/1) ratio, CSA (0.590 g, 2.54 mmol) was added and kept for stirring for 3-4h. The reaction was monitored by TLC, after completion of reaction, reaction mixture was concentrated under reduced pressure. Purification was done without workup by silica column by using EtOAc/Hexane solvent system to get compound **14**(no attached NMR). Compound **14** (0.83 g, 1.02 mmol) was dissolved in dry DCM in 10 Volume, Ac₂O (1.9 ml, 10.14 mmol) and Triethylamine (0.143 ml, 1.02 mmol) were added at 0°C and kept for stirring for overnight. The completion of the reaction was monitored by TLC, after completion of reaction, it was quenched with MeOH and did sat.NaHCO₃ workup then dried over Na₂SO₄. Purification was done by silica column in EtOAc/Hexane solvent system to get compound **15** in 65% yield.¹H NMR (400 MHz, Chloroform-*d*) 5.51 (d, $J = 1.8$ Hz, 1H), 5.29 (dt, $J = 2.4, 1.1$ Hz, 1H), 5.16 (s, 1H), 5.04 – 4.96 (m, 2H), 4.87 (d, $J = 11.5$ Hz, 1H), 4.76 (d, $J = 11.8$ Hz, 1H), 4.71 – 4.61 (m, 2H), 4.53 (d, $J = 11.8$ Hz, 1H), 4.31 – 4.23 (m, 2H), 4.22 – 4.16 (m, 2H), 4.03 – 3.91 (m, 2H), 3.85 – 3.68 (m, 2H), 2.54 (d, $J = 10.6$ Hz, 1H), 1.91 (s, 3H), 8.07 – 7.97 (m, 2H), 7.90 – 7.76 (m, 4H), 7.75 – 7.68 (m, 2H), 7.65 – 7.55 (m, 2H), 7.52 (dd, $J = 8.4, 1.7$ Hz, 1H), 7.50 – 7.37 (m, 7H), 7.37 – 7.30 (m, 2H), 7.28 (d, $J = 1.6$ Hz, 1H), 7.23 – 7.15 (m, 2H), 7.07 (dd, $J = 8.4, 1.7$ Hz, 1H) ¹³C NMR (101 MHz, Chloroform-*d*) δ 170.92, 135.54, 134.77, 133.91, 133.16, 132.97, 129.78, 129.62, 129.14, 128.92, 128.77, 128.47, 128.15, 127.91, 127.77, 127.75, 127.57, 127.16, 126.41, 126.32, 126.19, 126.01, 125.79, 125.58, 99.41, 95.23, 77.99,

77.27, 76.53, 75.26, 75.17, 74.17, 72.75, 71.74, 68.14, 66.91, 66.12, 65.55, 63.21, 20.73. HR-ESI-MS (m/z): [M+Na]⁺, calculated for C₄₈H₄₄O₁₂Na 835.2730; Found 835.2736.

Thiophenyl-((4,6-*O*-diacetyl-2-benzoyl-3-(2-naphthylmethyl))- α -L-idopyranosyl- α -(1 \rightarrow 4))(6-*O*-acetyl-2-benzoyl-3-*O*-(2-naphthylmethyl))- α -L-idopyranoside(13).

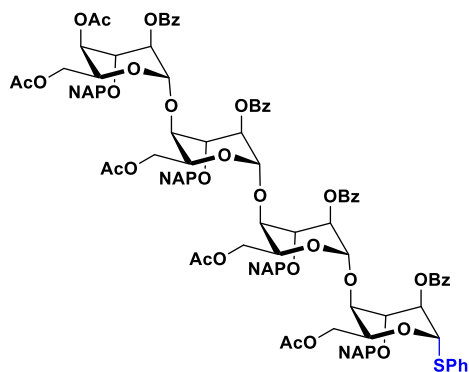


13

Compound **11** (730 mg, 0.813 mmol) was dissolved in Ac₂O (5 ml), Cu(OTf)₂ (29.5 mg, 0.0813 mmol) was added at 0 °C and kept for stirring for overnight. Completion of reaction was monitored by TLC, after completion, reaction mixture was concentrated under reduced pressure and rotavapour, then subsequently crude was extracted with EtOAc against sta. NaHCO₃ solution and dried over Na₂SO₄. The crude was concentrated and dried under reduced pressure, further it was taken to next step without purification, Crude Compound **12** (1.69 g, 1.693 mmol) and ZnI₂ (1.137 g, 3.56 mmol) was taken in a round bottom flask which is covered with aluminium foil, and was kept on high vacuum for 2 hours. The reaction mixture was dissolved in dry DCM and trimethyl(phenylthio)silane TMSSPh (0.962 g, 5.26 mmol) was added, kept for stirring for 1 hour. The reaction completion was monitored by TLC, after completion of reaction, clite filtration was done and then purified by silica column in a EtOAc/Hexane solvent system to get compound **13** in a 85% yield. ¹H NMR (400 MHz, Chloroform-*d*) 5.70 (d, *J* = 2.4 Hz, 1H), 5.63 (d, *J* = 1.4 Hz, 1H), 5.30 – 5.21 (m, 1H), 5.16 – 4.92 (m, 4H), 4.84 (t, *J* = 11.3 Hz, 2H), 4.58 – 4.40 (m, 4H), 4.32 – 4.18 (m, 1H), 3.88 – 3.74 (m, 3H), 3.37 (dd, *J* = 11.7, 4.2 Hz, 1H), 2.01 (s, 3H), 1.95 (s, 3H), 1.90 (s, 3H) 8.08 – 7.92 (m, 3H), 7.89 – 7.70 (m, 10H), 7.68 – 7.63 (m, 2H), 7.63 – 7.51 (m, 3H), 7.46 – 7.33 (m, 9H), 7.16 – 7.09 (m, 2H) ¹³C NMR (101 MHz, Chloroform-*d*) δ 170.59, 165.51, 134.78, 134.64, 133.61, 133.33, 133.04, 132.20, 129.98, 129.79, 129.02, 128.46, 128.36, 128.25, 128.19, 128.03, 127.97, 127.74, 127.69, 127.61, 126.81, 126.74, 126.17, 126.05, 126.03, 125.85, 125.81, 125.68, 101.72, 86.20, 77.48, 77.25, 74.50, 73.23, 72.57, 72.48, 68.73, 67.40, 66.90, 65.97, 64.14, 62.93, 62.75, 20.78, 20.53. HR-ESI-MS (m/z): [M+Na]⁺, calculated for C₆₀H₅₆O₁₅SNa 1071.3238; Found 1071.3239.

Thiophenyl-((4,6-*O*-diacetyl-2-*O*-benzoyl-3-*O*-(2-naphthylmethyl))- α -L-idopyranosyl- α -(1 \rightarrow 4))(6-*O*-acetyl-2-*O*-benzoyl-3-*O*-(2-naphthylmethyl))- α -L-idopyranosyl- α -(1 \rightarrow 4))(6-*O*-acetyl-2-*O*-

benzoyl-3-O-(2-naphthylmethyl))- α -L-idopyrnosyl- α -(1 \rightarrow 4)(6-O-acetyl-2-O-benzoyl-3-O-(2-naphthylmethyl))- α -L-idopyrnose (18).



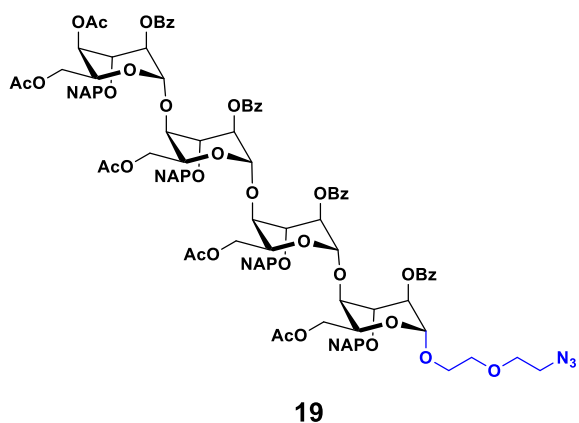
18

Compound **13** donor (1.02 g, 1.00 mmol) and Compound **26** acceptor (0.606 g, 0.708 mmol) was glycosylated to get compound **16** by using previous procedure. The crude product **16** was taken to next step without purification. Compound **16** (530 mg, 0.298 mmol) was dissolved in Ac₂O (5 ml), Cu(OTf)₂ (11 mg, 0.0298 mmol) was added at 0°C and kept for stirring for overnight. Completion of reaction was

monitored by TLC, after completion, reaction mixture was concentrated under reduced pressure and rotavapour, then subsequently crude was extracted with EtOAc against sta. NaHCO₃ solution and dried over Na₂SO₄. The crude was concentrated and dried under reduced pressure, Further it was taken to next step without purification, Crude Compound **17** (370 mg, 0.197 mmol) and ZnI₂ (132 mg, 0.413 mmol) was taken in a round bottom flask which is covered with aluminium foil, and was kept on high vacuum for 2 hours. The reaction mixture was dissolved in dry DCM and trimethyl(phenylthio)silane TMSSPh (116 μ l, 0.610 mmol) was added, kept for stirring for 1 hour. The reaction completion was monitored by TLC, after completion of reaction, clite filtration was done and then purified by silica column in a EtOAc/Hexane solvent system to get compound **18** in a 85% yield¹H NMR (400 MHz, Chloroform-*d*) 5.62 – 5.55 (m, 2H), 5.28 (dt, *J* = 6.8, 3.8 Hz, 2H), 5.19 (t, *J* = 2.1 Hz, 1H), 5.07 (d, *J* = 11.7 Hz, 1H), 5.00 – 4.81 (m, 9H), 4.78 (d, *J* = 11.5 Hz, 2H), 4.67 – 4.62 (m, 1H), 4.52 – 4.43 (m, 1H), 4.39 – 4.25 (m, 4H), 4.24 – 4.16 (m, 2H), 4.13 – 4.05 (m, 2H), 4.02 (t, *J* = 4.8 Hz, 1H), 3.89 – 3.82 (m, 2H), 3.79 (d, *J* = 11.5 Hz, 1H), 3.65 – 3.51 (m, 3H), 1.94 (s, 3H), 1.87 (d, *J* = 4.1 Hz, 6H), 1.82 (s, 3H), 1.74 (s, 3H), 8.01 (dd, *J* = 8.3, 1.4 Hz, 2H), 7.91 (dd, *J* = 9.9, 3.0 Hz, 3H), 7.87 – 7.79 (m, 7H), 7.78 – 7.72 (m, 5H), 7.65 (dd, *J* = 6.9, 2.2 Hz, 4H), 7.59 (tt, *J* = 7.9, 1.8 Hz, 6H), 7.55 – 7.50 (m, 2H), 7.47 – 7.43 (m, 2H), 7.43 – 7.41 (m, 2H), 7.40 – 7.36 (m, 6H), 7.35 – 7.29 (m, 7H), 7.24 – 7.14 (m, 7H)¹³C NMR (101 MHz, Chloroform-*d*) δ 165.28, 165.03, 134.93, 134.86, 134.60, 133.65, 133.35, 133.28, 133.20, 133.13, 133.08, 132.01, 130.10, 129.92, 129.89, 129.79, 129.30, 129.01, 128.93, 128.49, 128.32, 128.29, 128.24, 128.20, 128.08, 128.02, 127.88, 127.86, 127.80, 127.73, 127.66, 127.61, 127.55, 127.03, 127.00, 126.95, 126.83, 126.13, 126.11, 126.01, 125.95, 125.89, 125.85, 125.77, 125.69, 101.06, 100.42, 99.47, 86.02, 77.25, 76.49, 76.37, 75.46, 75.09,

74.91, 74.05, 73.33, 73.27, 73.08, 72.56, 68.92, 68.81, 68.39, 67.34, 66.97, 66.62, 66.19, 64.24, 62.75, 62.70, 62.24, 62.02, 20.77, 20.66, 20.62, 20.55. HR-ESI-MS (m/z): $[M+Na]^+$, calculated for $C_{112}H_{104}O_{29}SNa$ 1967.6282; Found 1967.6285.

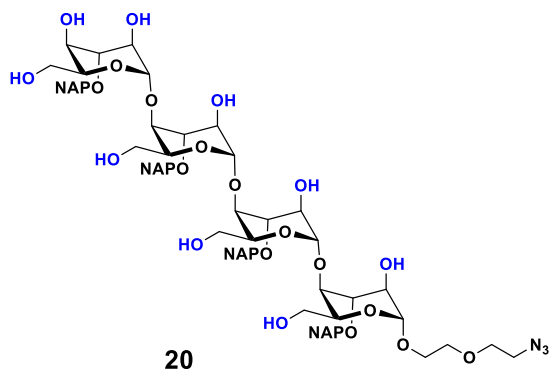
Ethoxy-2-azidoethoxyl-*O*-((4,6-*O*-diacetyl-2-*O*-benzoyl-3-*O*-(2-naphthylmethyl))- α -L-idopyrnosyl- α (1 \rightarrow 4)(6-*O*-acetyl-2-*O*-benzoyl-3-*O*-(2-naphthylmethyl))- α -L-idopyrnosyl- α (1 \rightarrow 4)(6-*O*-acetyl-2-*O*-benzoyl-3-*O*-(2-naphthylmethyl))- α -L-idopyrnosyl- α (1 \rightarrow 4)(6-*O*-acetyl-2-*O*-benzoyl-3-*O*-(2-naphthylmethyl))- α -L-idopyrnose (19).



Compound **18** donor (0.95 g, 0.490 mmol), azidoethoxy ethanol linker acceptor (178.7 mg, 0.735 mmol) and freshly dried 4 Å molecular sieves were taken in round bottom flask and was dissolved in dry DCM in 10 volume, kept for stirring for 2h under N_2 atmosphere. Then reaction mixture was cooled to $-10^\circ C$. Further, TMSOTf (62 μ l, 0.098 mmol) and NIS (0.486 g, 0.637 mmol) were added and kept for stirring. The reaction completion was monitored by TLC, after completion of reaction, it was neutralized with triethylamine Et_3N and did celite filtration and subsequently did sodium thiosulfate $Na_2S_2O_3$ workup and dried over Na_2SO_4 . Purification was done by silica column in EtOAc/Hexane solvent system to get compound **19** in a 55% yield. 1H NMR (400 MHz, Chloroform- d) 5.32 (ddd, $J = 13.9, 6.8, 3.0$ Hz, 3H), 5.24 – 5.11 (m, 1H), 5.07 – 4.71 (m, 12H), 4.65 (t, $J = 2.4$ Hz, 1H), 4.47 (ddt, $J = 7.8, 5.7, 2.4$ Hz, 2H), 4.41 – 4.33 (m, 2H), 4.32 – 4.24 (m, 2H), 4.24 – 4.02 (m, 6H), 3.95 – 3.78 (m, 5H), 3.72 – 3.49 (m, 8H), 3.12 (dt, $J = 5.9, 3.8$ Hz, 2H), 1.94 (s, 3H), 1.90 (s, 3H), 1.87 (s, 3H), 1.83 (s, 3H), 1.76 (s, 3H), 8.06 – 7.98 (m, 2H), 7.91 – 7.79 (m, 8H), 7.78 – 7.53 (m, 16H), 7.49 – 7.30 (m, 16H), 7.24 – 7.13 (m, 6H) ^{13}C NMR (101 MHz, Chloroform- d) δ 170.59, 170.50, 133.64, 133.31, 133.26, 133.13, 133.08, 132.96, 132.92, 130.00, 129.96, 129.87, 129.79, 129.37, 129.30, 128.48, 128.28, 128.20, 128.16, 128.07, 127.87, 127.80, 127.71, 127.60, 127.04, 127.00, 126.98, 126.55, 126.28, 126.13, 126.05, 125.98, 125.93, 125.90, 125.85, 125.76, 100.55, 100.31, 99.76, 98.32, 77.25, 76.35, 75.99, 75.61, 75.10, 74.85, 74.78, 73.32, 73.24, 72.80, 72.56, 72.51, 70.22, 70.16, 68.53, 68.47, 68.05, 67.78, 67.33, 66.97, 66.29, 65.38, 64.24, 62.74, 62.54, 62.20, 50.67, 20.77,

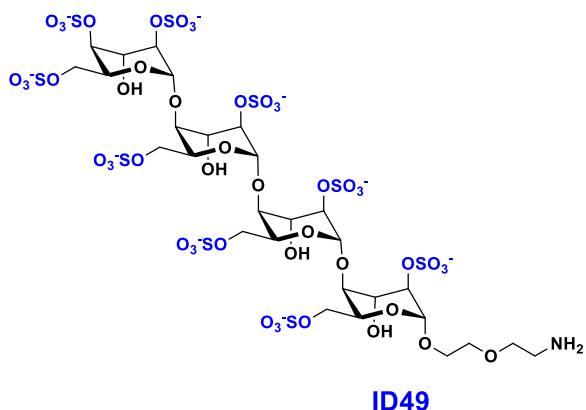
20.69, 20.63, 20.54. HR-ESI-MS (m/z): $[M+Na]^+$, calculated for $C_{110}H_{107}N_3O_{31}Na$ 1988.6786; Found 1988.6787.

Ethoxy-2-azidoethoxyl-*O*-((3-*O*-(2-naphthylmethyl))- α -L-idopyrnosyl- α (1 \rightarrow 4)(3-*O*-(2-naphthylmethyl))- α -L-idopyrnosyl- α (1 \rightarrow 4)(3-*O*-(2-naphthylmethyl))- α -L-idopyrnosyl- α (1 \rightarrow 4)(3-*O*-(2-naphthylmethyl))- α -L-idopyrrose (20**).**



Compound **19** (150 mg, 0.0763mmol) was dissolved in THF/MeOH/H₂O (4/2/1) and LiOH (16.0 mg, 0.381 mmol) was added at 0°C and kept for stirring for 3-4 hours. The reaction completion was monitored by TLC, after completion, reaction mixture was neutralized by amberlite 120 H⁺ resin, Further, reaction mixture was filtered by cotton plugh filtration, then it was concentrated under by reduced pressure, further it was purified by silica column in MeOH/DCM solvent system to get compound **20** in a 70% yield.¹H NMR (400 MHz, Chloroform-*d*) 4.86 (d, *J* = 11.9 Hz, 1H), 4.82 (s, 1H), 4.78 (s, 1H), 4.74 (d, *J* = 10.1 Hz, 3H), 4.69 (d, *J* = 5.8 Hz, 1H), 4.64 (d, *J* = 8.3 Hz, 1H), 4.59 (d, *J* = 10.6 Hz, 2H), 4.53 (s, 1H), 4.42 (s, 1H), 4.39 – 4.26 (m, 4H), 4.21 (t, *J* = 6.7 Hz, 1H), 4.12 (d, *J* = 11.2 Hz, 1H), 3.96 (dd, *J* = 7.6, 4.4 Hz, 2H), 3.93 – 3.74 (m, 8H), 3.72 (d, *J* = 3.7 Hz, 1H), 3.63 (ddtd, *J* = 22.0, 10.2, 5.1, 2.7 Hz, 9H), 3.52 (dt, *J* = 10.4, 5.1 Hz, 2H), 3.42 (dd, *J* = 9.5, 4.6 Hz, 4H), 3.31 – 3.23 (m, 1H), 3.15 (t, *J* = 5.0 Hz, 2H), 7.86 – 7.57 (m, 16H), 7.55 – 7.29 (m, 12H) ¹³C NMR (101 MHz, Chloroform-*d*) δ 134.38, 133.20, 133.17, 133.11, 128.51, 128.42, 128.16, 128.00, 127.98, 127.84, 127.79, 127.75, 127.56, 127.52, 127.50, 126.38, 126.35, 126.31, 126.27, 126.24, 126.20, 126.14, 126.09, 126.06, 125.73, 103.23, 102.96, 102.79, 101.34, 77.27, 74.40, 74.22, 74.00, 73.68, 73.19, 72.77, 72.61, 72.36, 71.98, 71.58, 70.38, 70.04, 69.97, 67.50, 66.96, 66.78, 66.54, 66.43, 66.32, 66.13, 65.85, 64.45, 62.00, 61.65, 60.98, 50.71. HR-ESI-MS (m/z): $[M+Na]^+$, calculated for $C_{72}H_{81}N_3O_{22}Na$ 1362.5209; Found 1362.5210.

Ethoxy-2-aminoethoxyl-*O*-((2,4,6-*O*-trisulfonato)- α -L-idopyrnosyl- α (1 \rightarrow 4)(2,6-*O*-trisulfonato)- α -L-idopyrnosyl- α (1 \rightarrow 4)(2,6-*O*-trisulfonato)- α -L-idopyrnosyl- α (1 \rightarrow 4)(2,6-*O*-trisulfonato)- α -L-idopyrnose (ID49).



Compound **20** (25 mg, 18.67 mmol) and SO₃.NMe₃ (250 mg, 1.68 mol) was thoroughly dried together under high vacuum, then was dissolved in dry DMF solvent and stirred at 60 °C for 72 h. Further DMF was evaporated under reduced pressure and then purified by Bound elute C-18 column to get compound **21** in 35% yield. The compound **21** (15 mg, 7.01 mmol) was dissolved in H₂O and Pd(OH)₂ (10% per wt) was added and stirred for 42 h under hydrogen atmosphere. Further, reaction mixture was filtered and concentrated, finally purified by Bound elute C-18 column by using H₂O as a solvent to get compound **22** (**ID49**) in a 50% yield. ¹H NMR (400 MHz, Deuterium Oxide) 5.07 (d, $J = 10.6$ Hz, 4H), 4.63 (t, $J = 7.6$ Hz, 2H), 4.50 – 4.40 (m, 1H), 4.34 – 4.15 (m, 17H), 3.86 (qd, $J = 12.1, 10.8, 5.8$ Hz, 5H), 3.77 – 3.68 (m, 5H), 3.15 (t, $J = 5.1$ Hz, 2H) ¹³C NMR (101 MHz, Deuterium Oxide) δ 100.35, 99.98, 98.56, 76.15, 75.92, 75.80, 74.92, 73.40, 72.70, 72.65, 71.88, 69.64, 68.13, 67.65, 67.52, 67.38, 67.00, 66.52, 66.22, 66.11, 65.66, 65.17, 64.20, 39.17. HR-ESI-MS (m/z): [M], calculated for C₂₈H₄₂NO₄₉S₉⁻⁹ 162.6485; Found 162.6489.

2.4.2 RDKit analysis

The similarity index value was computed using RDKit in Google Colab. A Python program, including libraries such as NumPy and Pandas, was imported and designed for the task. A comprehensive catalogue comprising 2304 HS tetrasaccharide chemical structures (PDF file), along with the similarity index (Excel file) and the program file (IPYNB), has been deposited on the Github server for free access. (<https://github.com/rkikkeri/HS-similarity-index>)

2.4.3 Synthesis and characterization of ID49-CRM₁₉₇

Solution of sugar (1 mg) in 100 μ l of anhydrous DMSO was added dropwise to the mixture of suberic acid bis(N-hydroxysuccinimide ester) (13 mole excess) and triethyl amine (5 mole excess) in 150 μ l of DMSO at RT and further stirred for 2 h. Next reaction mixture diluted

with 500 μ l of PBS pH 7.4 and extracted with chloroform (5 ml X 3) to remove non reacted linker. Further the aqueous phase was added slowly to the stirring solution of CRM₁₉₇ (1 mg) in 500 μ l of PBS pH 7.4 and continued stirring for 16 h at RT. Finally resulting conjugate was purified and concentrated using 10 KDa centrifugal filter and characterized using MLADI-TOF and gel-electrophoresis.

2.4.4 Immunization studies

Immunization studies were carried out using 6–8 week old female (C57BL/6) mice as per the protocol approved by the institutional ethical committee. Five groups of mice (n = 4) were immunized subcutaneously with 100 μ l of each formulation. **ID49-CRM₁₉₇** (6 μ g sugar per dose) added to equal volume of Freund's adjuvant with rigorous mixing to form oil emulsion. For alum adjuvant added equal volume of **ID49-CRM₁₉₇** (6 μ g sugar per dose) added to alum with mixing. CSF, CSA, alum, Freund's adjuvant, CRM₁₉₇ and PBS injected to mice on days 0, 14, and 28. The mice were bled on day 0, 15, 28, 37, 60 and the serum antibody titer was analyzed using ELISA.

2.4.5 General protocol to synthesize HS-thio derivatives

A solution of α -Lipoic acid (484.7mmol) in dry DCM was treated with pentafluorophenol (969.4mmol) in the presence of dibicyclohexylcarbodiimide (DCC) (969.4mmol) and kept for stirring for overnight under N₂ atmosphere, then reaction mixture was evaporated under reduced pressure, Further purification was done by column chromatography with a solvent system Hexane/EtOAc to get pentafluoro active ester of α -Lipoic acid. Further, HS ligands (1.29 mmol) was taken in dry DMF and was treated with pentafluoro active ester of α -Lipoic acid (2.59mmol) and Et₃N (5.19mmol) under N₂ atmosphere, kept for stirring for 4 h at 40°C. Further, DMF was evaporated under reduced pressure, purification was done with bond elute C18 column to get α -Lipoic acid conjugated HS ligands. Synthesis of NU and NAcetate domain HS ligands were already reported by our group.¹⁴ Synthesis of NS domain ligands are carried out by using literature protocols.³³

2.4.6 General protocol for BSA conjugation

Synthetic HS mimetic was treated with tris(2-carboxyethyl)phosphine (TCEP, 25 μ L of a 100 mM stock solution, pH 7.4) at room temperature for 1h and then added further to the solution

of maleimide activated BSA in PBS under stirring and continued stirring for 16 h at room temperature. Finally, the BSA-conjugated HS-mimetics were purified using 10 KDa centrifugal filter.

2.4.7 Characterization of ID49@CRM₁₉₇ and BSA conjugated HS mimetics.

All conjugates were characterized by MALDI-TOF and gel-electrophoresis.

2.4.8 Evaluation of Serum Antibody Titer using ELISA

The IgG antibody titers were determined using an ELISA protocol. 96-well plates (Nunc MaxiSorp® flat-bottom) were initially coated with 100 µl of BSA-conjugated sugars (from a stock solution of 2 µg/ml) in coating buffer (0.1 M Na₂HPO₄ in water, pH 9.3) overnight at 4°C. Following coating, the plates were washed three times with washing buffer (PBS + 0.1% Tween-20) and then blocked with blocking buffer (2% BSA) for 1 hour at room temperature. After blocking, the plates were washed again, and mice serum at various dilutions (1:1000, 1:10000, 1:100000) was added to the plates and incubated for 1 hour at room temperature, followed by another round of washing. Subsequently, HRP-conjugated IgG secondary goat anti-mouse antibody (diluted 1:2000, ThermoFisher) was added to the plates and incubated for 1 hour at room temperature. After another washing step, liquid TMB substrate solution was added, and the reaction was stopped by the addition of 0.5 M H₂SO₄. Finally, the absorbance was measured at 450 nm.

2.4.9 FACS analysis

Cells (5×10^5 cells per well) were seeded into a 6-well plate and incubated overnight. Subsequently, the cells were subjected to treatment with serum diluted at a ratio of 1:100 for 1 hour, followed by washing and incubation with Goat anti-mouse IgG secondary antibody conjugated with Alexa Fluor 488 for 1 hour at 37°C. Afterward, the cells were washed again and suspended in FACS buffer for analysis.

2.4.10 Immunohistochemistry of tissue sections

To assess the recognition of tissue section cell surface glycans by mouse serum antibodies, we conducted immunostaining on mouse tissue sections. For dewaxing and antigen retrieval of paraffin-embedded mouse tissue sections: Slides were initially heated at 60°C for 5

minutes, then placed into glass slide holders and subjected to dewaxing as follows: Twice in 100% xylene wash for 5 minutes each, followed by immersion in 100% isopropanol with brief agitation (10–20 seconds) for 3 minutes, and finally twice in H₂O with brief agitation. For antigen retrieval, sections were incubated with 0.1% trypsin for 1 hour at 37°C, followed by washing with PBS. Subsequently, tissue sections were treated with a 1:100 dilution of mouse serum for 1 hour at 4°C, followed by PBS washing. Finally, sections were treated with Goat anti-mouse IgG secondary antibody Alexa Fluor 568 (diluted 1:1000) for 2 hours at room temperature, followed by PBS washing, and then subjected to confocal imaging. For immunostaining with Heparinase treatment, tissue sections underwent a pretreatment step with heparinase (0.03 IU/ml) for 1 hour at 37°C. After PBS rinses, sections were treated with serum antibodies and then stained using Goat anti-mouse IgG secondary antibody Alexa Fluor 568, as described above.

2.4.11 Ex-vivo Blood Coagulation Assay

Freshly collected blood was utilized for assay without additional processing. Aliquots of 100 µL were prepared, to which Heparin (130 µM) and different dilutions of mice serum were added. These samples under different conditions were placed in Eppendorf tubes, and a picture was captured after 15 minutes. Clot formation was verified by gently rotating the Eppendorf vials.

2.5 References

1. Bishop, J. R.; Schuksz, M.; Esko, J. D. Heparansulfaate proteoglycans fine-tune mammalian physiology. *Nature*. **2007**, 446, 1030-1037
2. Lindahl, U.; Kusche-Gullberg, M.; Kjellen, L. Regulated diversity of heparan sulfate. *J. Biol. Chem.* **1998**, 273, 24979-24982.
3. Sarrazin, S.; Lamanna, W. C.; Esko, J. D. Heparan sulfate proteoglycans, *Cold Spring Harb. Perspect. Biol.* **2011**, 3, a004952.
4. Kreuger, J.; Spillmann, D.; Li, J.; Lindahl, U. Interactions between heparan sulfate and proteins: the concept of specificity. *J. Cell Biol.* **2006**, 174, 323-7.
5. Capila, I.; Linhardt, R. J. Heparin-protein interactions. *Angew. Chem. Int. Ed. Engl.* **2002**, 41, 391-412.

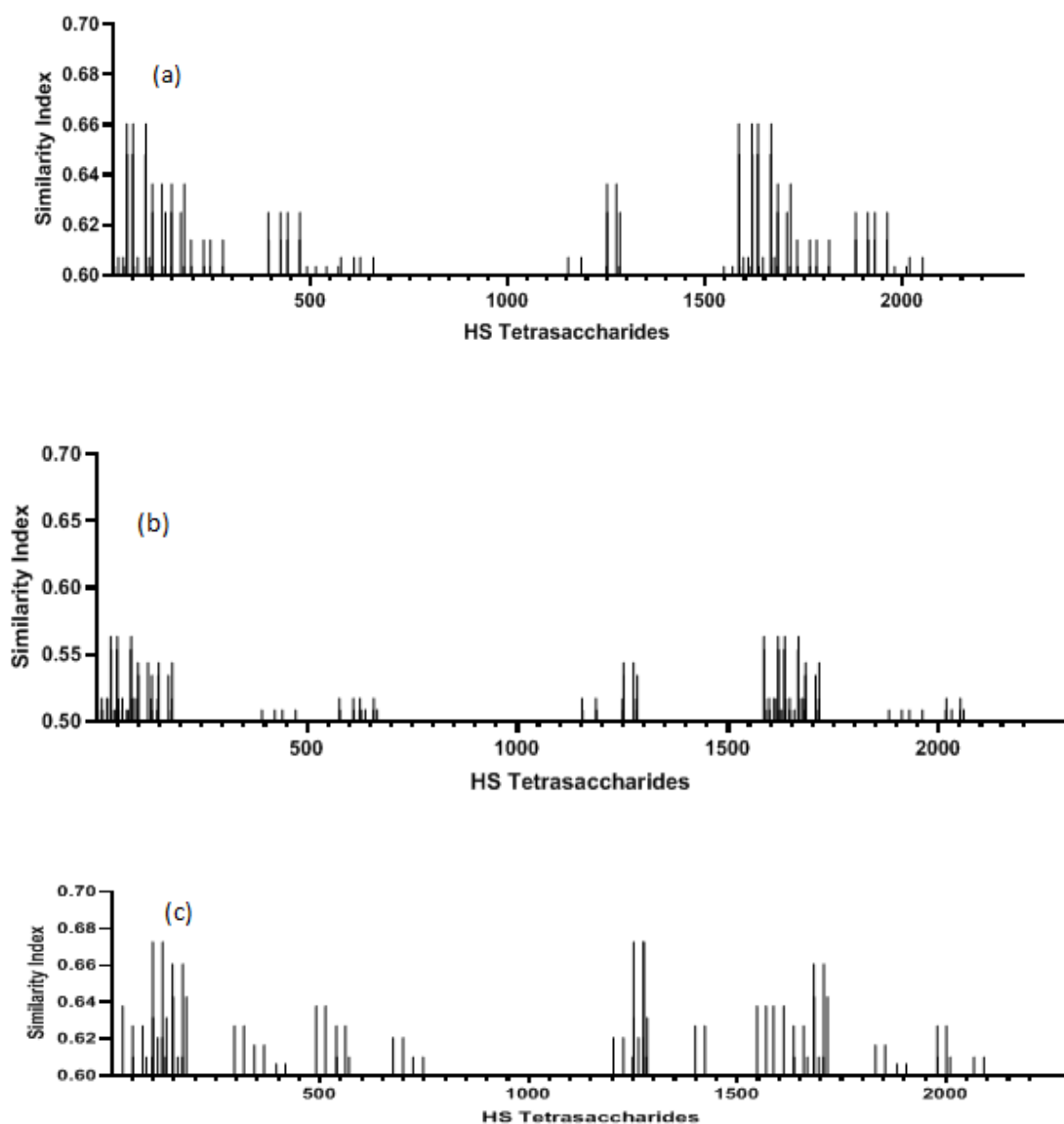
6. Xu, D.; Esko, J. D. Demystifying heparan sulfate-protein interactions. *Annu. Rev. Biochem.* **2014**, *83*, 129-157.
7. Kjellén, L.; Lindahl, U. Proteoglycans: structures and interactions. *Annu. Rev. Biochem.* **1991** *60*, 443–475.
8. , P. R.; Raigawali, R.; Mardhekar, S.; Anand, S.; Kikkeri, R. Synergistic interplay of uronic acid and sulfation composition of heparan sulfate on molecular recognition to activity. *Carbohydr. Res.* **2023**, *532*, 108919.
9. Wang, L.; Sorum, A. W.; Huang, B. S.; Kern, M. K.; Su, G.; Pawar, N.; Huang, X.; Liu, J.; Pohl, N. L. B.; Hsieh-Wilson. L. C. Efficient platform for synthesizing comprehensive heparan sulfate oligosaccharide libraries for decoding glycosaminoglycan-protein interactions. *Nat. Chem.* **2023**, *15*, 1108-1117.
10. Bayal, K. N.; Ramadan, S.; Su, S.; Huo, C.; Zhao, Y.; Liu, J.; Hsieh-Wilson, L. C.; Huang. X. Synthesis of a systematic 64-membered heparan sulfate tetrasaccharide library. *Angew. Chem. Int. Ed.* **2023**, *62*, e202211985.
11. Hu, Y. P.; Zhong, Y. Q.; Chen, Z. G.; Chen, C. Y.; Shi, Z.; Zulueta, M. M.; Ku, C. C.; Lee, P. Y.; Wang, C. C.; Hung, S. C. Divergent synthesis of 48 heparan sulfate-based disaccharides and probing the specific sugar-fibroblast growth factor-1 interaction. *J. Am. Chem. Soc.* **2012**, *134*, 20722-20727.
12. Hu, Y. P.; Lin. S. Y.; Huang, C. Y.; Zulueta, M. M.; Liu, J. Y.; Chang, W.; Hung, S. C. Synthesis of 3-O-sulfonated heparan sulfate octasaccharides that inhibit the herpes simplex virus type 1 host–cell interaction. *Nat. Chem.* **2011**, *3*, 557–563.
13. Zong, C.; Venot, A.; Li, X.; Lu, W.; Xiao, W.; Wilkes, J. S. L.; Salanga, C. L.; Handel, T. M.; Wang, L.; Wolfert, M. A.; Boons, G. J. Heparan sulfate microarray reveals that heparan sulfate–protein binding exhibits different ligand requirements *J. Am. Chem. Soc.* **2017**, *139*, 9534 – 9543.
14. Jain. P.; Shanthamurthy, C. D.; Leviatan Ben-Arye, S.; Woods, R. J.; Kikkeri, R.; Padler-Karavani, V. Discovery of rare sulfated N-unsubstituted glucosamine based heparan sulfate analogs selectively activating chemokines. *Chem. Sci.* **2021**, *12*, 3674-3681.
15. Chopra, P.; Joshi, A.; Wu, J.; Lu, W.; Yadavalli, T.; Wolfert, M. A.; Shukla, D.; Zaia, J.; Boons, G. J. The 3-O-sulfation of heparan sulfate modulates protein binding and lyase degradation. *PNAS*, **2021**, *118*, e2012935118.

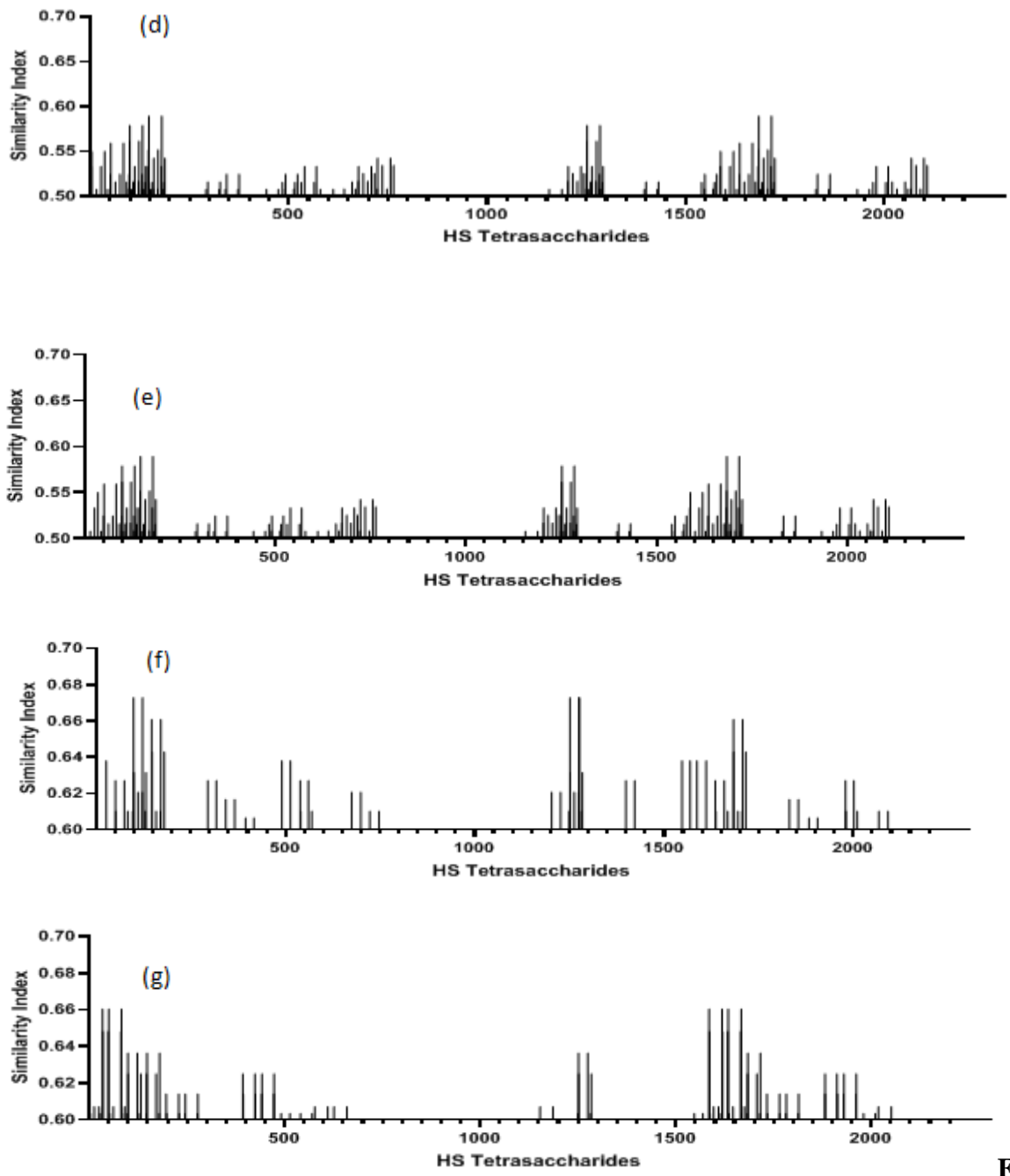
- O'Donnell and Shukla, 2008; Copeland et al., 2008
16. O'Donnell, C. D.; Shukla, D. The Importance of Heparan Sulfate in Herpesvirus Infection. *Virology*. 2008, 23, 383-393,
 17. Copeland, R.; Balasubramaniam, A.; Tiwari, V.; Zhang, F.; Bridges, A.; Linhardt, R. J.; Shukla, D.; Liu, J. Using a 3-O-sulfated heparin octasaccharide to inhibit the entry of herpes simplex virus type 1. *Biochemistry*. **2008**, 47, 5774-83,
 18. Mietzsch, M.; Broecker, F.; Reinhardt, A.; Seeberger, P. H.; Heilbronn, R. Differential adeno-associated virus serotype-specific interaction patterns with synthetic heparins and other glycans. *J. Virol.* **2014**, 88, 2991-3003.
 19. Clausen, T. M.; Sandoval, D. R.; Spliid, C. B.; Pihl, J.; Perrett, H. R.; Painter, C. D.; Narayanan, A.; Majowicz, S. A.; Kwong, E. M.; McVicar, R. N.; Thacker, B. E.; Glass, C. A.; Yang, Z.; Torres, J. L.; Golden, G. J.; Bartels, P. L.; Porell, R. N.; Garretson, A. F.; Laubach, L.; Feldman, J.; Yin, X.; Pu, Y.; Hauser, B. M.; Caradonna, T. M.; Kellman, B. P.; Martino, C.; Gordts, P. L. S. M.; Chanda, S. K.; Schmidt, A. G.; Godula, K.; Leibel, S. L.; Jose, J.; Corbett, K. D.; Ward, A. B.; Carlin, A. F.; Esko, J. D. SARS-CoV-2 Infection depends on cellular heparan sulfate and ACE2. *Cell*. **2020**, 183, 1043-1057.e15.
 20. Liu, L.; Chopra, P.; Li, X.; Bouwman, K. M.; Tompkins, S. M.; Wolfert, M. A.; de Vries, R. P.; Boons, G. J. Heparan Sulfate Proteoglycans as Attachment Factor for SARS-CoV-2. *ACS Cent. Sci.* **2021**, 7, 1009-1018,
 21. David, G.; Bai, X. M.; Van der Schueren, B.; Cassiman, J. J.; Van den Berghe, H. Developmental changes in heparan sulfate expression: in situ detection with mAbs. *J. Cell. Biol.* **1992**, 119, 961-75.
 22. van den Born, J.; Salmivirta, K.; Henttinen, T.; Ostman, N.; Ishimaru, T.; Miyaura, S.; Yoshida, K.; Salmivirta, M. Novel heparan sulfate structures revealed by monoclonal antibodies. *J. Biol. Chem.* **2005**, 280, 20516-20523.
 23. Leteux, C.; Chai, W.; Nagai, K.; Herbert, C. G.; Lawson, A. M.; Feizi, T. 10E4 antigen of Scrapie lesions contains an unusual nonsulfated heparan motif. *J. Biol. Chem.* **2001**, 276, 12539-12545.

24. Kure, S.; Yoshie, O. A syngeneic monoclonal antibody to murine meth-A sarcoma (HepSS-1) recognizes heparansulfate glycosaminoglycan (HS-GAG): Cell density and transformation dependent alteration in cell surface HS-GAG defined by HepSS-1. *J Immunol.* **1986** 137, 3900—3908.
25. van den Born, J.; van den Heuvel, L. P.; Bakker, M. A.; Veerkamp, J. H.; Assmann, K. J.; Berden, J. H. A monoclonal antibody against GBM heparan sulfate induces an acute selective proteinuria in rats. *Kidney Int.* **1992**, 41, 115-23.
26. Suzuki, K.; Yamamoto, K., Kariya, Y.; Maeda, H.; Ishimaru, T.; Miyaura, S.; Fujii, M.; Yusa, A.; Joo, E. J.; Kimata, K.; Kannagi, R.; Kim, Y. S.; Kyogashima, M. Generation and characterization of a series of monoclonal antibodies that specifically recognize [HexA(+/-2S)-GlcNAc]_n epitopes in heparan sulfate. *Glycoconj. J.* **2008**, 25, 703-712.
27. Sela-Passwell, N.; Kikkeri, R.; Dym, O.; Rozenberg, H.; Margalit, R.; Arad-Yellin, R.; Eisenstein, M.; Brenner, O.; Shoham, T.; Danon, T.; Shanzer, A.; Sagi, I. Antibodies targeting the catalytic zinc complex of activated matrix metalloproteinases show therapeutic potential. *Nat. Med.* **2011**, 18, 143-147.
28. Ferro, V.; Liu, L.; Johnston, K. D.; Winner, N.; Karoli, T.; Handley, P.; Rowley, J.; Dredge, K.; Li, C. P.; Hammond, E.; Davis, K.; Sarimaa, L.; Harenberg, J.; Beytheway, I. (2012) Discovery of PG545: A highly potent and simultaneous inhibitor of angiogenesis, tumor growth and metastasis. *J. Med. Chem.* **2012**, 55, 3804-3813.
29. Shanthamurthy, C. D.; Leviatan Ben-Arye, S.; Kumar, N. V.; Yehuda, S.; Amon, R.; Woods, R. J.; Padler-Karavani, V.; Kikkeri, R. Heparan Sulfate Mimetics Differentially Affect Homologous Chemokines and Attenuate Cancer Development. *J. Med. Chem.* **2021**, 64, 3367-3380.
30. Toraskar, S.; Chaudhary, P. M.; Kikkeri, R. The Shape of Nanostructures Encodes Immunomodulation of Carbohydrate Antigen and Vaccine Development. *ACS Chem. Biol.* **2022**, 17, 1122-1130.
31. Hassan, N.; Greve, B.; Espinoza-Sánchez, N. A.; Götte, M. Cell-surface heparan sulfate proteoglycans as multifunctional integrators of signaling in cancer. *Cell. Signalling.* **2021**, 77, 109822.
32. Damen, L. A. A., van de Westerlo, E. M. A.; Versteeg, E. M. M.; van Wessel, T.; Daamen, W. F.; van Kuppevelt, T. H. Construction and evaluation of an antibody phage display library targeting heparan sulfate. *Glycoconj. J.* **2020**, 37, 445-455.

33. Sakamoto, K.; T. Ozaki, T.; Ko, Y. C.; Tsai, C. F.; Gong, Y.; Morozumi, M.; Ishikawa, Y.; Uchimura, K.; Nadanaka, S.; Kitagawa, H.; Zulueta, M. M. L.; Bandaru, A.; Tamura, J. I.; Hung, S. C.; Kadomatsu, K. Glycan sulfation patterns define autophagy flux at axon tip via PTPR σ -cortactin axis. *Nat Chem. Biol.* **15**, 699-709 (2019).

2.6 Similarity index of heparin mimics





Fig

re 6. Similarity index of heparin mimics against 2304 HS tetrasaccharides (a) I45; (b) I49; (c) ID49; (d) G413; (e) GA49; (f) G49; (g) GA45

2.7 SDS-PAGE of BSA-Conjugate

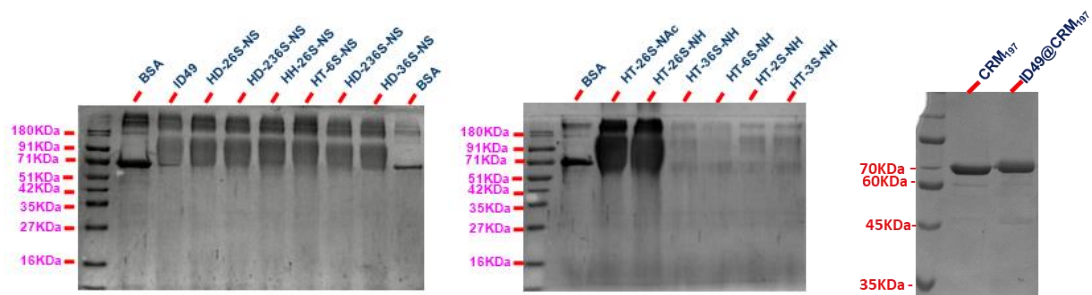
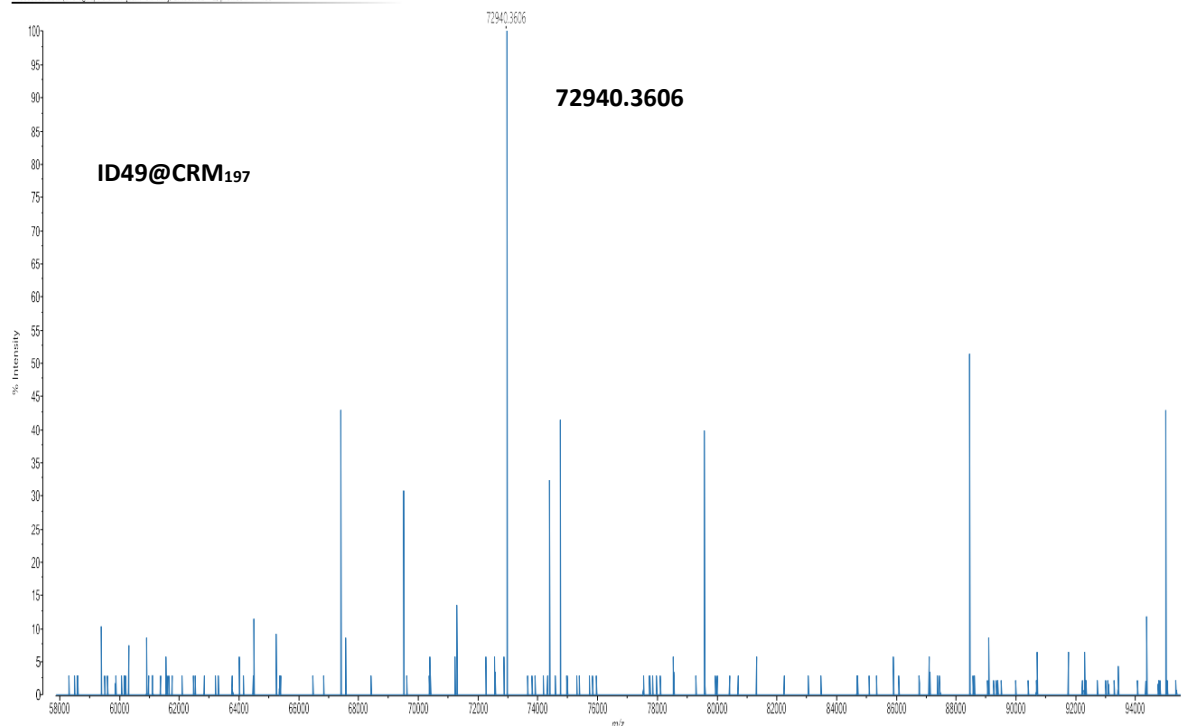
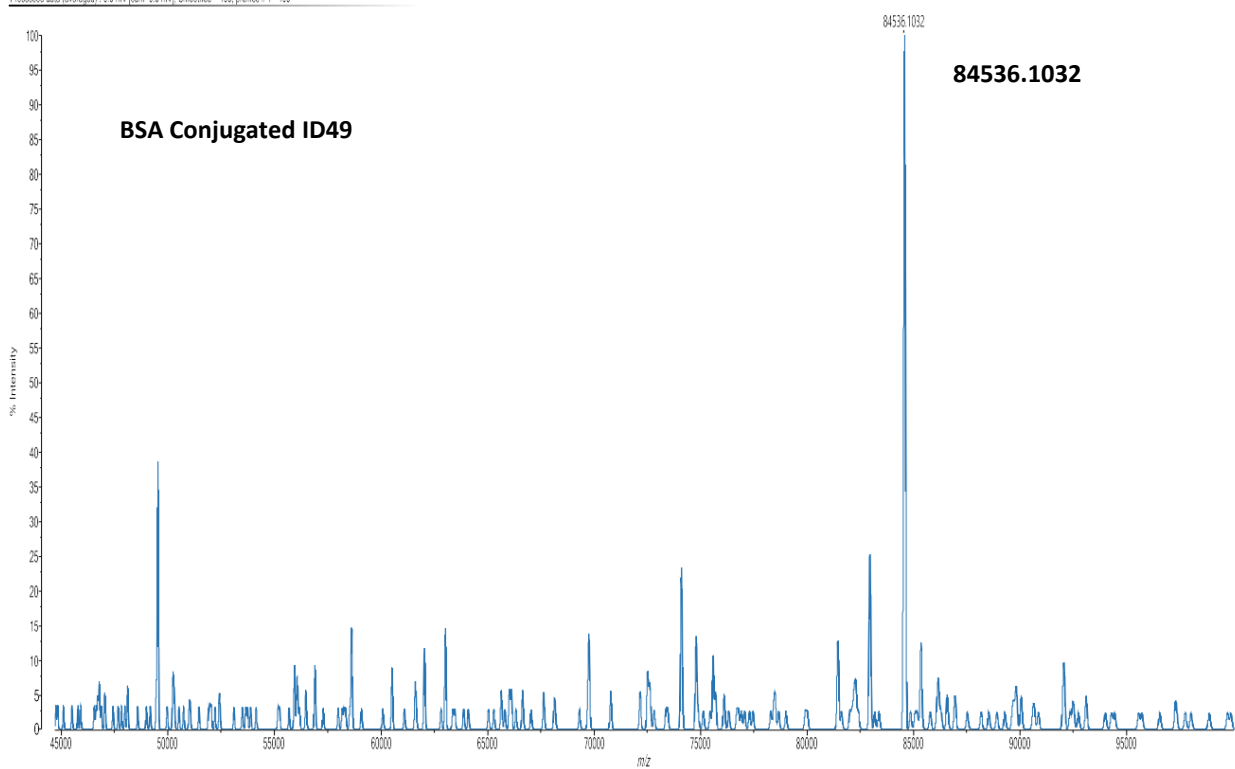


Figure 7. SDS-Gel page of all BSA conjugated HS-Mimetics and **ID49@CRM197**

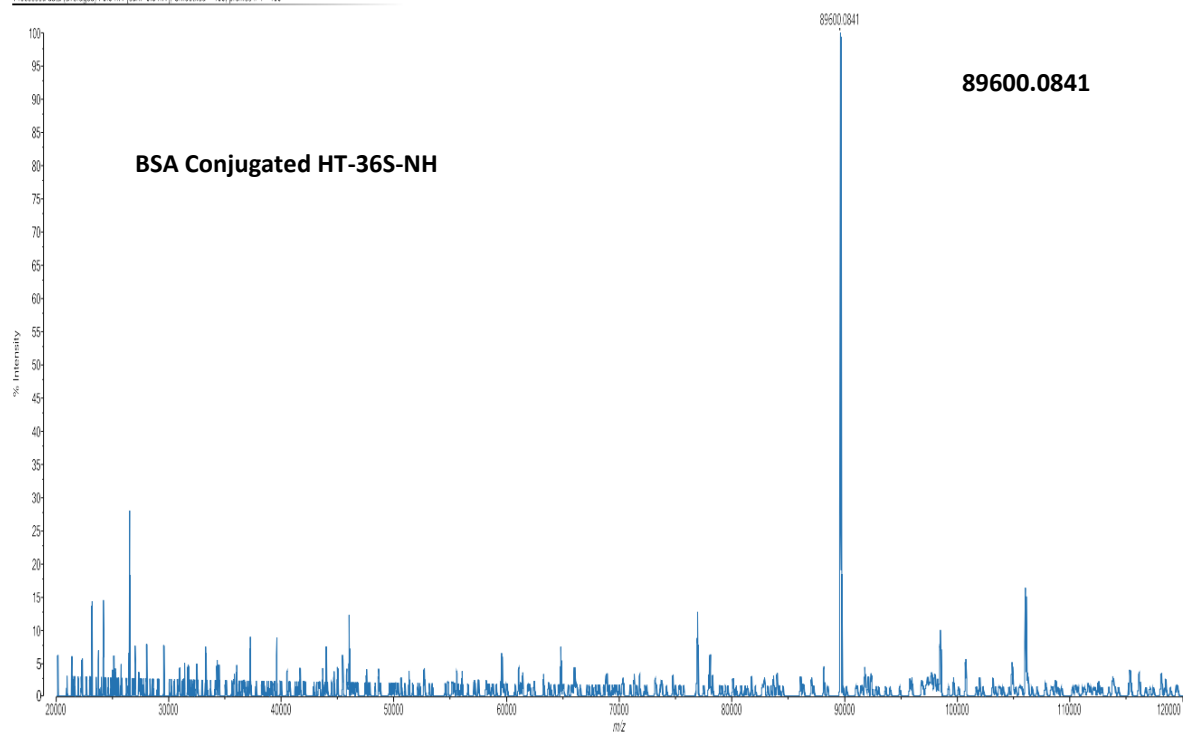
Created By MALDI Solutions Admin, Date: New Acquisition 1261104 July 2023 16:31:49 Cal: Named Calibration "Linear mass calibration" by MALDI Solutions Admin on 24 February 2023 12:17:42 (Original)
 Shimadzu MALDI-8020, Tuning: Linear, Power: 76, P.Ext at 70000.00 (pin 6-6E), Ion Gate Blanking: 10000.00
 Processed data (averaged): 0.0 mV (sum=0.7 mV), Smoothed = 2, profiles # 1 - 100



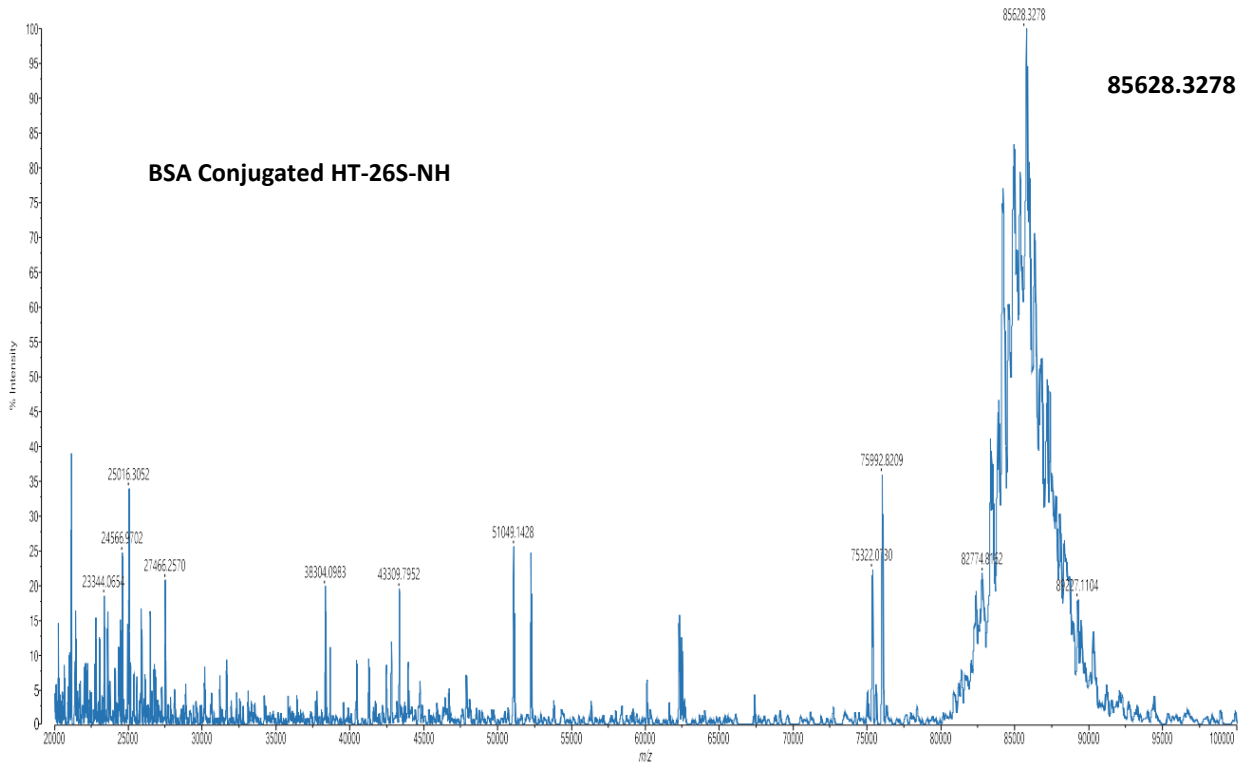
Created By: MALDI Solutions Admin, Date: New Acquisition 26_0001.C2.23 October 2023 11:41:00 Cal: Named Calibration "Linear mass calibration" by MALDI Solutions Admin on 24 February 2023 12:17:42 (Original)
Shimadzu MALDI-8020, Tuning: Linear, Power: 50, P.Et: at 70000.00 (bin 646), Ion Gate Blanking: 10000.00
Processed data (averaged): 1.0.0 mV (sum=0.0 mV), Smoothed = 100, profiles # 1 - 100



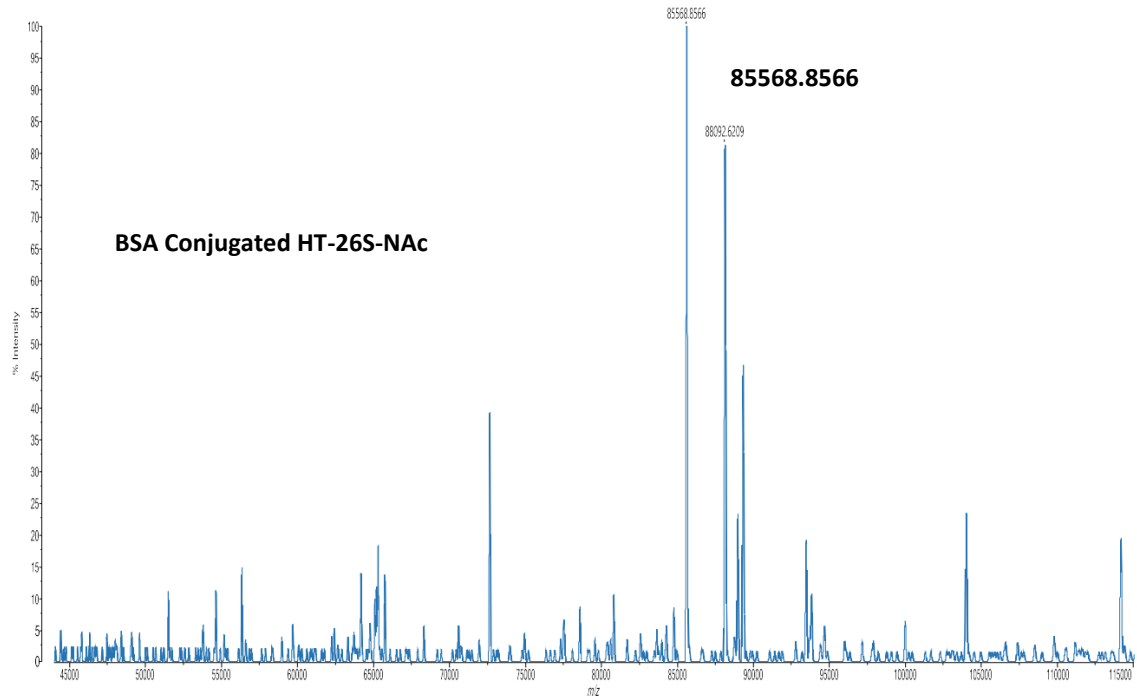
Created By: MALDI Solutions Admin, Date: New Acquisition 209_0001.O3.20 December 2023 16:50:15 Cal: Named Calibration "Linear mass calibration" by MALDI Solutions Admin on 24 February 2023 12:17:42 (Original)
Shimadzu MALDI-8020, Tuning: Linear, Power: 66, P.Et: at 75000.00 (bin 695), Ion Gate Blanking: 20000.00
Processed data (averaged): 1.0.0 mV (sum=0.0 mV), Smoothed = 100, profiles # 1 - 100



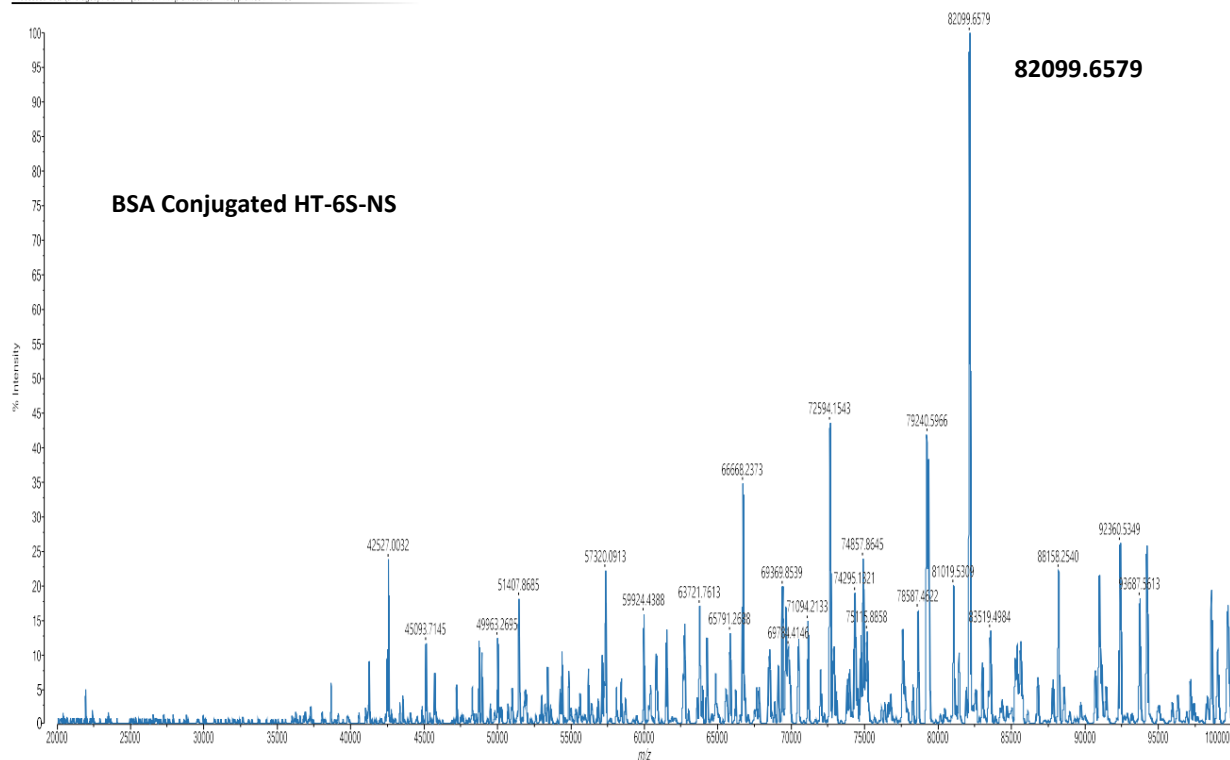
Created By MALDI Solutions Admin, Data: New Acquisition 165_0001.D1 20 December 2023 16:12:43 Cal Named Calibration 'Linear mass calibration' by MALDI Solutions Admin on 24 February 2023 12:17:42 (Original)
Shimadzu MALDI-8020 Tuning Linear, Power 75, P.Ext at 75000.00 (bin 669), Ion Gate Blanking: 20000.00
Processed data (averaged): 0.0 mV (sum=0.1 mV), Smoothed = 100, profiles # 1 - 100



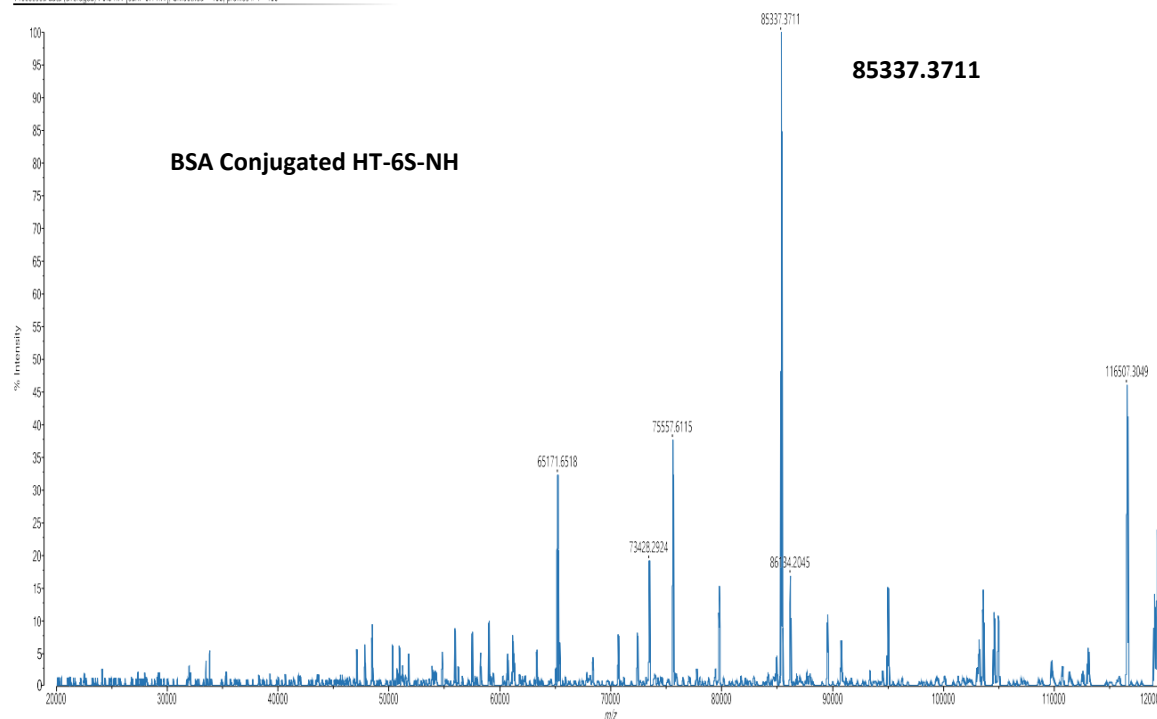
Created By MALDI Solutions Admin, Data: New Acquisition 234_0001.E1 20 December 2023 17:07:28 Cal Named Calibration 'Linear mass calibration' by MALDI Solutions Admin on 24 February 2023 12:17:42 (Original)
Shimadzu MALDI-8020 Tuning Linear, Power 66, P.Ext at 85000.00 (bin 712), Ion Gate Blanking: 20000.00
Processed data (averaged): 0.0 mV (sum=0.0 mV), Smoothed = 100, profiles # 1 - 100



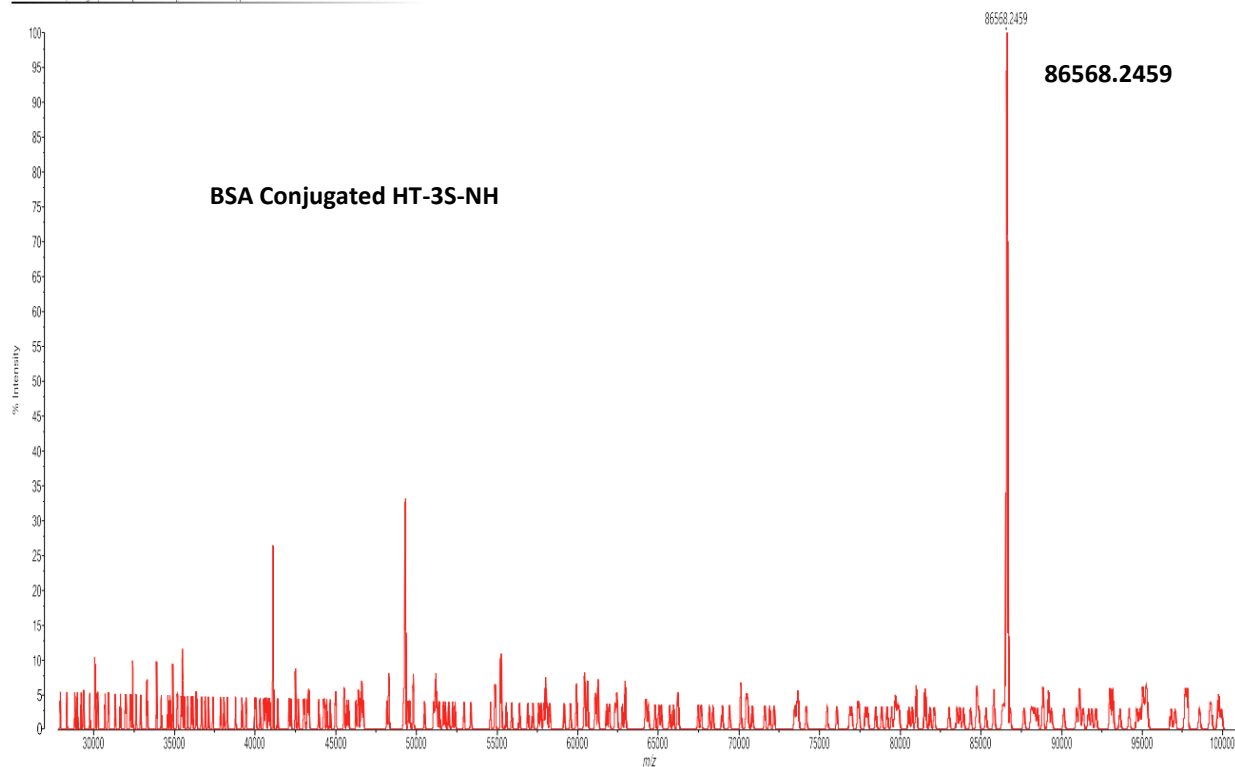
Created By: MALDI Solutions Admin, Date: New Acquisition: 279_0001.E3.20 December 2023 17:39:29 Cal: Named Calibration 'Linear mass calibration' by MALDI Solutions Admin on 24 February 2023 12:17:42 (Original)
Shimadzu MALDI-8020 Tuning: Linear, Power: 69, P.Exit at: 85000.00 (bin 712), Ion Gate Blanking: 20000.00
Processed data (averaged): 0.0 mV (sum=0.1 mV), Smoothed = 100, profiles # 1 - 100



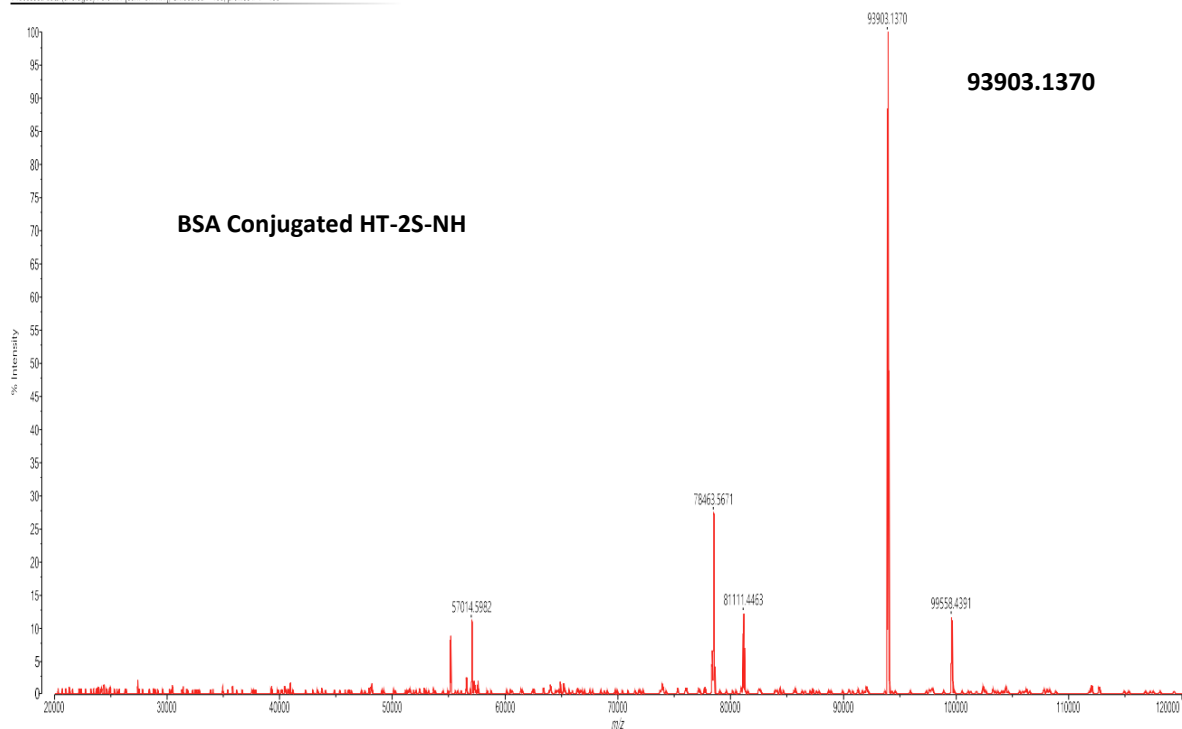
Created By: MALDI Solutions Admin, Date: New Acquisition: 222_0001.04.20 December 2023 16:58:54 Cal: Named Calibration 'Linear mass calibration' by MALDI Solutions Admin on 24 February 2023 12:17:42 (Original)
Shimadzu MALDI-8020 Tuning: Linear, Power: 64, P.Exit at: 75000.00 (bin 669), Ion Gate Blanking: 20000.00
Processed data (averaged): 0.0 mV (sum=0.1 mV), Smoothed = 100, profiles # 1 - 100



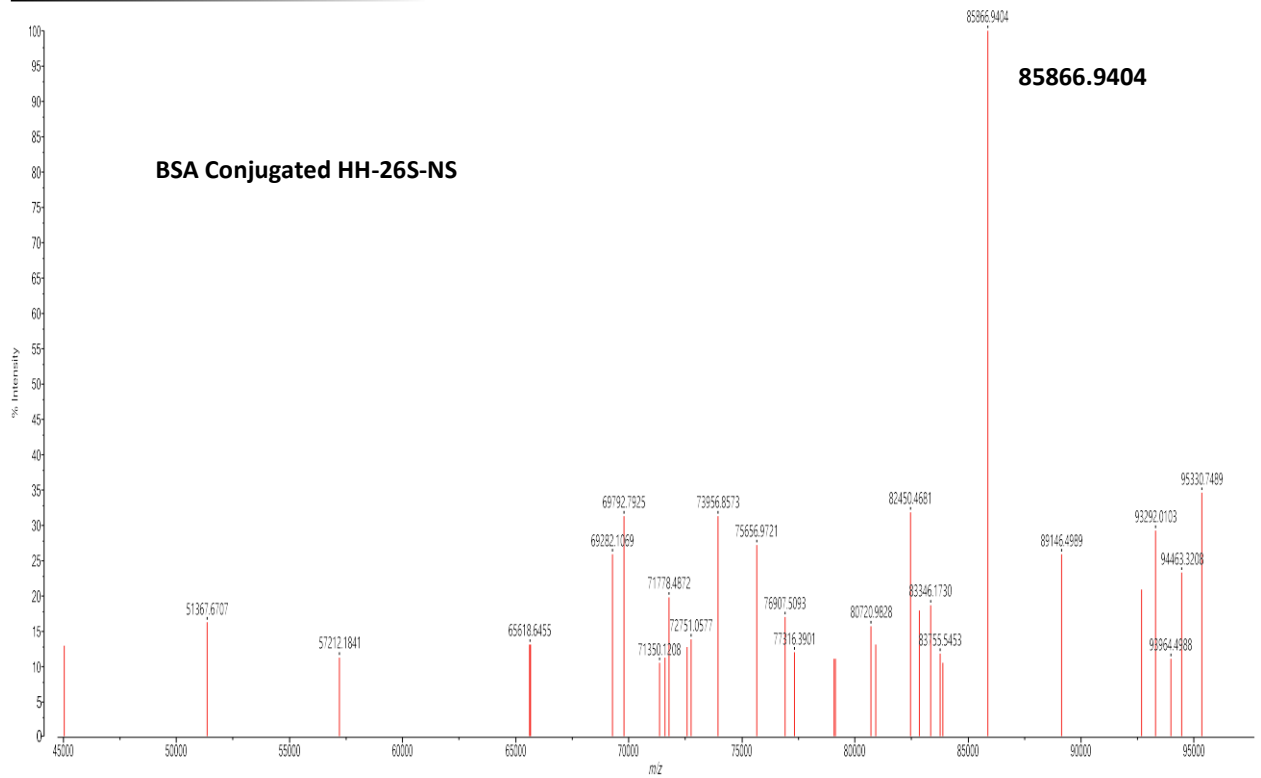
Created by MALDI Solutions Admin. Data: New Acquisition 252_0001.E2 20 December 2023 17:23:24 Cal/Named Calibration "Linear mass calibration" by MALDI Solutions Admin on 24 February 2023 12:17:42 (Original)
Shimadzu MALDI-8020 Tuning Linear, Power 77, P.Ext at 85000.00 (bin 112), Ion Gate Blanking: 20000.00
Processed data (averaged): 0.0 mV (sum=0.0 mV), Smoothed = 100, profiles # 1 - 100



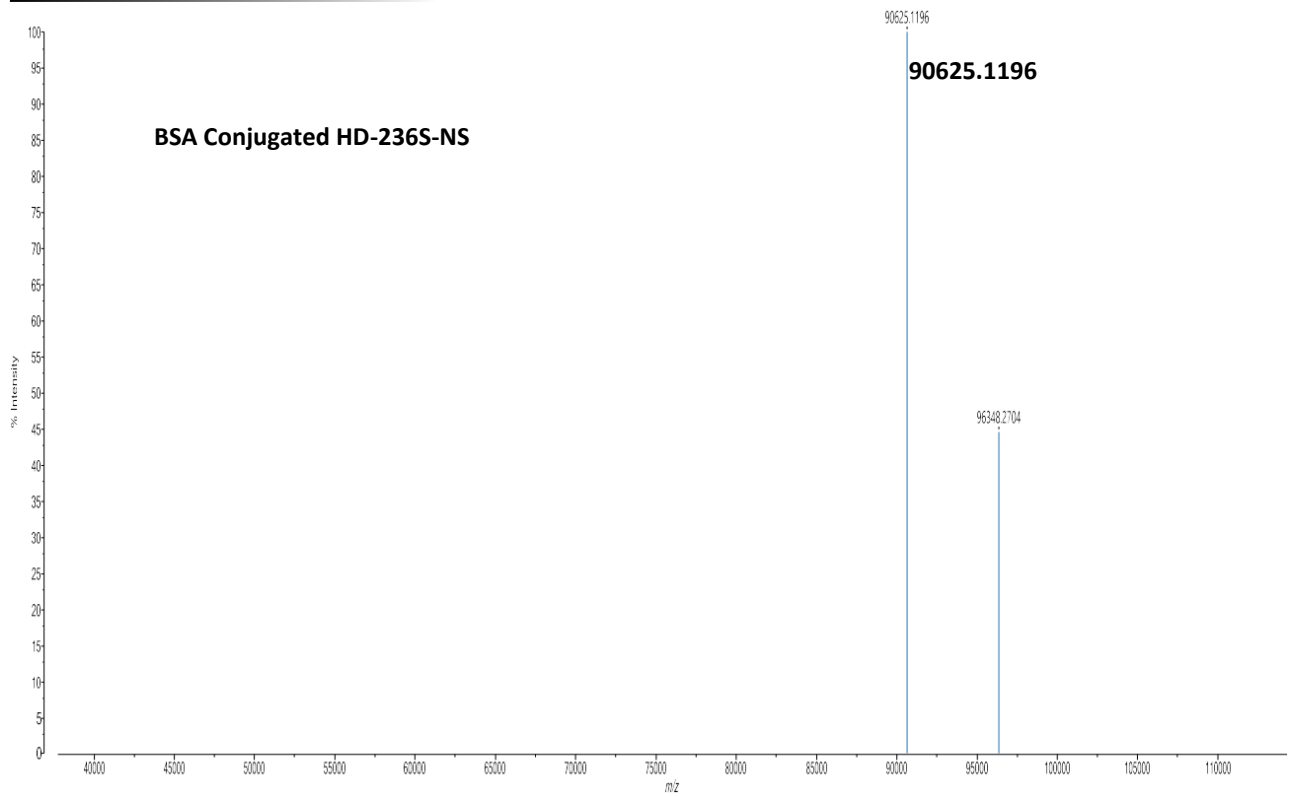
Created by MALDI Solutions Admin. Data: New Acquisition 194_0001.D2 20 December 2023 16:41:24 Cal/Named Calibration "Linear mass calibration" by MALDI Solutions Admin on 24 February 2023 12:17:42 (Original)
Shimadzu MALDI-8020 Tuning Linear, Power 68, P.Ext at 75000.00 (bin 669), Ion Gate Blanking: 20000.00
Processed data (averaged): 0.0 mV (sum=0.1 mV), Smoothed = 100, profiles # 1 - 100



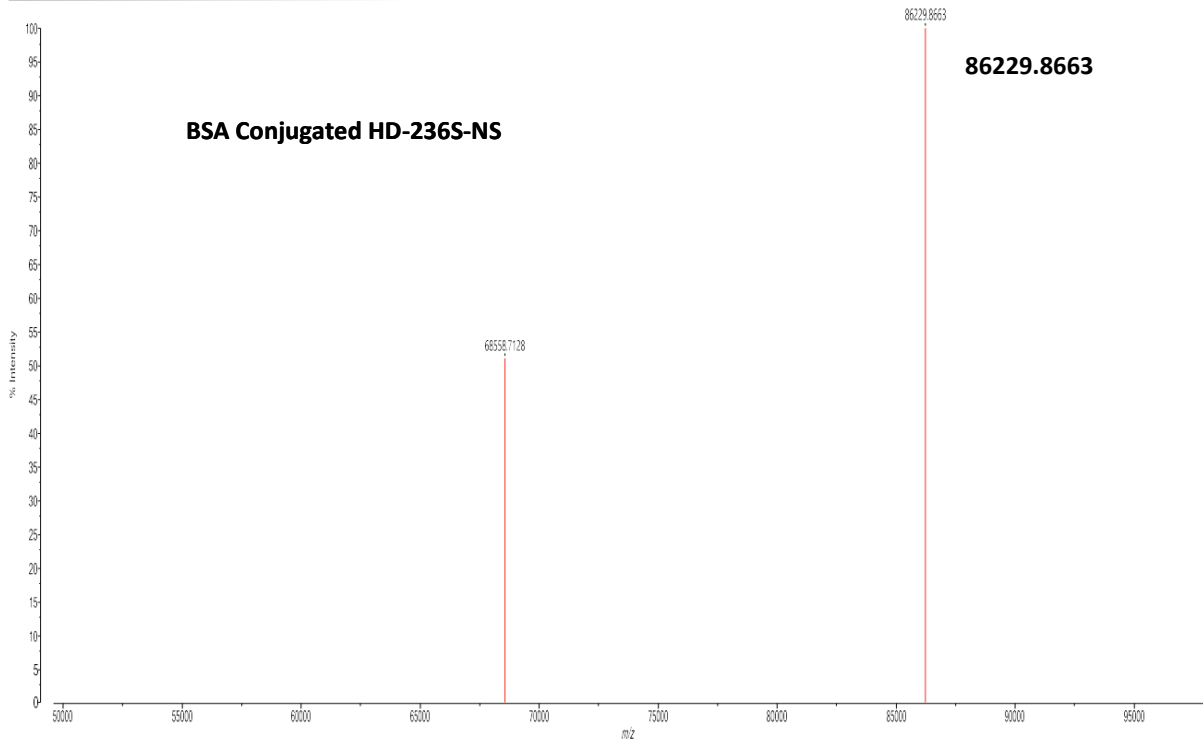
Created By MALDI Solutions Admin, Data: New Acquisition 1066_000114 07 February 2024 17:56:56, Cal Named Calibration "Linear mass calibration" by MALDI Solutions Admin on 24 February 2023 12:17:42 (Original)
Shimadzu MALDI-8020 Tuning Linear, Power 67, P.Exit at 85000.00 (bin 712), Ion Gate Blanking: 20000.00
Peaks: 0.0 mV, processing type=Threshold (Centroid 25%), profiles # 1 - 100



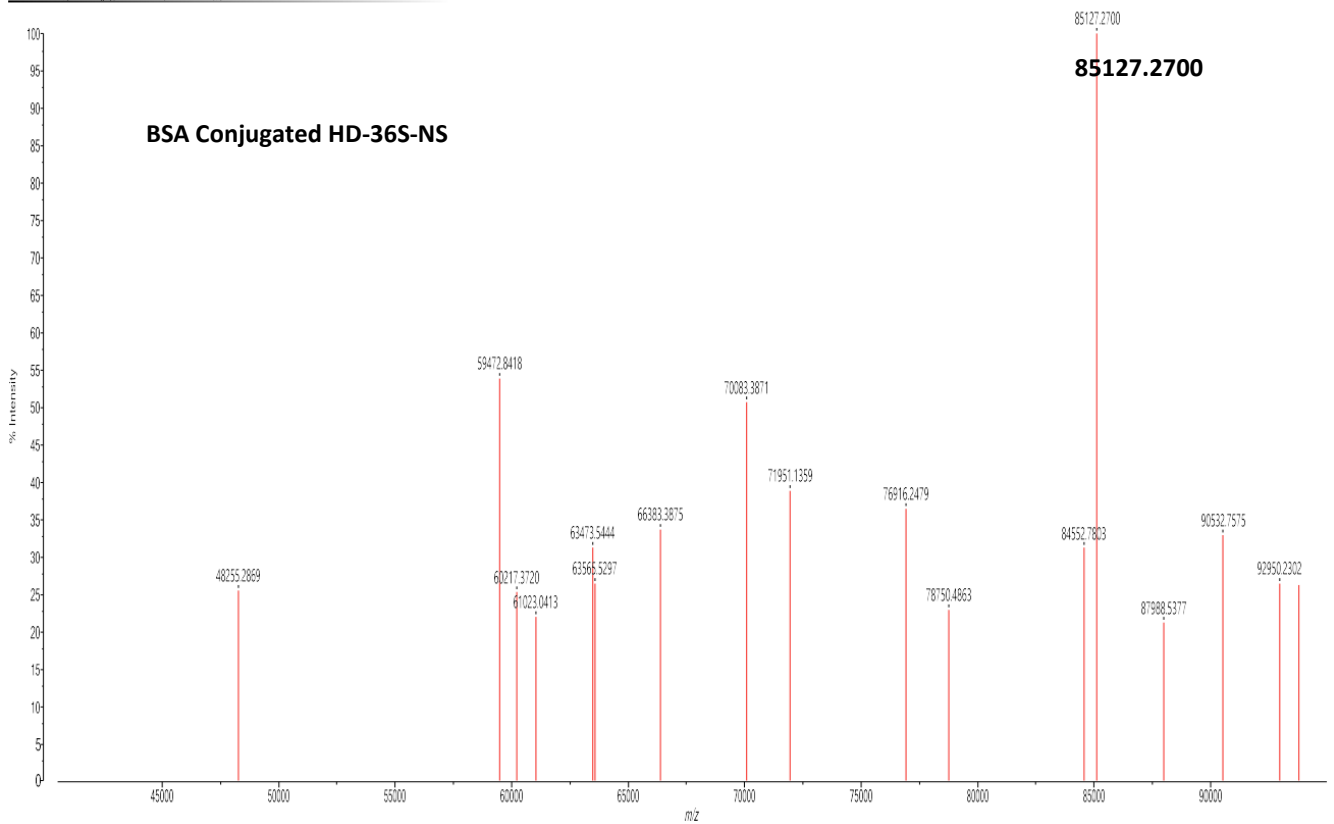
Created By MALDI Solutions Admin, Data: New Acquisition 1029_000111 07 February 2024 17:33:51, Cal Named Calibration "Linear mass calibration" by MALDI Solutions Admin on 24 February 2023 12:17:42 (Original)
Shimadzu MALDI-8020 Tuning Linear, Power 69, P.Exit at 85000.00 (bin 712), Ion Gate Blanking: 20000.00
Peaks: 0.0 mV, processing type=Threshold (Centroid 25%), profiles # 1 - 100



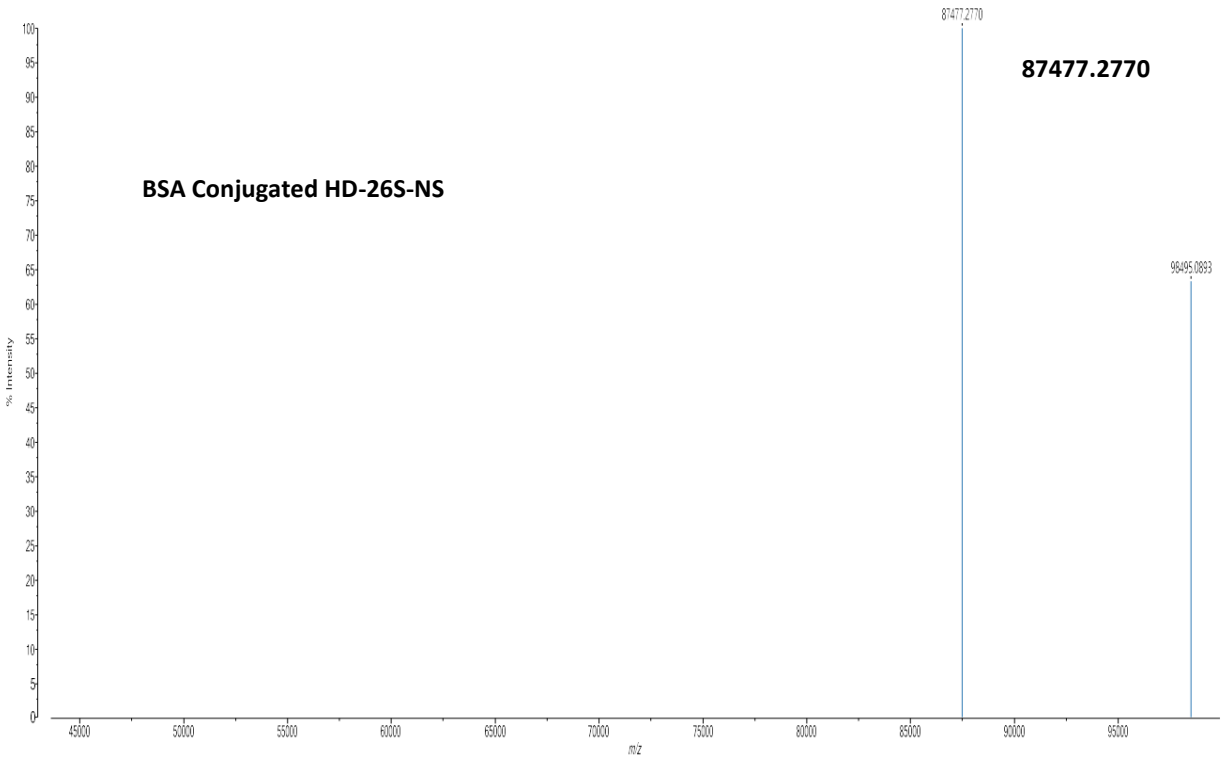
Created By MALDI Solutions Admin, Data: New Acquisition 1038_000112 07 February 2024 17:39:52 Cal Named Calibration "Linear mass calibration" by MALDI Solutions Admin on 24 February 2023 12:17:42 (Original)
Shimadzu MALDI-8020 Tuning Linear, Power 85, P.Ext at 85000.00 (bin 712), Ion Gate Blanking: 20000.00
Peaks: 0.0 mV, processing type=Threshold (Centroid 25%), profiles # 1 - 100



Created By MALDI Solutions Admin, Data: New Acquisition 1040_000113 07 February 2024 17:43:00 Cal Named Calibration "Linear mass calibration" by MALDI Solutions Admin on 24 February 2023 12:17:42 (Original)
Shimadzu MALDI-8020 Tuning Linear, Power 85, P.Ext at 85000.00 (bin 712), Ion Gate Blanking: 20000.00
Peaks: 0.0 mV, processing type=Threshold (Centroid 25%), profiles # 1 - 100



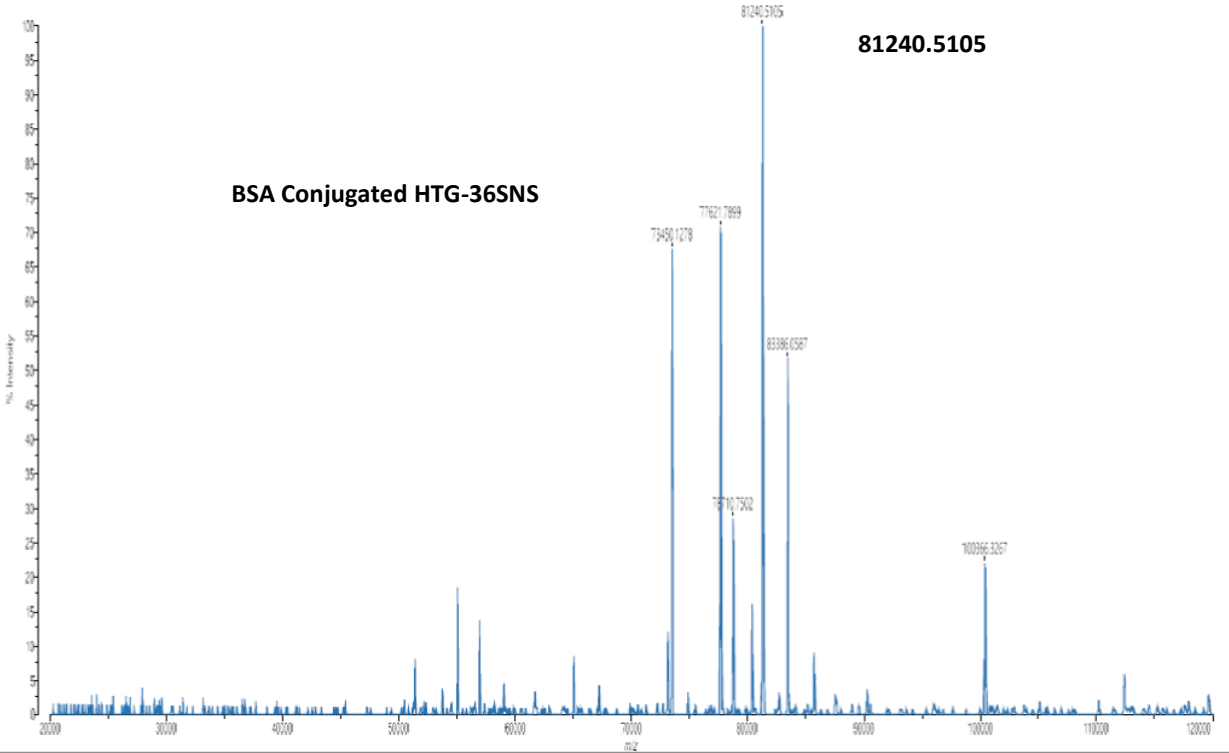
Created by MALDI Solutions Admin, Data: New Acquisition 1030_0001.H1 07 February 2024 17:22:30 CalName: Calibration 'Linear mass calibration' by MALDI Solutions Admin on 24 February 2023 12:17:42 (Original)
Shimadzu MALDI-8020 Tuning Linear, Power 60, P.Exit at 85000.00 (bin 712), Ion Gate Blanking: 20000.00
Peaks: 0.0 mV, processing type=Threshold (Contrast 25%), profiles # 1 - 100



Created by MALDI Solutions Admin, Data: New Acquisition 134-4 18 June 2024 11:53:22 CalName: Calibration 'Linear mass calibration' by MALDI Solutions Admin on 24 February 2023 12:17:42 (Original)
Shimadzu MALDI-8020 Tuning Linear, Power 94, P.Exit at 80000.00 (bin 691), Ion Gate Blanking: 40000.00
Processed data (averaged), 0.0 mV (scan=0.0 mV), Smoothed = 100, profiles # 1 - 100



Created By MALDI Solutions Admin, Data: New Acquisition 192_000102 20 December 2023 16:40:06 Cal: Named Calibration "Linear mass calibration" by MALDI Solutions Admin on 24 February 2023 12:17:42 (Original)
Shimadzu MALDI-8020 Tuning Linear, Power 68, F/L: at 75000.00 (bin 659), Ion Gate Blanking: 20000.00
Processed data (averaged), 0.0 mV (sum=0.0 mV), Smoothed = 100, profiles # 1 - 100



Created By MALDI Solutions Admin, Data: New Acquisition 1050_000104 07 February 2024 17:49:44 Cal: Named Calibration "Linear mass calibration" by MALDI Solutions Admin on 24 February 2023 12:17:42 (Original)
Shimadzu MALDI-8020 Tuning Linear, Power 70, F/L: at 85000.00 (bin 712), Ion Gate Blanking: 20000.00
Peaks: 0.0 mV, processing type: Threshold (Centroid 25%), profiles # 1 - 100

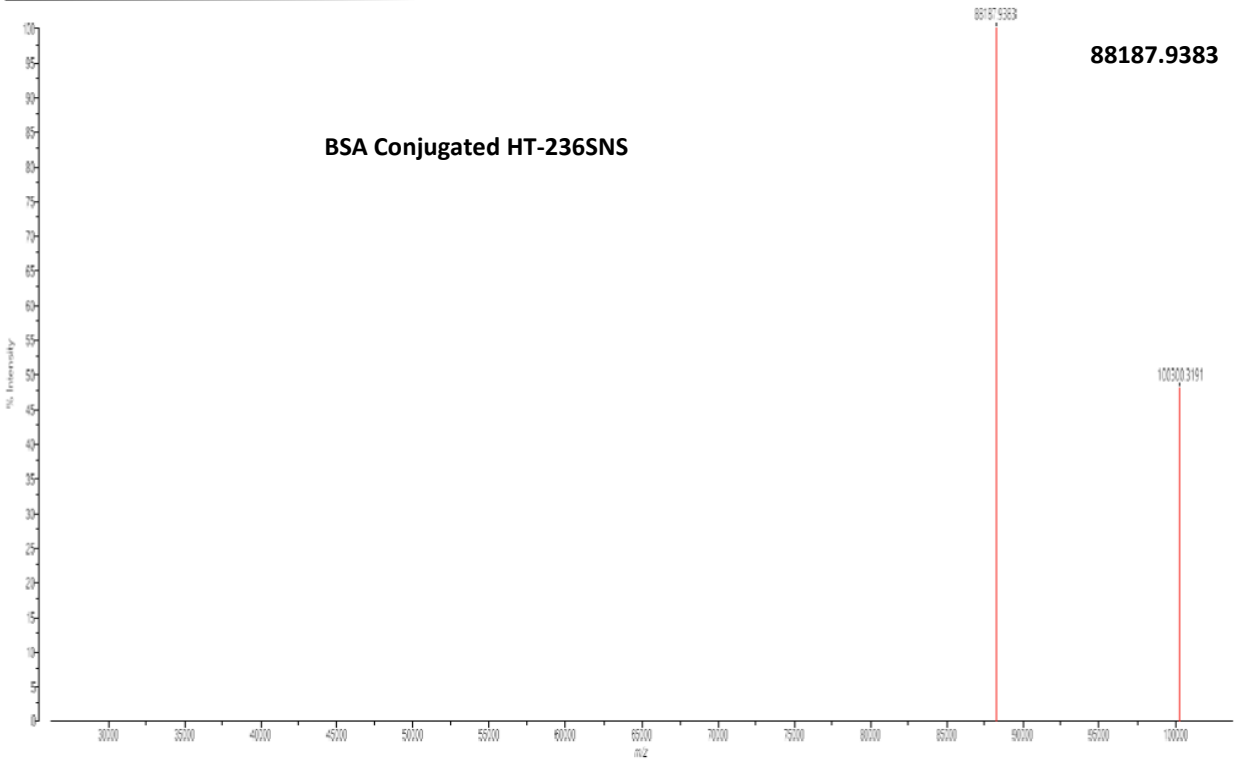
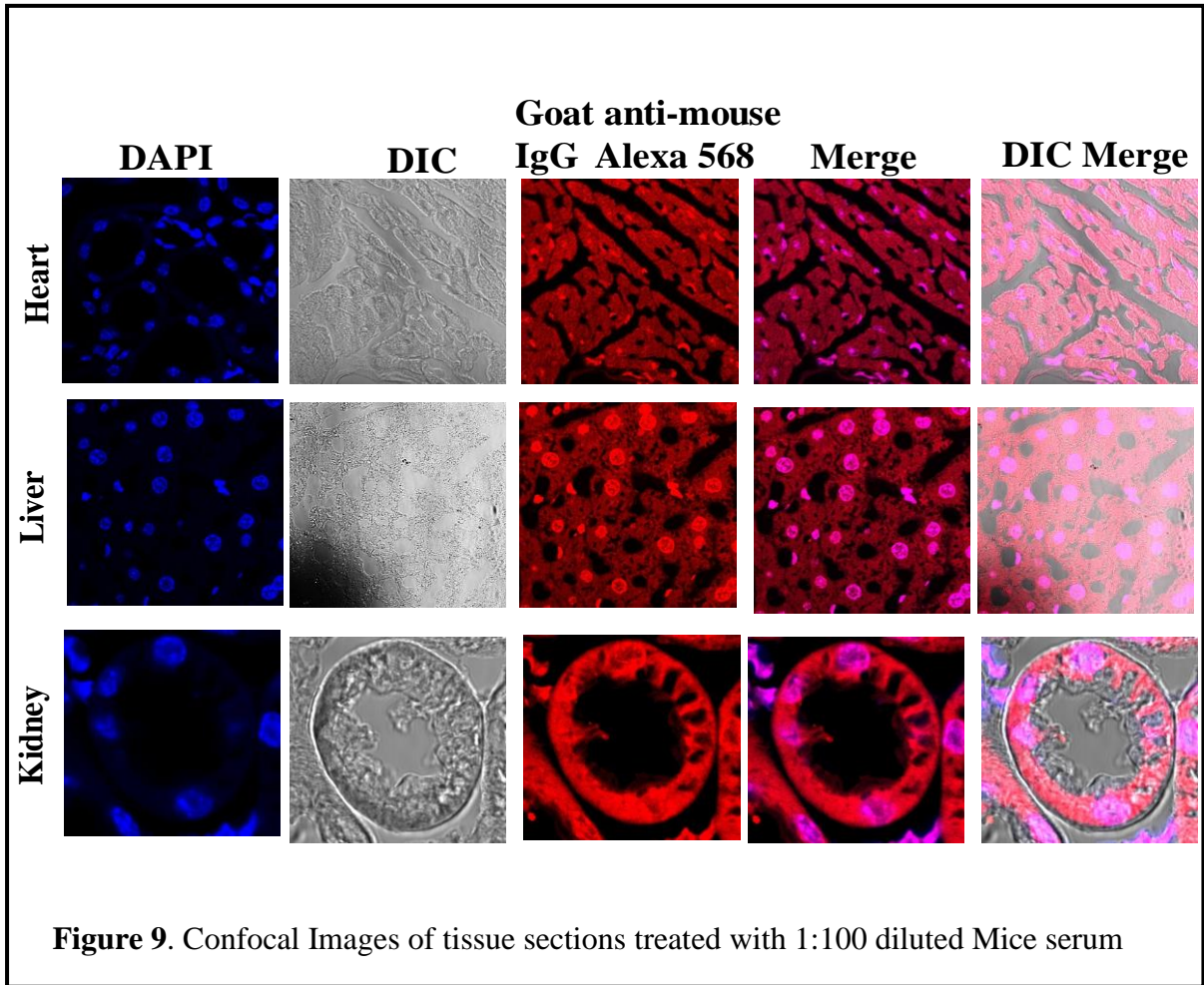


Figure 8. MALDI-TOF spectra of **ID49@CRM₁₉₇** and BSA conjugated HS ligands.

Table 1. MALDI-TOF masses of all BSA conjugated HS ligands.

Sr. No	BSA@HS-mimetics	MALDI-TOF Mass	Number of sugar per BSA molecule
1	BSA-HT-26S-NAc	85568.8566	~ 10
2	BSA-HT-26S-NH	85628.3278	~ 10
3	BSA-HT-36S-NH	89600.0841	~ 13
4	BSA-HT-6S-NH	85337.3711	~ 11
5	BSA -HT-2S-NH	93903.1370	~ 20
6	BSA-HT-3S-NH	86568.2459	~ 12
7	BSA-HT-6S-NS	82099.6579	~ 7
8	BSA-ID49	84563.7032	~ 6
9	BSA-HD-236S-NS	86229.8663	~ 11
10	BSA-HD-36S-NS	85127.2700	~ 10
11	BSA-HD-26S-NS	87477.2770	~ 12
12	BSA-HD-236S-NS	90625.1196	~ 15
13	BSA-HH-26S-NS	85866.9404	~ 10
14	BSA-HTG-36S-NS	81240.105	~ 4
15	BSA-HTG-236S-NS	84127.8900	~ 6
16	BSA-HT-236S-NS	88187.9383	~ 8



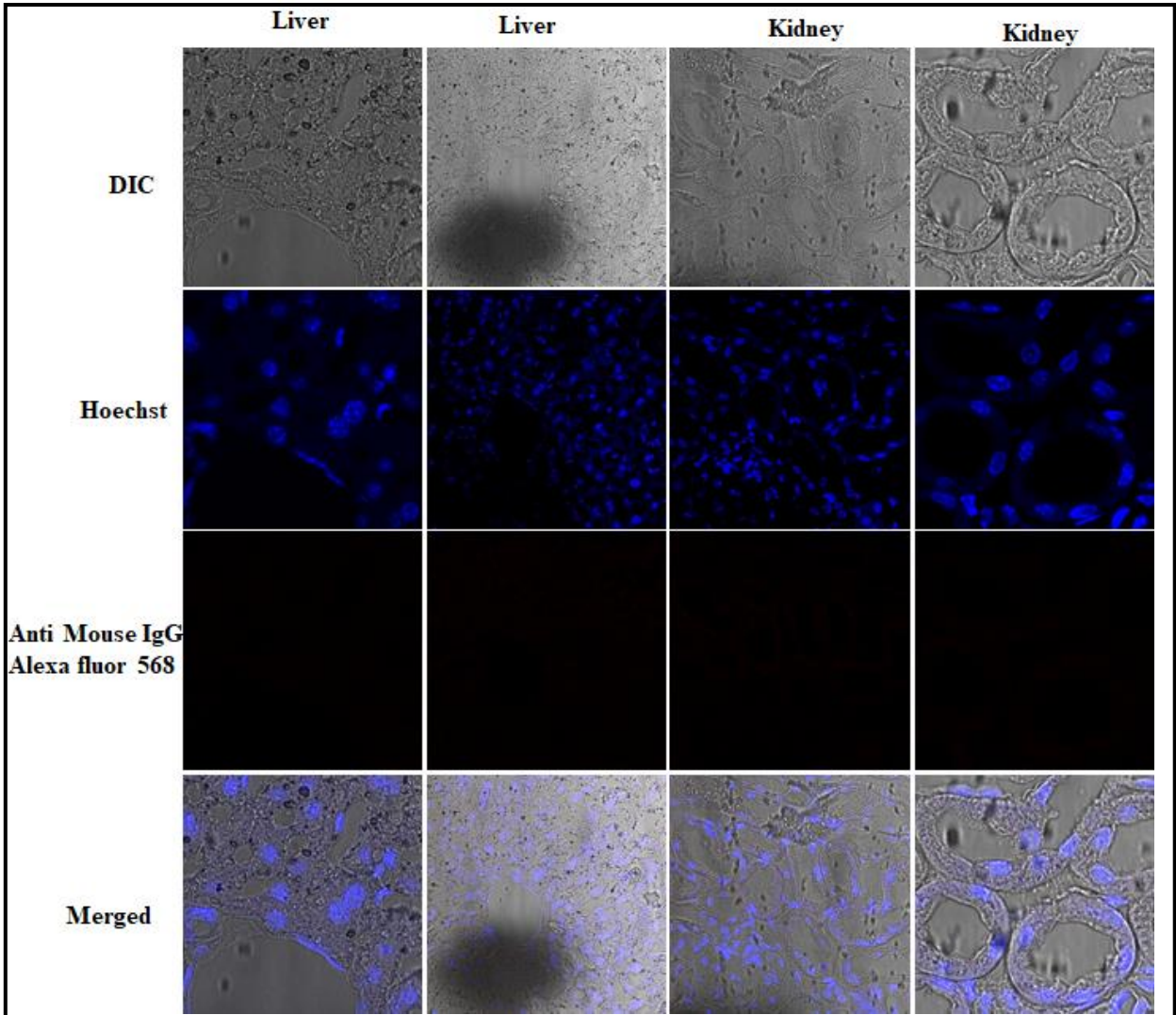
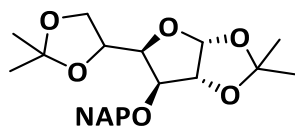
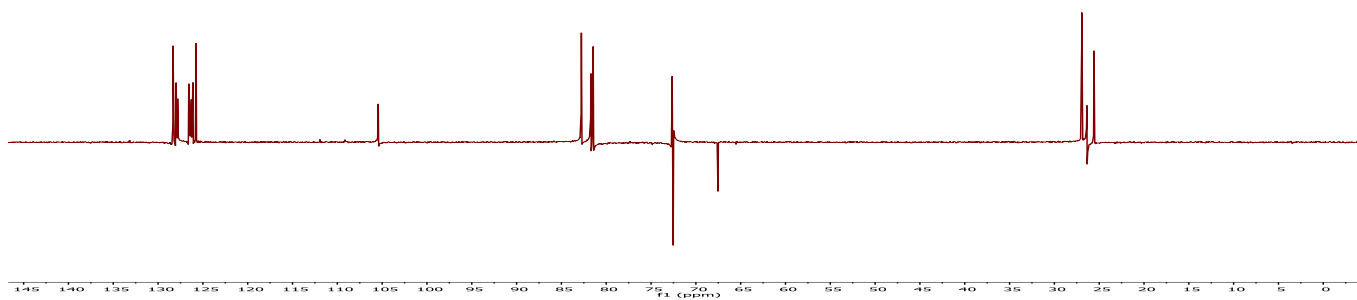
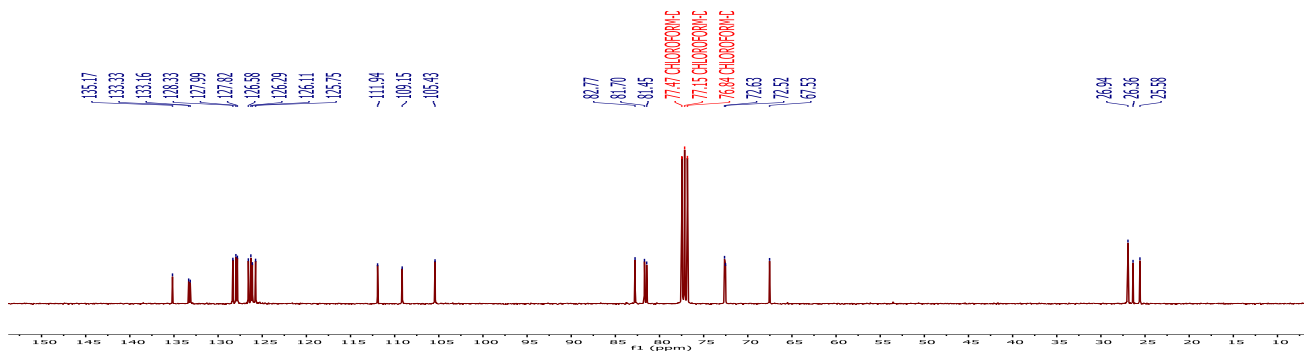
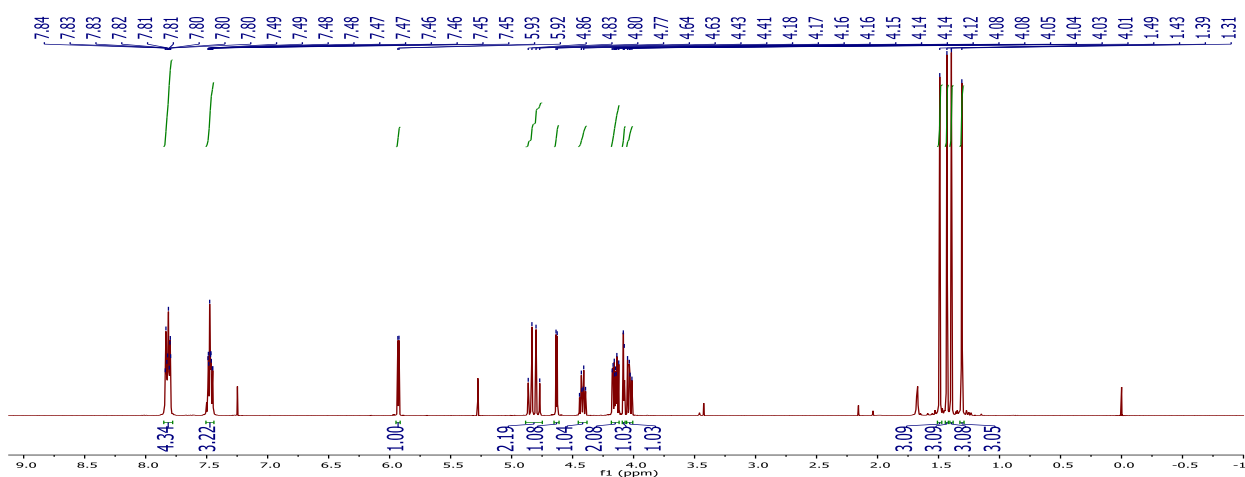


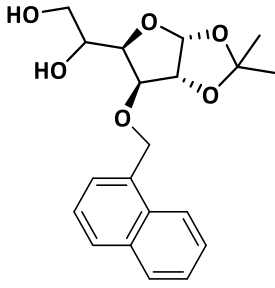
Figure 10. Confocal Images of heparinase treated tissue sections treated with 1:100 diluted Mice serum

2.8 NMR

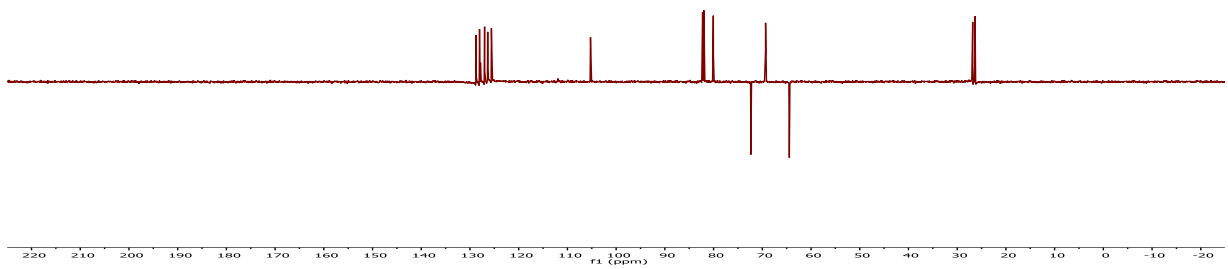
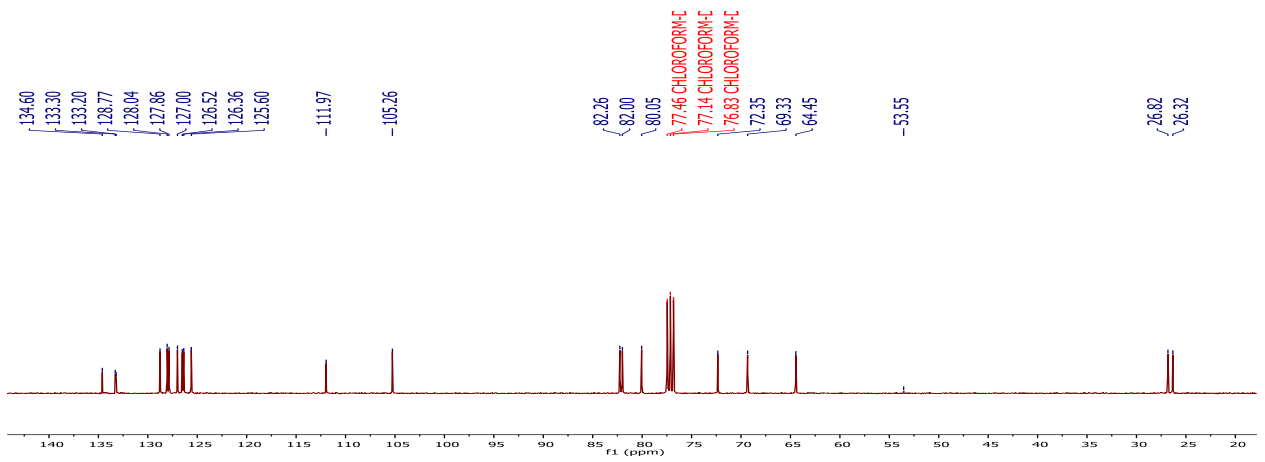
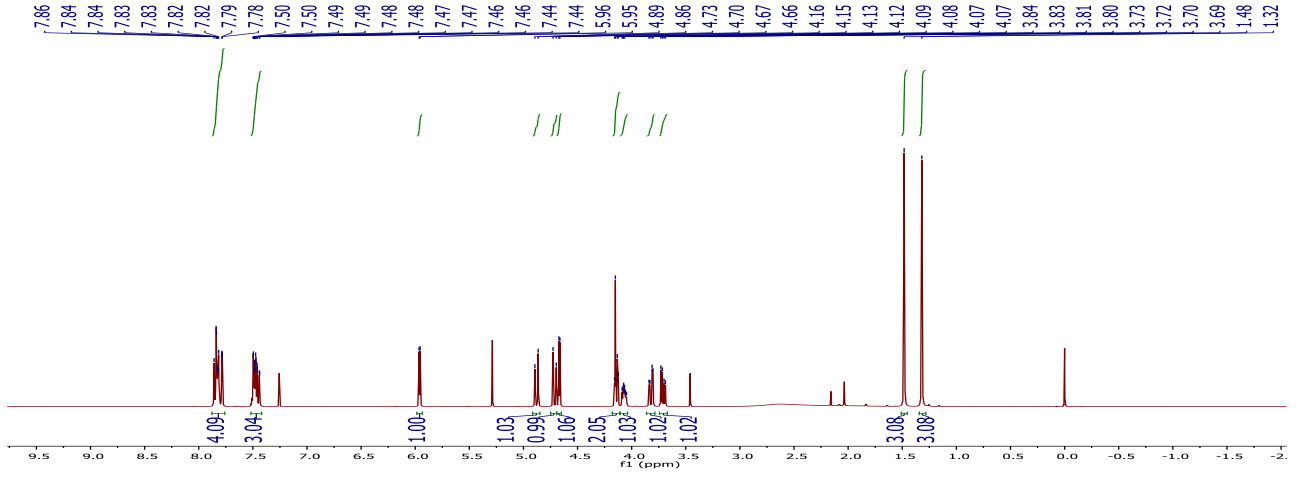


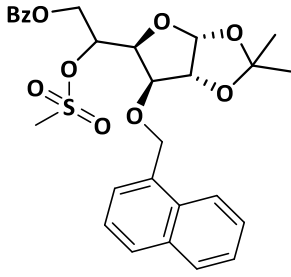
2



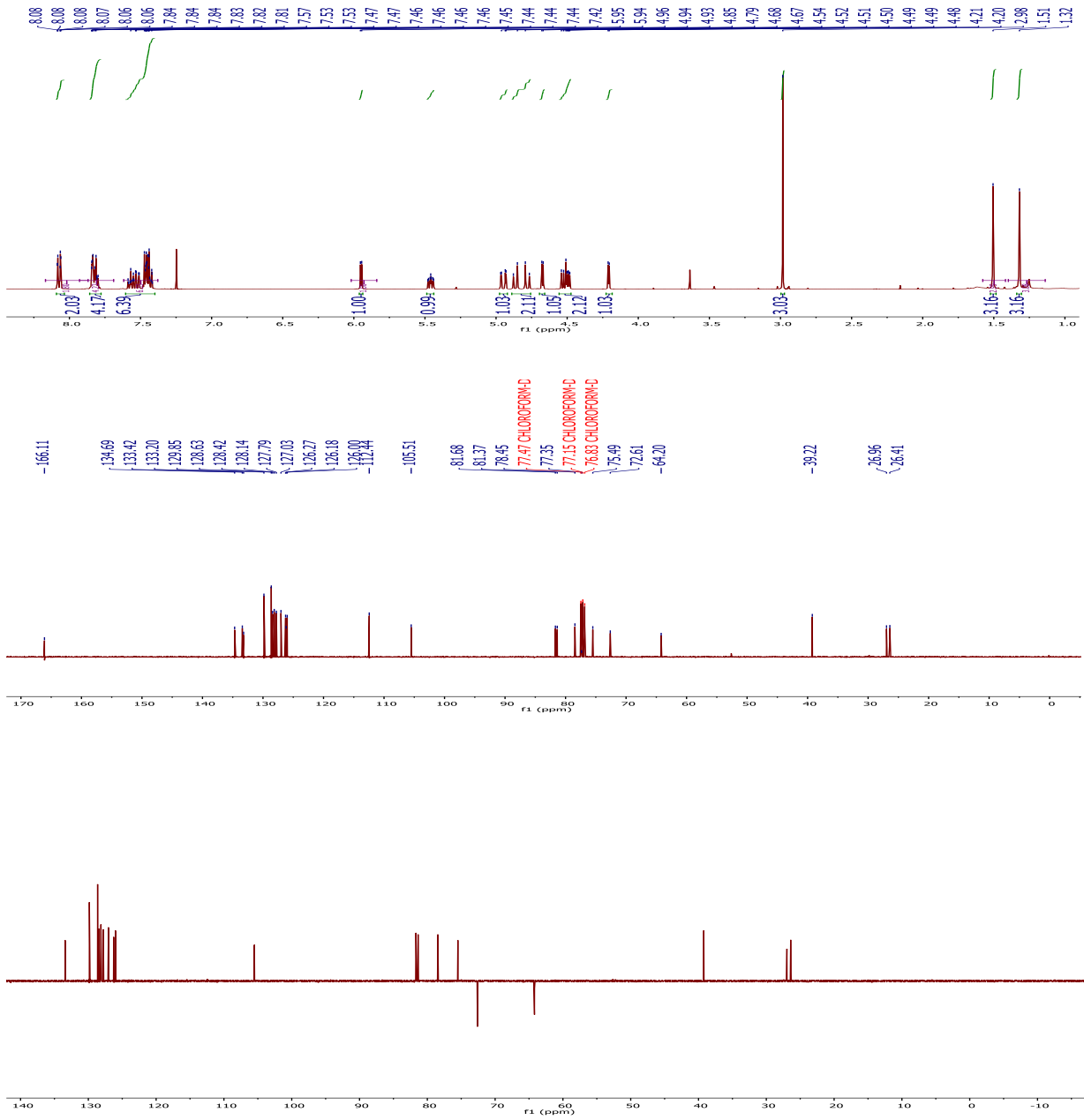


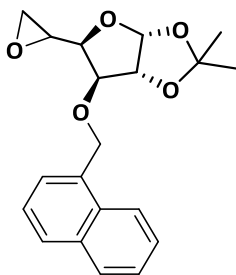
3



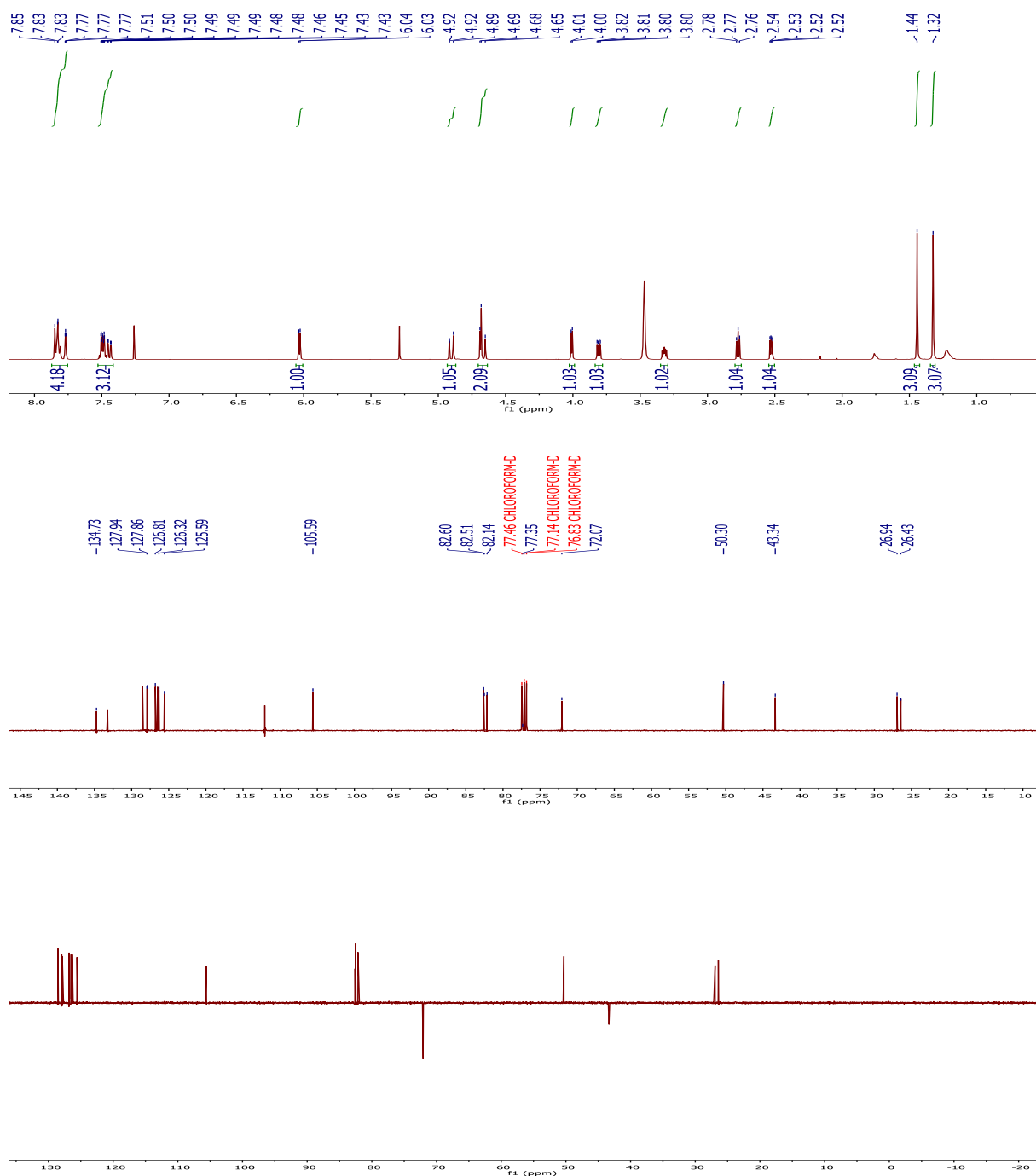


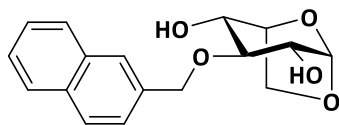
5



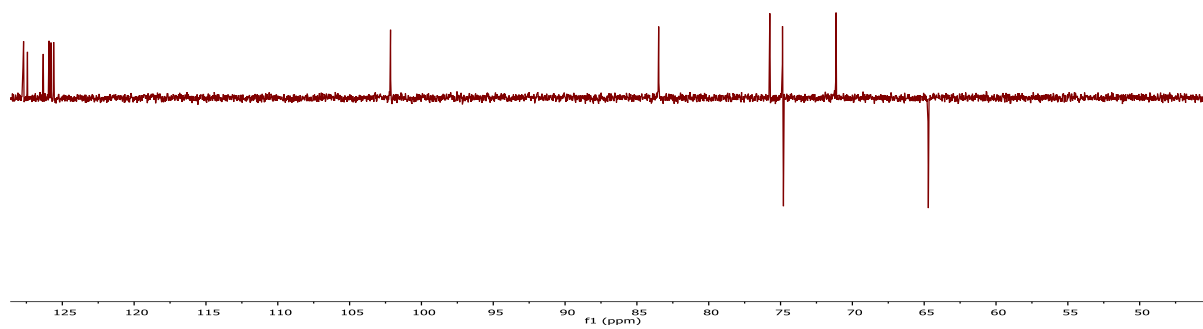
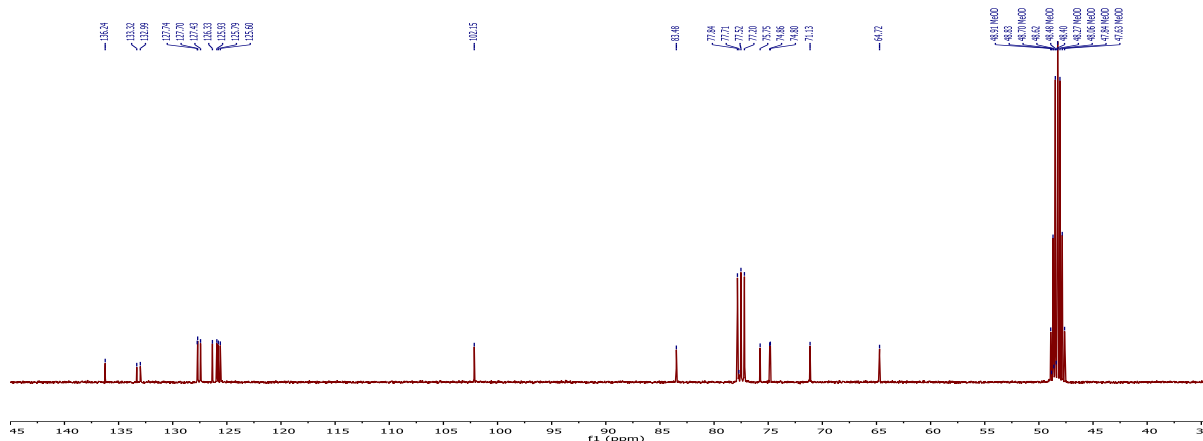
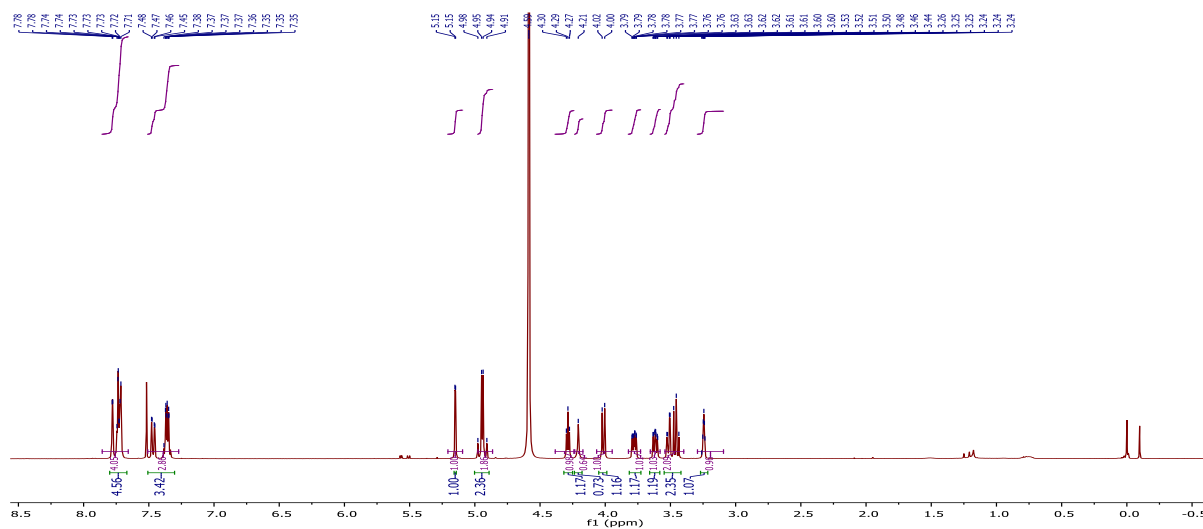


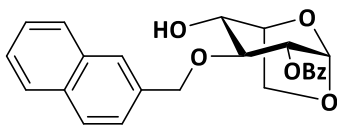
6



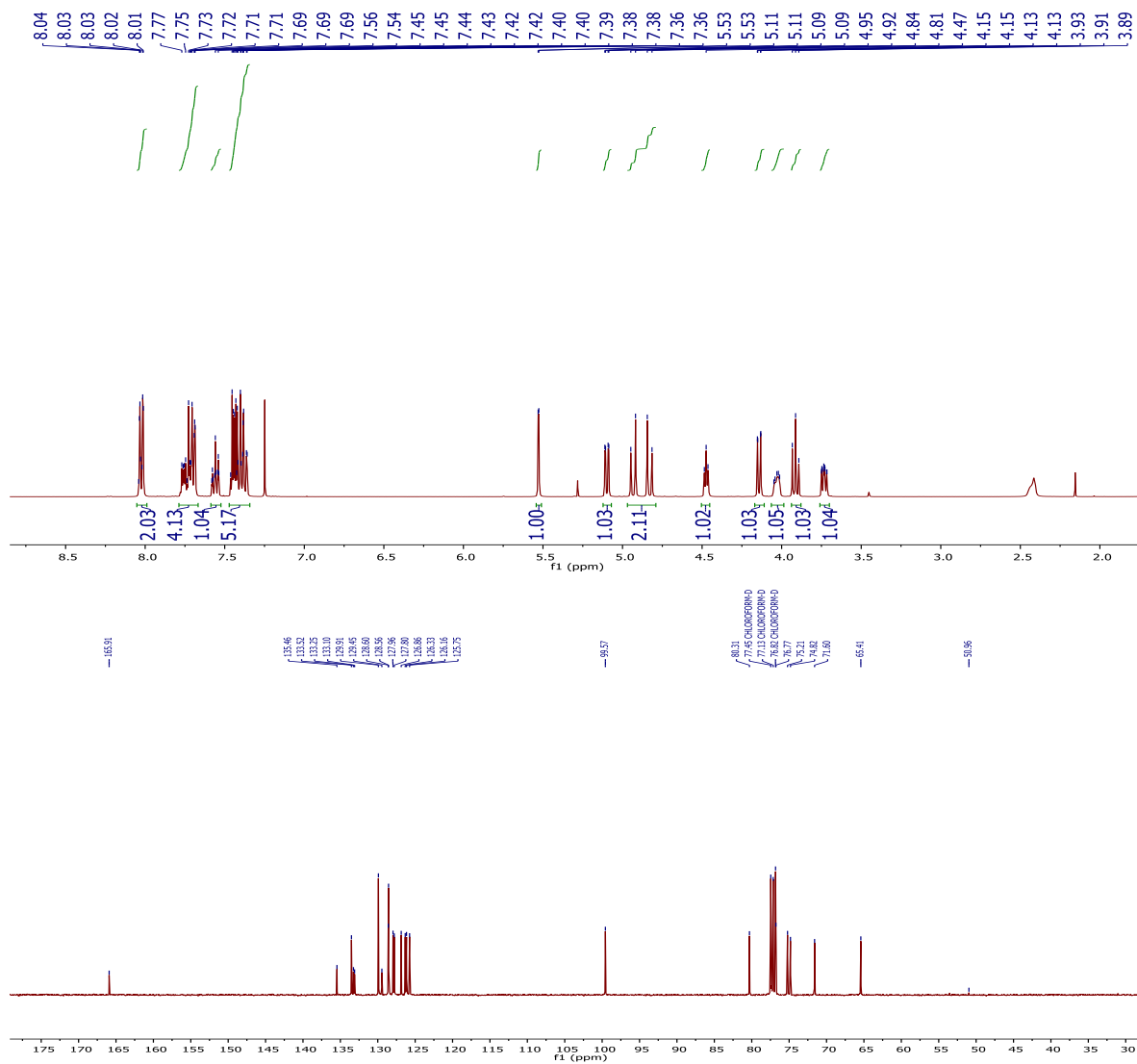


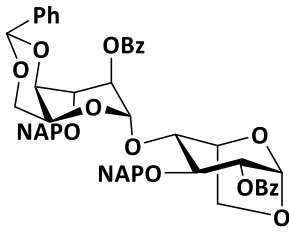
7



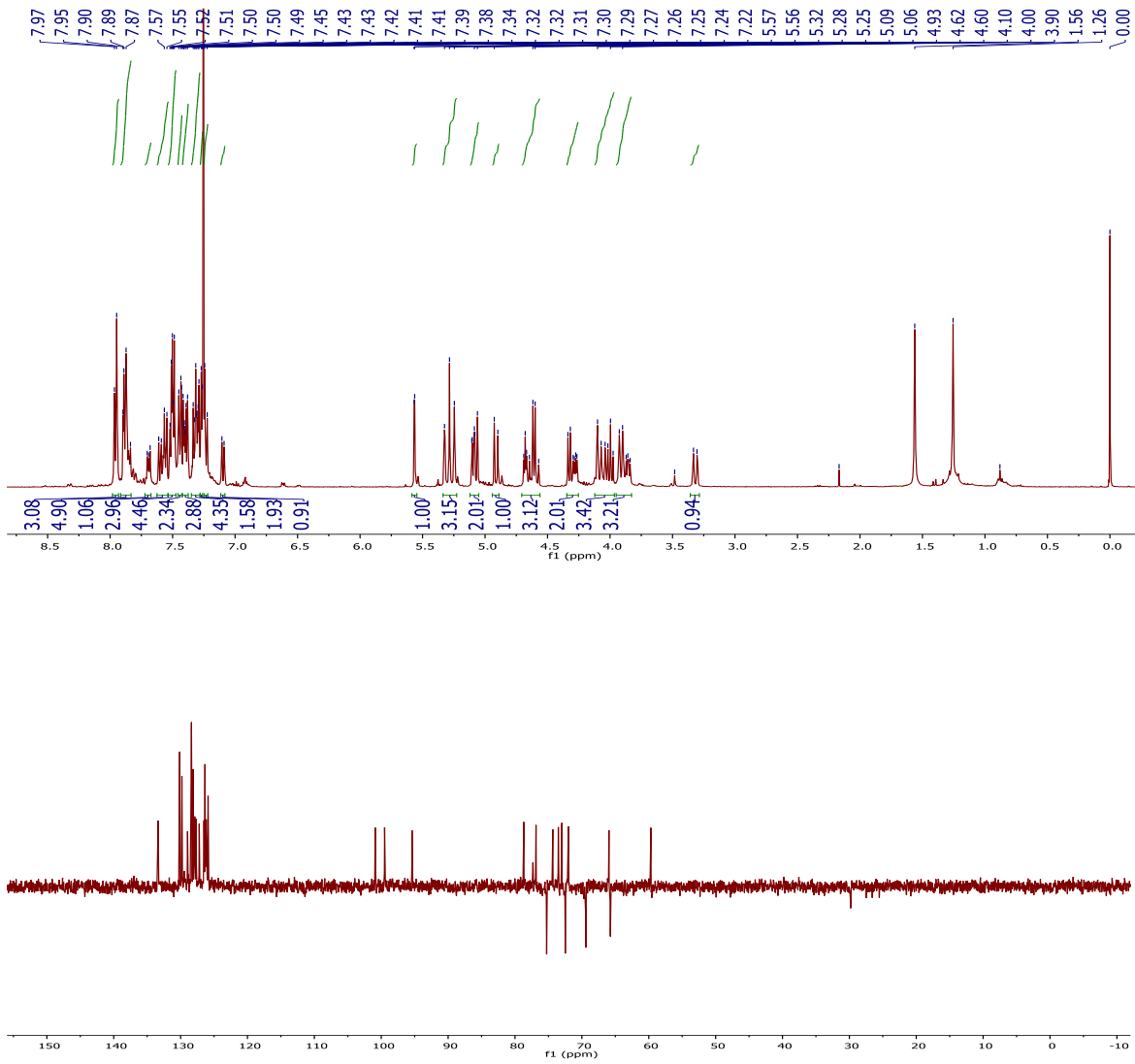


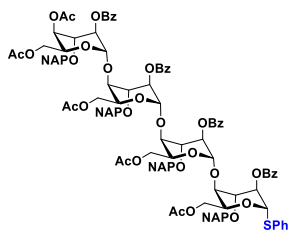
8



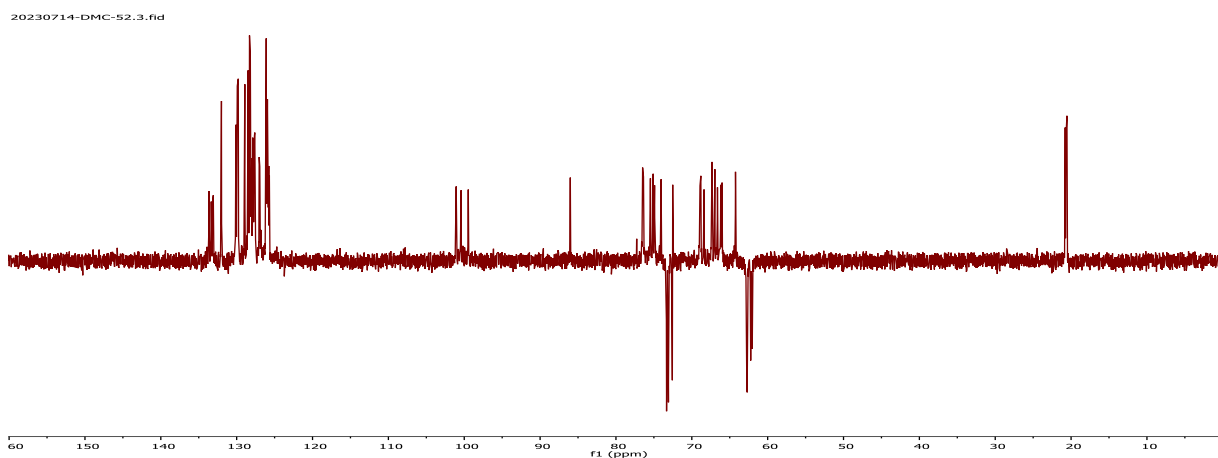
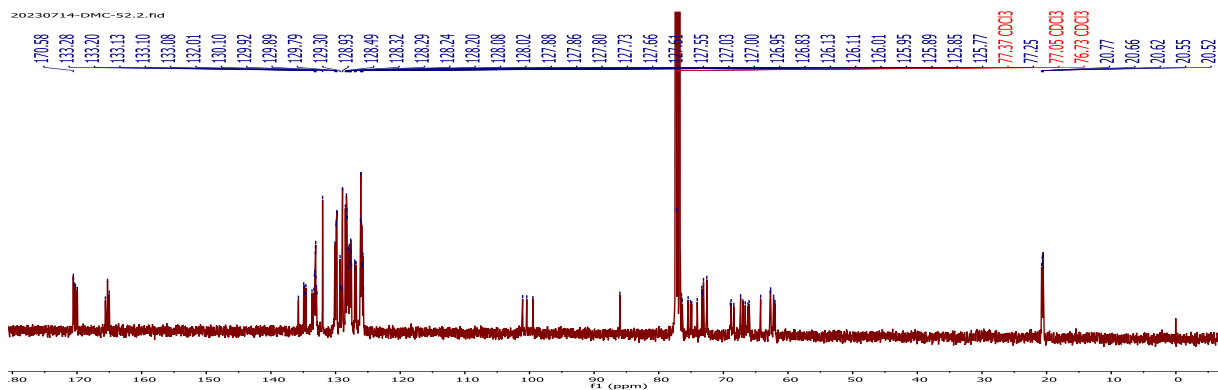
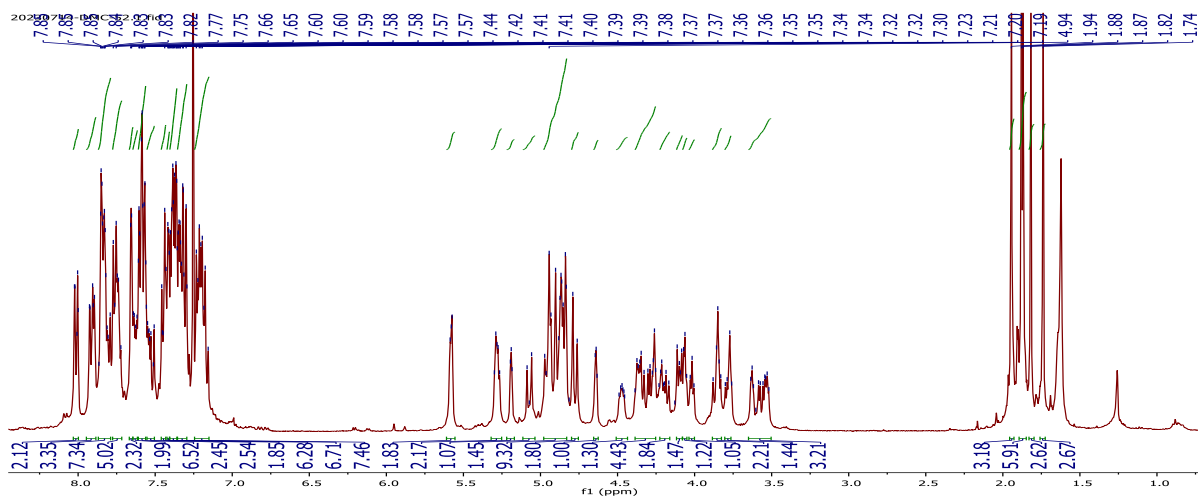


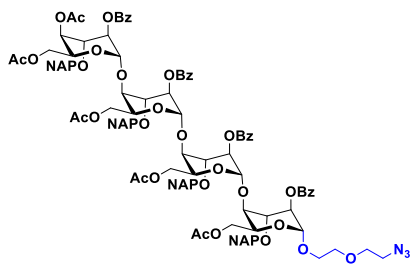
11



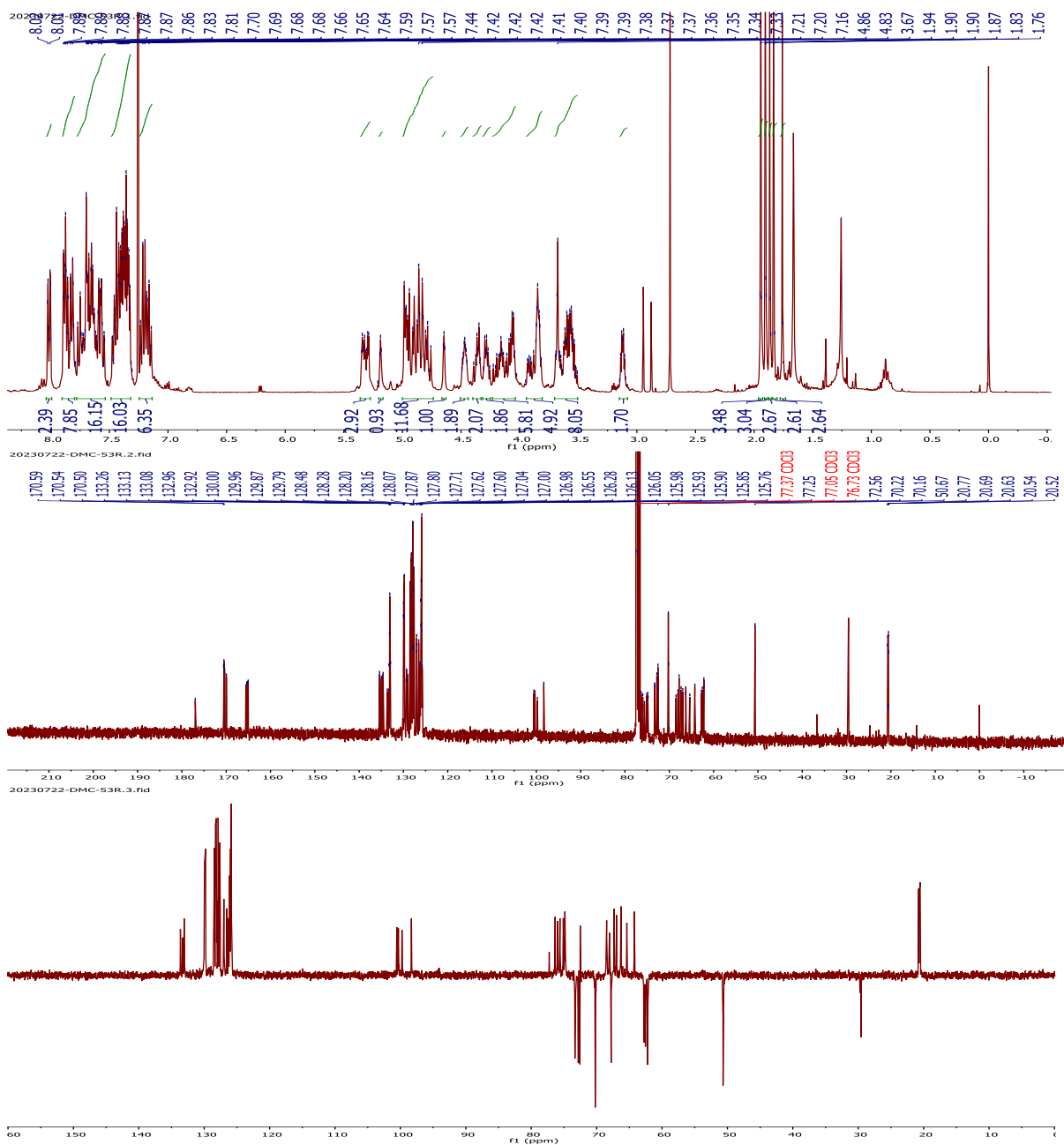


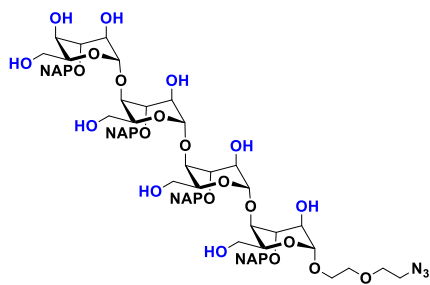
18



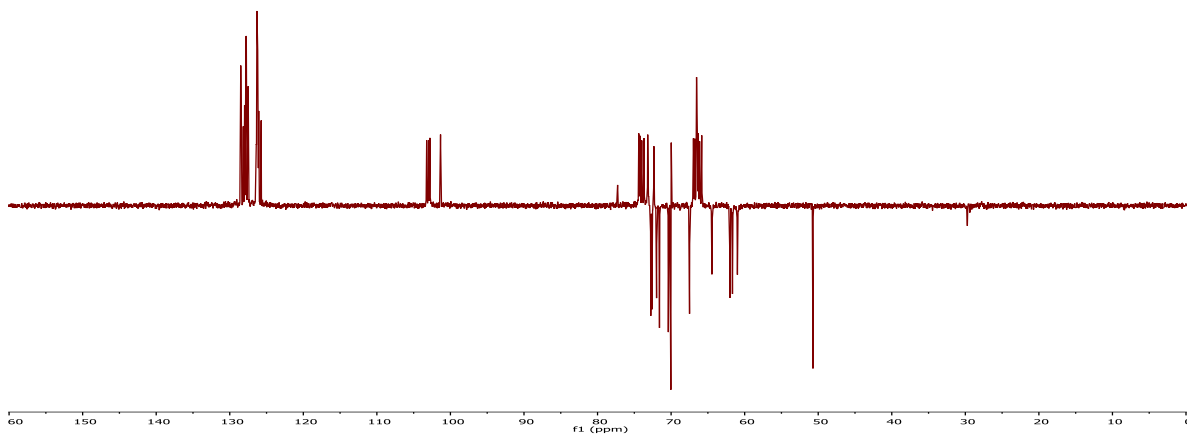
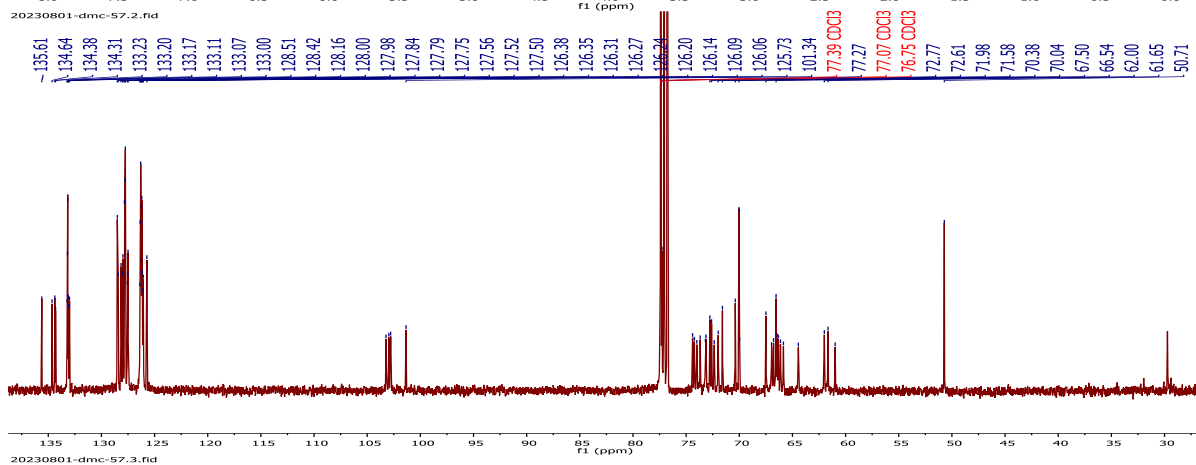
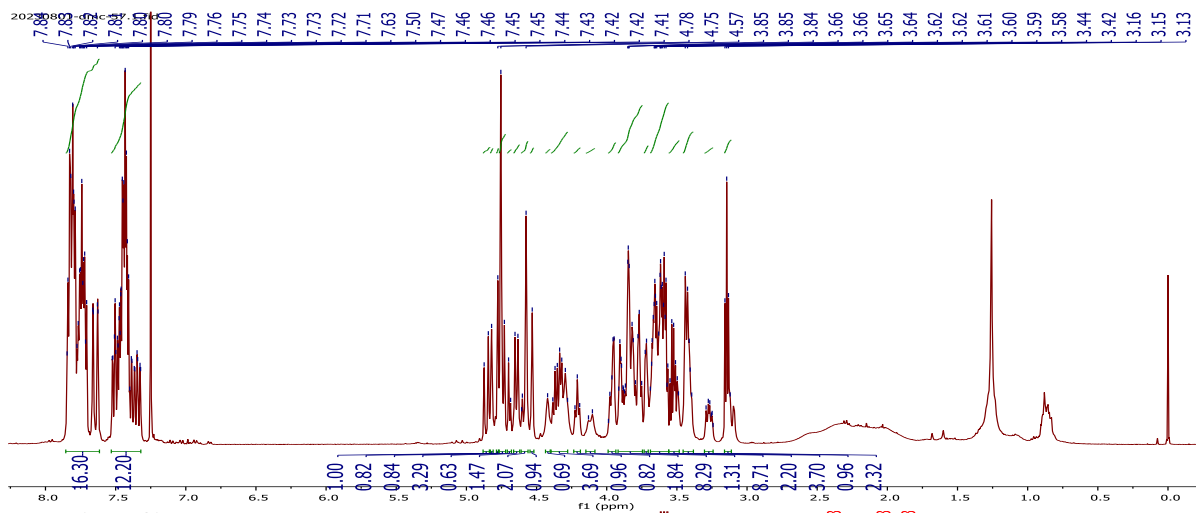


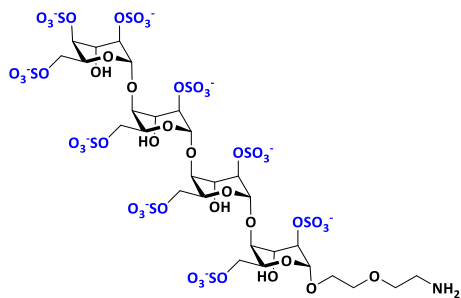
19



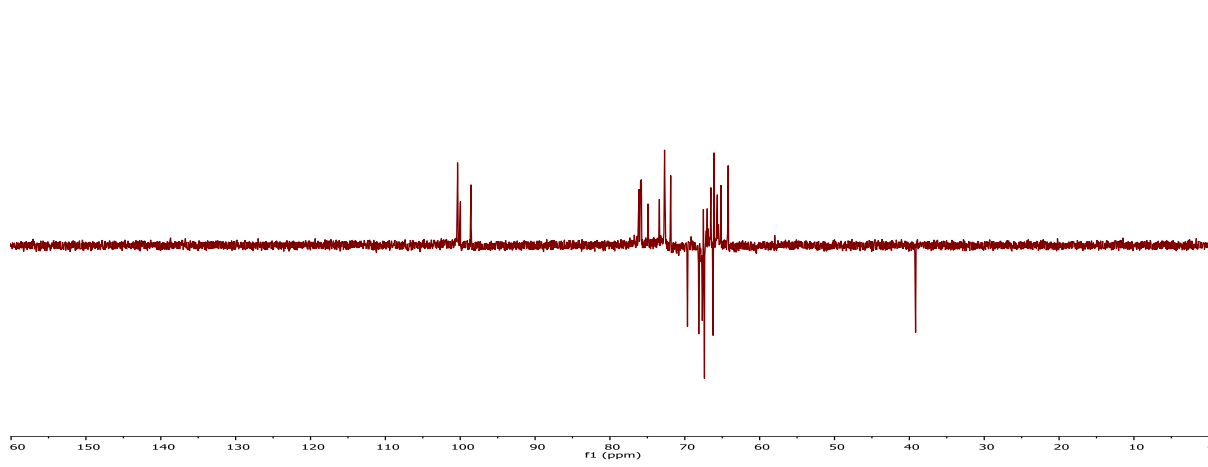
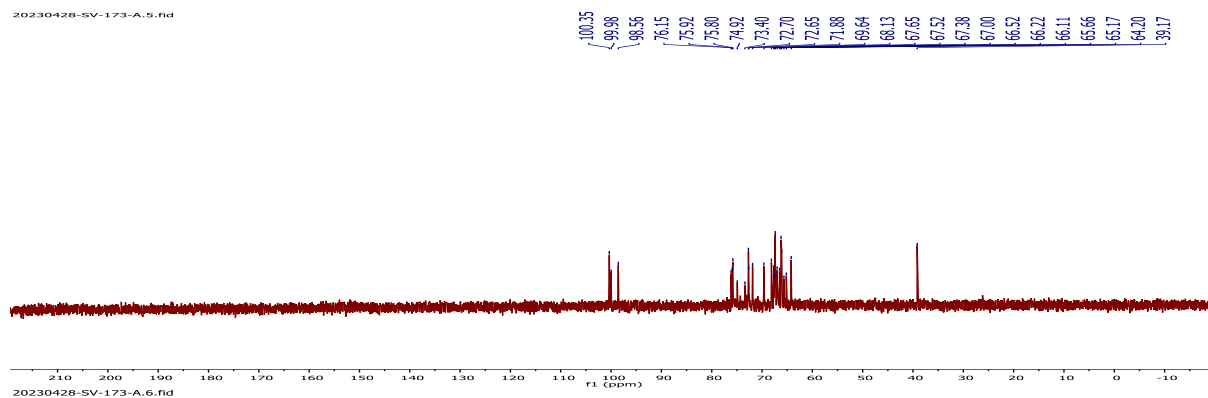
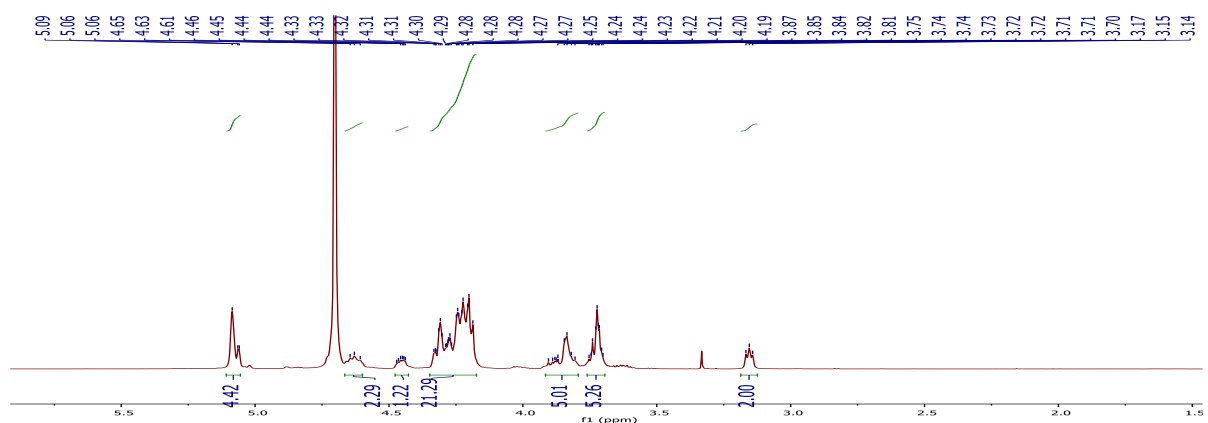


20





22



CHAPTER-3

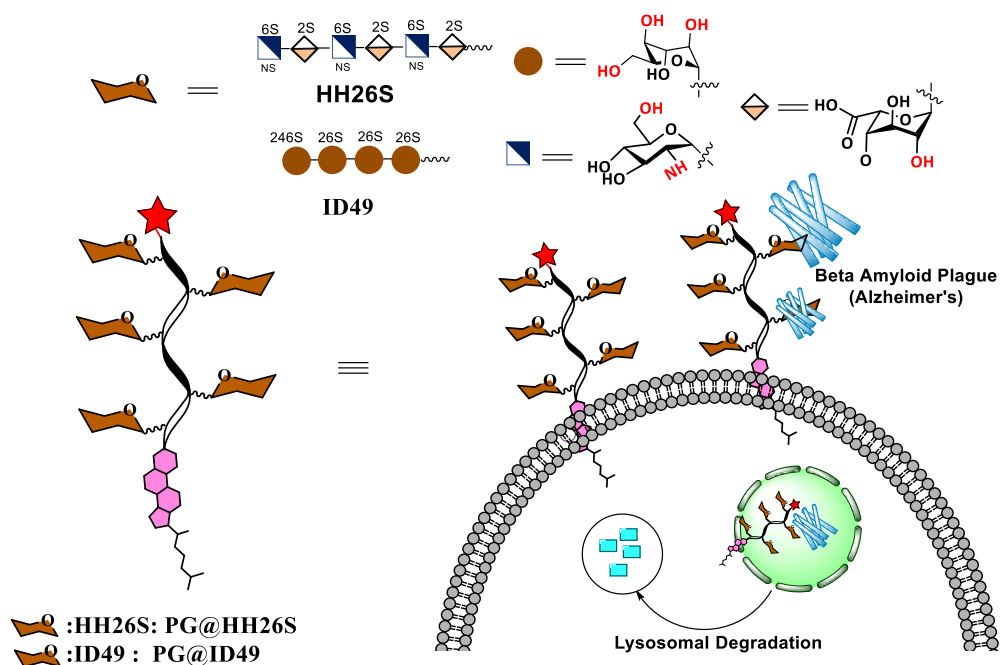
**Heparan Sulfate Neoproteoglycan Promotes
Lysosome Targeting Chimeras of Amyloid- β
Protein.**

Abstract

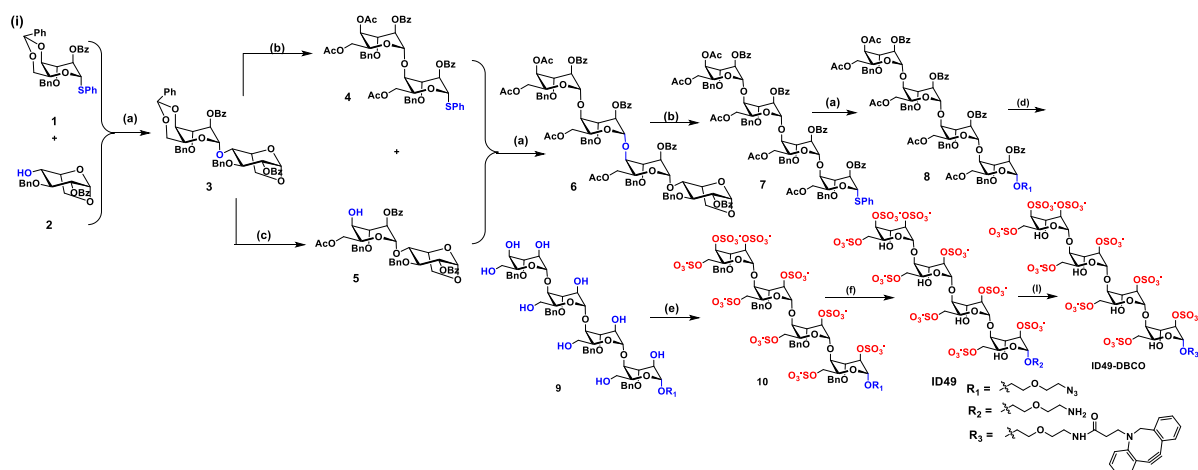
Lysosome targeting chimaeras (LYTAC) represent a promising strategy for clearing unwanted toxic extracellular and membrane proteins. However, challenges include the identification of potential ligands for these proteins and the lysosome-driving module. Herein, we developed the first synthetic heparan sulfate-based neoproteoglycan modular system that anchors on the cell membrane for an extended period to pull the amyloid-beta ($A\beta$) into the lysosomal compartment for degradation. We have identified sulfated oligo L-Idose tetrasaccharide (**ID49**) and heparan sulfate hexasaccharides (**HH26S**) as potential micromolar range ligands for $A\beta(1-42)$ peptide. When these molecules are expressed on the peptide-based fluorescent neoproteoglycan backbone, **PG@HH26S** persist on the cell membrane and facilitate the $A\beta(1-42)$ endocytosis to the lysosomal compartment and subsequent degradation. Overall, neoproteoglycan open a new avenue to generate LYTAC platforms for degrading plethora of HS binding proteins, including growth factor (receptor)s, morphogens and toxic secreted proteins in the future.

3.1 Introduction

Alzheimer's disease (AD) is a progressive neurodegenerative disorder that has significantly impacted the lives of millions globally.¹ Despite the approval of drugs such as aducanumab, lecanemab, and donanemab,² AD continues to be a major global health challenge. With the rapid increase in the incidence of AD, especially among the elderly population, there is a critical need to investigate alternative treatment methods. Studies on AD have revealed that the formation of neuritic plaques composed of Amyloid β -peptide ($A\beta$) and the toxicity regulated by these aggregates are major hallmarks of the condition.³⁻⁴ Consequently, significant efforts have been made to develop small molecule inhibitors for $A\beta$ aggregates.⁵⁻⁸ Alternatively, targeted protein degradation (TPD) represents a potent strategy to degrade selective protein aggregates in the brain for treating AD. TPD approaches, such as proteolysis-targeting chimeras (PROTACs) and molecular glues, exploit selective protein inhibitors and the ubiquitin-proteasome system to design small molecule probes.⁹⁻¹¹ Nevertheless, designing TPD for $A\beta$ plaques is particularly challenging due to their extracellular aggregation.¹² Consequently, researchers have opted alternate strategies involving targeting of $A\beta$ cross-interacting proteins to create TPD models.



Scheme 1. Lysosomal-targeting chimera of $A\beta$ aggregates using neoproteoglycans.



Scheme 2. (I) Synthesis of ID49 : Reagents and Conditions: (a) NIS TMSOTf, 4Å M.S., -10°C, 90% (3); 55% (6); R₁ Linker, 63% (8); (b) i) Cu(OTf)₂, Ac₂O, 0°C, 90%; ii) ZnI₂, TMSSPh, DCM, 85% (4) 80% (7); (c) i) p-TSA, MeOH/DCM (2/1) 77%; ii) Ac₂O, TEA, DCM, 0°C, 75% (d) i) LiOH, THF/MeOH/H₂O (4/2/1), 0°C, 70%; (e) SO₃.NMe₃, DMF, 60°C, 90%; (f) Pd(OH)₂/C/H₂, H₂O, 79%;

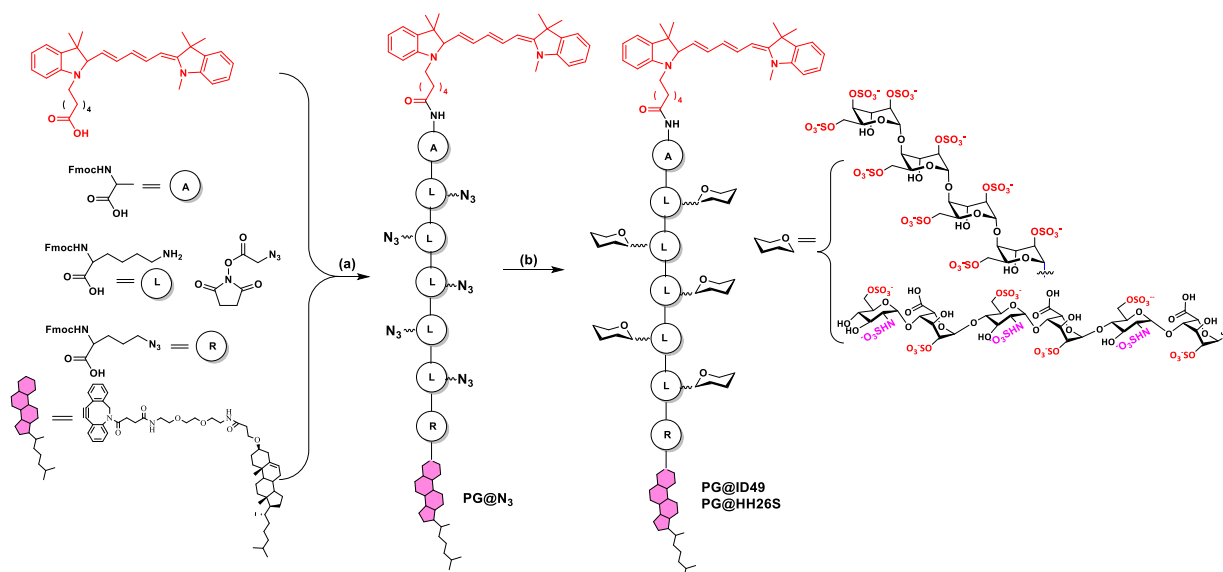
For example, PROTACs have been used to target tau protein, leading to a reduction in amyloid-beta (Aβ) aggregates, as tau aggregates cross-interact with Aβ aggregates.¹³ Similarly, PROTACs have targeted tau phosphorylating kinases, such as glycogen synthase kinase-3, to decrease tau phosphorylation and the subsequent production of Aβ peptides.¹⁴ While, TRAFACs (transcription factors targeted degradation chimeras) were designed to inhibit Aβ-mediated activation of transcription factors such as NF-κB and FoxOs.¹⁵⁻¹⁶ Additionally, the cross-interaction between Aβ and transthyretin (TTR) was targeted to develop a targeted protein stabilization system, deubiquitinase-target chimera (DUBTAC), aimed at enhancing the stability of the tetrameric form of the TTR protein and improving the clearance of Aβ aggregates.¹⁷ Although TRAFACs, DECTACs, and PROTACs have shown potential for treating AD, their indirect ability to target Aβ aggregates lessens their efficacy in AD applications. In contrast, lysosomal targeting chimeras (LYTACs) have emerged as a promising strategy for targeting extracellular and membrane proteins degradation.¹⁸⁻²⁵ Bertozzi et al. previously demonstrated that LYTAC-mediated degradation of apolipoprotein E4 and other membrane proteins reduces cancer cell proliferation.²⁶⁻²⁸ However, to the best of our knowledge, LYTAC degradation of Aβ has not been reported thus far. Herein, we introduce the first steps towards developing a LYTAC model system based on the heparan sulfate proteoglycan (HSPG) platform to degrade Aβ aggregates (Scheme 1). The choice of the HSPG platform for the LYTAC probe is based on the principle that HSPGs naturally

clear A β aggregates by binding to them and transporting them to lysosomal compartments for degradation, thereby mitigating neurotoxicity.²⁹⁻³¹ Hence, identifying specific HSPG epitopes to regulate protein degradation and modelling them on synthetic backbones is a promising strategy for designing LYTAC probes.

3.2 Results and Discussion

To design an effective HSPG-based LYTAC model, we first need to identify heparan sulfate (HS) ligands suitable for A β binding. HS is a heterogeneous sulfated polymer composed of D-glucosamine and uronic acid based disaccharide repeating units. The structural diversity of HS arises from the sulfation pattern and uronic composition. For example, HS tetrasaccharide can be assembled into 2,304 combinations.³² Previously, Hung et al. showed that a highly sulfated *N*-sulfated ligand with a minimum hexasaccharide length (**HH26S**) is suitable for A β binding.³³⁻³⁶ Accordingly, we synthesized **HH26S** and HS mimetics (**ID49**) carrying the same charge density (+9) to determine how the structural heterogeneity and conserved charge composition modulate A β binding and LYTAC modeling.

ID49 was synthesized from L-idose monosaccharide donor **1** and acceptor **2** (Scheme 2(i)), which were derived from 1,6-anhydro- β -L-idopyranosyl-4-alcohol as previously described.³⁷⁻⁴⁰ The glycosylation of compounds **1** and **2** in the presence of *N*-iodosuccinimide (NIS) and a catalytic amount of trimethylsilyl trifluoromethanesulfonate (TMSOTf) in DCM at -10°C yielded 90% of compound **3**. Compound **3** was converted into disaccharide donor **4** by a one-pot anhydrous ring opening and acetylation using copper(II) trifluoromethanesulfonate (Cu(OTf)₂) in the presence of acetic anhydride, followed by treatment with trimethyl(phenylthio)silane (TMSSPh) in the presence of ZnI₂ in DCM at room temperature. Compound **3** was also converted into an acceptor by treatment with *p*-TSA in MeOH/DCM (2/1) to obtain benzylidene-protected disaccharide, which was then subjected to selective acetylation, yielding 73% (over 2 steps) of compound **5**. Glycosylation of donor **4** with acceptor **5** in the presence of NIS and a catalytic amount of TMSOTf in DCM at -10°C yielded compound **6**, which was subsequently converted into thiophenol donor **7** using Cu(OTf)₂ and TMSSPh/ZnI₂. Tetrasaccharide donor **7** was then glycosylated with an azidoethoxyethanol linker to yield compound **8**. Lithium hydroxide (LiOH) mediated deacetylation and debenzoylation of compound **8** yielded 70% of **9**, which was sulfated in the presence of sulfur trioxide trimethylamine



Scheme 3. Synthesis of neoproteoglycan carrying HH26S and ID49 ligands. (a) Rink amide resin peptide synthesis; (b) HH26S-DBCO or ID49-DBCO in DMF at RT for 7 days complex in DMF at 60°C, yielded compound **10**. which was then subjected to hydrogenation, resulting in a 65% yield of the **ID49** ligand.

Comp	n	K_D (μM)	ΔH (cal/mol)	ΔS (cal/mol/deg)
ID49	1.87 ± 0.205	9.44 ± 7.41	-2.88 ± 0.616	-6.86
HH26S	2.07 ± 0.310	10.9 ± 10.3	-2.06 ± 0.574	-6.77

Table 1. ITC data for ID49 and HH26S with A β 1-42 (0.05 mM). Data are the average of 3 titrations \pm SD.

To validate the binding affinity and specificity of the native and heparin mimetics with the A β peptide, isothermal titration calorimetry (ITC) experiments were performed using **HH26S** and **ID49** with A β 1-42 in a 0.05 mM pH 5.6 sodium acetate buffer.⁴⁸ The ITC measurements indicated similar binding affinities, with dissociation constants (K_D) of 9.44 and 10.9 μM , respectively (Table 1, Figure 3). These results suggest that highly sulfated ligands are preferred for A β binding. Although **HH26S** and **ID49** have the same charge density, **HH26S** showed a slightly better binding affinity compared to **ID49**. This warrants further investigation of both molecules as potential ligands for LYTAC modelling. Motivated by the

strong binding of both ligand (**ID49** and **HH26S**), we next constructed neoproteoglycans (neoPG: **PG@ID49** and **PG@HH26S**) using **PG@N₃**, which was synthesized as reported previously.³⁷ First **ID49** and **HH26S** ligand was treated with DBCO active ester linker, followed by copper free click reaction using stoichiometric amount of **PG@N₃** and HS ligands for seven days (Scheme 3). Compound was purified by preparative HPLC and characterized by mass spectra and NMR techniques. The purity of the compound was further characterized by analytical HPLC. UV-visible and fluorescent spectra of the final compound was characterized and summarized, as expected both compound showed characteristic peaks of Cy5 with 5-6 nm bathochromic shift compared to the Cy5 as such, indicating the glycoconjugation. Quantum yield of the both compounds was 22.7 and 22.8, compared to atto 655 quantum yield of 30. illustrating the brightness of the probe. Prior to conducting the LYTAC, we examined the potential of **PG@HH26S** and **PG@ID49** in cell surface engineering utilizing MDA-MB-468 and SH-SY-3 breast cancer and glioblastoma cells. The rationale for employing these cell lines stems from literature results that demonstrate the A β ability to inhibit cancer cell proliferation and mitigate the metastasis of breast cancer cells.⁴⁹⁻⁵⁰ A solution of neoPG (1 μ M) was added to the cells and washed after 30 min incubation and confocal images displayed significant difference in the plasma membrane (PM) expression and internalization of the neoPGs.

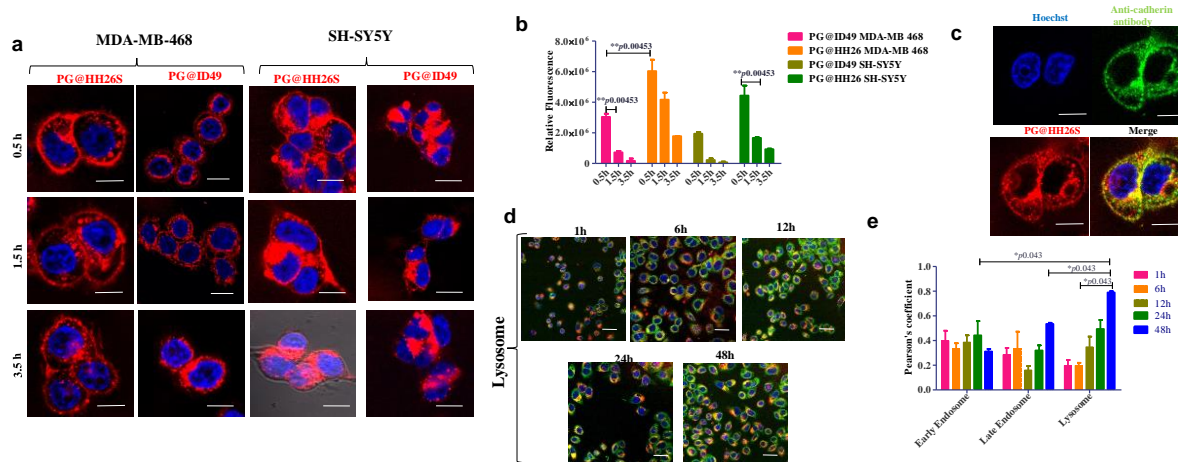


Figure 1. Confocal images illustrating time-dependent uptake of proteoglycan mimic in MDA-MB-468 and SH-Sy-3 cell lines (scale bar 10 μ m); (b) Statistics of cell surface decoration by proteoglycan mimic at differing time intervals; (c) Co-localisation of **PG@HH26S** with anti-cadherin antibody on the cell surface of MDA-MB-468 cells; (d) Co-localisation with lysosomes at differing time intervals; (e) Statistical Pearson's coefficient quantification of **PG@HH26S** in early, late, and lysosomal compartments of MDA-MB-468 cells at differing time intervals (scale bar 10 μ m).

To our surprise **PG@ID49** showed internalization within 30 mins (Figure 1a & 1b), whereas **PG@HH26S** displayed intense fluorescence on PM and continue to express even after 3.5 h in MDA-MB-468 cell line, indicating that native HS structure support cell membrane decoration over its mimetics. We observed a similar trend in SH-SY-3 cell line, but both neoPGs absolutely internalized after 3.5 h, indicating the glycoclayx composition modulate the cell membrane decoration of neoPG. Additionally, it was observed that **PG@HH26S** efficiently labels the cell membrane at a mere 100 nM concentration (Figure4), highlighting the commercial value of the probe. We also found that a reduction in neoPG concentration leads to more prominent cell membrane expression compared to internalisation after 1 h. We validated the decoration of the cell membrane by **PG@HH26S** using co-staining with a green fluorescent anti-cadherin antibody. Figure 1c displays colocalization of green and red fluorescence on the cell membrane and inside the cells, indicating that the **PG@HH26S** managed to draw some cadherin receptors into the cells. Next, we used early, late endosome and lysosomal markers at different time interval (Fig. 1d, 1e &5) to investigate the endocytosis pathway of the **PG@HH26S**. We observed that most of the **PG@HH26S** was sequestered in either early or late endosome in the first 6 h. After that the peptide was repopulated from late endosomal to lysosomal region. After 48 h, **PG@HH26S** was found majorly sequestered in late endosome and lysosomal region. Based on these studies, we hypothesize that **PG@HH26S** could be a potential LYTAC model for targeting A β protein. Inspired by the lysosomal sequestration of neoPG, we then sought to determine if **PG@HH26S** guides the A β aggregate to the lysosomal compartment and induce LYTAC. To achieve this, We first carried out an MTT assay of **PG@HH26S** and A β alone and in combination to evaluate the cytotoxic protection ability of neoPG against A β . As shown in Figure 2a, A β induced toxicity within the range of 15-30 μ M in the MDA-MB-468 cell line, whereas **PG@HH26S** demonstrated the least toxicity even at 20 μ M concentration (Fig 2b). We then mixed 30 μ M of A β with different concentrations of **PG@HH26S** peptide, hoping that neoPG binds to A β and reduce the toxicity by degrading the peptide. Figure 2c clearly illustrate that 2 μ M onward was effectively block the toxicity of A β . Overall, **PG@HH26S** showed promising results in blocking the cytotoxicity of the A β . Next, to understand the mechanism of mitigate the A β toxicity by neoPG, we examined confocal images of **PG@HH26S** (500 nM) and FITC-labelled A β (2 μ M) at various time intervals. Here, we used lower concentration of neoPG and A β compared to MTT assay, which facilitated a clearer visualisation of the endocytosis process. The colocalization is expected to reveal the molecular-level interaction between the neoproteoglycan and A β peptide. As

expected, following incubation for 1 h, we noted a promising colocalization of PG@HH26S and the A β peptide at the plasma membrane (Fig 2a). Performing the assay without neoPG for 1 hour showed no green fluorescence of the A β peptide either on the cell membrane or inside the cells (Fig 2d), suggesting that PG@HH26S is necessary for the cell membrane arrangement of the A β internalization (Fig 2d & 2f). As depicted in Figure 2d, with increasing time, the colocalisation of PG@HH26S and A β was observed both on the cell membrane and inside the cells. Pearson coefficient measurements at different time intervals showed that PG@HH26S facilitated A β peptide binding and endocytosis. Without PG@HH26S, only a small fraction of the peptide was detected inside the cells after 4 hours (Fig 2e). These results clearly indicate that the molecular-level interaction between the hexasaccharide ligand of PG@HH26S and the A β peptide is vital for driving the peptide into the cell.

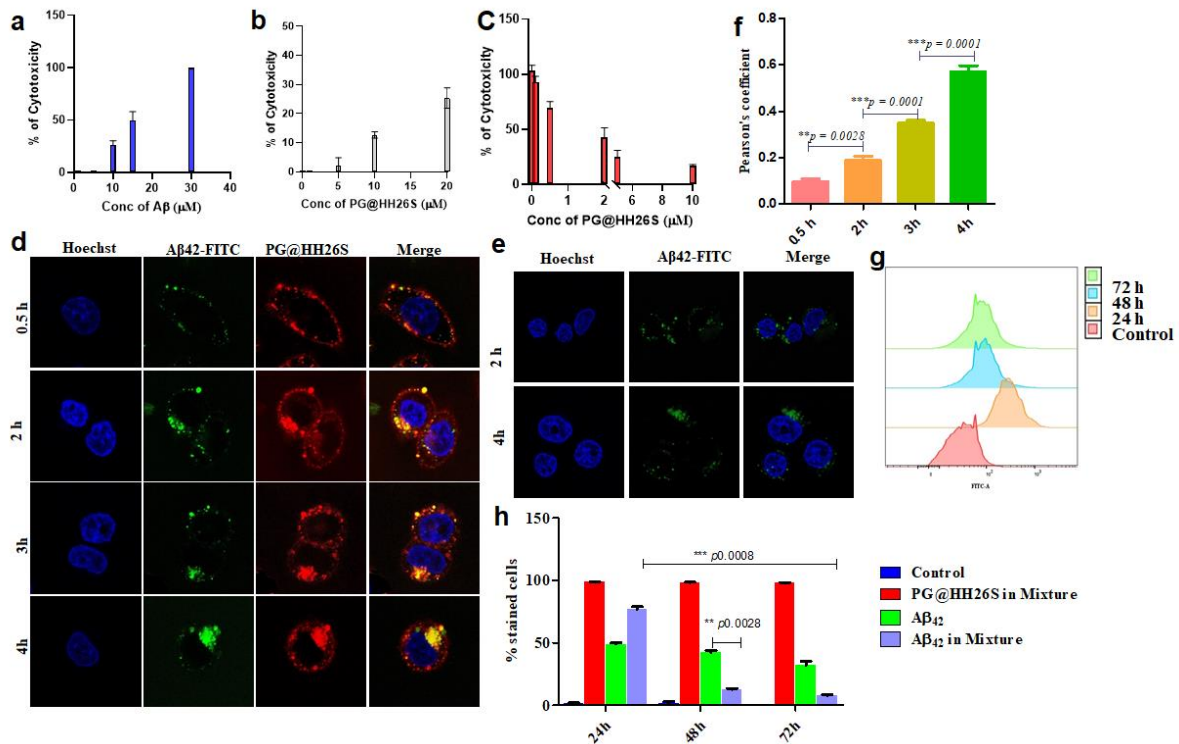


Figure 2. (a) Cytotoxicity of A β peptide to MDA-MB-468 cells after 48 hours of incubation; (b) Cytotoxicity induced by **PG@HH26S** to MDA-MB-468 cells following 48 hours of incubation; (c) Cytotoxicity induced by A β (30 μ M) in the presence of **PG@HH26S** at different levels; (d) Confocal images for LYTAC of FITC-A β in the presence of **PG@HH26S** at various times (0.5 - 4 hours) in MDA-MB-468 cells (Scale bar = 10 μ m); (e) Confocal images for FITC-A β in the absence of **PG@HH26S** after 2 hours and 4 hours respectively; (f) Pearson's coefficient for the co-localisation of **PG@HH26S** and FITC-A β ;

(g) FACS data for LYTAC of beta-amyloid FITC-A β in the presence of **PG@HH26S** at different time points; (h) Quantification of FACS data.

Next, we sought to determine whether the driven peptide undergoes LYTAC. We quantified the LYTAC of the peptide through FACS measurements taken at different time intervals (24 h, 48 h, and 72 h) (Fig 2g, 2h & 6). The FACS quantification data indicated that the A β peptide underwent LYTAC over time, with a notable amount decrease in the FITC fluorescent of peptide after 48 h. Whereas, A β peptide without **PG@HH26S** showed slow degree of LYTAC, indicating the **PG@HH26S** enhance the LYTAC compared to native proteoglycans. Interestingly, **PG@HH26S** did not undergo fragmentation even after 72 hours. These findings are consistent

with those of Bertozzi et al.,⁵¹ where it was shown that neoproteoglycan peptides are prone to recycling and are expressed on the cell membrane. Overall, our findings clearly reveal that **PG@HH26S** not only binds to the A β peptide but also has LYTAC potential of A β peptide.

3.3 Conclusion

To summarize, we have successfully demonstrated a novel synthetic heparan sulfate-based LYTAC platform that functions independent of antibody conjugation, making it applicable in any environment. As a prototype, we used HS hexasaccharide (**HH26S**) and a sulphated Oligo-L-idose (**ID49**) peptide conjugated system for A β binding and A β -LYTAC. We have demonstrated that native HS ligands carrying peptide (**PG@HH26S**) has greater potential to be expressed on the cell membrane compared to their mimetics (**PG@ID49**). Cytotoxicity assay, confocal and FACS measurement successfully demonstrated A β targeted degradation *via* lysosomal pathway. HS serves as a ligand for more than 500 proteins, playing a role in numerous pathological conditions.⁵²⁻⁵³ The targeted degradation of HS-binding proteins using synthetic neoproteoglycan backbone is critically needed for various therapeutic and clinical applications. We are currently in the process of expanding this LYTAC platform.

3.4 Experimental Part

3.4.1 General Information

All chemicals were reagent grade and used without further purification unless otherwise noted. Reactions were carried out in anhydrous solvents under a nitrogen atmosphere. Reaction progress was monitored by analytical thin-layer chromatography (TLC) on Merck silica gel 60 F₂₅₄. Spots on TLC plate were visualized under UV light or by dipping the TLC

plate in CAM/ninhydrin solution followed by heating. Column chromatography was carried out using Flukakieselgel 60 (230-400 mesh). ^1H and ^{13}C NMR spectra of compounds were measured with Bruker 400 MHz, Bruker 600 MHz and Jeol 400 MHz using residual solvents as an internal reference (CDCl_3 δH 7.26 ppm, δC 77.3 ppm, CD_3OD δH 3.31 ppm, δC 49.0 ppm, and D_2O δH 4.79 ppm). The chemical shifts (δ) are reported in ppm and coupling constants (J) in Hz. UV-visible measurements were performed with Evolution 300 UV-visible spectrophotometer (Thermo Fisher Scientific, USA). Fluorescence spectra were measured with FluoroMax-4 spectrofluorometer (Horiba Scientific, U.S.A.). All microscopy images were captured using Leica SP8 confocal microscope and processed using Image J software. The fluorescent tagged $\text{A}\beta$ was purchased from (Anaspec, USA) and non-fluorescent $\text{A}\beta$ was purchased from (Biolinkk, Delhi).

3.4.2 Isothermal titration calorimetry(ITC)

The thermodynamic analysis of amyloid- β_{42} ($\text{A}\beta_{42}$) against ID49 and HH26SNS Heparan mimetic oligosaccharides was conducted using an isothermal titration calorimeter (MicroCal PEAQ-ITC). The sample cell contained $\text{A}\beta_{42}$ (0.05mM) in sodium acetate buffer at pH 5.6. and was titrated against sulfated oligosaccharide (1mM) in sodium acetate buffer at pH 5.6. individually. Titrant was added in 2 μL increments, with a 150 s delay between injections. Heat of reaction was measured after each addition of titrant. To ensure thorough mixing of the solutions, the stirring speed was maintained at 750 rotations/min. The cell temperature was held constant at 298 K and nearly three successive titrations were averaged to obtain the ITC curves.

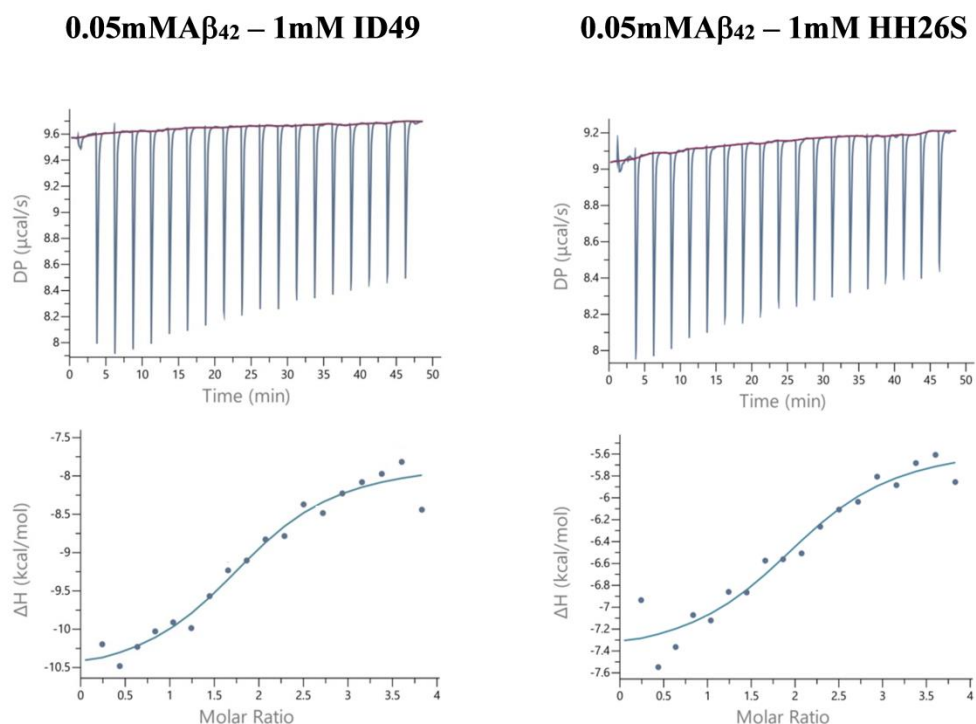


Figure 3:ITC data for ID-49 and HH26S compound.

3.4.3 Synthesis of PG@HH26S and PG@ID49

3.4.3.1 General Procedure for Conjugation of Sugar Molecules

The sugar derivative was dissolved in 400 μL of dry DMF and stirred for 5 minutes. Next, NEt_3 (2 equivalents) was added, followed by dropwise addition of the solution of DBCO-NHS in 400 μL , while stirring at room temperature. After 12 hours, DMF was evaporated, and the crude product was purified using LH-20 size exclusion chromatography. Then, a compound with an azide linker (1 eq.) was dissolved in 500 μL of CHCl_3 and 500 μL of MeOH. Subsequently, a solution of sugar molecules (1.2 eq. per azide of peptide) in H_2O (1 mL) was added, followed by the addition of another 500 μL of MeOH. The resulting solution was stirred for 7 – 8 days at room temperature. The progress of the reaction was monitored by infrared spectroscopy (IR). After the completion of the reaction (approximately 7 - 8 days), the solvent was evaporated under reduced pressure and first purified using 10kD cutoff filter followed by purification using HPLC (MeOH: H_2O). The compound was characterized using ^1H NMR, IR, HR-ESI-MS. The purity of compound was checked using reverse-phase high-performance liquid chromatography (HPLC) using (95% H_2O + 5% MeOH) and (95% MeOH + 5% H_2O) at the flow rate of 0.5mL/min.

PG@HH26S

The compound was characterized using ^1H NMR, IR and HR-ESI-MS (m/z): $[\text{M}/44]^-$, calcd is 299.9601; found, 299.9444. The purity of compound was checked using reverse-phase high performance liquid chromatography (HPLC) the elution time is ~ 12.4 min.

PG@ID49

The compound was characterized using ^1H NMR, IR and HR-ESI-MS (m/z): $[\text{M}/44]^-$, calcd is ; found 255.2322. The purity of compound was checked using reverse-phase high performance liquid chromatography (HPLC) the elution time is ~ 12.7 min.

3.4.4 Cell surface engineering studies:

A total of 20,000 cells were seeded into 8-well confocal imaging plates and incubated overnight at 37°C . The next day, the cells were treated with **PG@ID49** and **PG@HH26S** ($1\ \mu\text{M}$ to $100\ \text{nM}$ each) for 30 minutes. After treatment, the cells were washed three times with PBS, and the nuclei were stained with Hoechst 33342. Following the staining, fresh media was added, and fluorescent images were captured using a Leica SP8 microscope.

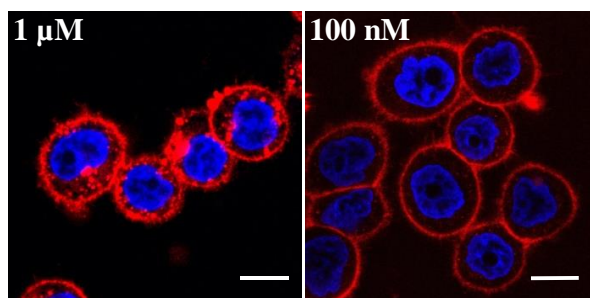


Figure 4. Confocal images of **PG@HH26S** at different dilution (scale bar $10\ \mu\text{m}$).

3.4.5 Co-localization studies:

To study the cellular co-localization of **PG@HH26S**, MDA-MB 468 cells were grown on cover glass (10,000 cells per well) overnight. The cells were treated with $1\ \mu\text{M}$ **PG@HH26S** for various time intervals (1 to 48 hours), followed by treatment with different organelle markers. For lysosome labelling, the cells were treated with Lyso Green for 1 hour at 37°C , followed by staining with Hoechst for 10 minutes. The cells were then fixed with 4% paraformaldehyde and the glass slides were mounted.

For early and late endosome co-localization, the cells were first fixed with 4% paraformaldehyde, then permeabilized with 0.1% Triton X-100 for 10 minutes, followed by blocking with 2% BSA for 45 minutes at room temperature. The cells were then labelled with

primary EEA1 and LAMP2 antibodies overnight at 4°C, followed by washing with PBS and treatment with secondary antibody at a 1:2000 dilution for 45 minutes at room temperature. The coverslips were washed and mounted on glass slides for imaging.

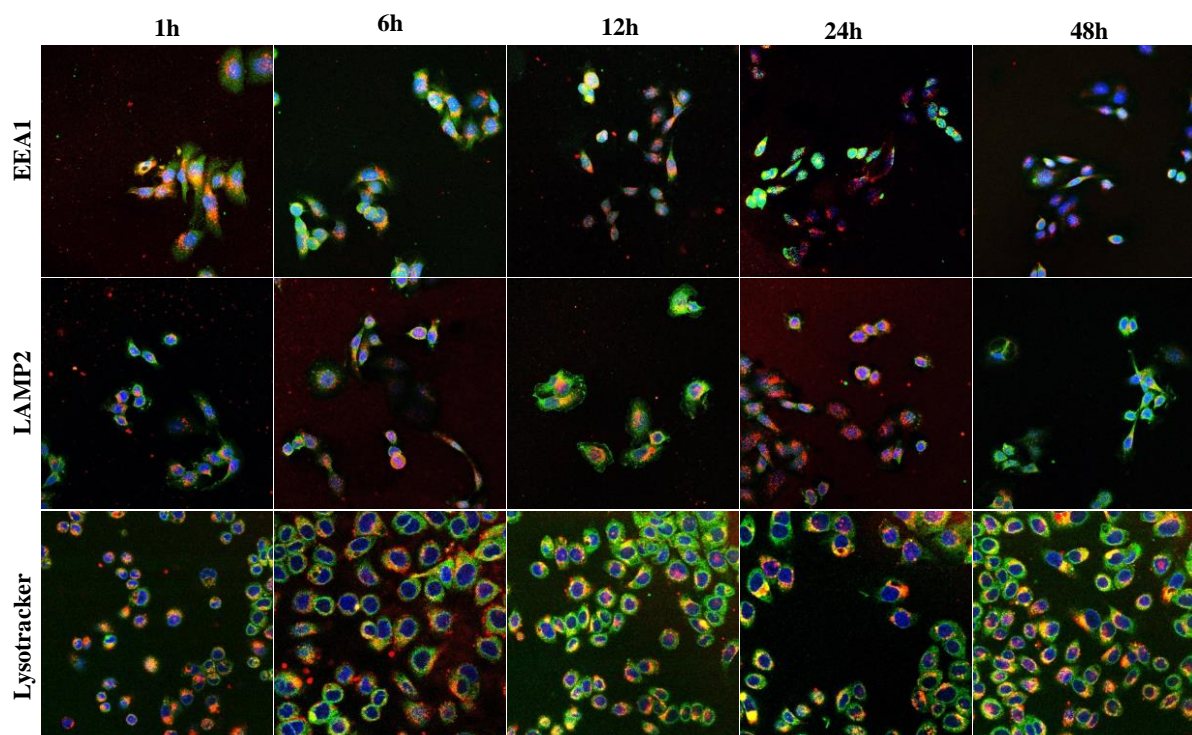


Figure 5. Colocalization of PG@HH26S at different time interval.

3.4.6 MTT assay.

MTT assay was used to check cell proliferation. MDA-MB-468 cells (5×10^3 cells per well) were plated in 96 well plate in DMEM medium and incubated overnight followed by treatment with different concentration of A β (0 – 30 μ M), PG@HH26S (0 - 20 μ M and A β (30 μ M) with different concentration of PG@HH26S (0 – 10 μ M) and further incubation for 48 h. Afterward 10 μ l of MTT (5 mg/ml) reagent was added to each well and incubated plates further for 4h at 37 °C. Purple precipitate formed was dissolved by adding 100 μ l of DMSO and plate was read at 570 nm.

3.4.7 Confocal imaging of Lysosomal degradation chimera of A β (1-42).

A total of 20,000 cells were seeded into 8-well confocal imaging plates and incubated overnight at 37°C. The next day, the cells were treated with FITC-A β 1-42 (2 μ M) followed by PG@HH26S (1 μ M) for 30 minutes. After treatment, the cells were washed three times with PBS, and the nuclei were stained with Hoechst 33342. Following the staining, fresh media was added, and fluorescent images were captured using a Leica SP8 microscope.

3.4.8 FACS Study.

MDA-MB 468 cells (1×10^6 cells per well) were seeded in 6 well tissue culture plate and incubated at 37 °C overnight. Cells treated with **PG@HH26S** ($1 \mu\text{M}$) for 1 h followed by washing and then treated with FITC-A β_{1-42} ($2 \mu\text{M}$) and continued incubation at 37 °C for different time intervals. On completion of incubation cells were washed with PBS and fixed with 4% paraformaldehyde at room temperature for 15 min followed by washing with PBS. Finally, cells were suspended in FACS buffer taken for the analysis.

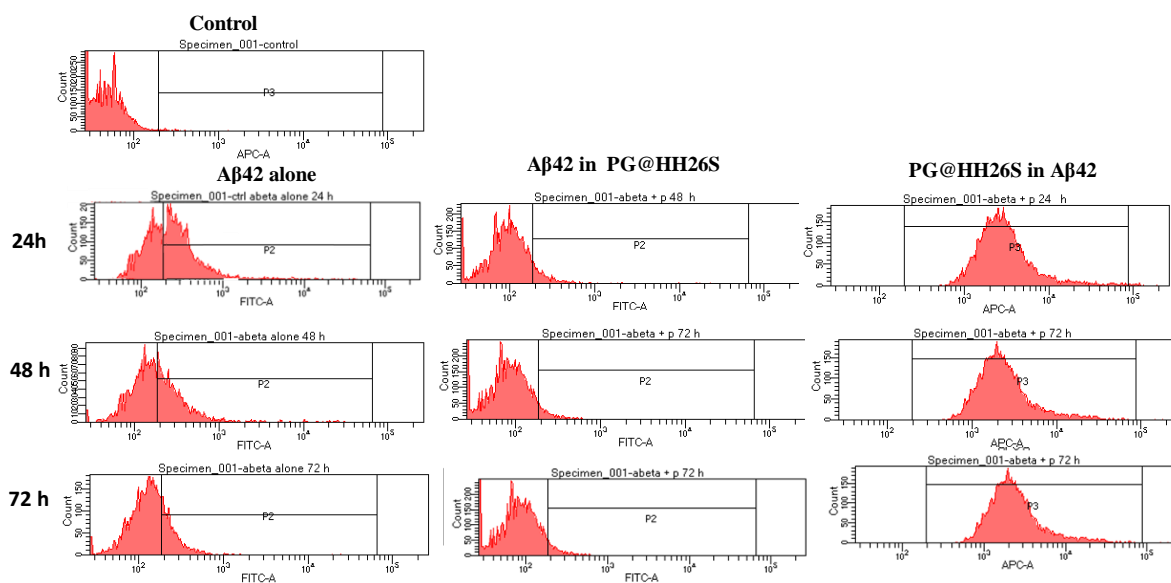
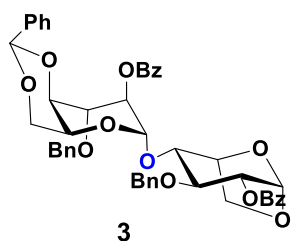


Figure 6: FACS data for LYTAC of A β in MDA-MB468 cells

3.4.9 Synthesis of ID49 tetrasaccharide

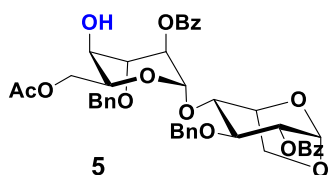
(4,6-benzylidiny-2-benzoyl-3-O-benzyl)- α -L-idopyranosyl- α (1 \rightarrow 4)(2-O-benzoyl-3-O-benzyl-1,6-anhydro)- β -L-idopyranoside(3).



Monosaccharide donor **1** (1 g, 1.80 mmol), acceptor **2** (0.514 g, 1.44 mmol) and freshly dried 4 Å molecular sieves were taken in round bottom flask and was dissolved in dry DCM in 10 volumes, kept for stirring for 2h under N₂ atmosphere. Then reaction mixture was cooled to -10 °C. Further, TMSOTf (65 μl , 0.360 mmol) and NIS (0.527 g, 2.345 mmol) were added and kept for stirring. The reaction completion was monitored by TLC, after completion of reaction, it was neutralized with triethylamine Et₃N and did celite filtration and subsequently did sodium thiosulfate Na₂S₂O₃ workup and dried over Na₂SO₄. Purification was done by silica column in EtOAc/Hexane solvent system to get compound **3** in a 90%

yield. ¹H NMR (400 MHz, Chloroform-*d*) 5.56 (d, *J* = 1.7 Hz, 1H), 5.44 (s, 1H), 5.33 – 5.18 (m, 2H), 5.09 (dd, *J* = 8.3, 1.8 Hz, 1H), 4.89 (d, *J* = 11.5 Hz, 1H), 4.74 (d, *J* = 11.5 Hz, 1H), 4.64 (t, *J* = 4.5 Hz, 1H), 4.59 – 4.47 (m, 2H), 4.31 – 4.19 (m, 2H), 4.07 (td, *J* = 6.5, 5.8, 1.6 Hz, 2H), 3.97 – 3.78 (m, 4H) 3.48 (dd, *J* = 13.0, 2.0 Hz, 1H), 7.99 (ddd, *J* = 30.4, 8.2, 1.4 Hz, 4H), 7.61 – 7.54 (m, 1H), 7.53 – 7.37 (m, 9H), 7.36 – 7.16 (m, 9H), 7.08 (dd, *J* = 6.6, 3.0 Hz, 2H) ¹³C NMR (101 MHz, Chloroform-*d*) δ 165.87, 138.06, 137.62, 133.38, 133.33, 130.08, 129.87, 128.91, 128.55, 128.48, 128.31, 128.20, 128.16, 128.13, 128.10, 127.87, 127.63, 126.34, 100.90, 99.43, 95.41, 78.47, 76.91, 75.08, 74.26, 73.52, 72.98, 72.25, 71.96, 69.35, 65.85, 65.64, 59.59. HRMS *m/z* calculated for C₄₈H₄₆O₁₁Na, 798.3040; Found 798.3044.

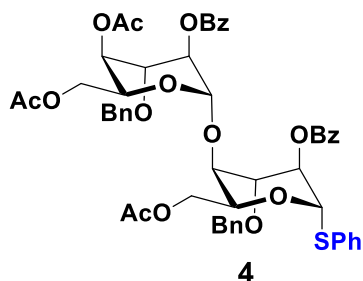
(6-O-acetyl-2-O-benzoyl-3-O-benzyl)-α-L-idopyranosyl-α(1→4)(2-O-benzoyl-3-O-benzyl-1,6-anhydro)-β-L-idopyranoside (5).



Compound **3** (1.143 g, 1.42mmol) was dissolved in DCM/MeOH (2/1) ratio, CSA (0.397 g, 1.71mmol) was added and kept for stirring for 3-4h. The reaction was monitored by TLC, after completion of reaction, reaction mixture was concentrated under reduced pressure. Purification was done without workup by silica column by using EtOAc/Hexane solvent system to get selective benzylidene deprotected intermediate product (no attached NMR). Further, this benzylidene deprotected intermediate product (0.83 g, 1.6mmol) was dissolved in dry DCM in 10 Volume, Ac₂O (1.1 ml, 11.65mmol) and Triethylamine (0.223 ml, 1.6mmol) were added at 0°C and kept for stirring for overnight. The completion of the reaction was monitored by TLC, after completion of reaction, it was quenched with MeOH and did sat. NaHCO₃ workup then dried over Na₂SO₄. Purification was done by silica column in EtOAc/Hexane solvent system to get compound **5** in 65% yield. ¹H NMR (400 MHz, Chloroform-*d*) 5.52 (d, *J* = 1.8 Hz, 1H), 5.18 (dt, *J* = 2.5, 1.1 Hz, 1H), 5.11 (s, 1H), 5.01 (dd, *J* = 8.3, 1.8 Hz, 1H), 4.81 (d, *J* = 11.6 Hz, 1H), 4.72 – 4.61 (m, 3H), 4.59 – 4.49 (m, 2H), 4.25 – 4.18 (m, 2H), 4.15 (dd, *J* = 6.0, 2.0 Hz, 2H), 3.90 (t, *J* = 8.4 Hz, 1H), 3.85 (ddd, *J* = 3.6, 2.6, 1.2 Hz, 1H), 3.78 (ddd, *J* = 7.9, 5.1, 1.2 Hz, 1H), 3.71 (dd, *J* = 10.9, 3.4 Hz, 1H), 2.53 – 2.48 (m, 1H), 1.99 (s, 3H), 8.00 (dd, *J* = 8.4, 1.3 Hz, 2H), 7.94 (dd, *J* = 8.3, 1.3 Hz, 2H), 7.66 – 7.51 (m, 2H), 7.50 – 7.44 (m, 2H), 7.44 – 7.36 (m, 5H), 7.36 – 7.28 (m, 2H), 7.11 – 7.06 (m, 3H), 7.06 – 7.02 (m, 2H) ¹³C NMR (101 MHz, Chloroform-*d*) δ 138.10, 137.45, 133.99, 133.41, 129.94, 129.85, 128.85, 128.66, 128.48, 128.27, 128.21, 128.14, 127.96, 127.55, 99.46, 95.42, 75.20, 75.15, 74.29, 72.58,

71.88, 68.15, 67.10, 66.16, 65.63, 63.38, 20.96. HRMS m/z calculated for $C_{43}H_{44}O_{12}Na$, 752.2833; Found 752.2836.

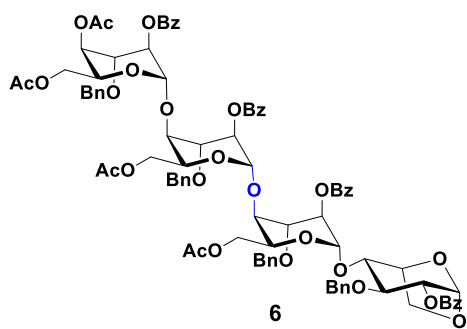
Thiophenyl-((4,6-O-diacetyl-2-O-benzoyl-3-O-benzyl)- α -L-idopyranosyl- α (1 \rightarrow 4))(6-O-acetyl-2-benzoyl-3-O-benzyl))- α -L-idopyranoside(4).



Compound **3** (730 mg, 0.911 mmol) was dissolved in Ac_2O (5 ml), $Cu(OTf)_2$ (33 mg, 0.0911 mmol) was added at $0^\circ C$ and kept for stirring for overnight. Completion of reaction was monitored by TLC, after completion, reaction mixture was concentrated under reduced pressure and rotavapor, then

subsequently crude was extracted with EtOAc against sat. $NaHCO_3$ solution and dried over Na_2SO_4 . The crude was concentrated and dried under reduced pressure, further it was taken to next step without purification, Further, this crude compound (1.69 g, 1.881 mmol) and ZnI_2 (1.26 g, 3.95 mmol) was taken in a round bottom flask which is covered with aluminum foil, and was kept on high vacuum for 2 hours. The reaction mixture was dissolved in dry DCM and trimethyl(phenylthio)silane (TMSSPh) (1.11 ml, 5.83 mmol) was added, kept for stirring for 1 hour. The reaction completion was monitored by TLC, after completion of reaction, celite filtration was done and then purified by silica column in a EtOAc/Hexane solvent system to get compound **4** in a 85% yield. 1H NMR (400 MHz, Chloroform- d) 5.64 (t, $J = 2.2$ Hz, 1H), 5.59 (s, 1H), 5.24 – 5.19 (m, 1H), 5.07 – 4.91 (m, 3H), 4.84 (d, $J = 11.3$ Hz, 1H), 4.67 (dd, $J = 20.7, 11.5$ Hz, 2H), 4.53 – 4.35 (m, 4H), 4.17 (t, $J = 3.0$ Hz, 1H), 3.91 – 3.73 (m, 3H), 3.44 (dd, $J = 11.6, 4.4$ Hz, 1H), 2.03 (s, 3H), 1.95 (s, 3H), 1.90 (s, 3H), 8.02 (dd, $J = 8.3, 1.4$ Hz, 2H), 7.92 (dd, $J = 8.2, 1.4$ Hz, 2H), 7.59 (ddt, $J = 8.4, 7.0, 1.1$ Hz, 3H), 7.51 – 7.39 (m, 7H), 7.39 – 7.25 (m, 8H), 7.22 (t, $J = 7.7$ Hz, 3H). ^{13}C NMR (101 MHz, Chloroform- d) δ 175.24 – 168.64 (m), 165.32 (d, $J = 48.6$ Hz), 137.39, 137.18, 135.72, 133.61, 133.40, 131.69, 130.09, 129.77, 129.34, 129.11, 128.96, 128.52, 128.48, 128.43, 128.35, 128.23, 128.03, 127.96, 127.65, 127.53, 101.79, 86.08, 74.33, 72.82, 72.55, 72.43, 68.69, 67.72, 66.90, 65.95, 64.28, 62.76 (d, $J = 6.2$ Hz), 23.29 – 14.44 (m). HRMS m/z calculated for $C_{52}H_{52}O_{15}SNa$, 948.3027; Found 948.3031.

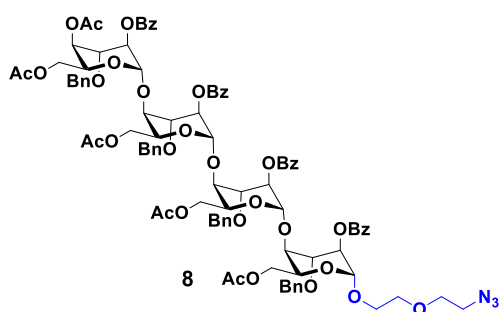
(4,6-O-diacetyl-2-O-benzoyl-3-O-benzyl)- α -L-idopyranosyl- α (1 \rightarrow 4))(6-O-acetyl-2-O-benzoyl-3-O-benzyl))- α -L-idopyranosyl- α (1 \rightarrow 4))(6-O-acetyl-2-O-benzoyl-3-O-benzyl))- α -L-idopyranosyl- α (1 \rightarrow 4))(1,6-anhydro-2-O-benzoyl-3-O-benzyl)- α -L-idopyranose(6).



Compound **6** was synthesised by using synthetic procedure of compound **3** in a 53% yield. ¹H NMR (400 MHz, Chloroform-*d*) 5.50 (d, *J* = 1.8 Hz, 1H), 5.35 (t, *J* = 3.1 Hz, 1H), 5.27 (t, *J* = 2.7 Hz, 1H), 5.13 (dt, *J* = 2.7, 1.1 Hz, 1H), 5.08 (d, *J* = 2.1 Hz, 1H), 5.02 – 4.96

(m, 2H), 4.90 (s, 1H), 4.87 – 4.78 (m, 3H), 4.77 – 4.70 (m, 1H), 4.68 (d, *J* = 11.5 Hz, 2H), 4.64 – 4.60 (m, 2H), 4.59 – 4.53 (m, 3H), 4.45 (ddd, *J* = 8.0, 4.6, 1.8 Hz, 1H), 4.37 – 4.16 (m, 4H), 4.17 – 4.06 (m, 3H), 4.05 – 3.95 (m, 2H), 3.91 – 3.77 (m, 4H), 3.69 – 3.61 (m, 1H), 3.58 – 3.51 (m, 2H), 1.94 (s, 3H), 1.91 – 1.87 (m, 6H), 1.84 (s, 3H), 8.04 – 7.99 (m, 2H), 7.97 – 7.86 (m, 6H), 7.63 – 7.15 (m, 32H) ¹³C NMR (101 MHz, Chloroform-*d*) δ 170.57, 170.55, 170.42, 169.93, 165.79, 165.67, 165.35, 165.01, 138.13, 137.52, 137.42, 137.19, 133.64, 133.39, 133.30, 133.25, 130.08, 129.99, 129.87, 129.76, 129.44, 129.30, 129.11, 129.04, 128.47, 128.42, 128.37, 128.34, 128.21, 128.18, 128.03, 127.99, 127.92, 127.84, 127.50, 127.34, 100.83, 100.72, 99.35, 95.50, 77.72, 77.36, 77.05, 76.73, 76.60, 75.85, 74.97, 74.93, 74.63, 72.97, 72.82, 72.51, 72.39, 71.92, 68.22, 68.10, 67.46, 66.71, 65.98, 65.44, 64.12, 62.77, 62.36, 62.14, 20.76, 20.58, 20.56, 0.02. HRMS *m/z* calculated for C₈₈H₈₈O₂₈Na, 1592.5462; Found 1592.5467.

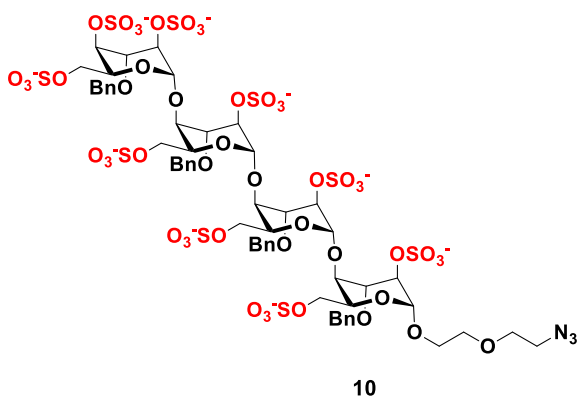
Ethoxy-2-azidoethoxyl-O-((4,6-O-diacetyl-2-O-benzoyl-3-O-benzyl)-α(1→4)-L-idopyrnosyl-(6-O-acetyl-2-O-benzoyl-3-O-benzyl)-α(1→4)-L-idopyrnosyl-(6-O-acetyl-2-O-benzoyl-3-O-benzyl)-α(1→4)-L-idopyrnosyl-(6-O-acetyl-2-O-benzoyl-3-O-benzyl)-α(1→4)-L-idopyrnoside (8).



Compound **8** was synthesised by using synthetic procedure of compound **3** in a 63% yield. ¹H NMR (400 MHz, Chloroform-*d*) 5.34 – 5.23 (m, 3H), 5.13 (d, *J* = 2.5 Hz, 1H), 5.03 – 4.95 (m, 2H), 4.93 – 4.75 (m, 6H), 4.71 – 4.60 (m, 4H), 4.57 (t, *J* = 2.4 Hz, 1H), 4.49 – 4.38 (m, 2H), 4.38 – 4.24 (m, 4H), 4.14 – 3.96 (m, 6H), 3.96 – 3.88 (m, 1H), 3.88 – 3.76 (m, 4H), 3.72 – 3.51 (m, 7H), 3.48 (t, *J* = 3.6 Hz, 1H), 3.19 (dt, *J* = 6.0, 4.0 Hz, 2H), 1.98 (s, 3H), 1.94 (s, 3H), 1.88 (s, 3H), 1.85 (s, 3H), 1.79 (s, 3H), 8.05 – 7.99 (m, 2H), 7.95 (ddd, *J* = 8.5, 3.6, 1.3 Hz, 4H), 7.92 – 7.85 (m, 2H), 7.63 – 7.55 (m, 1H), 7.51 – 7.41 (m, 8H),

7.36 (ddd, $J = 7.8, 6.7, 1.7$ Hz, 3H), 7.32 (p, $J = 1.5$ Hz, 3H), 7.30 – 7.27 (m, 4H), 7.27 – 7.26 (m, 3H), 7.25 – 7.20 (m, 6H), 7.20 – 7.14 (m, 4H) ^{13}C NMR (101 MHz, Chloroform- d) δ 170.50, 137.93, 137.53, 137.18, 133.62, 133.34, 133.08, 130.12, 130.06, 129.97, 129.75, 129.41, 129.29, 128.47, 128.41, 128.34, 128.32, 128.30, 128.25, 128.22, 128.17, 128.09, 128.02, 127.85, 127.80, 127.71, 127.65, 101.00, 100.64, 100.28, 98.35, 76.56, 76.16, 75.91, 74.96, 74.53, 72.91, 72.78, 72.45, 72.38, 72.28, 70.27, 70.17, 68.19, 67.72, 67.64, 67.50, 66.78, 66.04, 65.15, 64.16, 62.71, 62.17, 62.11, 50.72, 20.76, 20.74, 20.61, 20.53, 20.50. HRMS m/z calculated for $\text{C}_{94}\text{H}_{99}\text{N}_3\text{O}_{31}\text{Na}$, 1766.6296; Found 1766.6299.

Ethoxy-2-azidoethoxyl-O-((2,4,6-O-trisulfonato-3-O-benzyl)- α (1 \rightarrow 4)-L-idopyrnosyl-(2,6-O-disulfonato-3-O-benzyl)- α (1 \rightarrow 4)-L-idopyrnosyl-(2,6-O-disulfonato-3-O-benzyl))- α (1 \rightarrow 4)-L-idopyrnosyl-(2,6-O-disulfonato-3-O-benzyl))- α (1 \rightarrow 4)-L-idopyrnoside(10).

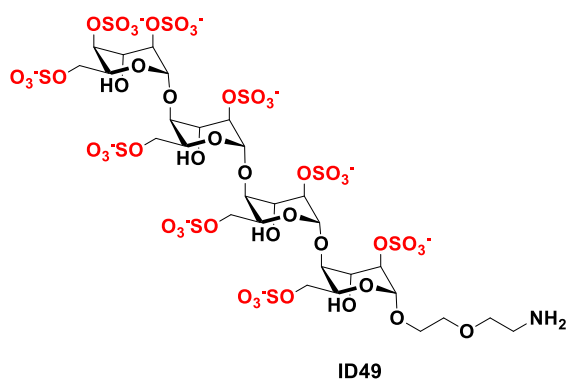


Compound **8** (106mg, 60.035mmol) was dissolved in THF/MeOH/H₂O (4/2/1) and LiOH (113.35mg, 2.701mol) was added at 0°C and kept for stirring for 3-4 hours. The reaction completion was monitored by TLC, after completion, reaction mixture was neutralized by amberlite 120 H⁺ resin,

Further, reaction mixture was filtered by cotton plough filtration, then it was concentrated under by reduced pressure, further it was purified by silica column in MeOH/DCM solvent system to get compound **9** in a 95% yield. Further, Compound **9** (36mg, 0.0315mmol) and SO₃.NMe₃ complex (395.72mg, 2.843mmol) was dissolved in dry DMF under N₂ atmosphere, reaction mixture was kept for stirring at 60°C for 36 h, Next DMF was evaporated under reduced pressure, resulting residue was purified using bond elute C18 column with ACN/H₂O solvent system to get compound **10** in a 90 % yield. ^1H NMR (600 MHz, Deuterium Oxide) 5.08 (s, 1H), 5.01 (d, $J = 11.5$ Hz, 1H), 4.91 (s, 2H), 4.81 – 4.72 (m, 7H), 4.65 (s, 1H), 4.63 – 4.49 (m, 2H), 4.45 – 4.33 (m, 5H), 4.31 (s, 1H), 4.27 – 4.20 (m, 1H), 4.20 – 4.11 (m, 6H), 4.06 (d, $J = 10.4$ Hz, 3H), 4.03 – 3.94 (m, 1H), 3.90 (d, $J = 10.6$ Hz, 1H), 3.74 (d, $J = 11.7$ Hz, 3H), 3.70 (dd, $J = 2.2, 1.3$ Hz, 2H), 3.68 – 3.63 (m, 3H), 3.59 (s, 1H), 3.37 – 3.32 (m, 2H), 7.51 – 7.44 (m, 5H), 7.44 – 7.29 (m, 15H) ^{13}C NMR (151 MHz, Deuterium Oxide) δ

137.68, 137.65, 137.61, 136.95, 128.66, 128.62, 128.60, 128.24, 128.11, 100.50, 100.41, 74.31, 73.86, 73.15, 73.02, 72.55, 71.45, 70.96, 70.29, 69.39, 69.29, 68.00, 65.85, 65.41, 55.51, 50.22, 50.17. HRMS m/z calculated for $C_{56}H_{64}N_3O_{49}S_9$ ⁻⁹, 205.5572; Found 205.5575.

Ethoxy-2-aminoethoxyl-O-((2,4,6-O-trisulfonato)- $\alpha(1\rightarrow4)$ -L-idopyrnosyl-(2,6-O-disulfonato)- $\alpha(1\rightarrow4)$ -L-idopyrnosyl-(2,6-O-disulfonato))- $\alpha(1\rightarrow4)$ -L-idopyrnoside (ID49).



The compound **10** (15mg, 8.10 mmol) was dissolved in H_2O and $Pd(OH)_2$ (10% per wt.) was added and stirred for 42h under hydrogen atmosphere. Further, reaction mixture was filtered and concentrated, finally purified by Bound elute C-18 column by using H_2O as a

solvent to get compound **ID49** in a 80% yield. 1H NMR (600 MHz, Deuterium Oxide) 5.07 (d, $J = 10.6$ Hz, 4H), 4.63 (t, $J = 7.6$ Hz, 2H), 4.50 – 4.40 (m, 1H), 4.34 – 4.15 (m, 17H), 3.86 (qd, $J = 12.1, 10.8, 5.8$ Hz, 5H), 3.77 – 3.68 (m, 5H), 3.15 (t, $J = 5.1$ Hz, 2H) ^{13}C NMR (151 MHz, Deuterium Oxide) δ 100.35, 99.98, 98.56, 76.15, 75.92, 75.80, 74.92, 73.40, 72.70, 72.65, 71.88, 69.64, 68.13, 67.65, 67.52, 67.38, 67.00, 66.52, 66.22, 66.11, 65.66, 65.17, 64.20, 39.17. HRMS m/z calculated for $C_{28}H_{42}NO_{49}S_9$ ⁻⁹, 162.6485; Found 162.6487.

3.5 References

1. Alzheimer's Dement. **2022**, *18*, 700-789.
2. Waite, L. M. Managing Alzheimer's Disease. *Aust. Prescr.* **2024**, *47*, 75-79.
3. LaFerla, F. M.; Green, K. N.; Oddo, S. Alzheimer's Disease: A Review. *Nat. Rev. Neurosci.* **2007**, *8*, 499-509.
4. Stewart, K. K.; Radford, S. E. Protein Misfolding and Disease. *Biophys. Rev.* **2017**, *9*, 405-419.
5. Hawkes, C. A.; Ng, V.; McLaurin, J. Alzheimer's Therapeutics. *Drug Dev. Res.* **2009**, *70*, 111-124.

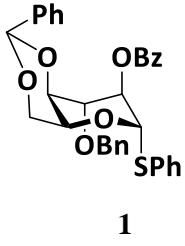
6. Tonali, N.; Kaffy, J.; Soulier, J. L.; Gelmi, M. L.; Ebra, E.; Taverna, M.; Van Heijenoort, C.; Ha-Dong, T.; Ongeri, S. Chemical Approaches to Alzheimer's. *Eur. J. Med. Chem.***2018**, *154*, 280-293.
7. Pellegrino, S.; Tonali, N.; Ebra, E.; Kaffy, J.; Taverna, M.; Contini, A.; Taylor, M.; Allsop, D.; Gelmi, M. L.; Ongeri, S. Novel Therapies for Alzheimer's. *Chem. Sci.***2017**, *8*, 1295-1302.
8. Kaffy, J.; Brinet, D.; Soulier, J. L.; Correia, I.; Tonali, N.; Fera, K. F.; Iacone, Y.; Hoffmann, A. R. F. Advances in Alzheimer's Drug Design. *J. Med. Chem.***2016**, *59*, 2025-2040.
9. Dong, G.; Ding, Y.; He, S.; Sheng, C. Progress in Alzheimer's Drug Development. *J. Med. Chem.***2021**, *64*, 10606-10620.
10. Békés, M.; Langley, D. R.; Crews, C. M. Targeted Protein Degradation: A New Paradigm in Drug Discovery. *Nat. Rev. Drug Discov.***2022**, *21*, 181-200.
11. Gilbertson, B.; Subbarao, K. Biotechnology and Drug Development. *Nat. Biotechnol.***2022**, *40*, 1328-1329.
12. Fang, Y.; Wang, J.; Zhao, M.; Zheng, Q.; Ren, C.; Wang, Y.; Zhang, J. New Advances in Medicinal Chemistry. *J. Med. Chem.***2022**, *65*, 11454-11477.
13. Chu, T. T.; Gao, N.; Li, Q. Q.; Chen, P. G.; Yang, X. F.; Chen, Y. X.; Zhao, Y. F.; Li, Y. M. Chemical Biology of Neurodegeneration. *Cell Chem. Biol.***2016**, *23*, 453-461.
14. Noh, M. Y.; Chun, K.; Kang, B. Y.; Kim, H.; Park, J. S.; Lee, H. C.; Kim, H. Y.; Ku, S.; Kim, S. H. Insights into Biochemical Pathways. *Biochem. Biophys. Res. Commun.***2013**, *435*, 274-281.
15. Yin, K.; Lee, J. M.; Chen, S.; Xu, J.; Hsu, C. Y. Neuroscience and Cell Signaling. *J. Neurosci.***2002**, *22*, 9764-9770.
16. Hu, W.; Yang, Z.; Yang, W.; Han, M.; Xu, B.; Yu, Z.; Shen, M.; Yang, Y. Progress in Neurobiology: Recent Advances. *Prog. Neurobiol.***2019**, *181*, 101645.
17. Ciccone, L.; Shi, C. H.; Di Lorenzo, D.; Van Baelen, A. C. Molecular Interactions in Drug Discovery. *Molecules***2020**, *25*, 2439.
18. Tian, Y.; Miao, Y.; Guo, P.; Wang, J.; Han, D. Innovations in Chemistry. *Angew. Chem. Int. Ed.***2024**, *63*, e202316089.
19. Wu, Y.; Lin, B.; Lu, Y.; Li, L.; Deng, K.; Zhang, S.; Zhang, H.; Yang, C.; Zhu, Z. Advances in Chemical Engineering. *Angew. Chem. Int. Ed.***2023**, *62*, e202218106.
20. Shao, J.; Lin, X.; Wang, H.; Zhao, C.; Yao, S. Q.; Ge, J.; Zeng, S.; Qian, L. Chemical Synthesis and Applications. *Angew. Chem. Int. Ed.***2024**, *63*, e202319232.

21. Wu, X.; Hu, J. J.; Yoon, J. *Frontiers in Chemical Research. Angew. Chem. Int. Ed.***2024**, *63*, e202400249.
22. Li, Y.; Liu, X.; Yu, L.; Huang, X.; Wang, X.; Han, D.; Yang, Y.; Liu, Z. *Chemical Innovations and Discoveries. J. Am. Chem. Soc.***2023**, *145*, 24506-24521.
23. Loppinet, E.; Besser, H. A.; Lee, C. E.; Zhang, W.; Cui, B.; Khosla, C. *Cutting-Edge Chemical Research. J. Am. Chem. Soc.***2023**, *145*, 18705-18710.
24. Luo, J.; Gao, Q.; Tan, K.; Zhang, S.; Shi, W.; Luo, L.; Li, Z.; Khedr, G. E.; Chen, J.; Xu, Y.; Luo, M.; Xing, Q.; Geng, J. *Chemistry and Molecular Science. J. Am. Chem. Soc.***2024**, *146*, 17728-17737.
25. Zhang, B.; Brahma, R. K.; Zhu, L.; Feng, J.; Hu, S.; Qian, L.; Du, S.; Yao, S. Q.; Ge, J. *Chemical Society Journal. J. Am. Chem. Soc.***2023**, *145*, 24272-24283.
26. Banik, S. M.; Pedram, K.; Wisnovsky, S.; Ahn, G.; Riley, N. M.; Bertozzi, C. R. *Advances in Chemical Biology. Nature***2020**, *584*, 291-297.
27. Ahn, G.; Riley, N. M.; Kamber, R. A.; Wisnovsky, S.; Von Has, S. M.; Bassik, M. C.; Banik, S. M.; Bertozzi, C. R. *Chemical Innovations in Science. Science***2023**, *383*, eadf6249.
28. Ahn, G.; Banik, S. M.; Miller, C. L.; Riley, N. M.; Cochran, J. R.; Bertozzi, C. R. *New Frontiers in Chemical Biology. Nat. Chem. Biol.***2021**, *17*, 937-946.
29. Maiza, A.; Chantepie, S.; Vera, C.; Fifra, A.; Huyuh, M. B.; Stettler, O.; Ouidja, M. O.; Papy-Garcia, D. *Insights in FEBS Letters. FEBS Lett.***2018**, *592*, 3806-3818.
30. Wesén, E.; Gallud, A.; Paul, A.; Lindberg, D. J.; Malmberg, P.; Esbjöner, E. K. *Biomembrane Studies. Biochim. Biophys. Acta, Biomembr.***2018**, *1860*, 2204-2214.
31. Liu, C.-C.; Zhao, N.; Yamaguchi, Y.; Cirrito, J. R.; Kanekiyo, T.; Holtzman, D. M.; Bu, G. *Translational Medicine Approaches. Sci. Transl. Med.***2016**, *8*, 332ra44.
32. Baryal, K. N.; Ramadan, S.; Su, G.; Huo, C.; Zhao, Y.; Liu, J.; Hsieh-Wilson, L. C.; Huang, X. *Advances in Chemical Engineering. Angew. Chem., Int. Ed.***2023**, *62*, e202211985.
33. Wang, P.; Zhao, J.; Nasr, S. H.; Otieno, S. A.; Zhang, F.; Qiang, W.; Linhardt, R. J.; Huang, X. *Chemical Biology Insights. ACS Chem. Biol.***2021**, *16*, 1894-1899.
34. Stewart, K. L.; Hughes, E.; Yates, E. A.; Akien, G. R.; Huang, T.-Y.; Lima, M. A.; Rudd, T. R.; Guerrini, M.; Hung, S.-C.; Radford, S. E.; Middleton, D. A. *Chemical Society Advances. J. Am. Chem. Soc.***2016**, *138*, 8328-8331.

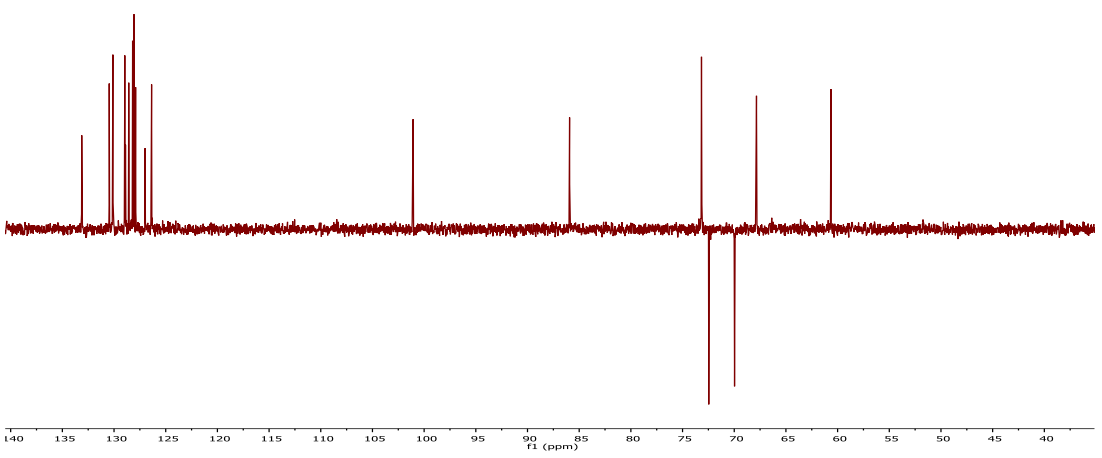
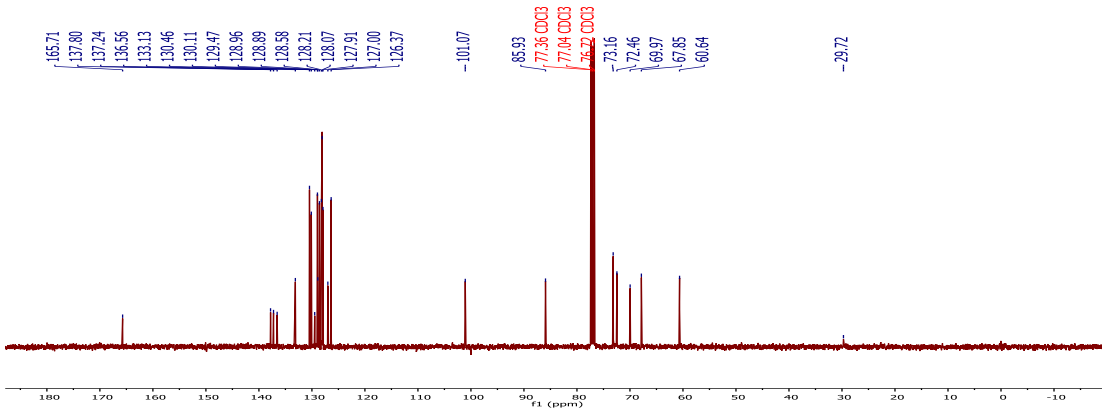
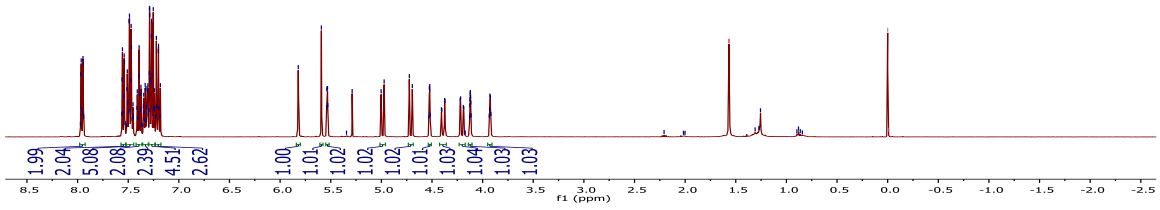
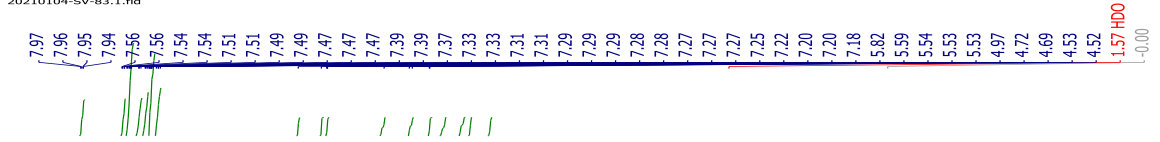
35. Madine, J.; Pandya, M. J.; Hicks, M. R.; Rodger, A.; Yates, E. A.; Radford, S. E.; Middleton, D. A. Chemical Communications. *Angew. Chem., Int. Ed.***2012**, *51*, 13140-13143.
36. Wang, T.; Jo, H.; DeGrado, W. F.; Hong, M. Advances in Chemical Research. *J. Am. Chem. Soc.***2017**, *139*, 6242-6252.
37. Anand, S.; Mardhekar, S.; Bhoge, P. R.; Mishra, S. K.; Kikkeri, R. Chemical Innovations. *Chem. Commun.***2024**, *60*, 4495-4498.
38. Chandra, A.; Bhoge, P. R.; Shanthamurthy, R. R. K. C. D.; Kikkeri, R. Recent Developments in Chemistry. *Chem. Commun.***2023**, *59*, 1213-1216.
39. Shanthamurthy, C. D.; Leviatan Ben-Arye, S.; Kumar, N. V.; Yehuda, S.; Amon, R.; Woods, R. J.; Padler-Karavani, V.; Kikkeri, R. Medicinal Chemistry Insights. *J. Med. Chem.***2021**, *64*, 3367-3380.
40. Shanthamaruthy, C. D.; Kikkeri, R. Organic Chemistry Perspectives. *Eur. J. Org. Chem.***2019**, *2019*, 2950-2953.
41. Sun, L.; Chopra, P.; Boons, G. J. Organic Chemistry Research. *J. Org. Chem.***2020**, *85*, 16082-16098.
42. Arungundram, S.; Al-Mafraji, K.; Asong, J.; Leach, F. E., III; Amster, I. J.; Venot, A.; Turnbull, J. E.; Boons, G. J. Advances in Chemical Society. *J. Am. Chem. Soc.***2009**, *131*, 17394-17405.
43. Jain, P.; Shanthamurthy, C. D.; Chaudhary, P. M.; Kikkeri, R. Chemical Science Innovations. *Chem. Sci.***2021**, *12*, 4021-4027.
44. Jain, P.; Shanthamurthy, C. D.; Leviatan Ben-Arye, S.; Woods, R. J.; Kikkeri, R.; Padler-Karavani, V. Advances in Chemical Science. *Chem. Sci.***2021**, *12*, 3674-3681.
45. Chopra, P.; Yadavalli, T.; Palmieri, F.; Jongkees, S. A. K.; Unione, L.; Shukla, D.; Boons, G. J. Chemical Communications. *Angew. Chem., Int. Ed.***2023**, *62*, e202309838.
46. Pawar, N. J.; Wang, L.; Higo, T.; Bhattacharya, C.; Kancharla, P. K.; Zhang, F.; Baryal, K.; Huo, C. X.; Liu, J.; Linhardt, R. J.; Huang, X.; Hsieh-Wilson, L. C. Organic Chemistry Discoveries. *Angew. Chem., Int. Ed.***2019**, *58*, 18577-18583.
47. Wang, L.; Sorum, A. W.; Huang, B. S.; Kern, M. K.; Su, G.; Pawar, N.; Huang, X.; Liu, J.; Pohl, N. L. B.; Hsieh-Wilson, L. C. Nature Chemistry Insights. *Nat. Chem.***2023**, *15*, 1108-1117.
48. Nguyen, K.; Rabenstein, D. L. Physical Chemistry Insights. *J. Phys. Chem. B***2016**, *120*, 2187-2197.

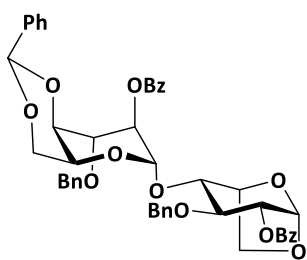
49. Zhao, H.; Zhu, J.; Cui, K.; Xu, X.; O'Brien, M.; Wong, K. K.; Kesari, S.; Xia, W.; Wong, S. T. C. Cancer Research Insights. *Cancer Cell Int.***2009**, *9*, 15.
50. Zhang, Y.; Chen, H.; Li, R.; Sterling, K.; Song, W. Signal Transduction and Targeted Therapy. *Signal Transduct. Target. Ther.***2023**, *8*, 248.
51. Woods, E. C.; Yee, N. A.; Shen, J.; Bertozzi, C. R. Innovations in Chemical Biology. *Angew. Chem., Int. Ed.***2015**, *54*, 15782-15788.
52. Ramadan, S.; Mayieka, M.; Pohl, N. L. B.; Liu, J.; Hsieh-Wilson, L. C.; Huang, X. Current Opinions in Chemical Biology. *Curr. Opin. Chem. Biol.***2024**, *80*, 102455.
53. Xu, D.; Esko, J. D. Annual Review of Biochemistry. *Annu. Rev. Biochem.***2014**, *83*, 129-157.

3.6 NMR

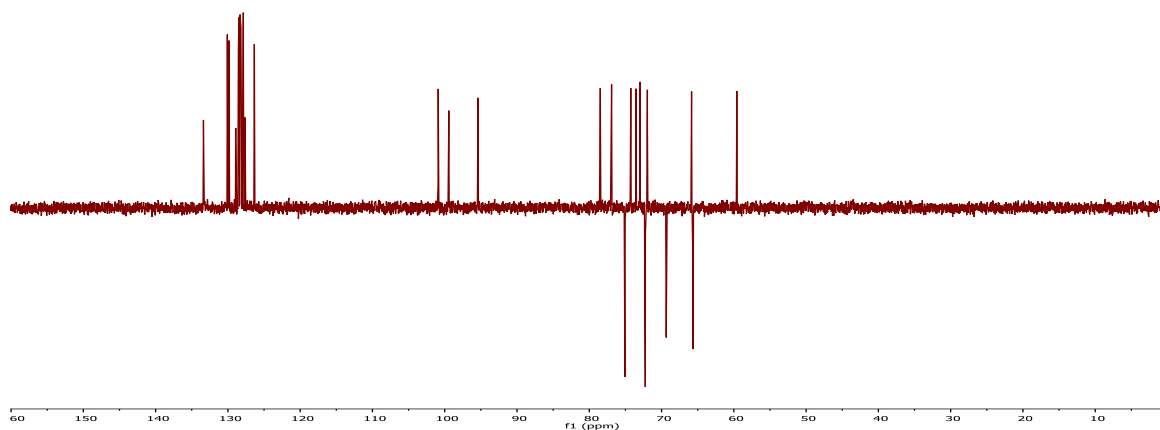
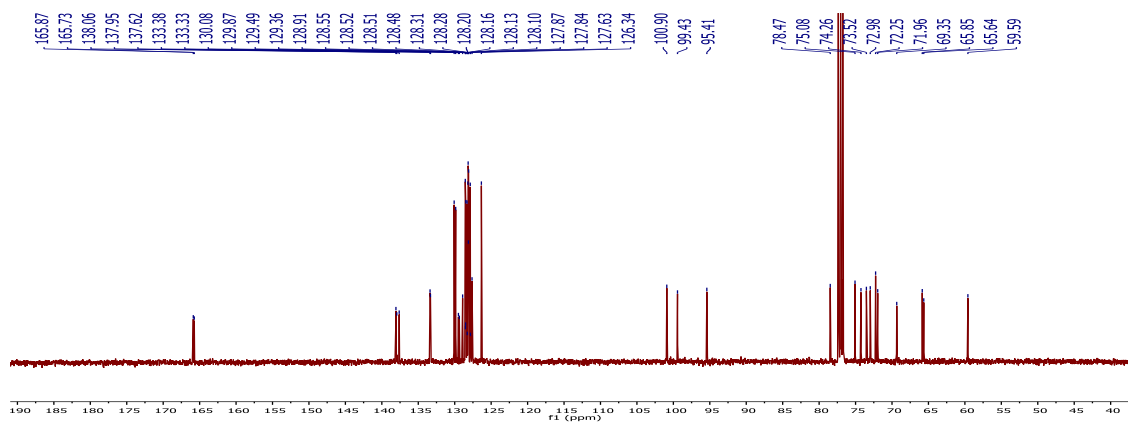
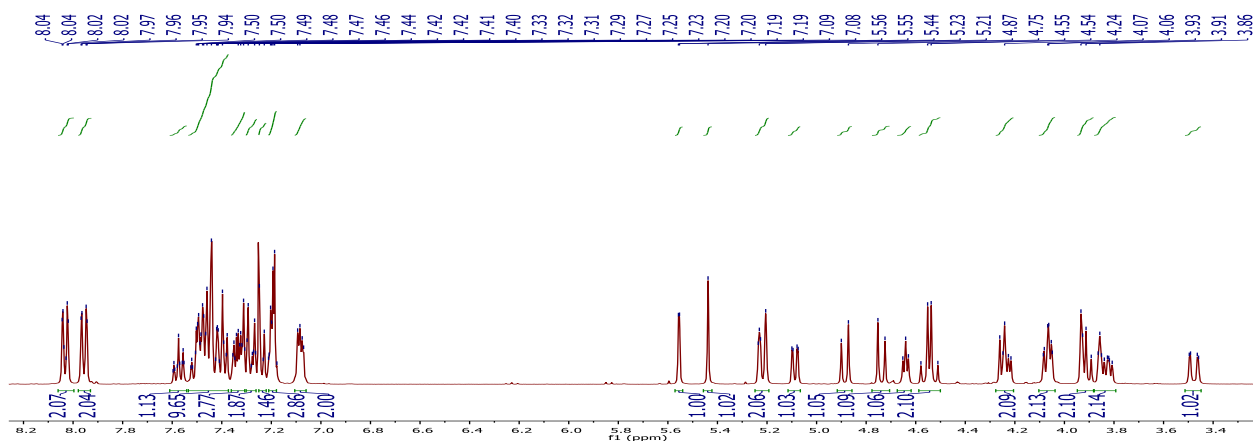


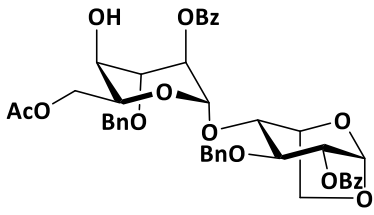
20210104-SV-83.1.fid



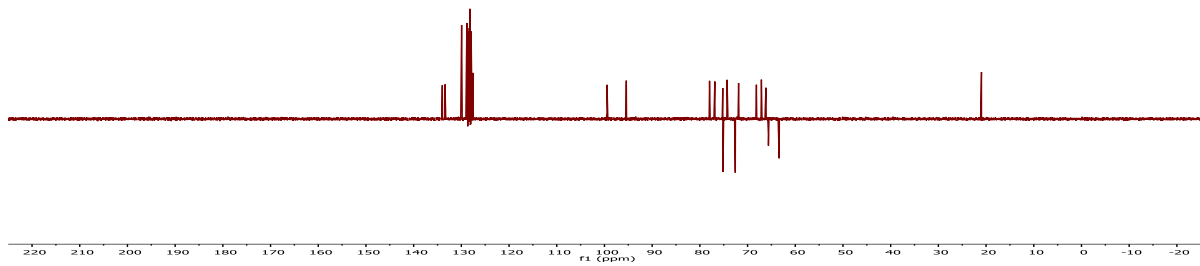
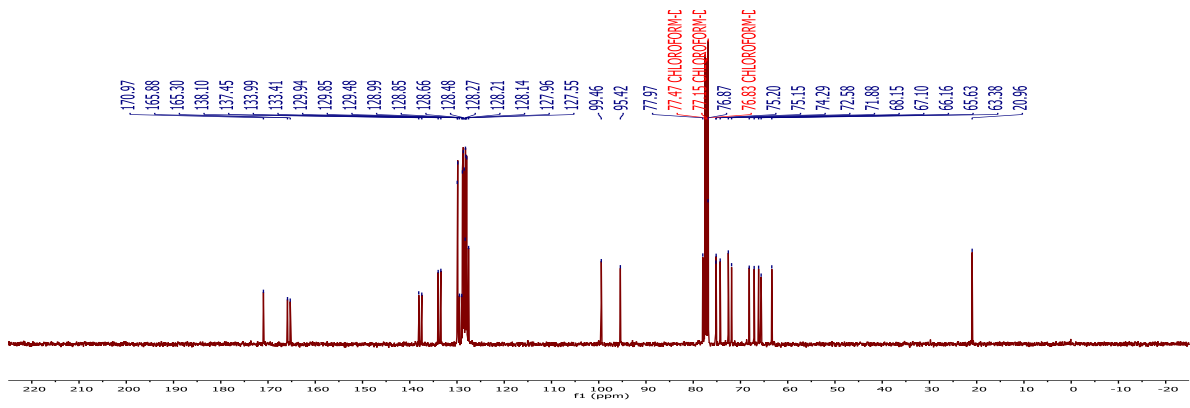
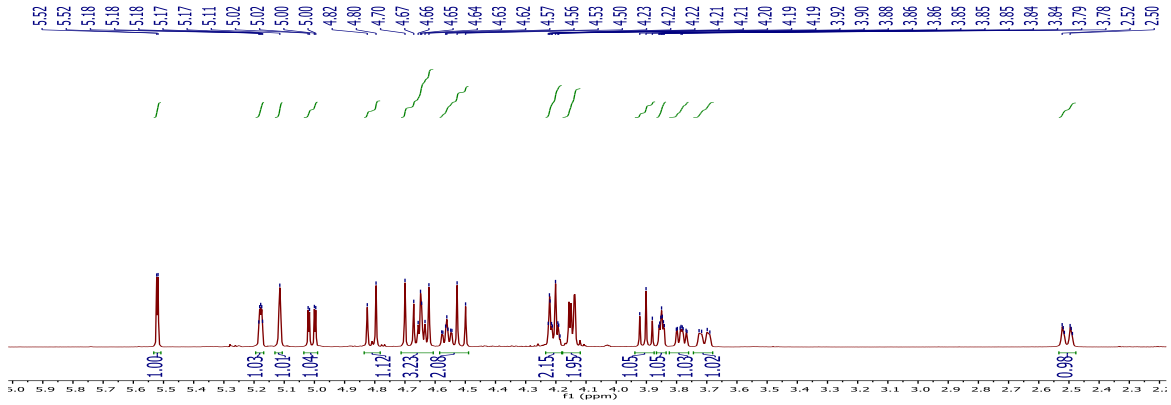


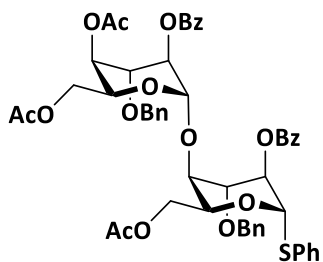
3



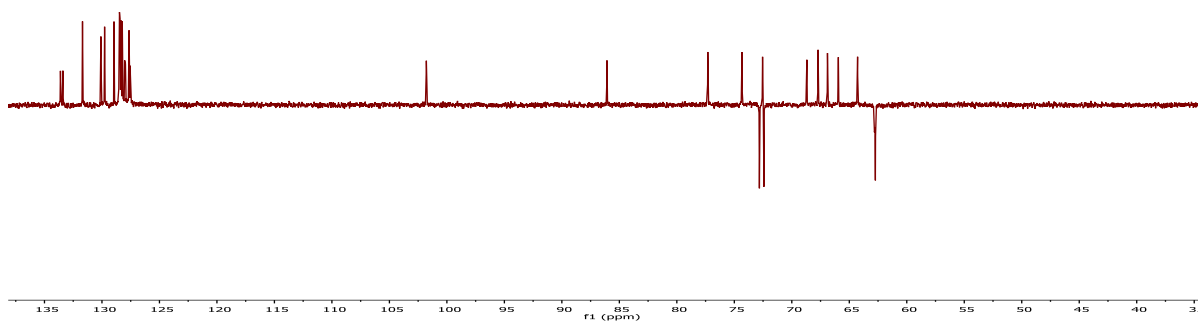
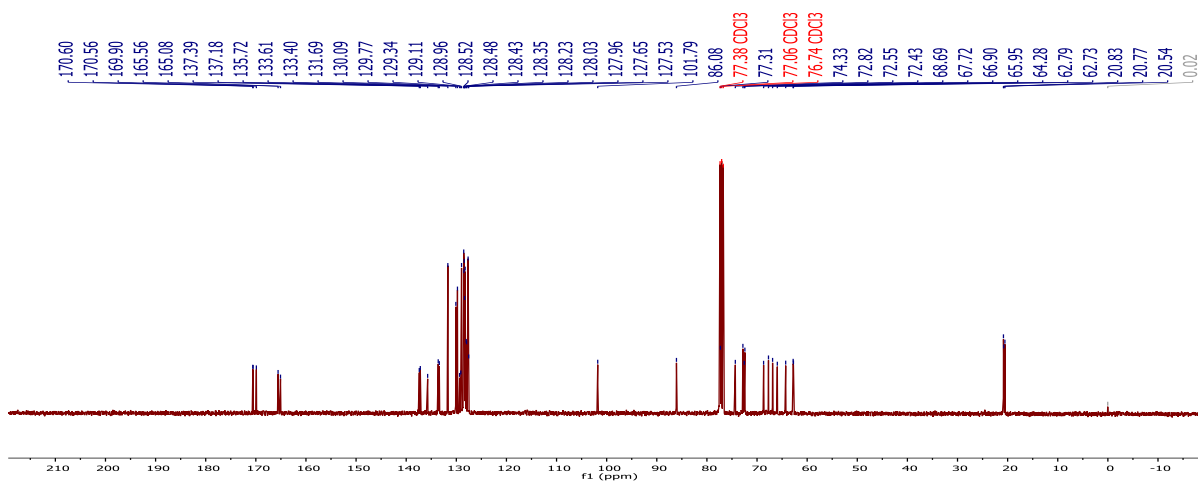
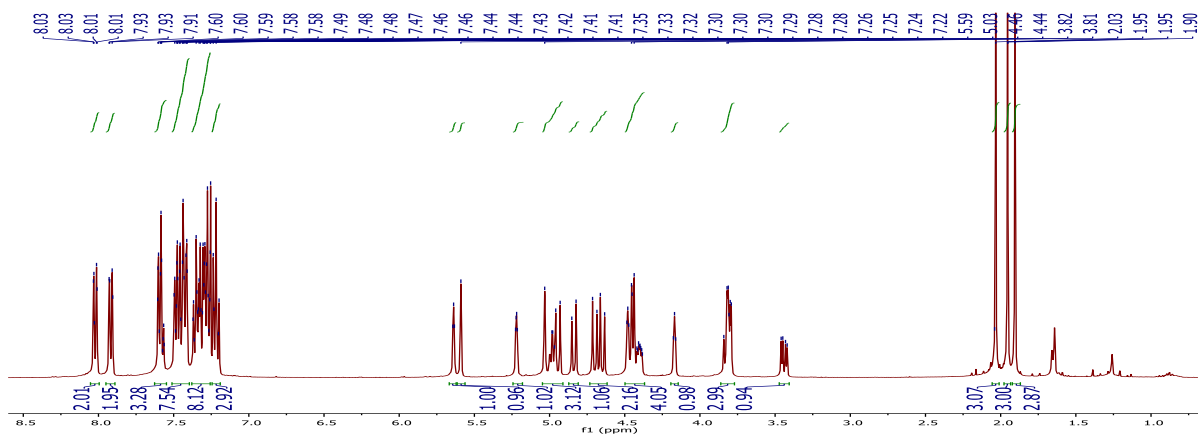


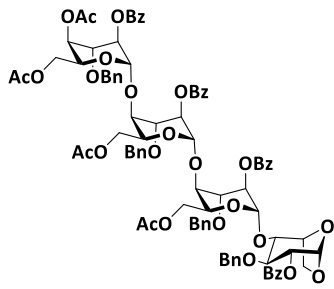
5



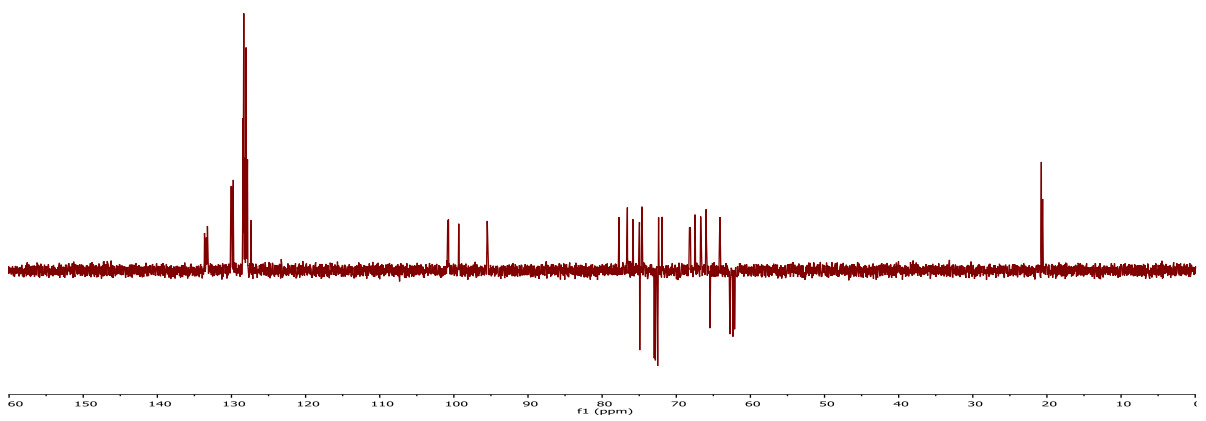
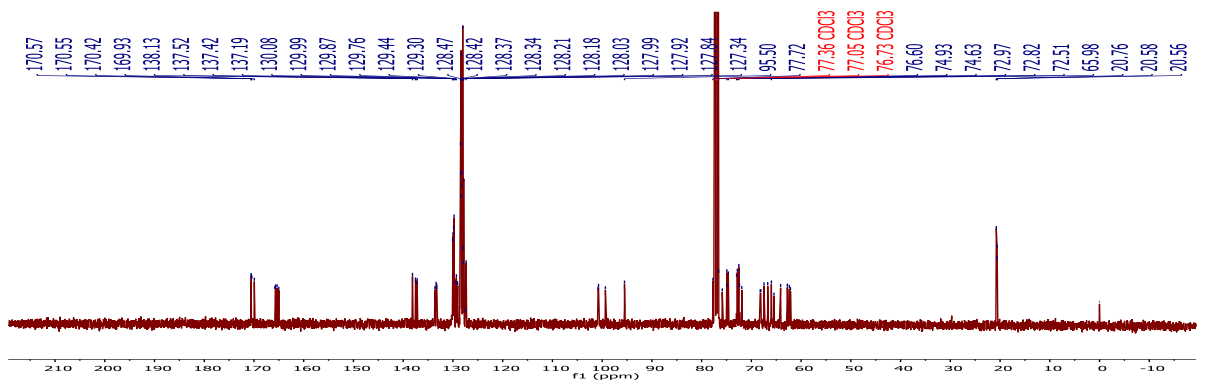
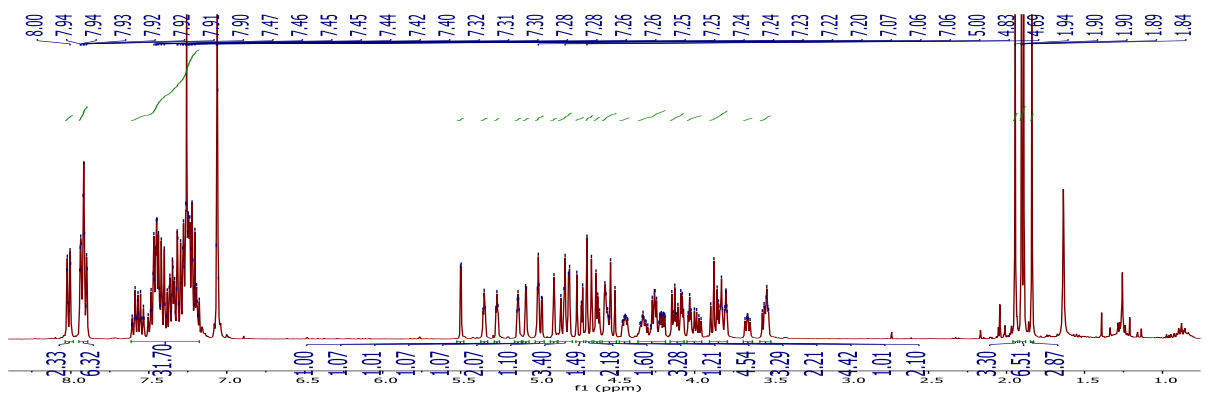


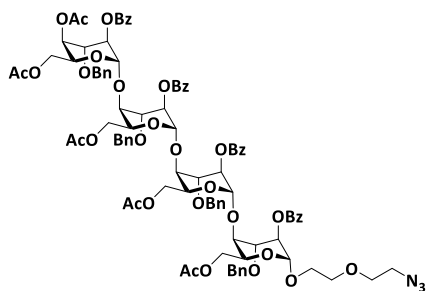
4



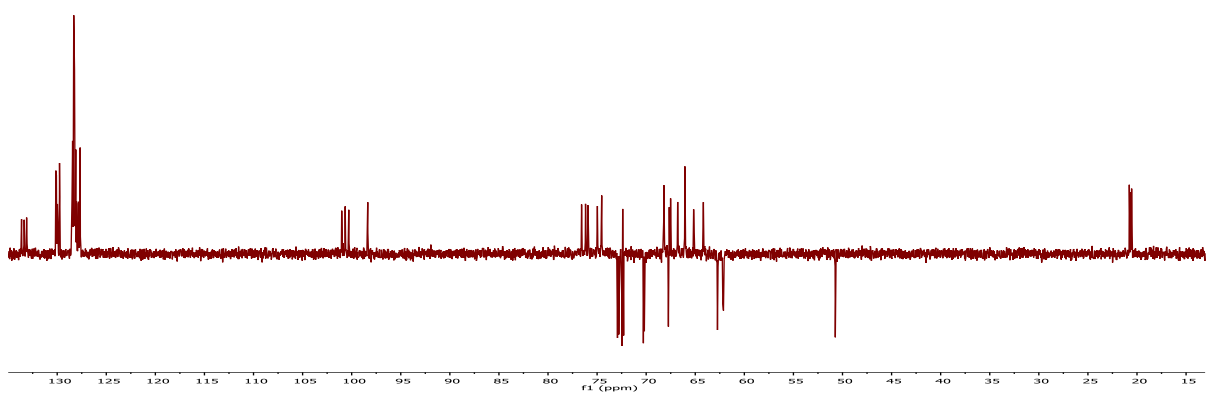
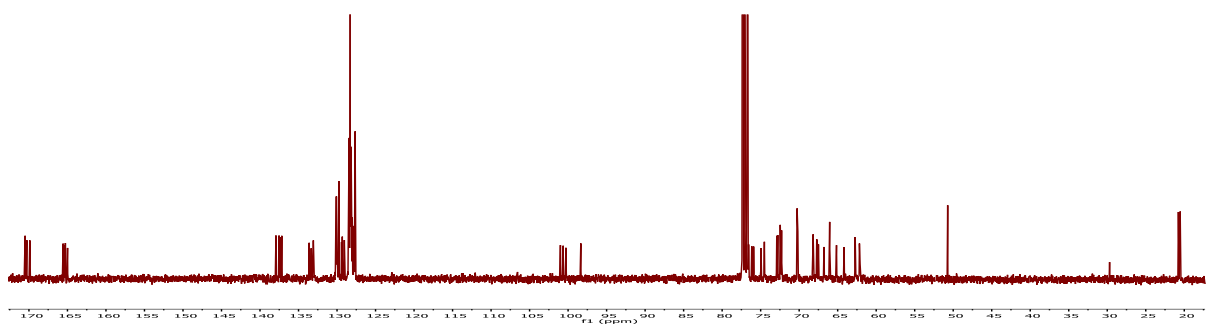
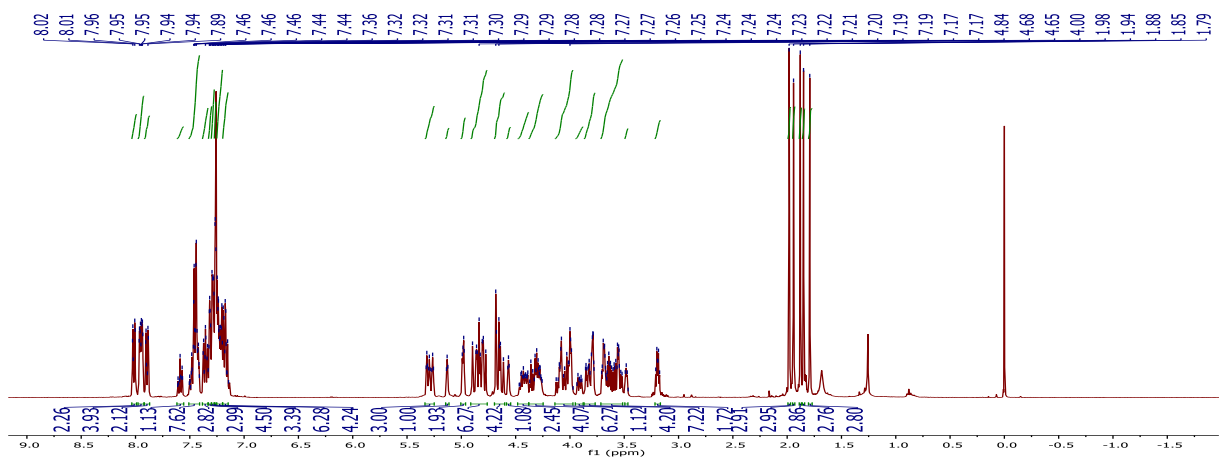


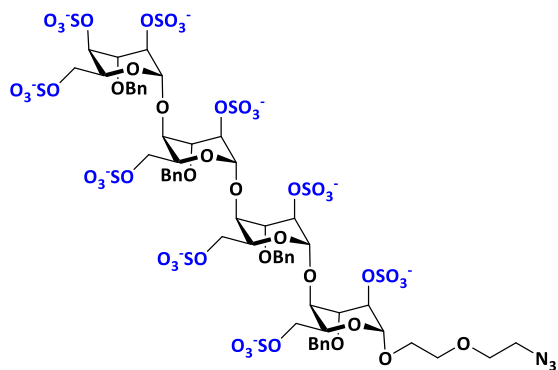
6



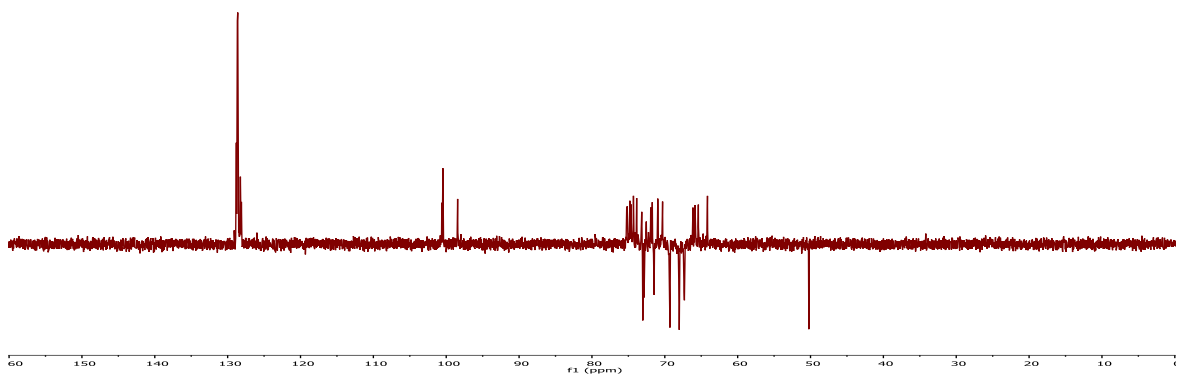
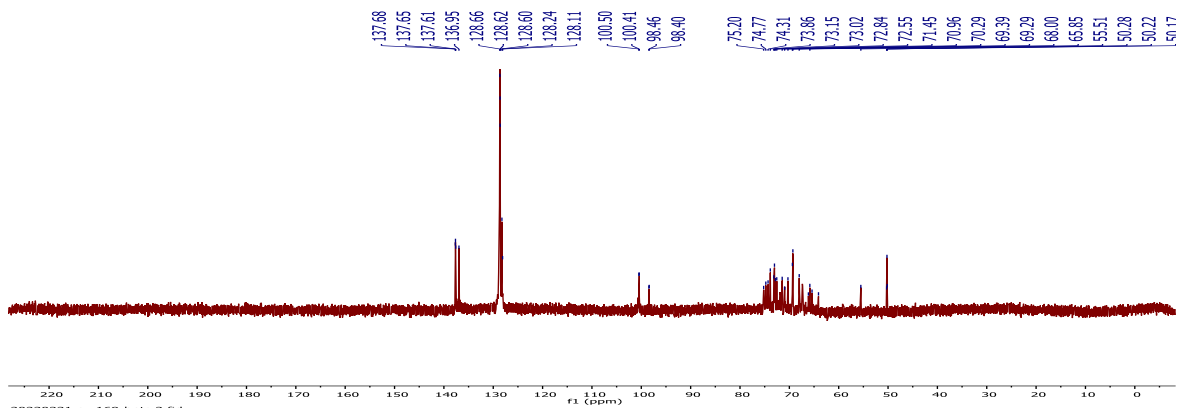
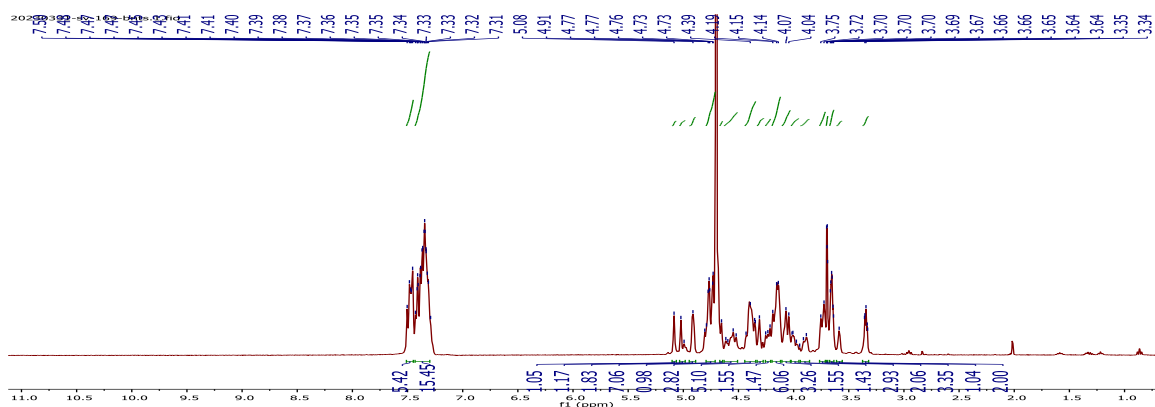


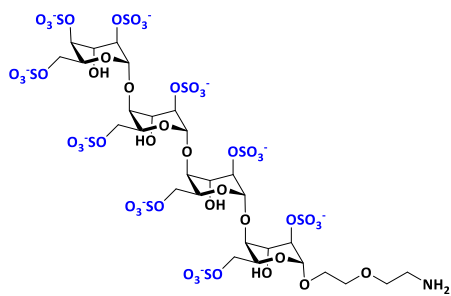
8



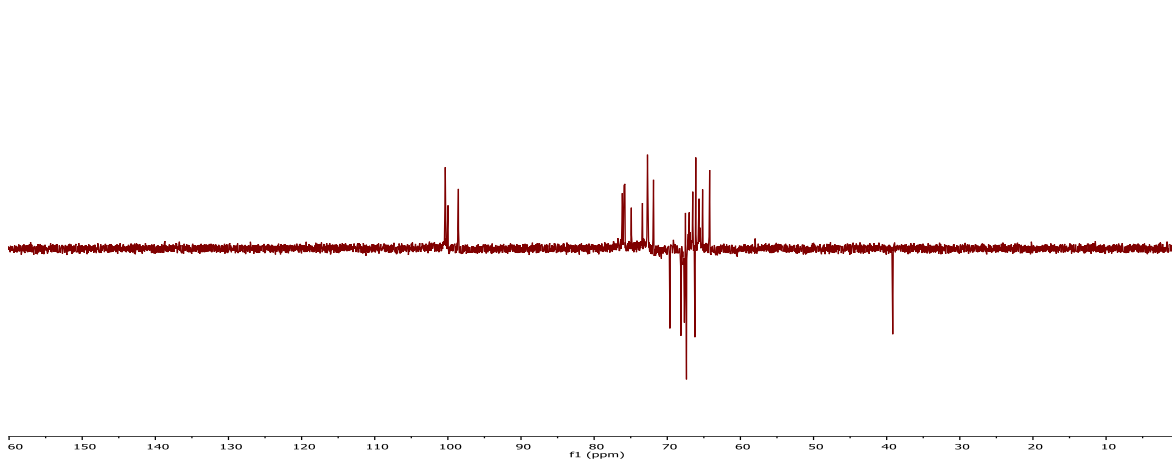
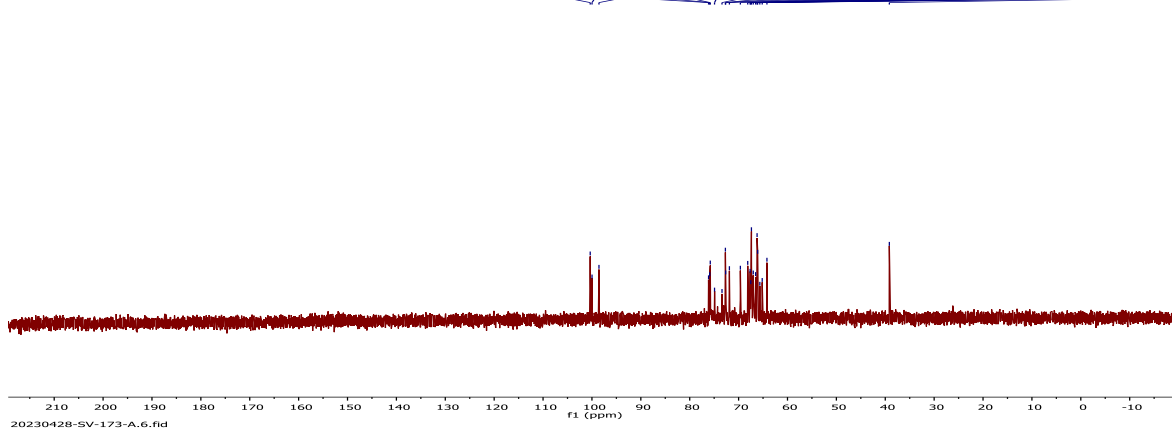
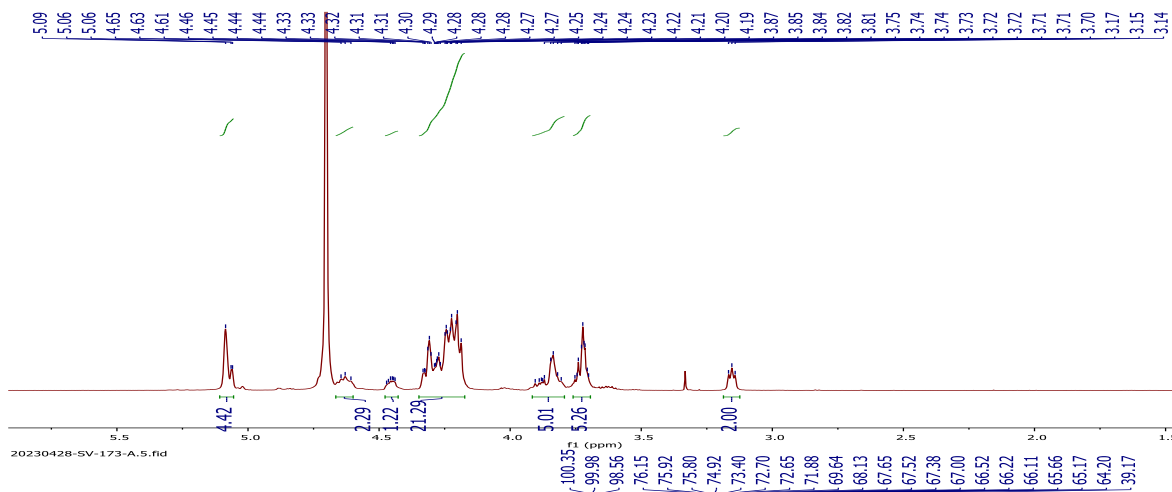


10

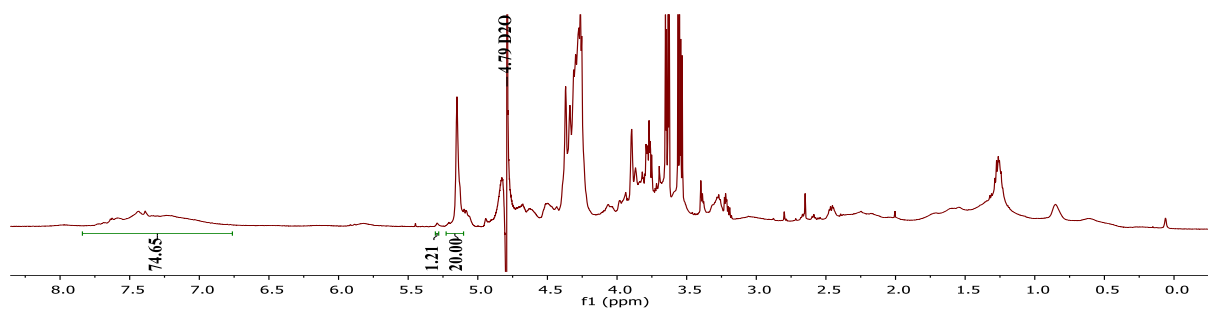




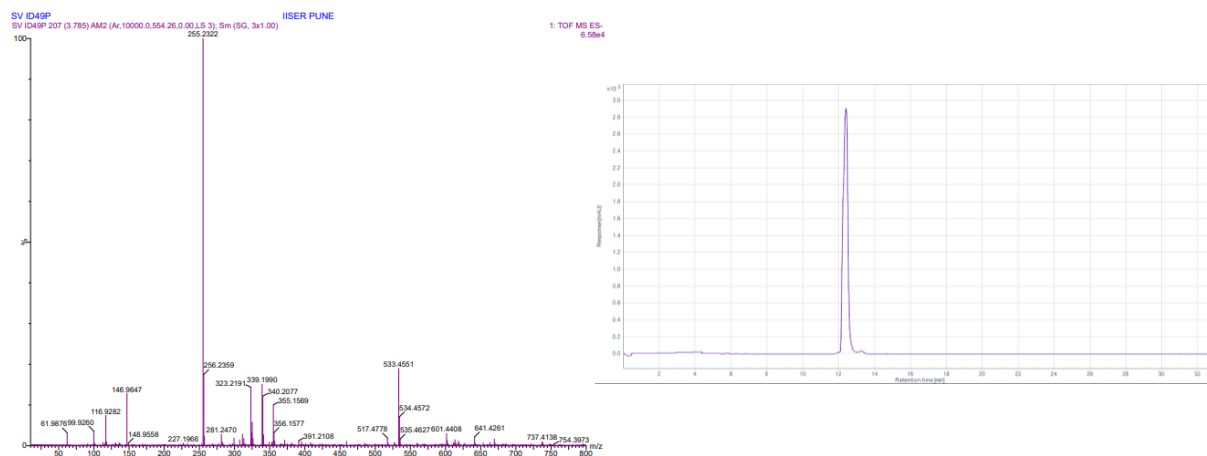
ID49



PG@ID49



HRMS & HPLC Profile of PG@ID49 :



CHAPTER-4

Amphiphilic Heparinoids as Potent Antiviral Agents Against SARS-CoV-2

Abstract

Herein, we report the synthesis and biological evaluation of a novel series of heparinoid amphiphiles as inhibitors of heparanase and SARS-CoV-2. By employing a tailor-made synthetic strategy, a library of highly sulfated homo-oligosaccharides bearing D-glucose or a C5-epimer (i.e., L-idose or L-iduronic acid) conjugated with various lipophilic groups was synthesized and investigated for anti-viral activity. Sulfated higher oligosaccharides of D-glucose or L-idose with lipophilic aglycones displayed potent anti-SARS-CoV-2 and anti-heparanase activity, similar to or better than pixatimod (PG545), and were more potent than their isosteric L-iduronic acid congeners. Lipophilic groups such as cholestanol and C₁₈-aliphatic substitution are more advantageous than functional group appended lipophilic moieties. These findings confirm that fine-tuning of higher oligosaccharide, degree of sulfation, and lipophilic groups could yield promising drug candidates for treating COVID-19.

4.1 INTRODUCTION

The SARS-CoV-2 coronavirus has caused widespread intestinal and respiratory infections worldwide, claiming millions of lives during the recent COVID-19 pandemic.¹ Despite the approval of several vaccines and drug molecules², SARS-CoV-2 continues to be a major pathogenic virus globally³. Given its high mutation rate and the rapid emergence of new variants, developing new drug molecules to complement vaccine programs is highly desirable. Studies of SARS-CoV-2 viral pathogenesis have revealed that the binding of the virus's spike protein to the glycosaminoglycan heparan sulfate (HS) and the angiotensin-converting enzyme 2 (ACE2) cell surface receptor is a critical factor in pathogenicity.⁴ Consequently, significant efforts have been made to determine the binding sequence of HS and its mimics to SARS-CoV-2 active sites to inhibit virus replication.⁵

Structurally, heparan sulfate (HS) is a highly sulfated polysaccharide composed of repeating units of (1→4)-linked glucosamine and uronic acid disaccharides. These disaccharides feature various O-sulfate and N-sulfate/N-acetate modifications on the uronic acid and glucosamine, respectively.⁶ Due to these modifications, there are 2,304 possible combinations of HS tetrasaccharides, making the identification of specific HS ligands for the spike protein challenging.⁷ Boons et al., Zhongping et al., Skidmore et al., and Desai et al. used a limited HS library to identify active HS ligands for the spike receptor binding domain (RBD) using microarray and surface plasmon resonance techniques.^{4b, 5a, 8} These studies suggest that the composition of iduronic acid and sulfation patterns, specifically 2-*O*, 6-*O*, or *N*-sulfation groups, are crucial for modulating SARS-CoV-2 activity.^{5a} Furthermore, Linhardt et al. reported that unfractionated heparin (UFH), enoxaparin, and 6-*O*-desulfated UFH demonstrated strong inhibition of SARS-CoV-2 binding to epithelial cells.⁹ Additionally, intranasal administration of these drugs showed low toxicity and bioavailability in blood, indicating their potential as therapeutic agents for SARS-CoV-2 infection.¹⁰

Although these studies provide insight into how spike proteins recognize native HS ligands, the structural complexity and synthetic challenges hinder the discovery of potential HS ligands for the spike protein. Alternatively, HS mimics represent potential therapeutic molecules for targeting SARS-CoV-2 infection.¹¹ Previous studies, including our own research, have demonstrated that HS mimics derived from L-iduronic acid can mimic many functions of native heparin/HS, including anti-viral activity. Notably, the heparinoid

amphiphile pixatimod (PG545, Fig. 1), originally developed as an anticancer drug ¹², is a potent inhibitor of heparanase—an enzyme that degrades HS and plays crucial roles in inflammation and viral pathogenesis, including SARS-CoV-2 ^{13, 14}. Early studies indicated that pixatimod exhibits antiviral activity both in vitro and in vivo against various viruses that use HS as an entry receptor, with EC50s ranging from 0.06 to 14 µg/mL, and demonstrates low toxicity and high selectivity indices. These viruses include HSV-2 ¹⁵, HIV ¹⁶, RSV ¹⁷, Ross River virus ¹⁸, Barmah Forest virus ¹⁸, CHIKV ¹⁸, and Dengue virus ¹⁹. Furthermore, in vivo evidence suggests that pixatimod possesses anti-inflammatory activities linked to the inhibition of IL-6 ^{18, 20}, a cytokine associated with respiratory failure in hospitalized symptomatic COVID-19 patients ²¹. Subsequently, pixatimod has been shown to effectively inhibit SARS-CoV-2 infection of cells at concentrations within its safe therapeutic dose range and to significantly reduce SARS-CoV-2 viral titers and COVID-19-like symptoms in the K18-hACE2 mouse model ²². Molecular modeling studies indicate that the steroid sidechain of pixatimod plays a crucial role in disrupting the spike-ACE2 interaction ²². The lipophilic side chains of amphiphilic heparinoids, such as pixatimod, confer several enhanced properties compared to their unmodified counterparts. Apart from binding to the heparin/HS binding sites of HS-binding proteins, these lipophilic side chains can also interact with nearby hydrophobic residues, often resulting in greater potency in many bioassays (e.g., heparanase inhibition) ¹². Importantly, they improve pharmacokinetics (i.e., longer half-life, increased bioavailability, lower plasma clearance), and exhibit low anticoagulant activity (high anticoagulant activity being a common undesirable side effect of heparinoids) ¹². Of particular relevance, these compounds can also exhibit virucidal activity, provided the side chain is sufficiently large and lipophilic ^{15-17, 23a}, a feature lacking in most unmodified HS mimics.

This article rationalizes the anti-viral activity of heparinoid amphiphiles by describing the design and synthesis of a library that manipulates the saccharide ligand's nature, oligosaccharide chain length, degree of sulfation, and lipophilic group. Compared to PG545, optimized L-idose-based oligosaccharides demonstrated effective inhibition of SARS-CoV-2. Importantly, many compounds exhibited higher inhibitory activity than PG545 in the heparanase inhibition assay. Isothermal titration calorimetry (ITC) binding studies and molecular docking highlighted the significance of oligosaccharide chain length and lipophilic group in spike protein binding. Overall, these findings pave the way for designing future HS mimics to target SARS-CoV-2 and other HS-dependent viral infections.

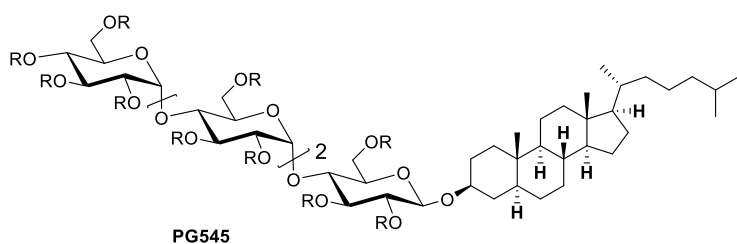


Figure 1. The structure of pixatimod (PG545). R = SO₃Na.

4.2 RESULTS AND DISCUSSION

To pinpoint optimal ligands for targeting SARS-CoV-2 virulence, we developed and synthesized a diverse library of six heparinoid amphiphiles featuring L-iduronic acid and L-idose saccharide moieties. This library encompasses highly sulfated di-, tri-, and tetra-L-iduronic acid/L-idosides paired with a cholesterol moiety (Fig. 2). Our hypothesis revolves around how variations in oligosaccharide chain length, saccharide ligand nature, degree of sulfation, and lipophilic group intricately modulate anti-viral activity. The selection of saccharide systems is expected to impact anti-viral efficacy by presenting diverse sulfate group conformations and arrangements. Recent studies have demonstrated the conformational adaptability of both sulfated L-iduronic acid homo-oligosaccharides and PG545.²⁴ The range of lipophilic groups includes variations in glycosidic configuration (α versus β), non-steroidal side chains, and modifications such as fluorescent or pro-fluorescent tags (e.g., azide, alkyne). Computational investigations underscore the critical role of PG545's lipophilic side chain in binding to target proteins, such as the SARS-CoV-2 spike protein²² and heparanase.^{24b} Prior research has also established that adequately sized lipophilic side chains can impart virucidal activity to amphiphilic heparinoids.¹⁵⁻

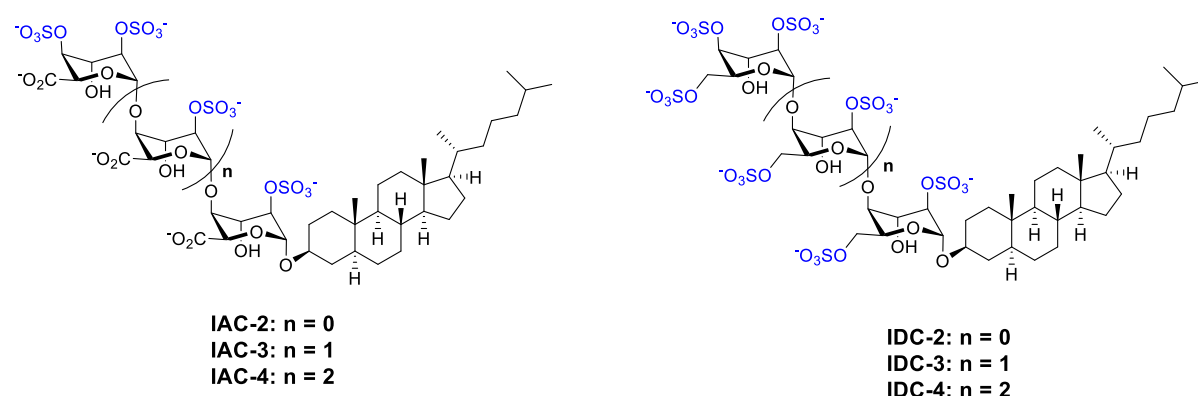
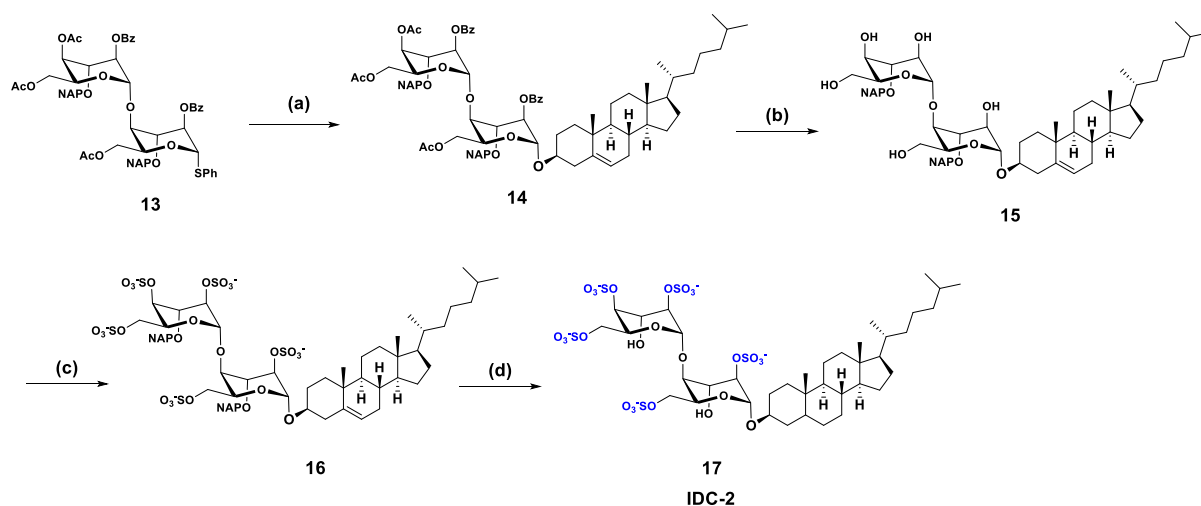


Figure 2. Structures of new heparinoid amphiphiles synthesized in this study.

4.2.1 Synthesis of L-idose and L-iduronic acid based amphiphiles

The synthesis of L-idose and L-iduronic acid based amphiphiles is highly challenging, as L-sugars are not commercially available, and controlling the stereoselective glycosylation between the saccharides and lipophilic groups is difficult. We have recently reported a novel linear approach to synthesize homo-oligoiduronic acid^{24a}. We employed a similar approach to synthesis the L-idose based amphiphiles (**IDC-2**, **IDC-3**, and **IDC-4**) from L-idose. Building block **1** was converted into the thiophenylL-idosyl donor by treatment with a mixture of acetic acid and Cu(OTf)₂ for anhydro-ring opening followed by glycosylation with thiophenol. The L-idose donor **10** was glycosylated with **8** using TMSOTf and NIS as an activator to yield 56% of the disaccharide precursor **11**. Compound **11** was converted to the disaccharide donor **13** by treatment with Cu(OTf)₂ and acetic acid and thioglycosylation. Compound **13** and cholesterol were coupled by using NIS and TfOH and subjected to deprotection of esters under basic conditions, and sulfation in the presence of SO₃.Et₃N yielding 69% of compound **16**. Finally, the hydrogenation of the 2-naphthylmethyl ether protecting groups over Pd/C produced the target compound **IDC-2**. In the case of the tri- and tetrasaccharides (**IDC-3** and **IDC-4**), the reaction sequences were similar to those of **IDC-2**. Similarly, di-, tri- and tetrasaccharide iduronic acid amphiphiles (**IAC-2**, **IAC-3** and **IAC-4**) were synthesized. (Scheme 1)



Scheme 1: Synthesis of **IDC-2**: Reagents and conditions: (a) Cholesterol, NIS, TfOH, CH₂Cl₂, 4 Å M.S., -10 °C; (b) NaOMe, MeOH/CH₂Cl₂(2:1), 85%; c) SO₃·Et₃N, DMF, 60 °C, 70% ; d) H₂, Pd(OH)₂, H₂O. 55%.

4.2.2 Biological Evaluation

Contemporary strategies for designing anti-viral drugs have increasingly focused on selectively inhibiting heparanase, a crucial enzyme that modulates heparan sulfate proteoglycans (HSPGs) on the cell surface, serving as receptors for numerous viruses¹³. The degradation of HS by heparanase facilitates viral spread to distant sites and has been notably implicated in COVID-19. Studies have demonstrated a correlation between increased plasma heparanase activity, elevated HS levels, and COVID-19 severity and outcomes,¹⁴ which has led to the evaluation of HS mimetics, including pixatimod.²²

Synthetic heparinoids were evaluated for their ability to inhibit heparanase using the fondaparinux assay²⁷, with PG545 as the positive control compound. The IC₅₀ values are summarized in Table 1. All heparinoids exhibited potent inhibition of heparanase, except for the shorter IAC-2, consistent with prior findings indicating that sulfated oligosaccharide chains in this class of compounds must be at least trisaccharides for strong inhibition¹². Heparanase inhibitory potency correlated with the oligosaccharide chain length; for instance, tetrasaccharide analogs like PG545 demonstrated robust inhibition. Additionally, an increase in oligosaccharide chain length from di- to tri- and tetrasaccharides (L-idose and L-iduronic acid derivatives) systematically enhanced potency against heparanase, underscoring the importance of sulfation levels.²⁶

Moreover, the glycosidic linkage between cholestanol and the sugar moiety also influenced potent inhibition. Furthermore, amphiphilic groups like azido, alkynyl, and fluorescent tags significantly enhanced heparanase inhibition compared to PG545, with some compounds exhibiting up to six-fold greater potency. Incorporating a C18 chain at the reducing end also yielded strong or comparable inhibition to PG545. These results highlight that D-oligomaltoside analogs are preferable for targeting heparanase over their L-idose or L-iduronic acid counterparts. The incorporation of hydrophobic moieties such as C18 or cholestanol, with or without fluorophores or other modifications, effectively modulates heparanase inhibition activity.

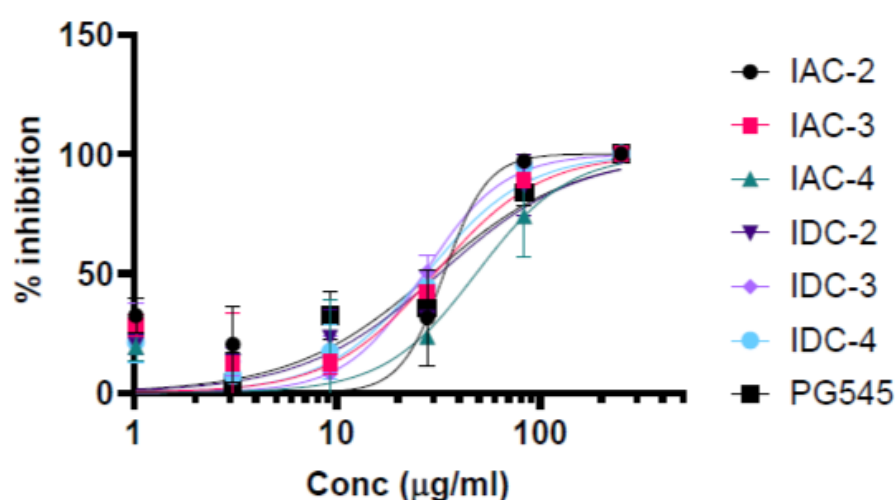


Figure 3: In vitro evaluation of antiviral property (PRNT) of IAC and IDC series compounds and PG545 against SARS-CoV-2 D614 variant

Following the assessment of anti-heparanase activity of the amphiphilic heparinoids, we investigated their anti-viral properties. The compounds were evaluated using a plaque reduction neutralization test (PRNT) against SARS-CoV-2 D614 and G614 isolates in Vero cells (Table 1 and Fig. 3). These strains were chosen as they are local (Australian) clinical isolates available to us. The D614 isolate represents an early clinical strain containing the ancestral D614 form of the Spike protein, initially identified in Wuhan, China. The G614 isolate carries the D614G mutation, which emerged in Europe in February 2020, conferring increased infectivity and becoming the dominant global variant by May 2020. However, it was subsequently replaced by newer variants and ceased circulation.²⁸ Comparing our new

compounds against these variants allowed benchmarking against PG545, known for its potent antiviral activity against SARS-CoV-2.²²

Due to limited availability of compounds, the IAC and IDC series were only tested against the ancestral D614 isolate. As shown in Table 1, the L-idose and L-iduronic acid analogs demonstrated activity dependent on the oligosaccharide chain length, with IC₅₀ values in the micromolar range. Among these, trisaccharide analogs IDC-3 and IAC-3 exhibited more potent activity than other analogs, showing similar IC₅₀ values to PG545 in this assay. These findings indicated that the trisaccharide scaffold is optimal for inhibiting SARS-CoV-2 within this series. Overall, these findings underscored the ability to distinguish between anti-heparanase and antiviral activities using amphiphilic heparinoid ligands.

Table 1. Inhibitory potency of test compounds against heparanase and SARS-CoV-2 isolates (PRNT). NI = no inhibition. NT = not tested.

Entry	Inhibitor	Heparanase (IC ₅₀ , μM) ^a	SARS-Cov-2 D614 (IC ₅₀ , μg/mL) ^b	SARS-CoV-2G614 (IC ₅₀ , μg/mL) ^b
1	PG545	0.123 ± 0.017	29.6 ± 5	NT
2	IAC-2	NI	33.7 ± 9.5	NT
3	IAC-3	3.54 ± 0.07	30.4 ± 6.5	NT
4	IAC-4	3.41 ± 0.14	48.5 ± 9	NT
5	IDC-2	10.42 ± 0.24	32.1 ± 7	NT
6	IDC-3	3.44 ± 0.06	26.9 ± 5	NT
7	IDC-4	3.19 ± 0.09	27.5 ± 4.5	NT

^aHeparanase inhibition in μM ± SE, n = 3. ^bPRNT in μg/mL ± SEM, n = 2.

To explore the interactions of the most potent compounds with the RBD domain of the SARS-CoV-2 spike protein, isothermal titration calorimetry (ITC) experiments were conducted using selected compounds and PG545 (as a control), with recombinant ancestral Spike protein RBD expressed in HEK 293 cells (GenBank: QHD43416). IAC-3 and IDC-3 were chosen based on their comparable or superior potency to PG545 in PRNT and heparanase assays

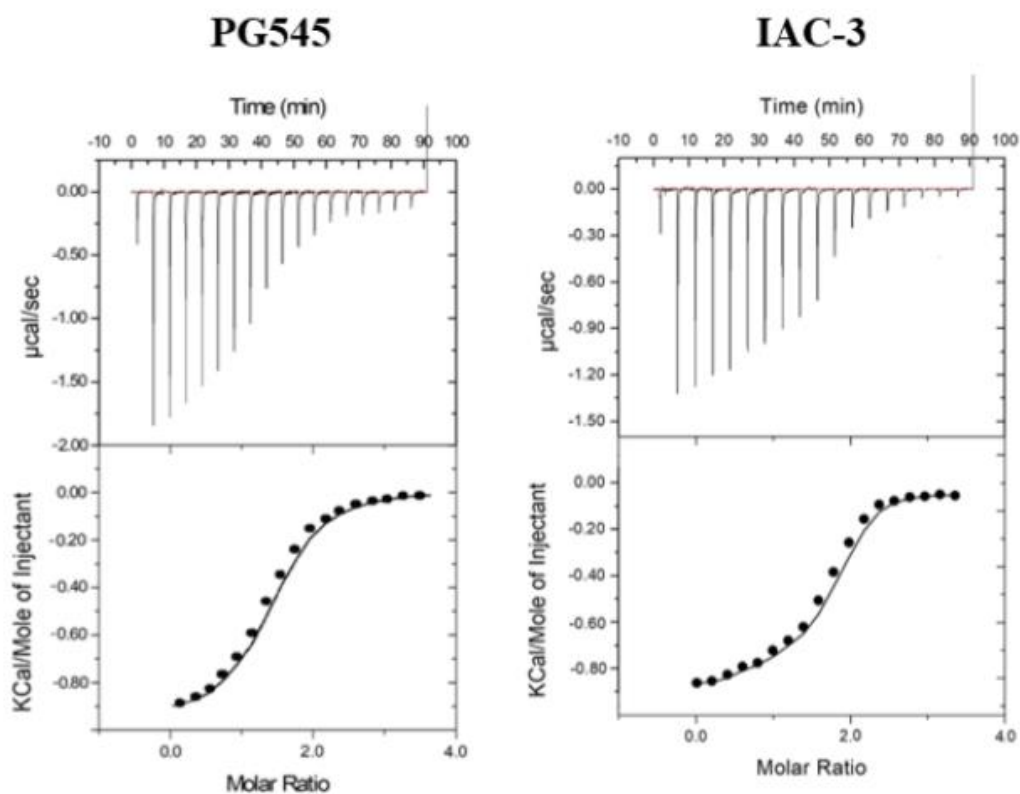


Figure 4: ITC profile for the interaction of selected heparinoids with spike protein.

The ITC measurements revealed that all compounds bound to the RBD with dissociation constants (K_D) ranging from 1.87 to 9.18 μM (Fig. 4, Table 2). Notably, IDC-3 exhibited similar affinity to the RBD compared to PG545,

Table2. ITC data for selected compounds. Data are the average of 3 titrations \pm SD.

Compound	n	K_D (μM)	ΔH (cal/mol)	ΔS (cal/mol/deg)
PG545	1.56 ± 0.03	9.12 ± 1.44	-8554 ± 196	12.4 ± 0.3
IAC-3	1.73 ± 0.12	9.18 ± 2.91	-8143 ± 107	13.2 ± 0.12
IDC-3	1.53 ± 0.05	2.11 ± 1.73	-4452 ± 114	11.8 ± 0.4

4.2.3 Molecular Docking Studies

IAC-3 and IDC-3 were subsequently docked using GlycoTorch Vina29 to investigate their interactions with heparanase and the SARS-CoV-2 spike protein RBD. The highest scoring

complexes of each ligand with the two proteins are depicted in Fig. 4 and 5, while the top four next-best scoring complexes and the ensemble cluster for each ligand are presented in the Supporting Information (Fig. 6-9). It has been previously reported that PG545 forms a complex with heparanase, orienting the cholesterol group towards heparin-binding domain II.

24b

Several similarities are observed between the docked conformations of PG545 and those of IAC-3 and IDC-3 bound to heparanase. Firstly, all ligands obstruct the catalytic residues of heparanase (Glu 225 and Glu 343), with the cholesterol side chain establishing crucial hydrophobic contacts. Additionally, all ligands interact within heparin-binding domains I and II. However, a distinguishing feature is the specific residues bound by each compound within these domains. PG545 interacts with three residues in the first binding domain (Lys 159, Phe 160, Lys 161) and two in the second binding domain (Arg 272, Lys 274). In contrast, IAC-3 and IDC-3 interact with two residues (Lys 159 and Phe 160) in the first binding domain, but engage with four residues (Gln 270, Arg 272, Lys 274, Thr 275) in the second binding domain. These additional binding interactions likely contribute to their enhanced heparanase inhibitory potency compared to IAC-3 and IDC-3.

IAC-3 and IDC-3 were further docked into the spike RBD, with the top scoring complex identified for each shown in Fig. 4. Previous studies have reported the conformation of PG545 in complex with the RBD-ACE2 complex.²² PG545 and the complexes of IAC-3 and IDC-3 share several common features. All ligands exhibit interactions with residues within heparin binding site I, facilitated by the sulfate groups within their structures.

Specifically, PG545 interacts with five residues within the binding site (Arg 346, Asn 354, Arg 355, Lys 356, Arg 466). In contrast, IAC-3 interacts with one residue (Arg 346) within the binding site, while IDC-3 engages with three residues (Arg 346, Asn 354, Arg 466), which likely contributes to its higher affinity compared to IAC-3. However, both IAC-3 and IDC-3 bind similarly to PG545 with some distinct interactions: IAC-3 interacts with Leu 452, whereas the tighter binding IDC-3 interacts additionally with Tyr 449 and Leu 452.

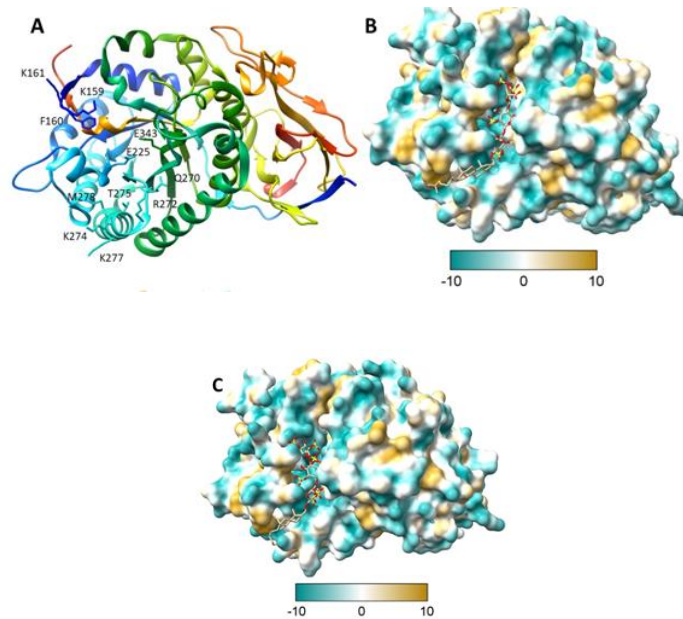


Figure 4. (A) Ribbon diagram of heparanase(PDB ID:5E9C) coloured blue to red from the N- to C-terminal with key residues involved in binding labelled. The top scoring complex obtained from docking with GlycoTorch Vina of (B) **IAC-3**, (C) **IDC-3**.,The surfaces (B-D) are in the same orientation as the ribbon diagram in (A). The enzyme surface is rendered using UCSF Chimera, wherein the hydrophobic regions of the surface are in tan and the hydrophilic in blue.

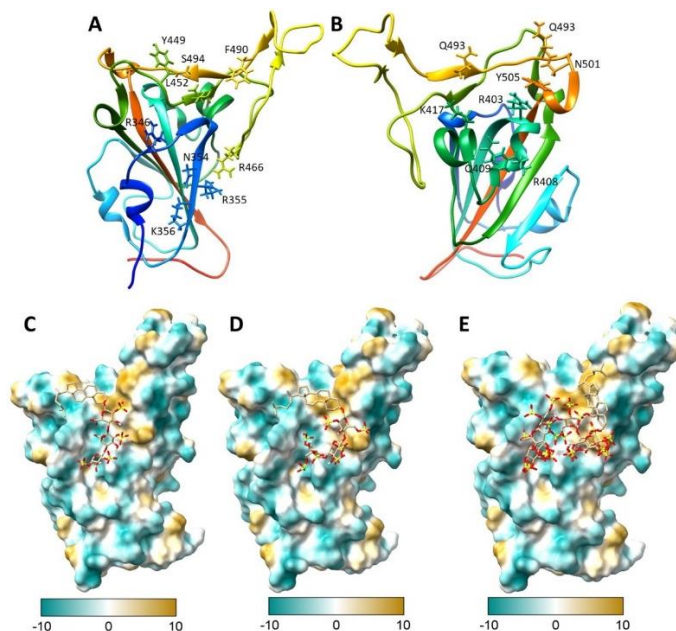


Figure 5. (A) Ribbon diagram of RBD of SARS-CoV-2 spike protein heparin binding site I (PDB ID: 6LZG). (B) Ribbon diagram of RBD of spike protein heparin binding site III. Both

diagrams coloured blue to red from the N- to C-terminal, with the residues responsible for binding labelled. The top scoring complex obtained from docking with GlycoTorch Vina of (C) **IAC-3**, (D) **IDC-3**. The receptor surface is rendered using UCSF Chimera, wherein the hydrophobic regions of the surface are in tan and the hydrophilic in blue. The surfaces (C-E) are oriented in the same orientation as the ribbon diagram in (A).

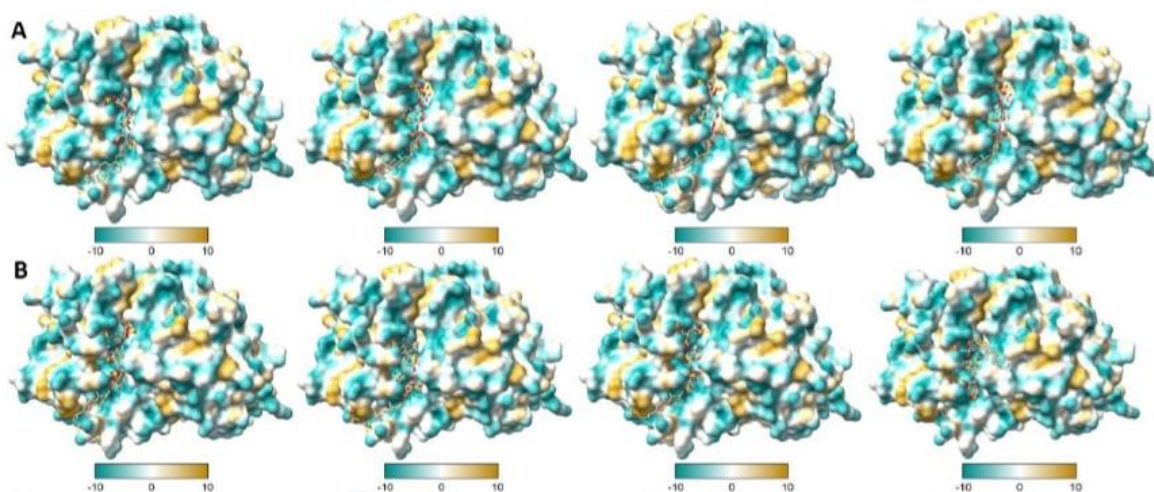


Figure 6: Second to fifth top scoring conformations calculated obtained from docking with GlycoTorch Vina of the three identified ligands with heparanase (PDB ID:5E9C). The enzyme surface is rendered using UCSF Chimera, wherein the surface's hydrophobic regions are tan and the hydrophilic in blue. The conformations of (A) IAC-3. (B) IDC-3. Amino acids are not shown for clarity.

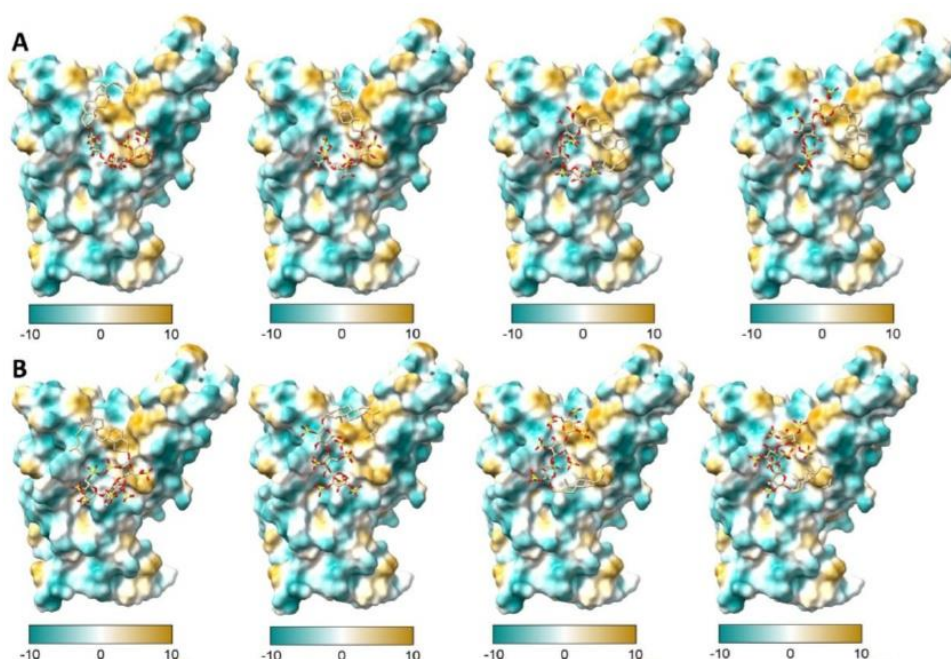


Figure 7: Second to fifth top scoring conformations calculated obtained from docking with GlycoTorch Vina of the three identified ligands with RBD of SARS-CoV-2 spike protein

(PDB ID: 6LZG). The enzyme surface is rendered using UCSF Chimera, wherein the surface's hydrophobic regions are tan and the hydrophilic in blue. The conformations of (A) IAC-3. (B) IDC-3. Amino acids are not shown for clarity.

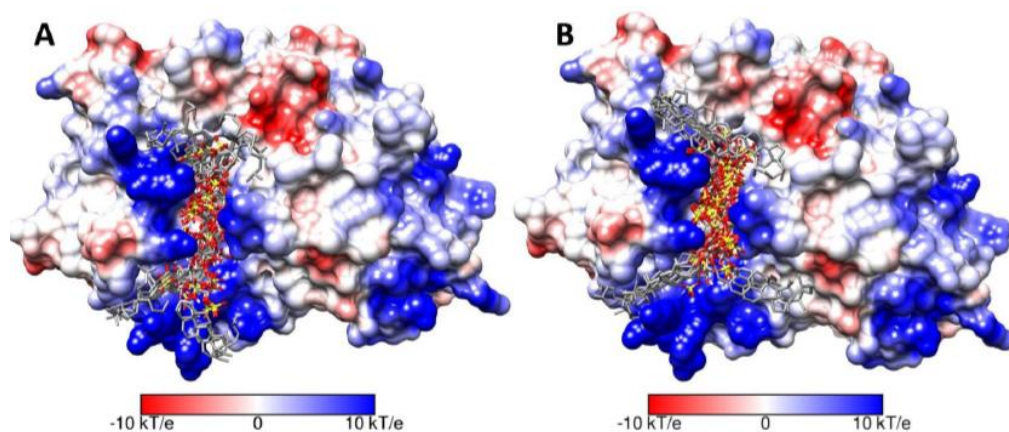


Figure 8: Ensemble cluster conformation obtained from docking with GlycoTorch Vina of the three identified ligands with heparanase (PDB ID:5E9C). The enzyme coulombic surface is rendered using UCSF Chimera using the default setting, wherein negative charges are coloured red, and positive charges are coloured blue. The conformation of (A) IAC-3. (B) IDC-3. Amino acids are not shown for clarity.

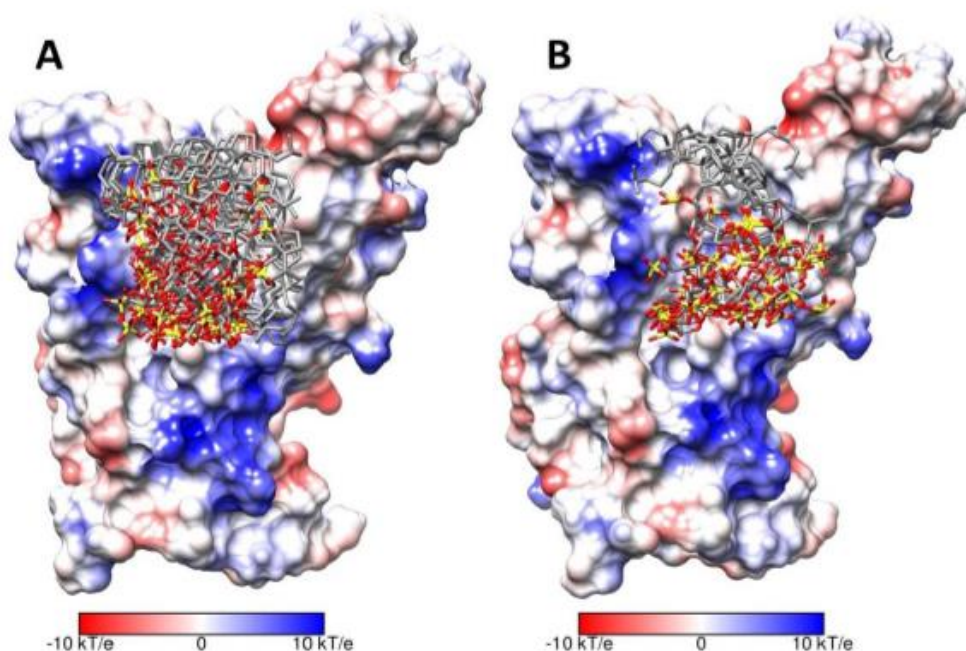


Figure 9: Ensemble cluster conformation obtained from docking with GlycoTorch Vina of the three identified ligands with RBD of SARS-CoV-2 spike protein (PDB ID: 6LZG). The

RBD coulombic surface is rendered using UCSF Chimera using the default setting, wherein negative charges are coloured red, and positive charges are coloured blue. The conformation of (A) IAC-3. (B) IDC-3. Amino acids are not shown for clarity.

4.3 CONCLUSIONS

Inspired by the amphiphilic HS mimetic pixatimod (PG545), a heparanase inhibitor in clinical trials showing promising activity against SARS-CoV-2, we synthesized a library of amphiphilic heparinoid mimetics as potential anti-SARS-CoV-2 agents. Employing a custom synthetic strategy, we varied the sulfated oligosaccharide moiety (highly sulfated, poly-L-idose, or poly-L-iduronic acid) with the lipophilic groups.

The compounds were assessed for their ability to inhibit heparanase and two SARS-CoV-2 isolates using a plaque reduction neutralization test. Sulfated higher oligosaccharides of L-idose with lipophilic aglycones exhibited potent anti-SARS-CoV-2 and anti-heparanase activities comparable to or superior to pixatimod (PG545), outperforming their isosteric L-iduronic acid counterparts. Notably, lipophilic groups like cholestanol and C18-aliphatic substitution provided greater advantages than other types of lipophilic moieties.

Confirmation of the binding of the most potent compounds to the RBD of the SARS-CoV-2 spike protein was achieved through ITC and molecular docking calculations. These results underscore the potential of fine-tuning higher oligosaccharide structure, degree of sulfation, and lipophilic groups in developing effective drug candidates for COVID-19 treatment. Specifically, IDC-4 shows promising potential to inhibit SARS-CoV-2 infection.

4.4 EXPERIMENTAL SECTION

4.4.1 General Information

General experimental details have been given previously.^{24, 25} High-resolution MS (HRMS) for polysulfated final products were performed in negative ion ESI mode using a Bruker MicroTOF Q II mass spectrometer, calibrated using Agilent calibration solution (G1969-85000, Agilent). The instrument was scanned from 50 – 3000 m/z with a scan time of 2

seconds. The purity of compounds **IAC-3**, **IAC-4**, **IDC-3**, **IDC-4** were determined to be $\geq 95\%$ pure by HPLC or SEC.

4.4.2 Synthesis of IAC and IDC Series:

General Procedure for Ester Deprotection

Compounds were dissolved in a THF/MeOH/H₂O water mixture (4/2/1). 50 eq of LiOH·H₂O was added and the reaction was stirred for 2-3 days. After completion, the reaction was quenched with Amberlite IR120 acidic resin (or Dowex 50WX8 H⁺ resin if the compound is sulfated), filtered and evaporated under reduced pressure, and the residue was purified by flash chromatography using DCM and MeOH as eluent to give the deprotected compounds.

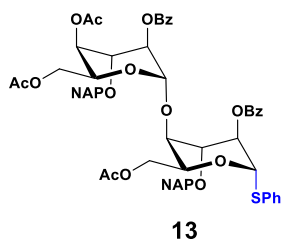
General Procedure for *O*-Sulfation

Compounds were dissolved in dry DMF (6 mL). SO₃·Et₃N (5 eq per OH group) was added and the reaction was stirred for 3 days at 60°C. After completion, the reaction was cooled to RT and aqueous NaHCO₃ (10 eq per OH group) was added and stirring continued for another 16h. The mixture was then filtered and washed with DCM/MeOH (1/1, 10 mL), solvents were evaporated under reduced pressure and the resulting residue was purified by using C-18 bond elute column eluting with increasing acetonitrile concentration in water, and passed through sodium (Na⁺) resin column using water as eluent. The product fraction was lyophilized to afford sulfated compounds as a white powder.

General Procedure for Hydrogenolysis

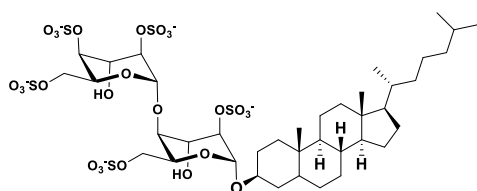
Compound was dissolved in dry methanol, 20% Pd(OH)₂ on carbon (0.025 g per benzyl group) was added and the reaction vessel was purged with hydrogen gas. The reaction mixture was stirred at RT for 2-3 days. The mixture was filtered through celite, and the filtrate was evaporated under reduced pressure. The residue was purified through bond elute C-18 column eluted with water. Sulfated compounds were passed through sodium (Na⁺) resin. The product fraction was lyophilized to afford sulfated compounds as a white powder.

Thiophenyl-((4,6-*O*-diacetyl-2-benzoyl-3-(2-naphthylmethyl))- α -L-idopyranosyl- α -(1 \rightarrow 4)(6-*O*-acety-2-benzoyl-3-*O*-(2-naphthylmethyl))- α -L-idopyranoside(13).



Compound **11** (730 mg, 0.813 mmol) was dissolved in Ac₂O (5 ml), Cu(OTf)₂ (29.5 mg, 0.0813 mmol) was added at 0°C and kept for stirring for overnight. Completion of reaction was monitored by TLC, after completion, reaction mixture was concentrated under reduced pressure and rotavapour, then subsequently crude was extracted with EtOAc against sta. NaHCO₃ solution and dried over Na₂SO₄. The crude was concentrated and dried under reduced pressure, further it was taken to next step without purification, Crude Compound **12** (1.69 g, 1.693 mmol) and ZnI₂ (1.137 g, 3.56 mmol) was taken in a round bottom flask which is covered with aluminium foil, and was kept on high vacuum for 2 hours. The reaction mixture was dissolved in dry DCM and trimethyl(phenylthio)silane TMSSPh (0.962 g, 5.26 mmol) was added, kept for stirring for 1 hour. The reaction completion was monitored by TLC, after completion of reaction, clite filtration was done and then purified by silica column in a EtOAc/Hexane solvent system to get compound **13** in a 85% yield. ¹H NMR (400 MHz, Chloroform-*d*) 5.70 (d, *J* = 2.4 Hz, 1H), 5.63 (d, *J* = 1.4 Hz, 1H), 5.30 – 5.21 (m, 1H), 5.16 – 4.92 (m, 4H), 4.84 (t, *J* = 11.3 Hz, 2H), 4.58 – 4.40 (m, 4H), 4.32 – 4.18 (m, 1H), 3.88 – 3.74 (m, 3H), 3.37 (dd, *J* = 11.7, 4.2 Hz, 1H), 2.01 (s, 3H), 1.95 (s, 3H), 1.90 (s, 3H) 8.08 – 7.92 (m, 3H), 7.89 – 7.70 (m, 10H), 7.68 – 7.63 (m, 2H), 7.63 – 7.51 (m, 3H), 7.46 – 7.33 (m, 9H), 7.16 – 7.09 (m, 2H) ¹³C NMR (101 MHz, Chloroform-*d*) δ 170.59, 165.51, 134.78, 134.64, 133.61, 133.33, 133.04, 132.20, 129.98, 129.79, 129.02, 128.46, 128.36, 128.25, 128.19, 128.03, 127.97, 127.74, 127.69, 127.61, 126.81, 126.74, 126.17, 126.05, 126.03, 125.85, 125.81, 125.68, 101.72, 86.20, 77.48, 77.25, 74.50, 73.23, 72.57, 72.48, 68.73, 67.40, 66.90, 65.97, 64.14, 62.93, 62.75, 20.78, 20.53. HR-ESI-MS (*m/z*): [M+Na]⁺, calculated for C₆₀H₅₆O₁₅SNa 1071.3238; Found 1071.3239.

3 β -Cholestanyl 2,4,6-tri-*O*-sulfonato- α -L-idopyranosyl-(1 \rightarrow 4)-2,6-di-*O*-sulfonato- α -L-idopyranoside (IDC-2)



17
IDC-2

The compound **16** (0.05 g, 0.039 mmol) was dissolved in dry methanol (2 mL), 20% Pd(OH)₂ on carbon (0.11 g, 0.017 mmol) was added and purged with hydrogen gas, and the mixture was stirred at RT for 24

h. The residue was filtered and the filtrate was evaporated under reduced pressure and purified through a bond elute C-18 column eluted with water. The product fraction was lyophilized to afford compound **IDC-2** (0.035 g, 57%). ¹H NMR (600 MHz, D₂O) δ 5.08 (d, J = 40.7 Hz, 2H), 4.78 – 4.74 (m, 1H), 4.46 (d, J = 8.0 Hz, 1H), 4.28 – 4.22 (m, 3H), 4.16 (dt, J = 10.9, 6.8 Hz, 6H), 3.77 (s, 1H), 3.65 (s, 1H), 1.87 (d, J = 12.4 Hz, 1H), 1.77 (s, 1H), 1.72 (s, 1H), 1.63 (s, 1H), 1.57 (s, 2H), 1.43 (td, J = 13.1, 7.3 Hz, 4H), 1.32 – 1.13 (m, 10H), 1.01 (dd, J = 14.2, 5.1 Hz, 6H), 0.92 (h, J = 12.5, 12.0 Hz, 5H), 0.81 (d, J = 6.6 Hz, 3H), 0.75 (dd, J = 6.6, 2.6 Hz, 6H), 0.72 (s, 3H), 0.56 (s, 3H). HRMS m/z calcd for C₃₉H₆₃O₂₆S₅⁵⁻: 1107.2239 found(m/z + 5H): 222.4530.

4.4.3 Plaque Reduction Neutralisation Test (PRNT)

The ability of the compounds to neutralize live SARS-CoV-2 virus was assessed using our established protocol.^{22, 31} Briefly, the compounds were titrated in DMEM in round bottom 96 well plates. For SARS-CoV-2, QLD02/2020—30/1/2020 (GISAID accession EPI_ISL_407896) and QLDID935/2020—25/03/2020 (GISAID accession EPI_ISL_436097), referred as D614 and G614, respectively, was isolated and obtained from Queensland Health, Brisbane, Australia. Viruses were passaged three times in Vero E6 cells and titrated by focus-forming assay on Vero E6 cells. The viruses were incubated with serial diluted compound or vehicle for 1 hour at 37 °C prior to adding to pre-seeded VeroE6 cells at 50 μ l/well. Mixtures were incubated onto cells for 30 minutes. Overlay were then subsequently added before proceeding as per immunoplaque assay protocol. IC₅₀ values were derived from a three-parameter dose response curve fit to plaque numbers obtained for compound titration performed in duplicate per condition. All work with viruses was performed in a biosafety

level 3 laboratory. *In vitro* work and protocol were approved by the University of Queensland Biosafety committee (IBC/447B/SCMB/2021).

4.4.4 Cytotoxicity assays

The cytotoxicity assay of compounds and vehicle was performed on Vero 76 cells and measured using the MTT assay in 96 wells plate format as described previously.¹⁹

4.4.5 Heparanase inhibition assays

For high-throughput screening of the compound library for heparanase inhibition, a colorimetric assay based on the cleavage of the synthetic heparin pentasaccharide fondaparinux (Arixtra)²⁷ was carried out. The assay measures the appearance of the disaccharide product of heparanase-catalyzed fondaparinux cleavage, colorimetrically using the tetrazolium salt WST-1. Assay solutions (100 μ L) were composed of 40 mM sodium acetate buffer (pH 5.0) and 100 mM fondaparinux (Arixtra) with or without inhibitor. Recombinant heparanase³² was added to a final concentration of 140 pM, to start the assay. The plates were incubated at 37°C for 18–21 h and the reaction was stopped by the addition of 100 μ L solution containing 1.69 mM 4-[3-(4-iodophenyl)-2-(4-nitrophenyl)-2H-5-tetrazolio]-1,3-benzene disulfonate (WST-1) in 0.1 M NaOH. The plates were developed at 60°C for 60 min, and the absorbance (OD) was measured at 584 nm. In each plate, a standard curve constructed with D-galactose as the reducing sugar standard was prepared in the same buffer and volume over the range of 2–100 μ M. In each experiment, each compound was examined in duplicate for its capacity to inhibit heparanase at increasing concentration ranging from 6.25 ng/ml to 3.125 mg/ml. A dose-response curve was then plotted and the IC₅₀ value calculated. Each experiment was repeated 2-3 times and the variation (SE) between the IC₅₀ values listed in table 1 did not exceed \pm 15% of the mean.

4.4.6 Isothermal titration calorimetry

The thermodynamic analysis of heparinoids and the spike protein (SAE1000, Sigma-Aldrich) was conducted using an isothermal titration calorimeter (ITC 200, USA). The titration cell contained spike protein (10 μ M) and was titrated with heparinoids (1 mM of 2 μ L) in a Tris buffer (10 mM Tris, 50 mM NaCl, pH 7.5). Each experiment comprised 18 injections with a consecutive time interval of 100 s between two injections. To ensure

thorough mixing of the solutions, the stirring speed was maintained at 1000 rotations/min. The cell temperature was held constant at 298 K, and nearly three successive titrations were averaged to obtain the ITC curves (Fig. 4).

4.4.7 Molecular docking

The crystal structure of the RBD-ACE2 complex (PDB ID: 6LZG)³³ was obtained from the RCSB Protein Data Bank. After removing water molecules, ACE2 chains, and any cofactors or ligands, UCSF Chimera 1.16³⁴ was utilised for structure editing and visualization. For docking three compounds, namely **IAC-3**, **IDC-3** the GlycoTorch Vina²⁹ docking program was employed. Glycam carbohydrate builder (Glycam.org) was used to build the sulfated backbone of oligosaccharides, which was then modified by adding a cholestanol group at the reducing end using Discovery Studio³⁵ to obtain the required structure. During the docking process, all sulfate and hydroxyl groups, as well as glycosidic torsion angles of the ligand, were treated as flexible. The box size was adjusted to cover both sites I and II, reported previously²² for PG545. Docking runs were carried out with an energy range of 12, an exhaustiveness of 80, chi_cutoff = 1, chi_coeff = 2, and the number of modes set to 100. The docking simulations were repeated twice to ensure accuracy and reliability. To identify common binding modes and oligosaccharide-protein interactions, a cluster analysis using UCSF Chimera 1.16 was performed on multiple docking solutions obtained from the docking process. This analysis aimed to identify poses that could potentially exhibit similar interactions with the ligand-RBD complex.

The same approach was used to dock the 3 ligands to heparanase. The 5E9C crystal structure cocrystallised with heparin tetrasaccharide,³⁶ was selected for docking studies. Water and all non-standard residues were removed before docking, and Glu225 was manually protonated. The active site was defined based on the co-crystallised ligand (heparin tetrasaccharide) with heparanase.

The results from the docking were visualised using UCSF Chimera version 1.16. The clusters were determined using the ensemble cluster tool within Chimera 1.16. Pose analysis was carried out using Biovia Discovery Studio Visualiser 2021, ligand interaction 2D diagram tool. Hydrophobic surfaces were created using ChimeraX 1.3,³⁷ and the coulombic surfaces were created using Chimera 1.16.

4.5 References

1. (a) Finkel, Y.; Mizrahi, O.; Nachshon, A.; Weingarten-Gabbay, S.; Morgenstern, D.; Yahalom-Ronen, Y.; Tamir, H.; Achdout, H.; Stein, D.; Israeli, O., et al. The coding capacity of SARS-CoV-2. *Nature***2021**, *589*, 125-130.(b) Harvey, W. T.; Carabelli, A. M.; Jackson, B.; Gupta, R. K.; Thomson, E. C.; Harrison, E. M.; Ludden, C.; Reeve, R.; Rambaut, A.; Consortium, C.-G. U., et al. SARS-CoV-2 variants, spike mutations and immune escape. *Nat. Rev. Microbiol.***2021**, *19*, 409-424.(c) Hu, B.; Guo, H.; Zhou, P.; Shi, Z. L. Characteristics of SARS-CoV-2 and COVID-19. *Nat. Rev. Microbiol.***2021**, *19*, 141-154.
2. Chaudhary, N.; Weissman, D.; Whitehead, K. A. mRNA vaccines for infectious diseases: principles, delivery and clinical translation. *Nat. Rev. Drug Discov.***2021**, *20*, 817-838.
3. Haddad, F.; Dokmak, G.; Karaman, R. A Comprehensive Review on the Efficacy of Several Pharmacologic Agents for the Treatment of COVID-19. *Life***2022**, *12*, 1758.
4. (a) Kearns, F. L.; Sandoval, D. R.; Casalino, L.; Clausen, T. M.; Rosenfeld, M. A.; Spliid, C. B.; Amaro, R. E.; Esko, J. D. Spike-heparan sulfate interactions in SARS-CoV-2 infection. *Curr. Opin. Struct. Biol.***2022**, *76*, 102439.(b) Liu, L.; Chopra, P.; Li, X.; Bouwman, K. M.; Tompkins, S. M.; Wolfert, M. A.; de Vries, R. P.; Boons, G. J. Heparan Sulfate Proteoglycans as Attachment Factor for SARS-CoV-2. *ACS Cent. Sci.***2021**, *7*, 1009-1018.(c) Clausen, T. M.; Sandoval, D. R.; Spliid, C. B.; Pihl, J.; Perrett, H. R.; Painter, C. D.; Narayanan, A.; Majowicz, S. A.; Kwong, E. M.; McVicar, R. N., et al. SARS-CoV-2 Infection Depends on Cellular Heparan Sulfate and ACE2. *Cell***2020**, *183*, 1043-1057 e15.
5. (a) Mycroft-West, C. J.; Su, D.; Pagani, I.; Rudd, T. R.; Elli, S.; Gandhi, N. S.; Guimond, S. E.; Miller, G. J.; Meneghetti, M. C. Z.; Nader, H. B., et al. Heparin Inhibits Cellular Invasion by SARS-CoV-2: Structural Dependence of the Interaction of the Spike S1 Receptor-Binding Domain with Heparin. *Thromb. Haemost.***2020**, *120*, 1700-1715.(b) Paiardi, G.; Richter, S.; Oreste, P.; Urbinati, C.; Rusnati, M.;

Wade, R. C. The binding of heparin to spike glycoprotein inhibits SARS-CoV-2 infection by three mechanisms. *J. Biol. Chem.***2022**, *298*, 101507.(c) Parafioriti, M.; Ni, M. H.; Petitou, M.; Mycroft-West, C. J.; Rudd, T. R.; Gandhi, N. S.; Ferro, V.; Turnbull, J. E.; Lima, M. A.; Skidmore, M. A., et al. Evidence for multiple binding modes in the initial contact between SARS-CoV-2 spike S1 protein and cell surface glycans. *Chem. Eur. J.***2022**, *29*, e202202599.(d) Schuurs, Z. P.; Hammond, E.; Elli, S.; Rudd, T. R.; Mycroft-West, C. J.; Lima, M. A.; Skidmore, M. A.; Karlsson, R.; Chen, Y. H.; Bagdonaite, I., et al. Evidence of a putative glycosaminoglycan binding site on the glycosylated SARS-CoV-2 spike protein N-terminal domain. *Comput. Struct. Biotechnol. J.***2021**, *19*, 2806-2818.

6. (a) Brickman, Y. G.; Ford, M. D.; Gallagher, J. T.; Nurcombe, V.; Bartlett, P. F.; Turnbull, J. E. Structural modification of fibroblast growth factor-binding heparan sulfate at a determinative stage of neural development. *J. Biol. Chem.***1998**, *273*, 4350-4359.(b) Feyzi, E.; Saldeen, T.; Larsson, E.; Lindahl, U.; Salmivirta, M. Age-dependent modulation of heparan sulfate structure and function. *J. Biol. Chem.***1998**, *273*, 13395-13398.(c) Gama, C. I.; Hsieh-Wilson, L. C. Chemical approaches to deciphering the glycosaminoglycan code. *Curr. Opin. Chem. Biol.***2005**, *9*, 609-619.(d) Nadanaka, S.; Kitagawa, H. Heparan sulphate biosynthesis and disease. *J. Biochem.***2008**, *144*, 7-14.(e) Xu, D.; Esko, J. D. Demystifying heparan sulfate-protein interactions. *Annu. Rev. Biochem.***2014**, *83*, 129-157.
7. (a) Hu, Y. P.; Zhong, Y. Q.; Chen, Z. G.; Chen, C. Y.; Shi, Z.; Zulueta, M. M.; Ku, C. C.; Lee, P. Y.; Wang, C. C.; Hung, S. C. Divergent synthesis of 48 heparan sulfate-based disaccharides and probing the specific sugar-fibroblast growth factor-1 interaction. *J. Am. Chem. Soc.***2012**, *134*, 20722-20727.(b) Pawar, N. J.; Wang, L.; Higo, T.; Bhattacharya, C.; Kancharla, P. K.; Zhang, F.; Baryal, K.; Huo, C. X.; Liu, J.; Linhardt, R. J., et al. Expedient Synthesis of Core Disaccharide Building Blocks from Natural Polysaccharides for Heparan Sulfate Oligosaccharide Assembly. *Angew. Chem. Int. Ed.***2019**, *58*, 18577-18583.(c) Zong, C.; Venot, A.; Li, X.; Lu, W.; Xiao, W.; Wilkes, J. L.; Salanga, C. L.; Handel, T. M.; Wang, L.; Wolfert, M. A., et al. Heparan Sulfate Microarray Reveals That Heparan Sulfate-Protein Binding Exhibits Different Ligand Requirements. *J. Am. Chem. Soc.***2017**, *139*, 9534-9543.(d) Zulueta, M. M. L.; Chyan, C. L.; Hung, S. C. Structural analysis of synthetic heparan sulfate

- oligosaccharides with fibroblast growth factors and heparin-binding hemagglutinin. *Curr. Opin. Struct. Biol.***2018**, *50*, 126-133.
8. (a) Chittum, J. E.; Sankaranarayanan, N. V.; O'Hara, C. P.; Desai, U. R. On the Selectivity of Heparan Sulfate Recognition by SARS-CoV-2 Spike Glycoprotein. *ACS Med. Chem. Lett.***2021**, *12*, 1710-1717.(b) Hao, W.; Ma, B.; Li, Z.; Wang, X.; Gao, X.; Li, Y.; Qin, B.; Shang, S.; Cui, S.; Tan, Z. Binding of the SARS-CoV-2 spike protein to glycans. *Sci. Bull. (Beijing)***2021**, *66*, 1205-1214.
9. (a) Kim, S. Y.; Jin, W.; Sood, A.; Montgomery, D. W.; Grant, O. C.; Fuster, M. M.; Fu, L.; Dordick, J. S.; Woods, R. J.; Zhang, F., et al. Characterization of heparin and severe acute respiratory syndrome-related coronavirus 2 (SARS-CoV-2) spike glycoprotein binding interactions. *Antiviral Res.***2020**, *181*, 104873.(b) Tandon, R.; Sharp, J. S.; Zhang, F.; Pomin, V. H.; Ashpole, N. M.; Mitra, D.; McCandless, M. G.; Jin, W.; Liu, H.; Sharma, P., et al. Effective Inhibition of SARS-CoV-2 Entry by Heparin and Enoxaparin Derivatives. *J. Virol.***2021**, *95*, e01987-20.
10. (a) Eder, J.; Bermejo-Jambrina, M.; Vlaming, K. E.; Kaptein, T. M.; Zaderer, V.; Kemper, E. M.; Wilflingseder, D.; Reitsma, S.; Bree, G. J. d.; Cohn, D. M., et al. Inhalation of Low Molecular Weight Heparins as Prophylaxis against SARS-CoV-2. *mBio***2022**, *13*, e02558-22.(b) van Haren, F. M. P.; van Loon, L. M.; Steins, A.; Smoot, T. L.; Sas, C.; Staas, S.; Vilaseca, A. B.; Barbera, R. A.; Vidmar, G.; Beccari, H., et al. Inhaled nebulised unfractionated heparin for the treatment of hospitalised patients with COVID-19: A multicentre case series of 98 patients. *Br. J. Clin. Pharmacol.***2022**, *88*, 2802-2813.
11. Chhabra, M.; Doherty, G. G.; See, N. W.; Gandhi, N. S.; Ferro, V. From Cancer to COVID-19: A Perspective on Targeting Heparan Sulfate-Protein Interactions. *Chem. Rec.***2021**, 3087-3101.
12. Ferro, V.; Liu, L. G.; Johnstone, K. D.; Wimmer, N.; Karoli, T.; Handley, P.; Rowley, J.; Dredge, K.; Li, C. P.; Hammond, E., et al. Discovery of PG545: A Highly Potent and Simultaneous Inhibitor of Angiogenesis, Tumor Growth, and Metastasis. *J. Med. Chem.***2012**, *55*, 3804-3813.

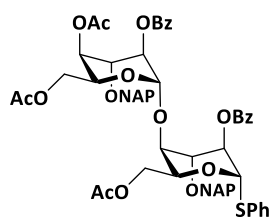
13. Agelidis, A.; Shukla, D. Heparanase, Heparan Sulfate and Viral Infection. *Adv. Exp. Med. Biol.***2020**, *1221*, 759-770.
14. (a) Buijssers, B.; Yanginlar, C.; de Nooijer, A.; Grondman, I.; Maciej-Hulme, M. L.; Jonkman, I.; Janssen, N. A. F.; Rother, N.; de Graaf, M.; Pickkers, P., et al. Increased Plasma Heparanase Activity in COVID-19 Patients. *Front. Immunol.***2020**, *11*, 575047.(b) Zechendorf, E.; Schroder, K.; Stiehler, L.; Frank, N.; Beckers, C.; Kraemer, S.; Dreher, M.; Kersten, A.; Thiemermann, C.; Marx, G., et al. The Potential Impact of Heparanase Activity and Endothelial Damage in COVID-19 Disease. *J. Clin. Med.***2022**, *11*.
15. Ekblad, M.; Adamiak, B.; Bergstrom, T.; Johnstone, K. D.; Karoli, T.; Liu, L.; Ferro, V.; Trybala, E. A highly lipophilic sulfated tetrasaccharide glycoside related to muparfostat (PI-88) exhibits virucidal activity against herpes simplex virus. *Antiviral Res.***2010**, *86*, 196-203.
16. Said, J.; Trybala, E.; Andersson, E.; Johnstone, K.; Liu, L.; Wimmer, N.; Ferro, V.; Bergstrom, T. Lipophile-conjugated sulfated oligosaccharides as novel microbicides against HIV-1. *Antiviral Res.***2010**, *86*, 286-295.
17. Lundin, A.; Bergstrom, T.; Andrighetti-Frohner, C. R.; Bendrioua, L.; Ferro, V.; Trybala, E. Potent anti-respiratory syncytial virus activity of a cholestanol-sulfated tetrasaccharide conjugate. *Antiviral Res.***2012**, *93*, 101-109.
18. Supramaniam, A.; Liu, X.; Ferro, V.; Herrero, L. J. Prophylactic Antiheparanase Activity by PG545 Is Antiviral In Vitro and Protects against Ross River Virus Disease in Mice. *Antimicrob. Agents Chemother.***2018**, *62*, e01944-17.
19. Modhiran, N.; Gandhi, N. S.; Wimmer, N.; Cheung, S.; Stacey, K.; Young, P. R.; Ferro, V.; Watterson, D. Dual targeting of dengue virus virions and NS1 protein with the heparan sulfate mimic PG545. *Antiviral Res.***2019**, *168*, 121-127.

20. Khamaysi, I.; Singh, P.; Nasser, S.; Awad, H.; Chowders, Y.; Sabo, E.; Hammond, E.; Gralnek, I.; Minkov, I.; Nosedá, A., et al. The Role of Heparanase in the Pathogenesis of Acute Pancreatitis: A Potential Therapeutic Target. *Sci. Rep.***2017**, *7*, 715.
21. Herold, T.; Jurinovic, V.; Arnreich, C.; Lipworth, B. J.; Hellmuth, J. C.; von Bergwelt-Baildon, M.; Klein, M.; Weinberger, T. Elevated levels of IL-6 and CRP predict the need for mechanical ventilation in COVID-19. *J. Allergy Clin. Immunol.***2020**, *146*, 128-136.e4.
22. Guimond, S. E.; Mycroft-West, C. J.; Gandhi, N. S.; Tree, J. A.; Le, T. T.; Spalluto, C. M.; Humbert, M. V.; Buttigieg, K. R.; Coombes, N.; Elmore, M. J., et al. Synthetic Heparan Sulfate Mimetic Pixatimod (PG545) Potently Inhibits SARS-CoV-2 by Disrupting the Spike-ACE2 Interaction. *ACS Cent. Sci.***2022**, *8*, 527-545.
23. Said, J. S.; Trybala, E.; Gorander, S.; Ekblad, M.; Liljeqvist, J. A.; Jennische, E.; Lange, S.; Bergstrom, T. The Cholesterol-Conjugated Sulfated Oligosaccharide PG545 Disrupts the Lipid Envelope of Herpes Simplex Virus Particles. *Antimicrob. Agents Chemother.***2016**, *60*, 1049-1057.
24. (a) Shanthamurthy, C. D.; Gimeno, A.; Leviatan Ben-Arye, S.; Kumar, N. V.; Jain, P.; Padler-Karavani, V.; Jimenez-Barbero, J.; Kikkeri, R. Sulfation Code and Conformational Plasticity of 1-Iduronic Acid Homo-Oligosaccharides Mimic the Biological Functions of Heparan Sulfate. *ACS Chem. Biol.***2021**, *16*, 2481-2489.(b) Chhabra, M.; Wilson, J. C.; Wu, L.; Davies, G. J.; Gandhi, N. S.; Ferro, V. Structural Insights into Pixatimod (PG545) Inhibition of Heparanase, a Key Enzyme in Cancer and Viral Infections. *Chem. Eur. J.***2022**, *28*, e202104222.
25. Chhabra, M.; Wimmer, N.; He, Q. Q.; Ferro, V. Development of Improved Synthetic Routes to Pixatimod (PG545), a Sulfated Oligosaccharide-Steroid Conjugate. *Bioconjugate Chem.***2021**, *32*, 2420-2431.

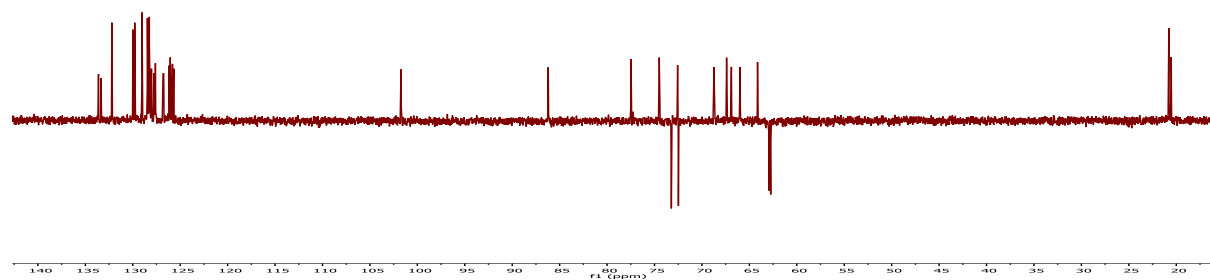
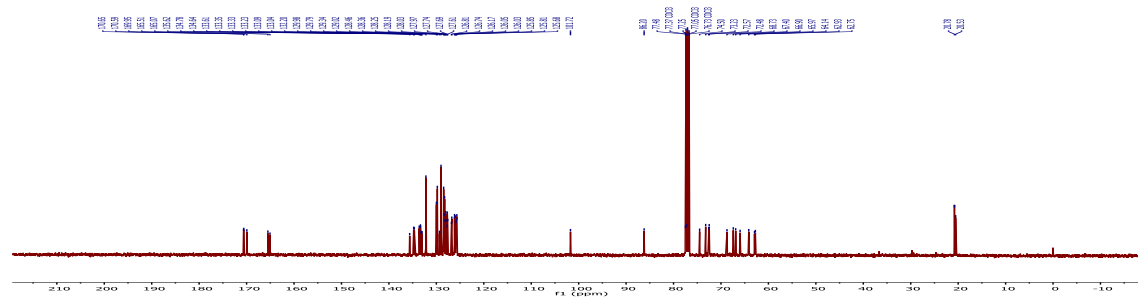
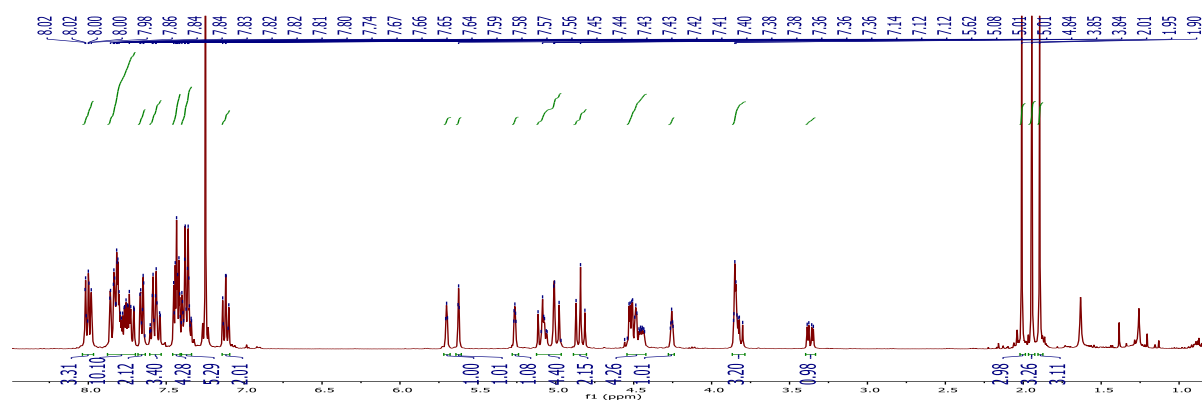
26. Xiang, J.; Lu, M.; Shi, M.; Cheng, X.; Kwakwa, K. A.; Davis, J. L.; Su, X.; Bakewell, S. J.; Zhang, Y.; Fontana, F., et al. Heparanase Blockade as a Novel Dual-Targeting Therapy for COVID-19. *J. Virol.***2022**, *96*, e0005722.
27. (a) Hammond, E.; Ferro, V. An Enzymatic Activity Assay for Heparanase That Is Useful for Evaluating Clinically Relevant Inhibitors and Studying Kinetics. *Methods Mol. Biol.***2023**, *2619*, 227-238.(b) Hammond, E.; Li, C. P.; Ferro, V. Development of a colorimetric assay for heparanase activity suitable for kinetic analysis and inhibitor screening. *Anal. Biochem.***2010**, *396*, 112-116.
28. Korber, B.; Fischer, W. M.; Gnanakaran, S.; Yoon, H.; Theiler, J.; Abfalterer, W.; Hengartner, N.; Giorgi, E. E.; Bhattacharya, T.; Foley, B., et al. Tracking Changes in SARS-CoV-2 Spike: Evidence that D614G Increases Infectivity of the COVID-19 Virus. *Cell***2020**, *182*, 812-827.e19.
29. Boittier, E. D.; Burns, J. M.; Gandhi, N. S.; Ferro, V. GlycoTorch Vina: Docking Designed and Tested for Glycosaminoglycans. *J. Chem. Inf. Model.***2020**, *60*, 6328-6343.
30. Ferro, V.; Karoli, T.; Liu, L.; Handley, P. N.; Johnstone, K. D.; Wimmer, N.; Hammond, E. T. Novel sulfated oligosaccharide derivatives. PCT Int. Appl. WO/2009/049370. **2009**.
31. Amarilla, A. A.; Modhiran, N.; Setoh, Y. X.; Peng, N. Y. G.; Sng, J. D. J.; Liang, B.; McMillan, C. L. D.; Freney, M. E.; Cheung, S. T. M.; Chappell, K. J., et al. An Optimized High-Throughput Immuno-Plaque Assay for SARS-CoV-2. *Front. Microbiol.***2021**, *12*, 625136.
32. Blich, M.; Golan, A.; Arvatz, G.; Sebbag, A.; Shafat, I.; Sabo, E.; Cohen-Kaplan, V.; Petcherski, S.; Avniel-Polak, S.; Eitan, A., et al. Macrophage activation by heparanase is mediated by TLR-2 and TLR-4 and associates with plaque progression. *Arterioscler. Thromb. Vasc. Biol.***2013**, *33*, e56-65.

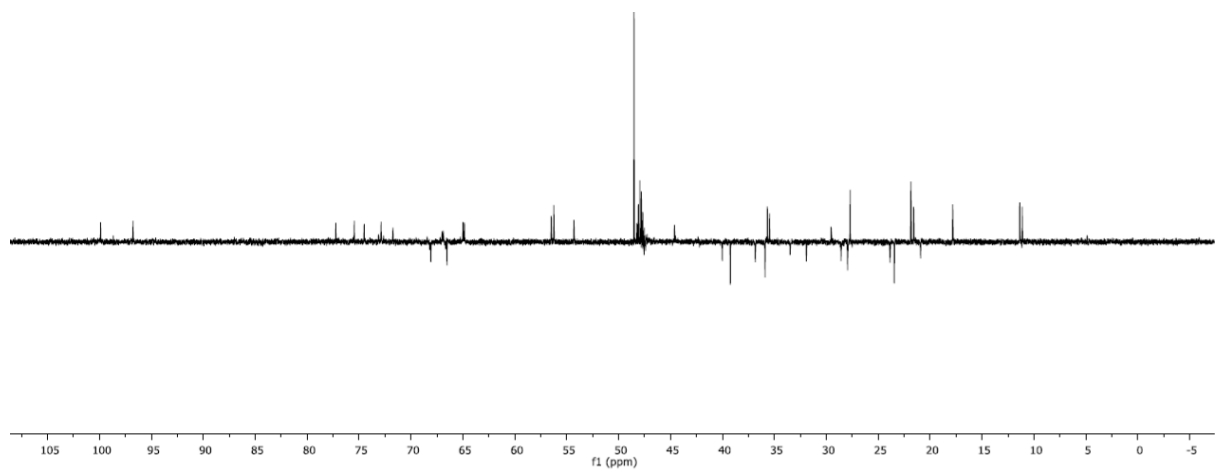
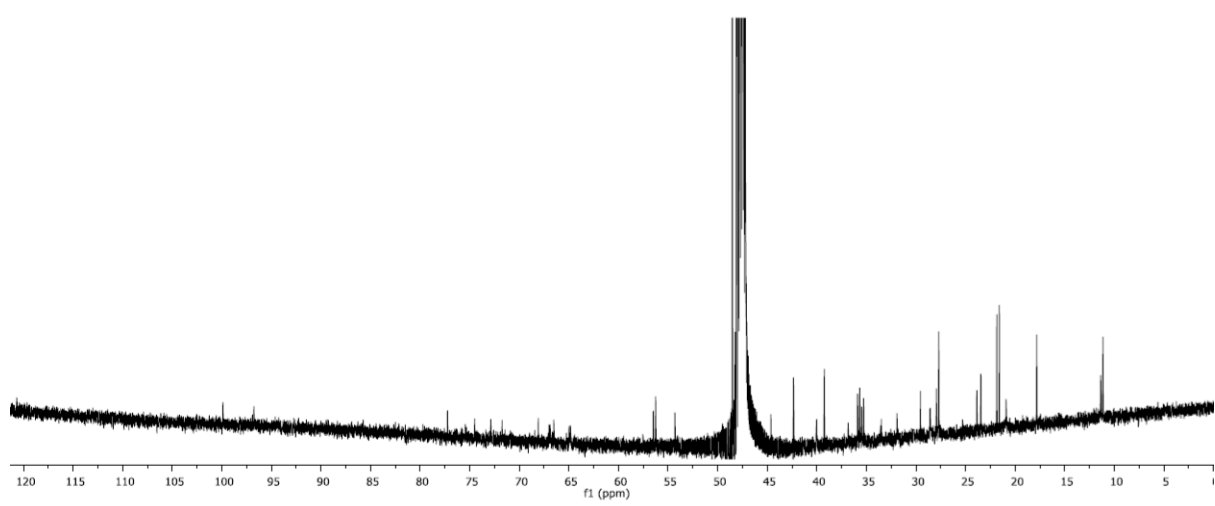
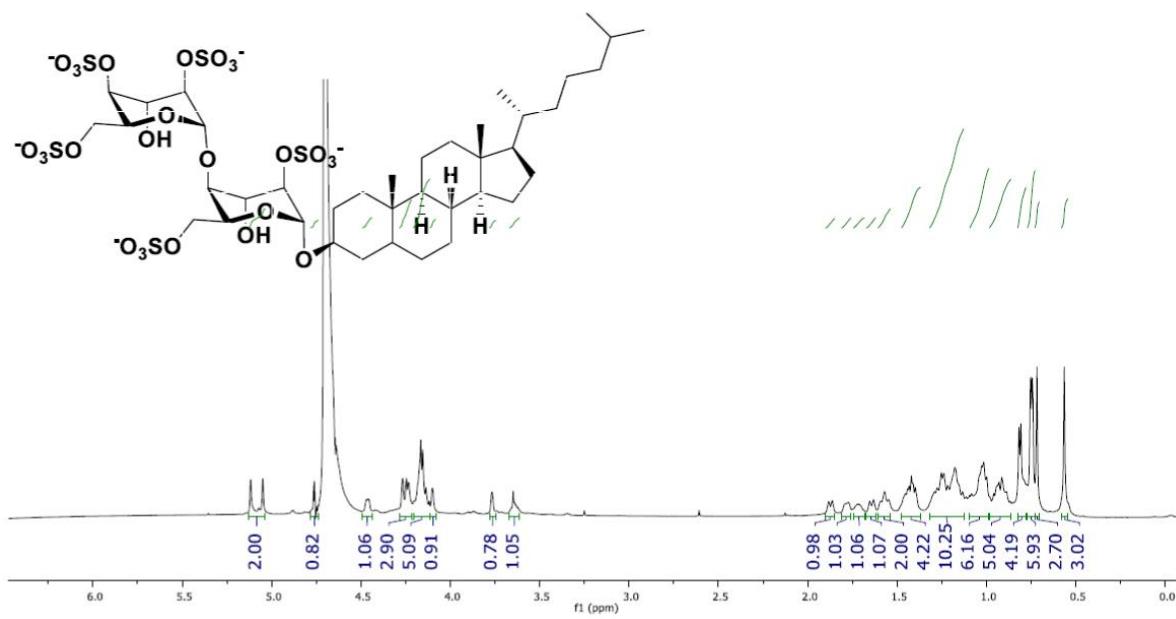
33. Wang, Q.; Zhang, Y.; Wu, L.; Niu, S.; Song, C.; Zhang, Z.; Lu, G.; Qiao, C.; Hu, Y.; Yuen, K.-Y., et al. Structural and Functional Basis of SARS-CoV-2 Entry by Using Human ACE2. *Cell***2020**, *181*, 894-904.e9.
34. Pettersen, E. F.; Goddard, T. D.; Huang, C. C.; Couch, G. S.; Greenblatt, D. M.; Meng, E. C.; Ferrin, T. E. UCSF Chimera—A visualization system for exploratory research and analysis. *J. Comput. Chem.***2004**, *25*, 1605-1612.
35. BIOVIA, Dassault Systèmes, Discovery Studio Visualizer, 21.1.0.20298, San Diego: Dassault Systèmes, **2021**.
36. Wu, L.; Viola, C. M.; Brzozowski, A. M.; Davies, G. J. Structural characterization of human heparanase reveals insights into substrate recognition. *Nat. Struct. Mol. Biol.***2015**, *22*, 1016-1022.
37. Goddard, T. D.; Huang, C. C.; Meng, E. C.; Pettersen, E. F.; Couch, G. S.; Morris, J. H.; Ferrin, T. E. UCSF ChimeraX: Meeting modern challenges in visualization and analysis. *Protein Sci.***2018**, *27*, 14-25.

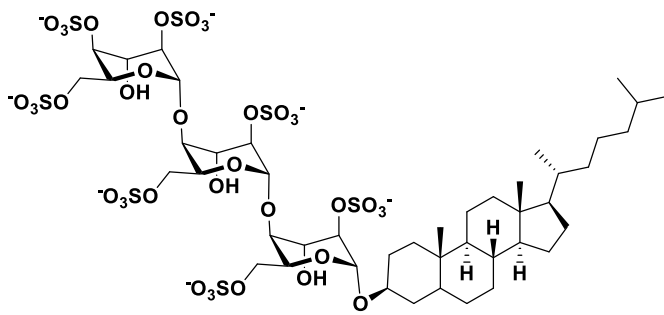
4.6 NMR



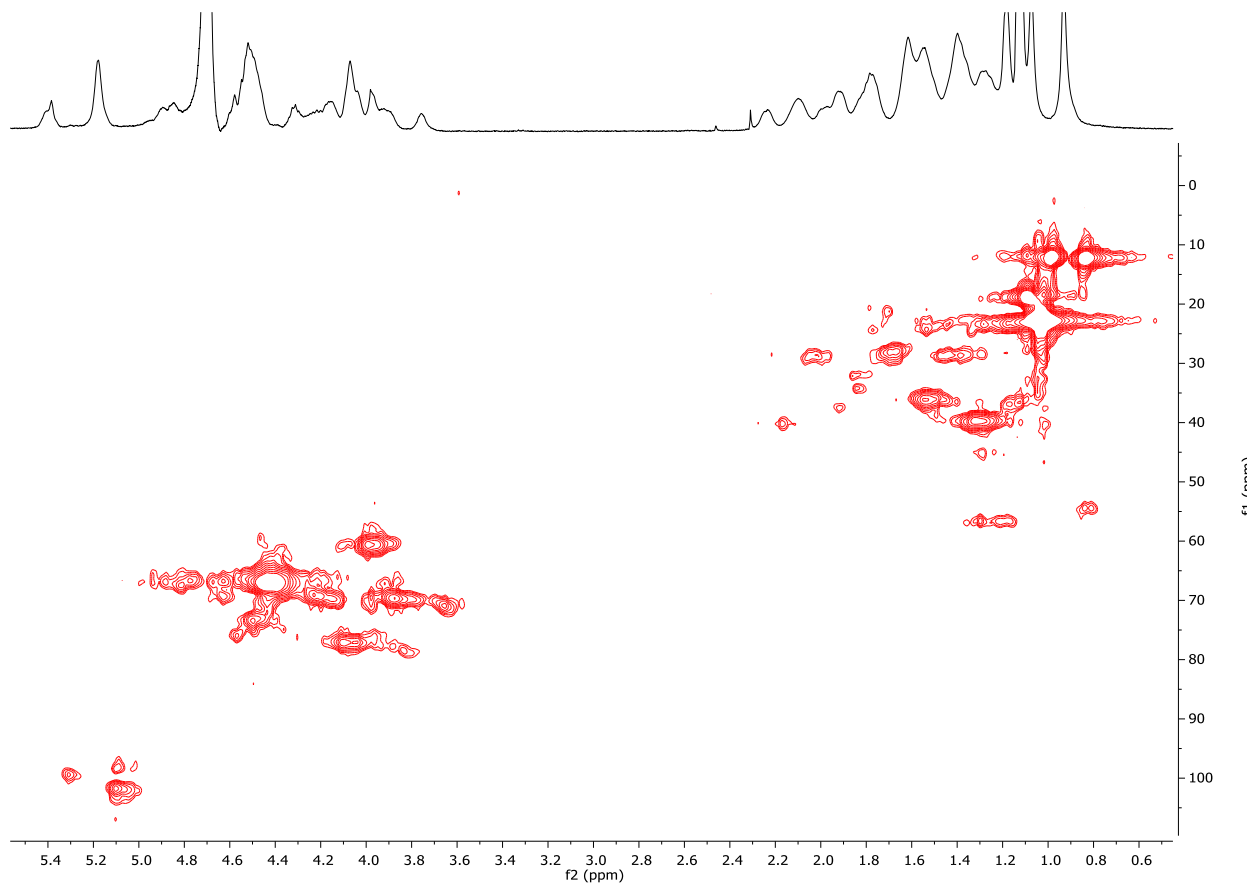
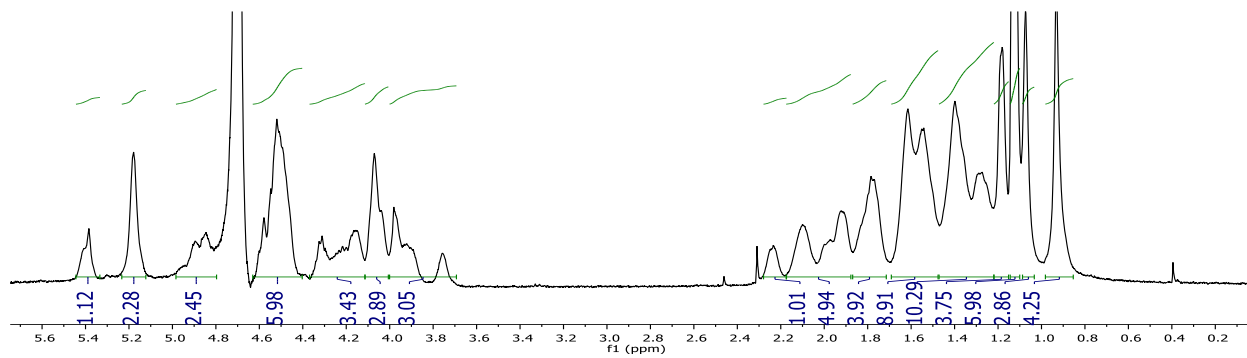
13

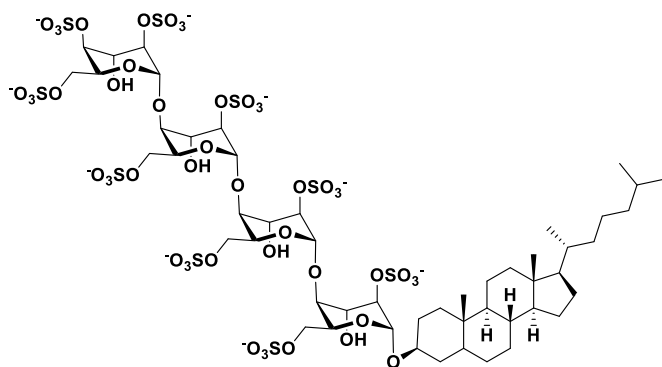




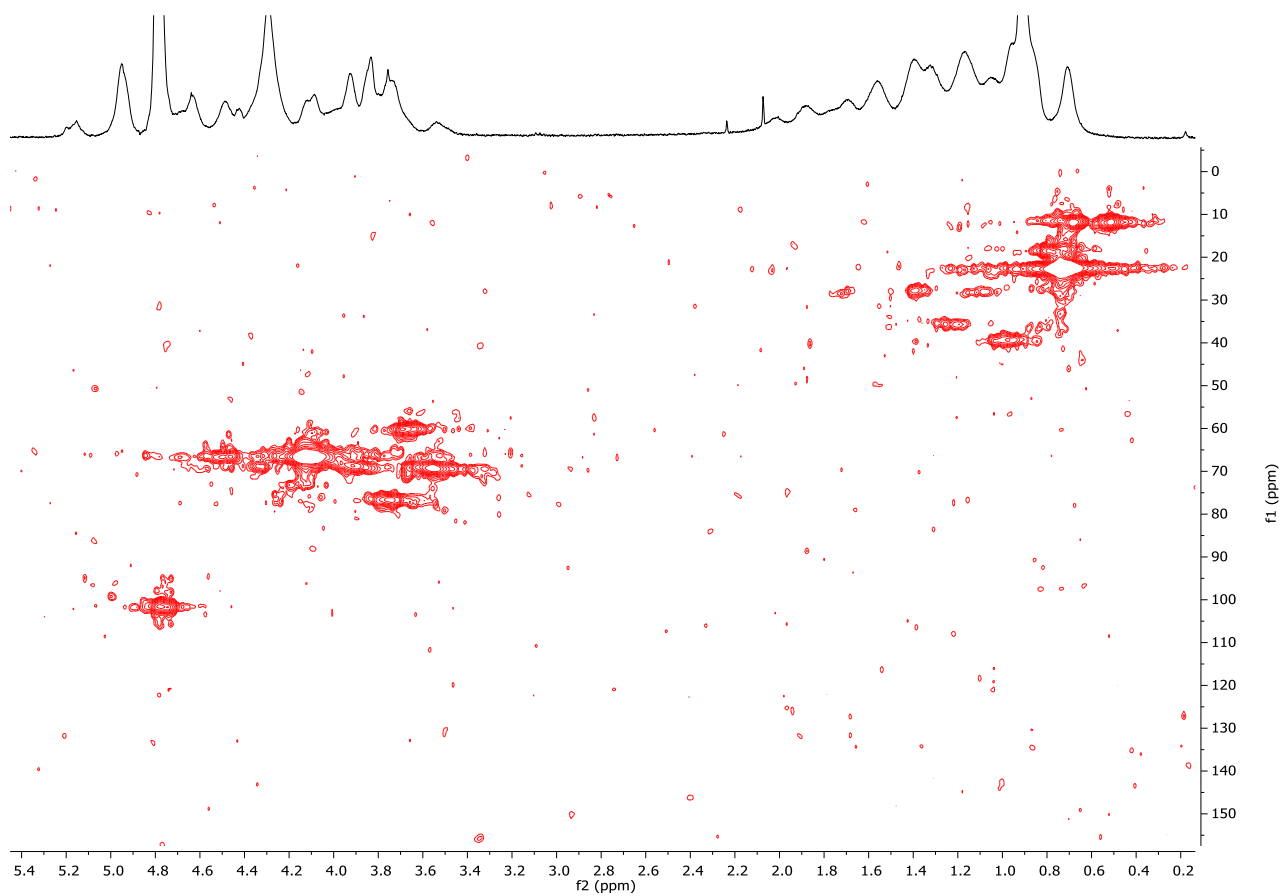
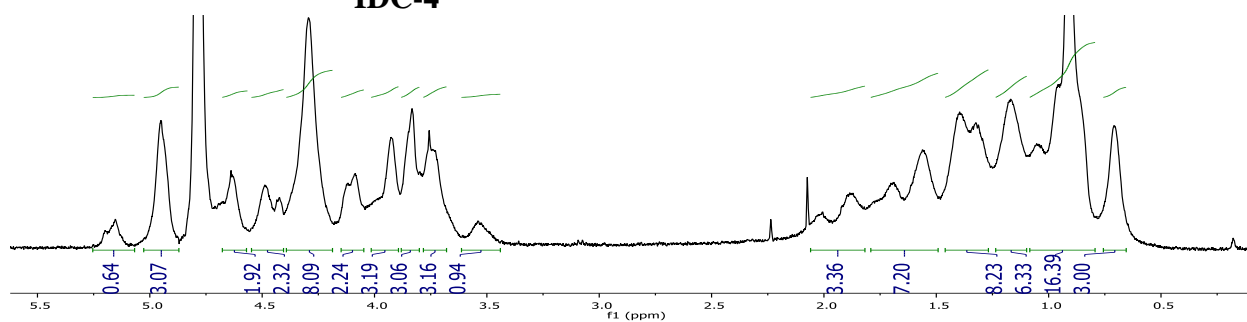


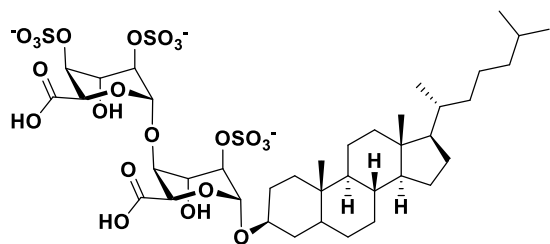
IDC-3



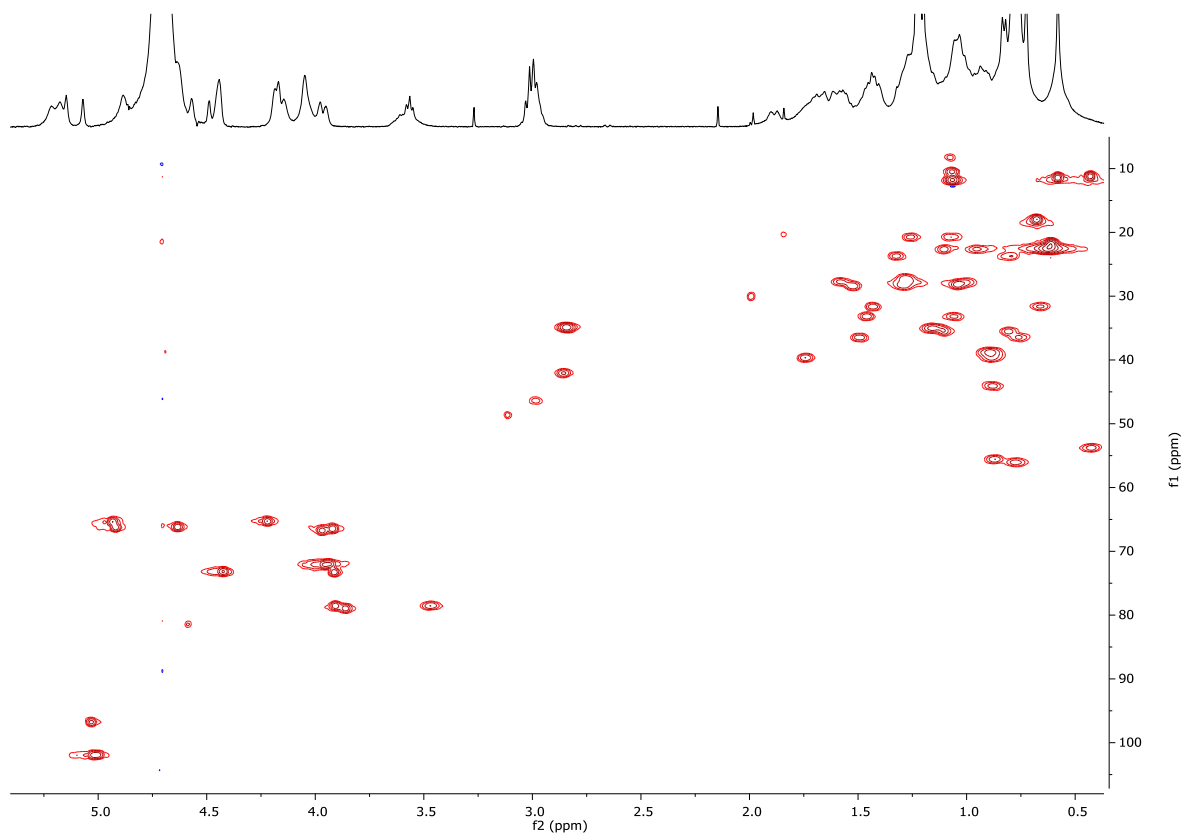
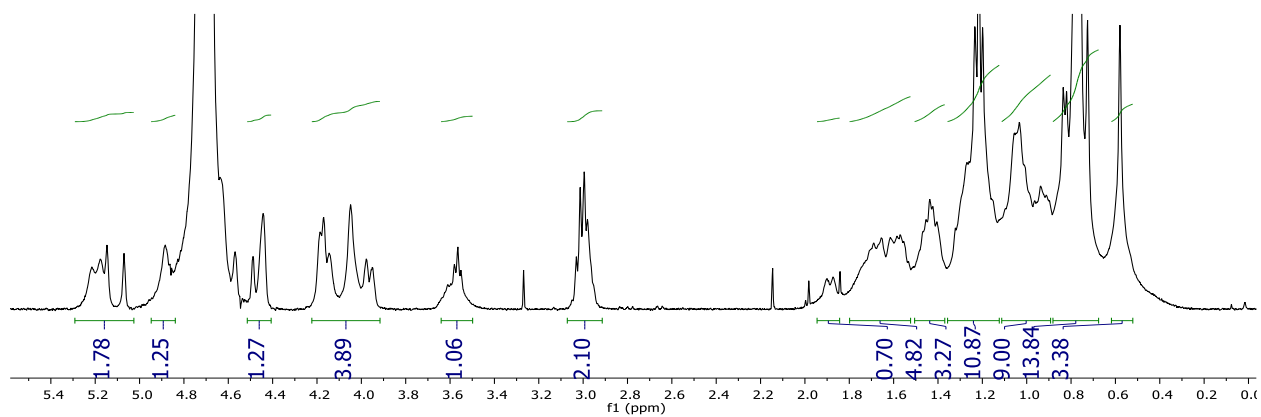


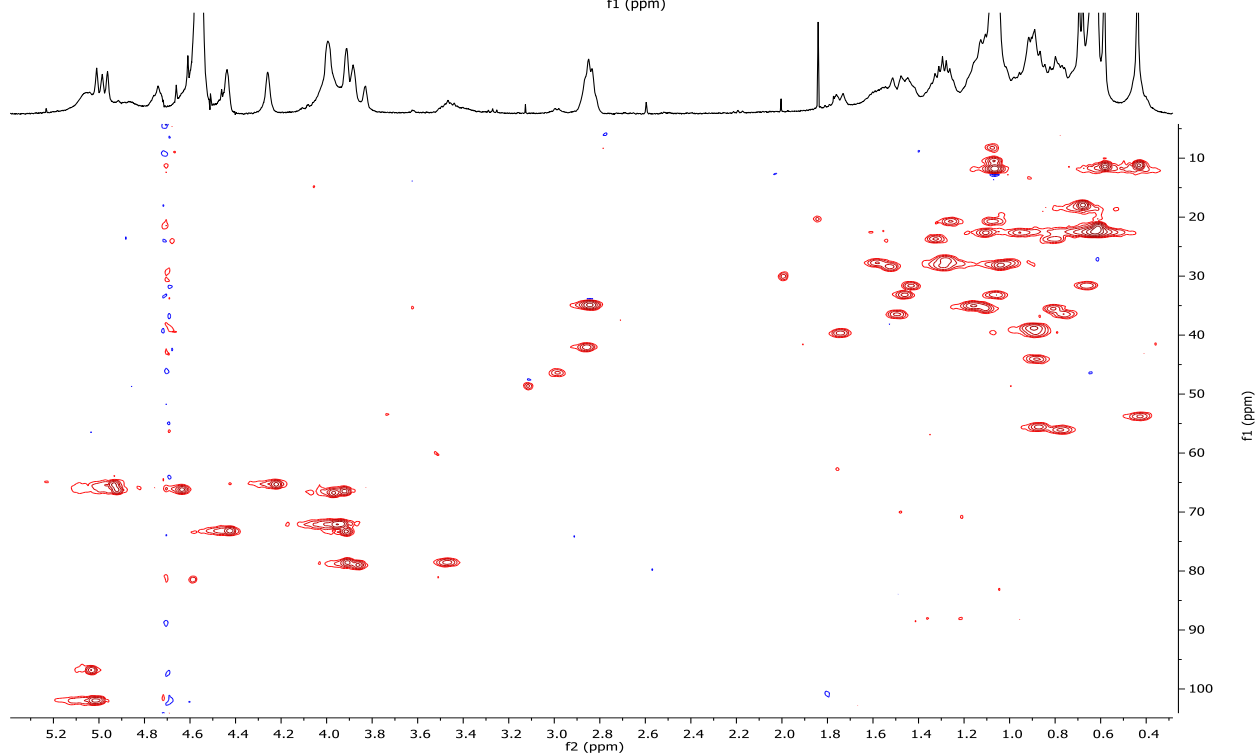
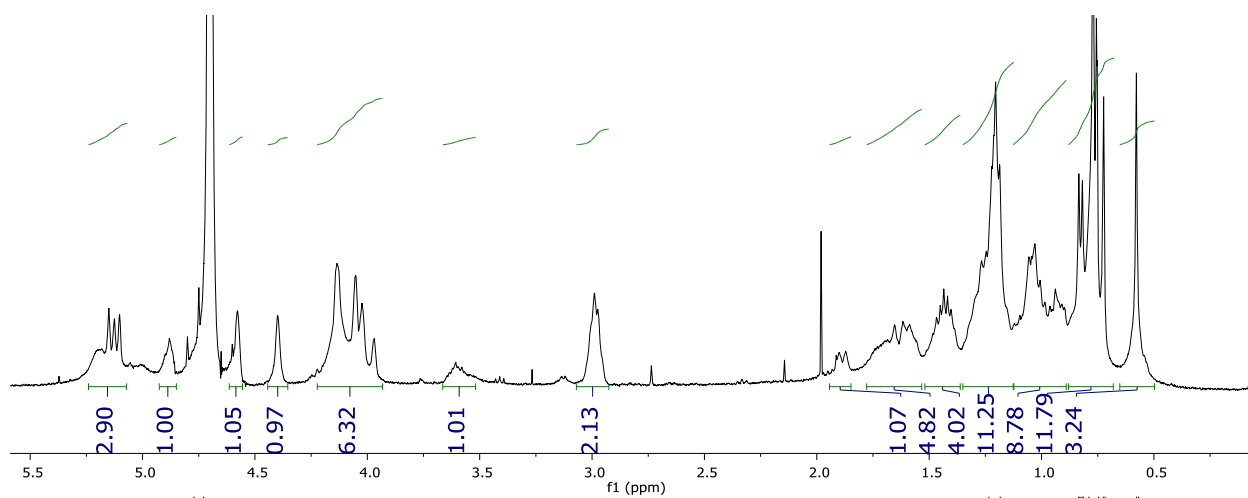
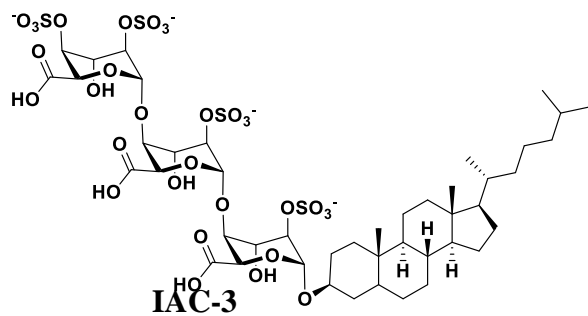
IDC-4

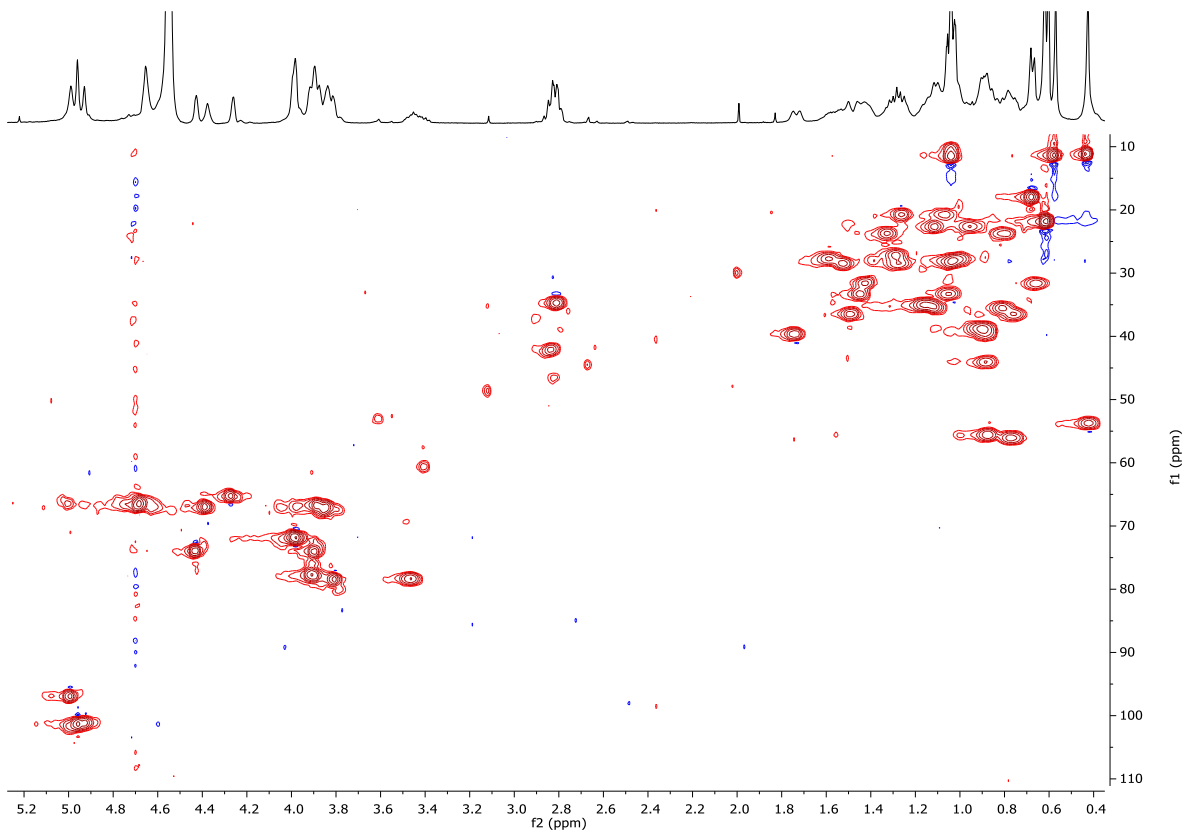
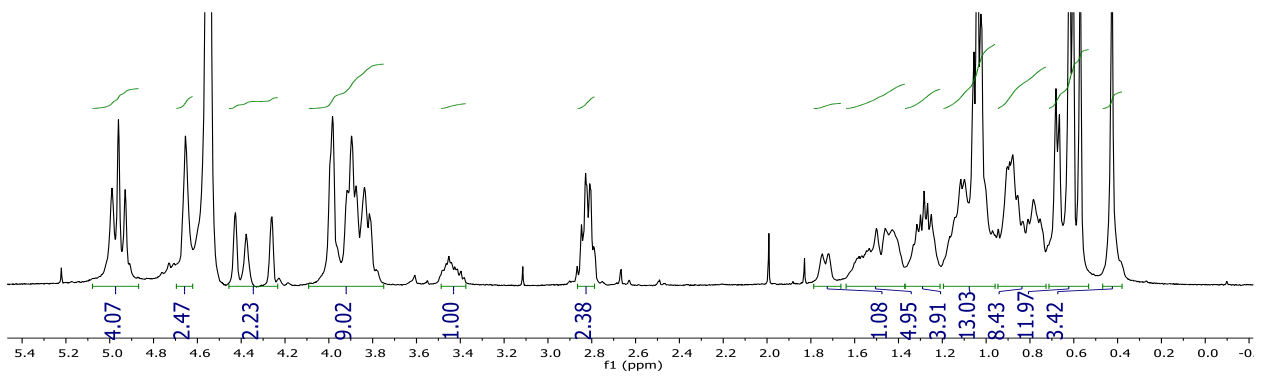
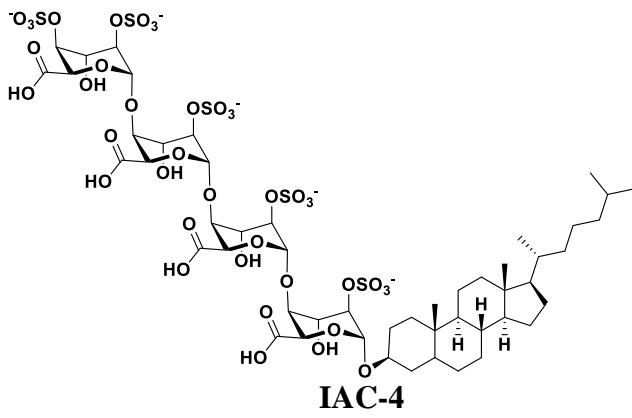




IAC-2







CHAPTER-5

Modulation of the Growth Factors and Chemokines Specificity of Heparan Sulfate Through Charge Diversity

Abstract

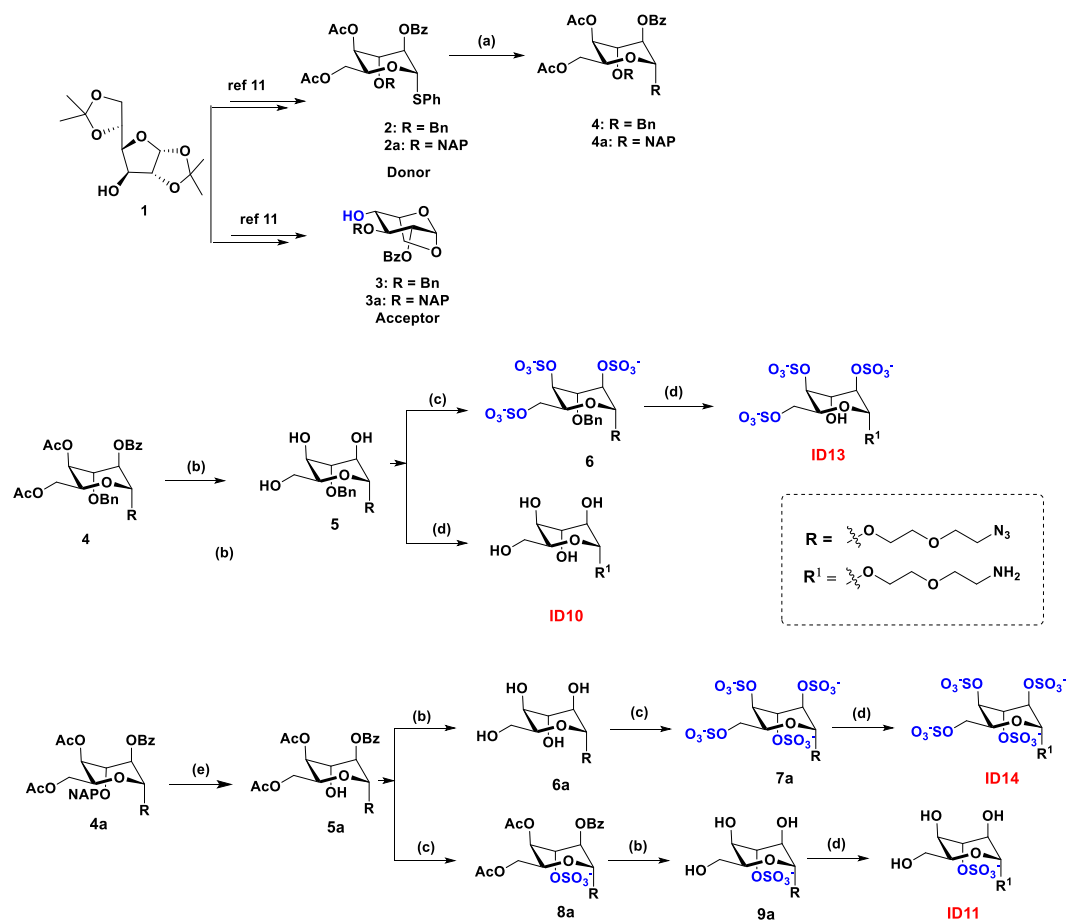
Heparan sulfate mimetics, derived from homooligosaccharides are potential candidates for drug development in cancer and viral therapy. Consequently, the synthesis of HS mimetics with diverse sulfation patterns and the assessment of their biological activity is an active area of research. Here, we present the synthesis of oligo L-idose-based HS mimetics, aiming to fine-tune the growth factors and chemokines biological activities. A comparative study on the interaction of HS binding proteins with sulfated oligo L-idose and oligo L-iduronic acid has revealed the synergistic role of charge diversity in the form of carboxylate and sulfate group in protein binding and activation. This insight paves the way for designing therapeutic molecules targeting cancer and immunology.

5.1 Introduction

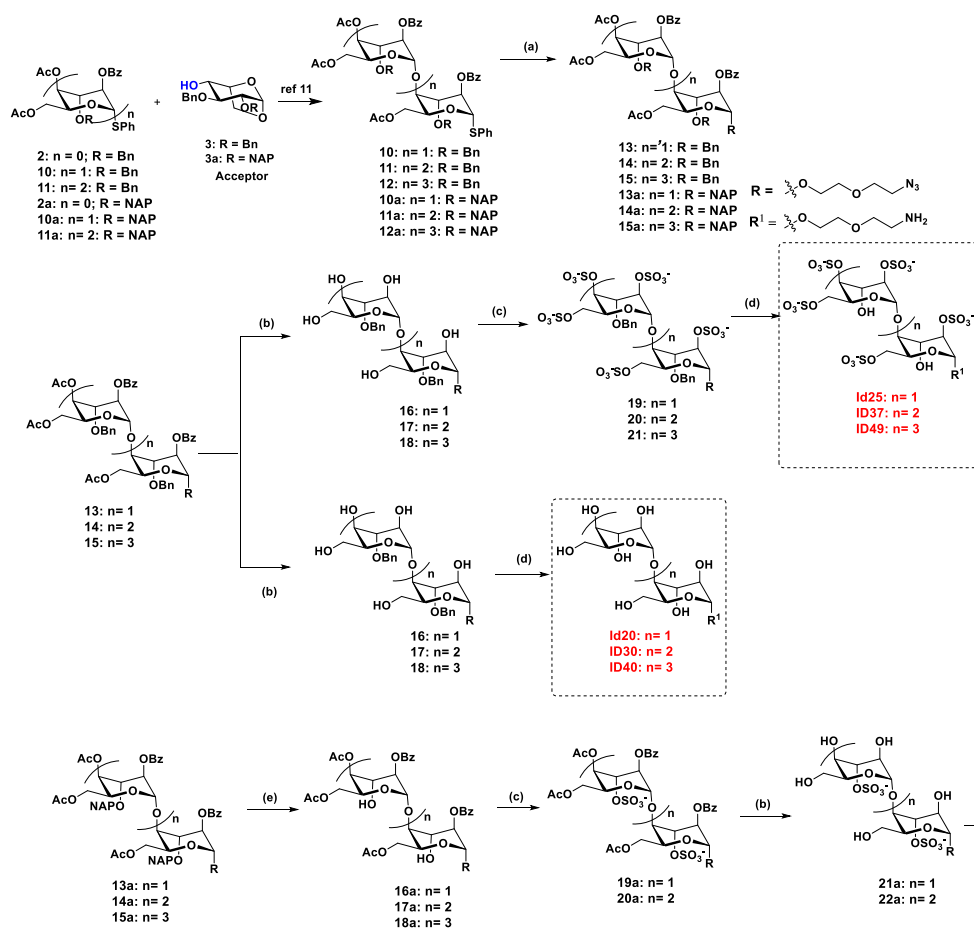
Mammalian cell surfaces are densely covered with polysaccharide units, typically known as glycosaminoglycans (GAGs). Heparan sulfate is the most heterogeneous GAG structure, featuring $\alpha(1,4)$ -linked D-glucosamine and hexuronic acid units, which can be L-iduronic acid or D-glucuronic acid.¹ The structural heterogeneity of HS results from the sulfate groups located at various positions on the saccharides and the differing compositions of hexuronic acid. Sulfation patterns that are most frequently observed include *O*-sulfation at C-6 and C-3 of glucosamine and C-2 of the uronic acid unit, with *N*-sulfation at glucosamine being another important sulfation. Additionally, glucosamine residues are *N*-acetylated and remain *N*-unsubstituted, forming NAc, NU, and NS domains in heparan sulfate.^{1,2} Among these domains, NS and NAc are recognized for their ability to bind numerous proteins that are abundantly present on the cell surface and in the extracellular matrix. HS binds to a diverse spectrum of growth factors/morphogens and their receptors, enzymes, cell adhesion molecules, chemokines, and various microbial proteins.^{3,4} Elucidating the molecular-level details of these interactions is vital for drug discovery. The groundbreaking research conducted by the Linhardt, Seeberger, Boons, Hung, Hsieh-Wilson, Desai, Turnbull, Liu, and Gardiner labs has unveiled a combinatorial library of HS oligosaccharides to decode the structure-activity relationship of proteins.^{5,6,7,8} These studies have demonstrated that electrostatic interactions between negatively charged sulfates and carboxylates and the positively charged lysine and arginine side chains of proteins are crucial for HS-protein interactions. Furthermore, these anionic residues and hydroxyls groups of HS are involved in hydrogen bonding, van der Waals forces, and coordination bonding with proteins, thereby strengthening the interaction.⁹ Nevertheless, at physiological pH, the carboxylate group tends to engage in hydrogen bonding networks instead of ionic interactions. Consequently, it is still uncertain why nature has opted for two different anionic residues on the HS backbone. How do these residues work synergistically and independently to affect protein binding specificity? What is the ideal charge density necessary for precise HS-protein interactions? To address these fundamental questions, it is necessary to develop a combinatorial library of HS mimetics, where uronic acid/uranate residues are varied with different sulfation patterns. Conducting systematic binding studies on these molecules could potentially result in the discovery of advanced drug molecules that inhibit specific HS-protein interactions. Herein, we report the synthesis of a library of sulfate and non-sulfate L-idose oligosaccharides.¹⁰ We compare the binding specificity to various growth factors and chemokines along with sulfated

L-iduronic acid oligosaccharides of similar charge density and unique charge diversity through microarray screening. We further evaluate specificity using SPR and the best candidate is then utilized to inhibit specific HS-protein interactions.

5.2 Results and Discussion



Scheme 1. Synthesis of sulfated L-idose monosaccharide derivatives. (a) azidoethoxyethanol, NIS TMSOTf, 4Å M.S., -10°C (b) LiOH, THF/MeOH/H₂O (4/2/1), 0°C (c) SO₃.NMe₃, DMF, 60°C (d)H₂/Pd(OH)₂/C, H₂O;(e)DDQ, DCM/H₂O (18/1).



Scheme 2. Synthesis of non-sulfated and sulfated L-idose oligosaccharides: Reagents and conditions: **(a)** azidoethoxyethanol, NIS TMSOTf, 4Å M.S., -10°C **(b)** LiOH, THF/MeOH/H₂O (4/2/1), 0°C **(c)** SO₃.NMe₃, DMF, 60°C **(d)** H₂/Pd(OH)₂/C, H₂O; **(e)** DDQ, DCM/H₂O (18/1).

The synthesis of sulfated L-idose monosaccharide derivatives was performed using an idose-thiophenol donor (Scheme 1) which was synthesized according to a literature procedure.¹¹ We synthesized 3-*O*-benzyl and 3-*O*-naphthyl protected idose thiophenol separately to achieve different sulfation patterns. The 3-*O*-benzyl protected idose thiophenol was deacetylated and debenzoylated to yield precursor **5**, which was subjected to hydrogenolysis to produce **ID10**, or to sulfation and hydrogenolysis to produce **ID13**. The synthesis of **ID14** and **ID11** was performed using the **4a** precursor, which was subjected to selective NAP deprotection using DDQ, yielding **5a**. **5a** intermediate was then either subjected to 3-*O*-sulfation and hydrogenolysis or to lithium hydroxide-based deacetylation and debenzoylation, followed by sulfation and hydrogenolysis, resulting in the formation of **ID11** and **ID14**, respectively.

The synthesis of oligo L-idose (Scheme 2) is not straightforward as controlling the α -glycosidic linkages between the successive idose residue is difficult. Recently, we have reported a new linear approach to synthesize oligo-idose using 1,6-anhydro- β -L-idopyranosyl 4- alcohol (**2**) acceptor and idose-thiophenol (**3**) donor.¹⁴ We synthesized these two building block from 1,2:5,6-di-O-isopropylidene- α -D-glucofuranose (**1**) using literature procedure with 6-8 steps with overall yield of 0.2 %. Glycosylation of **2** and **3** was carried out using NIS and TMSOTf promotor, followed by acetolysis of the anhydro-ring in the presence of copper(II) trifluoromethanesulfonate [Cu(OTf)₂] and acetic anhydride, and finally anomeric acetate was converted to thiophenol donor using TMSSPh/ZnI₂ method yielded the di-Idose donor. Glycosylation of di-Idose donor with an azide-linker yielded fully protected di-Idose intermediate (**13**). Similar reaction conditions with di- or tri-IdoA donor (**11** and **12**) and acceptor **3** yielded tri- and tetra-IdoA precursors (**14** and **15**). Global deprotection of these precursors yielded desired non-sulfate IdoA ligands (**ID20**, **ID30**, and **ID40**) (Figure 2). Further deacetylation and debenzoylation, sulfation and hydrogenolysis yielded highly sulfated idose oligosaccharide series (**ID25**, **ID37** and **ID49**). For 3-O-sulfated idose (**I-22** and **I-33**), we first synthesized 3-O-NAP protected oligosaccharide donor (**10a**, **11a** and **12a**) and linker glycosylated oligosaccharide (**13a**, **14a** and **15a**) using above procedure, followed by selectively NAP deprotection, sulfation and global deprotection yielded final compounds. Overall, we synthesized 12 different idose mono to tetrasaccharide derivatives and all final compounds were purified by ion-exchange resin chromatography, followed by a bond elute column. Their structures and purity were confirmed by standard NMR and mass spectrometry techniques.

Sulfation	ID	Charge			Growth Factors					%
		Sulfate	Carboxylate	Net	FGF2	VEGF	HB-EGF	Amphireulin	BMP2	
None	ID10	0	0	0	14	0	9	14	6	100
	ID20	0	0	0	1	0	5	5	2	75
	ID30	0	0	0	3	0	5	9	5	50
	ID40	0	0	0	13	0	9	15	11	25
	I-10	0	-1	-1	35	23	22	52	41	0
	I-20	0	-2	-2	35	13	25	47	35	
	I-30	0	-3	-3	26	8	22	65	45	
	I-40	0	-4	-4	27	24	28	59	47	
Mono-Sulfated	ID11	-1	0	-1	87	30	31	60	50	
	I-11	-1	-1	-2	40	89	55	60	83	
	I-21	-1	-2	-3	54	99	47	66	91	
	I-31	-1	-3	-4	57	59	45	72	73	
	I-41	-1	-4	-5	49	5	20	67	47	
Di-Sulfated	ID22	-2	0	-2	82	78	65	72	90	
	I-12	-2	-1	-3	50	72	79	66	71	
Tri-Sulfated	ID33	-3	0	-3	90	85	72	70	86	
	ID13	-3	0	-3	81	74	61	59	62	
	I-23	-3	-2	-5	63	76	63	57	74	
Tetra-Sulfated	ID14	-4	0	-4	85	71	67	51	64	
	I-34	-4	-3	-7	97	76	97	93	73	
Penta-Sulfated	ID25	-5	0	-5	73	76	63	53	67	
	I-45	-5	-4	-9	41	70	48	51	66	
Hepta-Sulfated	ID37	-7	0	-7	92	84	90	42	87	
Nono-Sulfated	ID49	-9	0	-9	96	87	81	61	72	
Natural Heparin	HP	*	*	*	37	55	21	69	36	

Figure 1. Growth factors glycan microarray binding assay and structural analysis. Binding was tested at three serial dilutions, then detected with the relevant biotinylated secondary antibody (1 µg/mL) followed by Cy3-Streptavidin (1.5 µg/mL). Arrays were scanned, relative fluorescent units (RFU) obtained for each chemokine, and mean rank between the three dilutions was calculated for glycans printed at 100 µM concentration. For this purpose, the binding RFUs per dilution per glycan was determined, then maximum RFUs in each detection were determined and set as 100% binding and all other glycans were calculated as a ratio of max (percent). The rank for each glycan was averaged between the three dilutions for each detection and SEM was carried out. This analysis allowed to compare the glycans' binding patterns across chemokines. The mean rank is shown as a heatmap of all examined binding assays together (red highest, blue lowest, and white 50th percentile of ranking).

Sulfation	ID	Charge			A		B		C		D		%
		Sulfate	Carboxylate	Net	CCL13	CCL28	CXCL12	CCL21	CXCL10	CCL7	CCL2	CCL5	
Non-Sulfated	ID10	0	0	0	14	7	0	1	5	1	5	3	100
	ID20	0	0	0	4	0	0	0	0	0	0	0	75
	ID30	0	0	0	14	2	0	0	3	1	5	2	50
	ID40	0	0	0	20	0	2	0	2	0	5	1	25
	I-10	0	-1	-1	74	46	62	52	47	30	4	2	0
	I-20	0	-2	-2	82	58	66	63	45	30	2	2	
	I-30	0	-3	-3	69	72	38	46	24	17	0	1	
I-40	0	-4	-4	67	56	56	48	44	33	0	2		
Mono-Sulfated	ID11	-1	0	-1	70	20	55	77	33	37	60	50	
	I-11	-1	-1	-2	81	80	64	62	57	58	23	15	
	I-21	-1	-2	-3	94	84	79	71	67	55	25	38	
	I-31	-1	-3	-4	86	80	92	83	78	75	36	30	
	I-41	-1	-4	-5	72	54	45	60	23	12	0	10	
Di-Sulfated	ID22	-2	0	-2	74	50	73	80	75	72	65	47	
	I-12	-2	-1	-3	53	51	75	79	82	94	66	75	
Tri-Sulfated	ID33	-3	0	-3	97	100	73	61	96	83	73	43	
	ID13	-3	0	-3	78	56	63	36	65	72	74	88	
	I-23	-3	-2	-5	88	76	98	86	96	87	69	86	
Tetra-Sulfated	ID14	-4	0	-4	83	59	71	46	56	75	79	96	
	I-34	-4	-3	-7	67	84	82	80	74	79	67	80	
Penta-Sulfated	ID25	-5	0	-5	97	83	74	49	77	82	79	80	
	I-45	-5	-4	-9	70	72	91	50	87	80	88	91	
Hepta-Sulfated	ID37	-7	0	-7	87	26	86	35	51	78	83	90	
Nono-Sulfated	ID49	-9	0	-9	93	42	87	21	60	81	79	83	
Natural Heparin	HP	*	*	*	33	28	33	87	74	81	40	71	

Figure 2. Microarray analysis of chemokines.

To identify hidden HS mimetic-binding active sites on growth factors, we constructed a microarray platform of HS mimetics carrying both L-idose and L-iduronic acid based ligands. The synthetic HS mimetics were printed onto epoxide-functionalized microarray slides in replicates of four, as described in the Experimental Section, and tested on HS binding growth factors (FGF1, FGF2, VEGF, HB-EGF, amphiregulin and BMP2) and three homeostatic chemokines (CCL28, CXCL12, and CCL12) and six inflammatory chemokines [CXCL8 (IL-8), CXCL10 (IP-10), CCL2 (MCP-1), CCL7 (MCP-3), CCL13 (MCP-4), and CCL5 (RANTES)]. To validate the binding order of HS mimetics with growth factors, we ranked each glycan based on percentage of its relative fluorescent intensity against the optimal fluorescent signal. Our results showed that most of the growth factor and chemokines prefers highly sulfated oligosaccharides. Further investigation of specificity and selectivity is under progress.

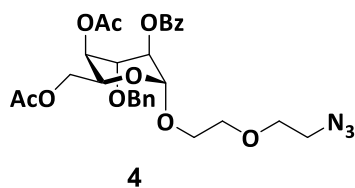
5.3 Conclusion

We report a novel, tailor-made heparan sulfate (HS) mimetic that features an exclusive L-idose scaffold with various sulfation patterns and oligosaccharide chain lengths as potential ligands to target chemokines and growth factors. Our preliminary analysis indicated that highly sulfated oligosaccharides demonstrated preferential binding to the majority of growth factors and chemokines. Further analyses, including surface plasmon resonance (SPR) binding studies and biological activity assessments of these molecules, are currently in progress.

5.4 EXPERIMENTAL SECTION

5.4.1 General Information

All chemicals were reagent grade and used without further purification unless otherwise noted. Reactions were carried out in anhydrous solvents under a nitrogen atmosphere. Reaction progress was monitored by analytical thin-layer chromatography (TLC) on Merck silica gel 60 F₂₅₄. Spots on TLC plate were visualized under UV light or by dipping the TLC plate in CAM/ninhydrin solution followed by heating. Column chromatography was carried out using Flukakieselgel 60 (230-400 mesh). ¹H and ¹³C NMR spectra of compounds were measured with Bruker 400 MHz, Bruker 600 MHz and Jeol 400 MHz using residual solvents as an internal reference (CDCl₃ δH 7.26 ppm, δC 77.3 ppm, CD₃OD δH 3.31 ppm, δC 49.0 ppm, and D₂O δH 4.79 ppm). The chemical shifts (δ) are reported in ppm and coupling constants (J) in Hz.

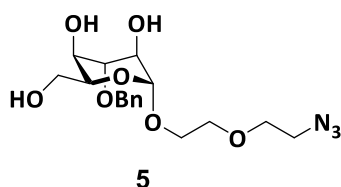


Ethoxy-2-azidoethoxyl-O-(4,6-O-diacetyl-2-O-benzoyl-3-O-benzyl)-α(1→4)-L-idopyrnoside (4)

Monosaccharide donor **2** (300 mg, 0.541 mmol), acceptor Azido ethoxy ethanol linker (56 mg, 0.433 mmol) and freshly dried 4 Å molecular sieves were taken in round bottom flask and was dissolved in dry DCM in 10 volumes, kept for stirring for 2h under N₂ atmosphere. Then reaction mixture was cooled to -10°C. Further, TMSOTf (24 μl, 0.1082 mmol) and NIS (158.2 mg, 0.703 mmol) were added and kept for stirring. The reaction completion was monitored by TLC, after completion of reaction, it was neutralized with triethylamine Et₃N and did celite filtration and subsequently did sodium thiosulfate Na₂S₂O₃ workup and dried over Na₂SO₄. Purification was done by silica column in EtOAc/Hexane

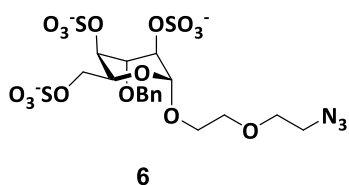
solvent system to get compound **4** in a 85% yield. ¹H NMR (400 MHz, Chloroform-*d*) 5.30 – 5.13 (m, 1H), 5.03 (s, 1H), 4.97 (t, *J* = 2.2 Hz, 1H), 4.84 (d, *J* = 11.6 Hz, 1H), 4.70 (d, *J* = 11.6 Hz, 1H), 4.58 (td, *J* = 6.4, 1.8 Hz, 1H), 4.24 (d, *J* = 6.4 Hz, 2H), 3.93 (ddd, *J* = 10.1, 5.4, 3.1 Hz, 1H), 3.84 (td, *J* = 2.7, 1.3 Hz, 1H), 3.78 – 3.47 (m, 5H), 3.21 (t, *J* = 5.0 Hz, 2H), 2.07 (s, 3H), 1.98 (s, 3H), 8.14 – 7.93 (m, 2H), 7.65 – 7.51 (m, 1H), 7.45 (t, *J* = 7.6 Hz, 2H), 7.42 – 7.23 (m, 5H). ¹³C NMR (101MHz, Chloroform-*d*) δ 170.68, 170.15, 137.64, 133.55, 129.81, 129.47, 128.45, 128.36, 127.84, 127.69, 98.18, 72.66, 72.23, 70.34, 70.15, 67.67, 67.06, 67.01, 63.66, 62.91, 50.76, 20.81. HRMS *m/z* calculated for C₂₈H₃₃N₃O₁₀Na, 571.2166; Found 571.2169.

Ethoxy-2-azidoethoxyl-O-(3-O-benzyl)-α(1→4)-L-idopyrnoside (5)



Compound**4** (106mg, 0.1855mmol) was dissolved in THF/MeOH/H₂O (4/2/1) and LiOH (234mg, 5.567 mmol) was added at 0°C and kept for stirring for 3-4 hours. The reaction completion was monitored by TLC, after completion, reaction mixture was neutralized by amberlite 120 H⁺ resin, Further, reaction mixture was filtered by cotton plugh filtration, then it was concentrated under by reduced pressure, further it was purified by silica column in MeOH/DCM solvent system to get compound**5** in a 95% yield. ¹H NMR (400 MHz, Chloroform-*d*) 4.94 (s, 1H), 4.71 (d, *J* = 11.5 Hz, 1H), 4.53 (d, *J* = 11.5 Hz, 1H), 4.20 – 4.08 (m, 1H), 4.06 – 3.81 (m, 5H), 3.75 – 3.48 (m, 6H), 3.21 (t, *J* = 5.0 Hz, 2H), 7.44 – 7.17 (m, 5H). ¹³C NMR (101MHz, Chloroform-*d*) δ 138.09, 128.37, 127.77, 127.60, 101.71, 75.51, 71.69, 70.36, 70.17, 67.58, 66.33, 65.65, 50.73. HRMS *m/z* calculated for C₁₇H₂₅N₃O₇Na, 383.1693; Found 383.1695.

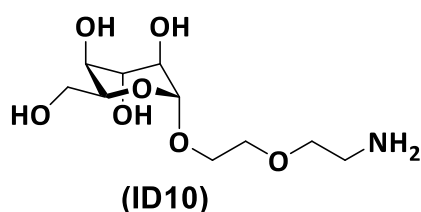
Ethoxy-2-azidoethoxyl-O-(2,4,6-O-trisulfonato-3-O-benzyl)-α(1→4)-L-idopyrnoside (13)



Compound**5** (32mg, 0.0835mmol) and SO₃.NMe₃ (348mg, 2.505mol) was thoroughly dried together under high vacuum, then was dissolved in dry DMF solvent and stirred at 60°C for 72h, Further DMF was evaporated under reduced pressure and then purified by

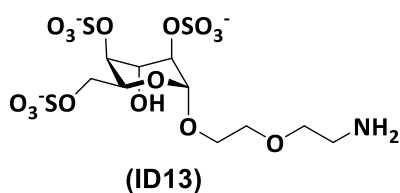
Bound elute C-18 column to get compound **6** in 80% yield. ^1H NMR (400 MHz, Deuterium Oxide) 5.17 (s, 1H), 4.82 (s, 2H), 4.64 (ddd, $J = 8.2, 3.5, 1.5$ Hz, 1H), 4.50 (ddt, $J = 18.5, 2.2, 1.3$ Hz, 2H), 4.38 – 4.25 (m, 3H), 4.02 (ddd, $J = 11.0, 4.8, 3.1$ Hz, 1H), 3.87 – 3.84 (m, 2H), 3.82 (s, 1H), 3.78 (dd, $J = 5.4, 4.3$ Hz, 2H), 3.51 – 3.44 (m, 2H), 7.58 – 7.45 (m, 5H). ^{13}C NMR (101 MHz, Deuterium Oxide) δ 137.03, 128.78, 128.56, 128.50, 98.30, 73.26, 72.36, 71.15, 70.67, 69.45, 69.41, 68.01, 67.39, 64.49, 55.61, 50.30. HRMS m/z calculated for $\text{C}_{17}\text{H}_{22}\text{N}_3\text{O}_{16}\text{S}_3^{-3}$, 206.6726; Found 206.6729.

Ethoxy-2-aminoethoxyl-*O*- $\alpha(1\rightarrow4)$ -*L*-idopyrnoside (ID10)



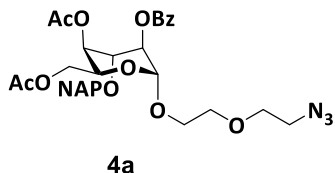
The compound **5** (15mg, 0.391mmol) was dissolved in H_2O and $\text{Pd}(\text{OH})_2$ (10% per wt) was added and stirred for 42h under hydrogen atmosphere. Further, reaction mixture was filtered and concentrated, finally purified by Bound elute C-18 column by using H_2O as a solvent to get **(ID10)** in a 90% yield. ^1H NMR (400 MHz, Chloroform- d) 4.74 (d, $J = 5.0$ Hz, 1H), 4.04 (dt, $J = 8.1, 4.1$ Hz, 1H), 3.89 (tdd, $J = 8.1, 4.7, 1.1$ Hz, 1H), 3.78 – 3.59 (m, 11H), 3.45 (ddd, $J = 7.4, 5.0, 1.1$ Hz, 1H), 3.14 – 3.09 (m, 2H). ^{13}C NMR (101 MHz, Deuterium Oxide) δ 100.24, 71.82, 71.75, 71.04, 70.26, 69.59, 67.63, 66.37, 59.45, 39.05. HRMS m/z calculated for $\text{C}_{10}\text{H}_{21}\text{NO}_7\text{Na}$, 267.1318; Found 267.1321.

Ethoxy-2-aminoethoxyl-*O*-(2,4,6-sulfonato)- $\alpha(1\rightarrow4)$ -*L*-idopyrnoside (ID13)



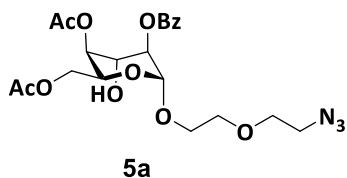
The compound **6** (15mg, 0.241mmol) was dissolved in H_2O and $\text{Pd}(\text{OH})_2$ (10% per wt) was added and stirred for 42h under hydrogen atmosphere. Further, reaction mixture was filtered and concentrated, finally purified by Bound elute C-18 column by using H_2O as a solvent to get **(ID13)** in a 91% yield. ^1H NMR (400 MHz, Chloroform- d) 5.03 (d, $J = 0.9$ Hz, 1H), 4.51 – 4.42 (m, 1H), 4.27 – 4.07 (m, 5H), 3.84 (td, $J = 6.9, 6.3, 4.0$ Hz, 1H), 3.69 (ddd, $J = 5.0, 3.7, 2.0$ Hz, 5H), 3.12 (t, $J = 5.1$ Hz, 2H). ^{13}C NMR (101 MHz, Deuterium Oxide) δ 98.40, 73.48, 73.23, 69.64, 67.98, 67.33, 66.56, 66.34, 64.63, 39.22. HRMS m/z calculated for $\text{C}_{10}\text{H}_{18}\text{NO}_{16}\text{S}_3^{-3}$, 167.9935; Found 167.9939.

Ethoxy-2-azidoethoxyl-O-(4,6-O-diacetyl-2-O-benzoyl-3-O-(2-naphthylmethyl)- α (1 \rightarrow 4)-L-idopyrnoside (4a)



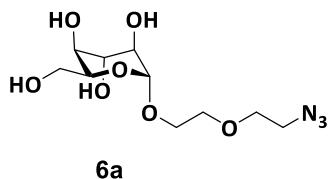
Compound **4a** was synthesised by using synthetic procedure of compound **4** in a 78% yield. ^1H NMR (400 MHz, Chloroform-*d*) 5.36 – 5.25 (m, 1H), 5.09 – 4.94 (m, 4H), 4.87 (d, $J = 11.8$ Hz, 1H), 4.61 (td, $J = 6.4, 1.8$ Hz, 1H), 4.28 – 4.15 (m, 2H), 4.06 – 3.86 (m, 2H), 3.77 – 3.50 (m, 5H), 3.15 (t, $J = 5.0$ Hz, 2H), 2.05 (s, 3H), 1.98 (s, 3H), 8.13 – 7.96 (m, 2H), 7.95 – 7.73 (m, 4H), 7.63 – 7.37 (m, 6H) ^{13}C NMR (101 MHz, Chloroform-*d*) δ 170.68, 170.16, 135.06, 133.55, 129.82, 128.45, 128.14, 127.94, 127.71, 126.53, 126.17, 126.01, 125.69, 98.22, 72.77, 72.34, 70.29, 70.17, 67.65, 67.11, 67.08, 63.73, 62.89, 50.72, 20.82, 20.78. HRMS m/z calculated for $\text{C}_{32}\text{H}_{35}\text{N}_3\text{O}_{16}\text{Na}$, 621.2322; Found 621.2326.

Ethoxy-2-azidoethoxyl-O-(4,6-O-diacetyl-2-O-benzoyl)- α (1 \rightarrow 4)-L-idopyrnoside (5a)



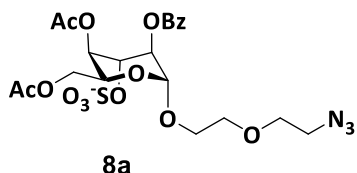
Compound **4a** (440 mg, 0.707 mmol) was dissolved in DCM/ H_2O (18:1) solvent mixture. To that DDQ (481.8 mg, 2.122 mmol) was added and kept stirring for overnight at RT, after completion of reaction, workup was done with sat. NaHCO_3 and dried over Na_2SO_4 . Filtered and concentrated, Purification was done by silica column in EtOAc/Hexane solvent system to get compound **5a** in a 83% yield. ^1H NMR (400 MHz, Chloroform-*d*) 5.12 (d, $J = 1.6$ Hz, 1H), 5.08 (dt, $J = 2.6, 1.2$ Hz, 1H), 4.97 (td, $J = 2.4, 1.2$ Hz, 1H), 4.58 (td, $J = 6.4, 2.0$ Hz, 1H), 4.26 (dd, $J = 6.4, 2.4$ Hz, 2H), 4.06 (s, 1H), 4.01 – 3.91 (m, 1H), 3.80 – 3.64 (m, 5H), 3.52 (q, $J = 10.8, 8.7$ Hz, 1H), 3.40 (dt, $J = 5.9, 4.7$ Hz, 2H), 8.15 – 7.99 (m, 2H), 7.65 – 7.54 (m, 1H), 7.50 – 7.40 (m, 2H) ^{13}C NMR (101 MHz, Chloroform-*d*) δ 170.65, 169.98, 165.13, 133.59, 129.87, 129.38, 128.44, 97.78, 70.20, 69.85, 68.58, 67.72, 66.89, 66.00, 63.20, 62.74, 50.74, 20.78, 20.76. HRMS m/z calculated for $\text{C}_{21}\text{H}_{27}\text{N}_3\text{O}_{10}\text{Na}$, 481.1696; Found 481.1697.

Ethoxy-2-azidoethoxyl-O- α (1 \rightarrow 4)-L-idopyrnoside (6a)



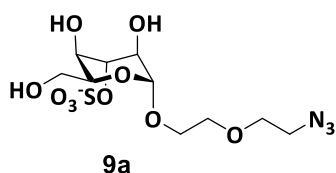
Compound **5a** (138 mg, 0.2907 mmol) was dissolved in THF/MeOH/H₂O (4:2:1) ratio, to that LiOH.H₂O (183 mg, 4.369 mmol) was added at 0°C and kept for overnight. After completion of reaction, it was neutralized in amberlite 120 H⁺ resin, Further, reaction mixture was filtered by cotton plug filtration, then it was concentrated under reduced pressure, further it was purified by silica column in MeOH/DCM solvent system to get compound **6a** in a 87% yield. ¹H NMR (400 MHz, Methanol-*d*₄) 4.71 (d, *J* = 2.7 Hz, 1H), 3.99 (ddd, *J* = 7.2, 4.9, 2.4 Hz, 1H), 3.88 – 3.78 (m, 1H), 3.72 – 3.51 (m, 9H), 3.46 (ddd, *J* = 4.7, 2.7, 1.0 Hz, 1H), 3.32 – 3.25 (m, 2H). ¹³C NMR (101 MHz, Methanol-*d*₄) δ 101.00, 70.54, 69.85, 69.80, 69.67, 68.87, 66.84, 61.22, 50.39. HRMS *m/z* calculated for C₁₀H₁₉N₃O₇Na, 293.1223; Found 293.1224.

Ethoxy-2-azidoethoxyl-O-(4,6-O-diacetyl-3-O-sulfonato-2-O-benzoyl)- α (1 \rightarrow 4)-L-idopyrnoside (8a)



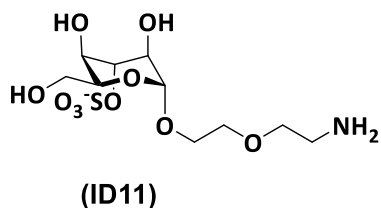
Compound **5a** (100 mg, 0.207 mmol) and SO₃.NMe₃ complex (289 mg, 2.077 mmol) was dissolved in dry DMF under N₂ atmosphere, reaction mixture was kept for stirring at 60°C for 24 h, Next DMF was evaporated under reduced pressure, resulting residue was purified using silica column with DCM/MeOH solvent system to get compound **8a** in a 85% yield. ¹H NMR (400 MHz, Methanol-*d*₄) 5.32 (dd, *J* = 2.6, 1.3 Hz, 1H), 5.27 (t, *J* = 2.3 Hz, 1H), 4.72 (td, *J* = 2.9, 1.1 Hz, 1H), 4.66 (ddd, *J* = 7.3, 5.2, 1.7 Hz, 1H), 4.36 – 4.20 (m, 2H), 3.99 (ddd, *J* = 11.0, 6.0, 3.3 Hz, 1H), 3.95 – 3.88 (m, 1H), 3.87 – 3.72 (m, 5H), 3.47 (t, *J* = 4.9 Hz, 2H). ¹³C NMR (151 MHz, Methanol-*d*₄) δ 171.15, 170.50, 133.50, 129.51, 129.37, 128.34, 97.86, 70.30, 70.27, 69.65, 67.96, 67.54, 66.81, 63.63, 62.60, 50.62, 48.13, 47.99, 47.85, 47.70, 47.56, 47.42, 19.53, 19.43. HRMS *m/z* calculated for C₂₁H₂₆N₃O₁₃S⁻¹, 560.1192; Found 560.1196.

Ethoxy-2-azidoethoxyl-O-(3-O-sulfonato)- α (1 \rightarrow 4)-L-idopyrnoside (9a)



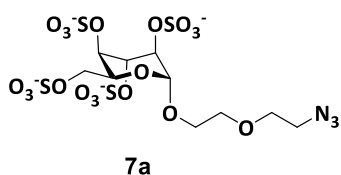
Compound **8a** (138 mg, 0.2907 mmol) was dissolved in THF/MeOH/H₂O (4:2:1) ratio, to that LiOH.H₂O (183 mg, 4.369 mmol) was added at 0°C and kept for overnight. After completion of reaction, it was neutralized, further, reaction mixture was filtered by cotton plug filtration, then it was concentrated under reduced pressure, further it was purified by silica column in MeOH/DCM solvent system to get compound **9a** in a 90% yield. ¹H NMR (400 MHz, Methanol-*d*₄) 4.72 (dd, *J* = 1.8, 1.0 Hz, 1H), 4.35 (td, *J* = 3.8, 1.0 Hz, 1H), 4.02 (ddd, *J* = 6.9, 5.0, 1.9 Hz, 1H), 3.87 – 3.77 (m, 2H), 3.76 – 3.69 (m, 2H), 3.69 – 3.61 (m, 5H), 3.53 (ddd, *J* = 11.0, 5.8, 3.9 Hz, 1H), 3.32 – 3.28 (m, 2H). ¹³C NMR (101 MHz, Methanol-*d*₄) δ 100.83, 75.04, 70.27, 69.72, 68.02, 67.80, 67.44, 67.11, 61.45, 50.56, 47.66, 47.44, 47.23, 47.02, 22.76. HRMS *m/z* calculated for C₁₀H₁₈N₃O₁₆S⁻¹, 372.0718; Found 372.0717.

Ethoxy-2-aminoethoxyl-O-(3-O-sulfonato)- α (1 \rightarrow 4)-L-idopyrnoside (ID11)



The compound **9a** (15mg, 0.403mmol) was dissolved in H₂O and Pd(OH)₂ (10% per wt) was added and stirred for 42h under hydrogen atmosphere. Further, reaction mixture was filtered and concentrated, finally purified by Bound elute C-18 column by using H₂O as a solvent to get (**ID11**) in a 85% yield. ¹H NMR (400 MHz, Deuterium oxide) 4.84 (dd, *J* = 1.8, 1.0 Hz, 1H), 4.36 (td, *J* = 3.6, 1.1 Hz, 1H), 4.07 (ddd, *J* = 7.0, 4.8, 1.9 Hz, 1H), 3.94 – 3.84 (m, 2H), 3.81 (ddd, *J* = 3.4, 2.0, 1.1 Hz, 1H), 3.79 – 3.68 (m, 6H), 3.67 – 3.60 (m, 1H), 3.17 – 3.11 (m, 2H). ¹³C NMR (101 MHz, Deuterium Oxide) δ 100.00, 75.48, 69.55, 68.17, 67.16, 66.92, 66.61, 66.17, 61.07, 39.16. HRMS *m/z* calculated for C₁₀H₂₀NO₁₀S⁻¹, 346.0813; Found 346.0816.

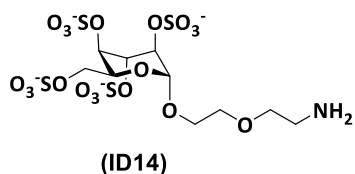
Ethoxy-2-azidoethoxyl-O-(2,3,4,6-O-sulfonato)- α (1 \rightarrow 4)-L-idopyrnoside (7a)



Compound **6a** (54mg, 0.184mmol) and SO₃.NMe₃ complex (717.5mg, 5.155mmol) was dissolved in dry DMF under N₂

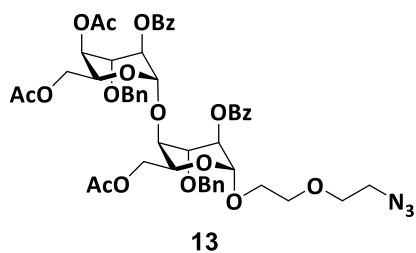
atmosphere, reaction mixture was kept for stirring at 60°C for 36 h, Next DMF was evaporated under reduced pressure, resulting residue was purified using silica column with DCM/MeOH solvent system to get compound **7a** in a 77 % yield. ¹H NMR (400 MHz, Deuterium oxide) 5.04 (d, *J* = 1.3 Hz, 1H), 4.90 (td, *J* = 2.5, 1.3 Hz, 1H), 4.54 – 4.43 (m, 3H), 4.25 – 4.10 (m, 2H), 3.93 – 3.82 (m, 1H), 3.78 – 3.71 (m, 4H), 3.71 – 3.62 (m, 1H), 3.43 (dd, *J* = 5.8, 4.1 Hz, 2H) ¹³C NMR (101 MHz, Deuterium Oxide) δ 98.02, 70.90, 70.74, 70.36, 69.52, 69.27, 67.95, 67.43, 64.17, 50.32. HRMS *m/z* calculated for C₁₀H₁₅N₃O₁₉S₄⁻⁴, 152.2301; Found 152.2305.

Ethoxy-2-aminoethoxyl-O-(2,3,4,6-O-sulfonato)-α(1→4)-L-idopyrnoside (ID14)



The compound **7a** (15mg, 0.0246mmole) was dissolved in H₂O and Pd(OH)₂ (10% per wt) was added and stirred for 42 h under hydrogen atmosphere. Further, reaction mixture was filtered and concentrated, finally purified by Bound elute C-18 column by using H₂O as a solvent to get **(ID14)** in a 80% yield. ¹H NMR (400 MHz, Deuterium oxide) 5.06 (s, 1H), 4.89 (dt, *J* = 2.9, 1.3 Hz, 1H), 4.53 – 4.38 (m, 3H), 4.26 – 4.09 (m, 2H), 3.93 – 3.82 (m, 1H), 3.81 – 3.62 (m, 5H), 3.14 (ddt, *J* = 6.8, 3.5, 1.6 Hz, 2H) ¹³C NMR (151 MHz, Deuterium Oxide) δ 97.99, 70.91, 70.66, 70.22, 69.54, 67.96, 67.40, 66.51, 64.24, 39.27. HRMS *m/z* calculated for C₁₀H₁₇NO₁₉S₄⁻⁴, 145.7325, Found 145.7327.

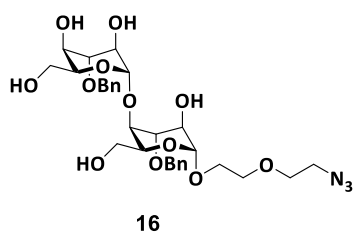
Ethoxy-2-azidoethoxyl-O-((4,6-O-diacetyl-2-O-benzoyl-3-O-benzyl)-α(1→4)-L-idopyrnosyl-(6-O-acetyl-2-O-benzoyl-3-O-benzyl))-α(1→4)-L-idopyrnoside (13)



Azido ethoxy ethanol linker glycosylated product **13** was obtained using synthetic procedure of compound **4** to get 78% yield. ¹H NMR (400 MHz, Chloroform-*d*) 5.41 (t, *J* = 2.2 Hz, 1H), 5.28 – 5.19 (m, 1H), 5.09 – 4.98 (m, 2H), 4.67 (dd, *J* = 11.3, 7.4 Hz, 2H), 4.56 – 4.33 (m, 5H), 4.18 – 4.05 (m, 1H), 4.02 – 3.88 (m, 1H), 3.88 – 3.79 (m, 3H), 3.76 – 3.53 (m, 5H), 3.41 (dd, *J* = 11.6, 4.3 Hz, 1H), 3.20 (dt, *J* = 6.0, 3.9 Hz, 2H), 2.07 (s, 3H), 1.95 (s, 3H), 1.93 (s, 3H), 8.07 – 7.98 (m, 2H), 7.92 – 7.82 (m, 2H), 7.64 – 7.51 (m, 3H), 7.50 – 7.39 (m, 3H), 7.38 – 7.26 (m, 7H), 7.22 (dt, *J* = 8.2, 6.9 Hz, 3H) ¹³C NMR (101 MHz, Chloroform-*d*) δ 170.63, 137.26, 133.60, 133.31, 130.03, 129.76,

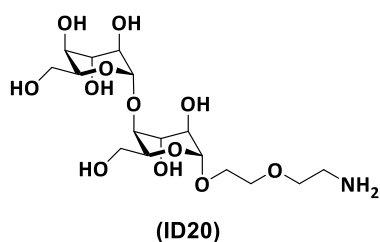
128.46, 128.44, 128.34, 128.31, 128.27, 128.02, 127.77, 127.62, 101.48, 98.49, 75.05, 72.48, 72.38, 70.33, 70.22, 67.72, 67.62, 67.51, 66.62, 65.05, 63.95, 62.97, 62.74, 50.74, 20.87, 20.77, 20.55. HRMS m/z calculated for $C_{50}H_{55}N_3O_{17}Na$, 969.3531; Found 969.3533.

Ethoxy-2-azidoethoxyl-O-((3-O-benzyl)- α (1 \rightarrow 4)-L-idopyrnosyl-(3-O-benzyl))- α (1 \rightarrow 4)-L-idopyrnoside (16)



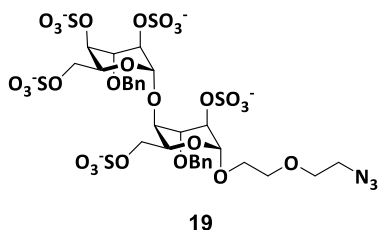
Compound **16** was obtained from esters group deprotection of compound **13** using synthetic procedure of compound **5** to get 85% yield. 1H NMR (400 MHz, Chloroform-*d*) 4.95 (s, 1H), 4.80 (s, 1H), 4.69 (d, $J = 11.9$ Hz, 1H), 4.58 – 4.49 (m, 3H), 4.29 (t, $J = 6.6$ Hz, 1H), 4.20 – 4.10 (m, 1H), 3.95 – 3.82 (m, 3H), 3.81 – 3.72 (m, 5H), 3.71 – 3.53 (m, 9H), 3.23 (t, $J = 5.0$ Hz, 2H), 7.37 – 7.19 (m, 10H). ^{13}C NMR (101 MHz, Chloroform-*d*) δ 130.98 – 122.77 (m), 103.03, 101.32, 74.17, 73.94 (d, $J = 4.3$ Hz), 72.59, 71.22, 70.35, 70.06, 69.74, 67.51, 66.52 – 65.92 (m), 64.35, 61.46, 50.71. HRMS m/z calculated for $C_{30}H_{41}N_3O_{12}Na$, 635.2690; Found 635.2692.

Ethoxy-2-aminoethoxyl-O-((2,3,4,6-anhydro)- α (1 \rightarrow 4)-L-idopyrnosyl-(2,3,6-anhydro))- α (1 \rightarrow 4)-L-idopyrnoside (ID20)



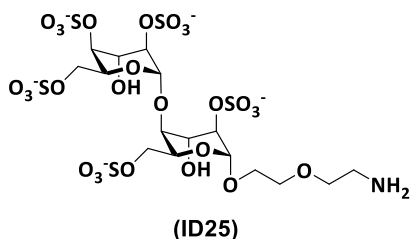
Hydrogenolysis of compound **10** was done by using the previous procedure of compound **(ID10)** to get compound **(ID20)** in a yield 89% yield. 1H NMR (600 MHz, Deuterium Oxide) 4.76 (dd, $J = 6.2, 4.4$ Hz, 2H), 4.15 (dq, $J = 8.8, 4.6$ Hz, 2H), 3.89 (dt, $J = 9.2, 5.4$ Hz, 2H), 3.82 – 3.60 (m, 14H), 3.52 (ddd, $J = 12.6, 6.9, 4.4$ Hz, 2H), 3.19 – 3.07 (m, 2H). ^{13}C NMR (151 MHz, Deuterium Oxide) δ 101.39, 100.35, 77.52, 71.43, 71.34, 70.49, 70.33, 70.19, 70.17, 69.93, 69.57, 67.52, 66.36, 59.84, 59.70, 39.05. HRMS m/z calculated for $C_{16}H_{31}NO_{12}Na$, 429.1846; Found 429.1847.

Ethoxy-2-azidoethoxyl-O-((2,4,6-O-trisulfonato-3-O-benzyl)- α (1 \rightarrow 4)-L-idopyrnosyl)-(2,6-O-disulfonato-3-O-benzyl)- α (1 \rightarrow 4)-L-idopyrnoside (19)



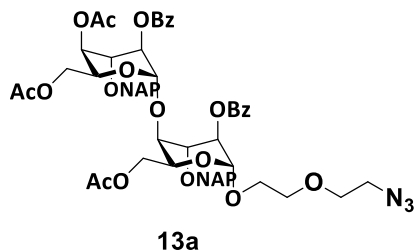
Compound **19** was obtained by performing sulfation reaction of compound **16** using synthetic procedure of compound **6** to get 75% yield. ^1H NMR (400 MHz, Deuterium Oxide) 5.20 (s, 1H), 5.11 (s, 1H), 4.95 – 4.83 (m, 4H), 4.61 – 4.49 (m, 3H), 4.40 (dt, $J = 2.1, 1.0$ Hz, 1H), 4.29 (pd, $J = 7.5, 6.5, 3.2$ Hz, 5H), 4.23 – 4.16 (m, 1H), 4.04 – 3.90 (m, 2H), 3.87 – 3.65 (m, 6H), 3.45 – 3.40 (m, 2H), 7.56 (ddd, $J = 8.4, 4.6, 1.8$ Hz, 3H), 7.51 (dt, $J = 7.4, 1.5$ Hz, 2H), 7.49 – 7.40 (m, 4H) ^{13}C NMR (101 MHz, Deuterium Oxide) δ 137.72, 137.03, 130.94 – 125.11 (m), 100.39, 98.50, 75.17, 73.77, 73.19, 72.31, 72.14, 71.66, 71.14, 70.40, 69.40 (d, $J = 10.0$ Hz), 68.22, 67.70, 67.45, 65.65, 64.44, 50.25. HRMS m/z calculated for $\text{C}_{30}\text{H}_{36}\text{N}_3\text{O}_{27}\text{S}_5^{-5}$, 206.0033; Found 206.0039.

Ethoxy-2-aminoethoxyl-O-((2,4,6-O-trisulfonato)- α (1 \rightarrow 4)-L-idopyrnosyl)-(2,6-O-disulfonato)- α (1 \rightarrow 4)-L-idopyrnoside (ID25)



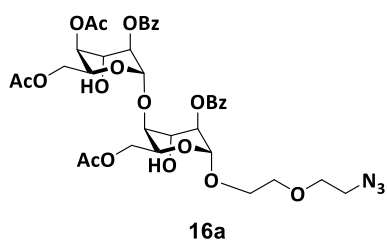
Compound (**ID25**) was obtained by doing hydrogenolysis reaction of compound **19** using synthetic procedure of compound (**ID13**) to get 85% yield. ^1H NMR (400 MHz, Deuterium Oxide) 5.06 – 4.99 (m, 2H), 4.41 (ddd, $J = 8.4, 3.8, 2.0$ Hz, 1H), 4.30 – 4.12 (m, 10H), 3.89 – 3.79 (m, 1H), 3.78 – 3.74 (m, 1H), 3.71 – 3.63 (m, 5H), 3.15 – 3.04 (m, 2H) ^{13}C NMR (101 MHz, Deuterium Oxide) δ 100.14, 98.59, 76.12, 74.27, 72.83, 72.33, 69.65, 68.17, 67.52, 67.40, 67.05, 66.37, 66.31, 65.62, 64.43, 39.23. HRMS m/z calculated for $\text{C}_{16}\text{H}_{26}\text{NO}_{27}\text{S}_5^{-5}$, 164.7865; Found 164.7867.

Ethoxy-2-azidoethoxyl-O-((4,6-O-diacetyl-2-O-benzoyl-3-O-(2-naphthylmethyl))- α (1 \rightarrow 4)-L-idopyrnosyl-(6-O-acetyl-2-O-benzoyl-3-O-(2-naphthylmethyl))- α (1 \rightarrow 4)-L-idopyrnoside (13a)



Compound **13a** was synthesised by using synthetic procedure of compound **4a** in a 78% yield. ^1H NMR (400 MHz, Chloroform-*d*) 5.49 – 5.38 (m, 1H), 5.28 (p, $J = 1.1$ Hz, 1H), 5.08 – 4.94 (m, 4H), 4.83 (dd, $J = 19.9, 11.5$ Hz, 2H), 4.60 – 4.40 (m, 5H), 4.16 (t, $J = 3.3$ Hz, 1H), 4.01 – 3.92 (m, 1H), 3.92 – 3.81 (m, 3H), 3.70 (dt, $J = 4.4, 3.1$ Hz, 3H), 3.66 – 3.52 (m, 2H), 3.42 (dd, $J = 11.6, 4.1$ Hz, 1H), 3.14 (dt, $J = 6.0, 3.8$ Hz, 2H), 2.03 (s, 3H), 1.95 (s, 3H), 1.92 (s, 3H), 8.04 – 7.93 (m, 3H), 7.90 – 7.69 (m, 9H), 7.69 – 7.54 (m, 2H), 7.50 – 7.34 (m, 8H), 7.21 – 7.10 (m, 2H) ^{13}C NMR (101 MHz, Chloroform-*d*) δ 170.70, 170.66, 169.98, 165.45, 165.08, 135.27, 134.71, 133.60, 133.29 (d, $J = 4.9$ Hz), 133.13 (d, $J = 2.2$ Hz), 132.96, 129.90, 129.79, 129.36, 129.14, 128.45, 128.24, 128.11, 127.98, 127.87, 127.67 (d, $J = 4.6$ Hz), 126.92, 126.54, 126.11, 125.95, 125.79, 101.09, 98.44, 75.24, 72.93, 72.55 (d, $J = 2.8$ Hz), 70.26, 70.19, 68.04, 67.77, 67.35, 65.29, 64.02, 63.00, 62.62, 50.68, 20.81, 20.78, 20.56. HRMS m/z calculated for $\text{C}_{58}\text{H}_{59}\text{N}_3\text{O}_{17}\text{Na}$, 1069.3844; Found 1069.3847.

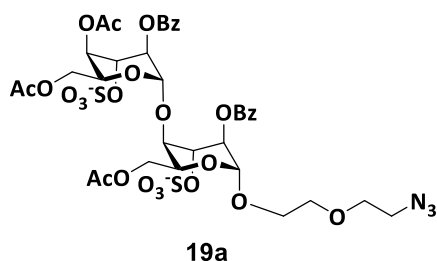
Ethoxy-2-azidoethoxyl-O-((4,6-O-diacetyl-2-O-benzoyl)- α (1 \rightarrow 4)-L-idopyrnosyl-(6-O-acetyl-2-O-benzoyl))- α (1 \rightarrow 4)-L-idopyrnoside (16a)



Compound **16a** was obtained by doing selective NAP-deprotection reaction of compound **13a** using synthetic procedure of compound **5a** to get 82% yield. ^1H NMR (400 MHz, Chloroform-*d*) 5.23 (dd, $J = 4.5, 2.5$ Hz, 1H), 5.13 – 5.02 (m, 3H), 4.57 – 4.52 (m, 1H), 4.51 – 4.37 (m, 3H), 4.35 – 4.24 (m, 2H), 4.15 – 4.07 (m, 1H), 4.15 – 4.07 (m, 1H), 3.99 (s, 1H), 3.95 – 3.88 (m, 1H), 3.86 (t, $J = 3.5$ Hz, 1H), 3.76 (dd, $J = 11.7, 3.4$ Hz, 1H), 3.70 – 3.56 (m, 7H), 3.37 – 3.30 (m, 2H), 2.05 (s, 3H), 2.02 (s, 3H), 1.99 (s, 3H), 8.13 – 8.06 (m, 2H), 8.07 – 7.97 (m, 2H), 7.70 – 7.33 (m, 6H) ^{13}C NMR (101 MHz, Chloroform-*d*) δ 170.82, 170.70, 170.25, 165.26, 133.63, 133.58, 129.99, 129.80, 129.29, 129.21, 128.62, 128.45, 100.89, 98.28, 78.61, 70.09, 69.96, 69.92, 69.46, 69.33,

68.28, 67.12, 64.97, 64.87, 62.74, 62.20, 50.67, 20.76, 20.70, 20.51. HRMS m/z calculated for $C_{36}H_{43}N_3O_{17}Na$, 789.2592; Found 789.2594.

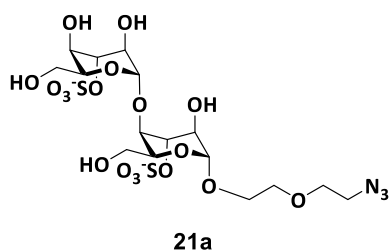
Ethoxy-2-azidoethoxyl-O-((4,6-O-diacetyl-3-O-sulfonato-2-O-benzoyl)- $\alpha(1\rightarrow4)$ -L-idopyrnosyl-(6-O-acetyl-3-O-sulfonato-2-O-benzoyl)- $\alpha(1\rightarrow4)$ -L-idopyrnoside (19a)



Compound **19a** was obtained by doing selective sulfation reaction of compound **16a** using synthetic procedure of compound **8a** to get 75% yield. 1H NMR (400 MHz, Methanol- d_4) 5.50 – 5.43 (m, 1H), 5.42 – 5.33 (m, 1H),

5.19 (t, $J = 1.3$ Hz, 1H), 5.10 – 5.02 (m, 1H), 5.00 (d, $J = 1.6$ Hz, 1H), 4.70 (td, $J = 3.5, 0.9$ Hz, 1H), 4.63 (ddd, $J = 8.1, 4.0, 2.0$ Hz, 1H), 4.58 – 4.40 (m, 3H), 4.16 (q, $J = 3.8, 2.7$ Hz, 1H), 4.03 – 3.89 (m, 2H), 3.84 (dt, $J = 10.8, 4.9$ Hz, 1H), 3.80 – 3.73 (m, 3H), 3.72 (d, $J = 4.0$ Hz, 2H), 3.42 (t, $J = 4.9$ Hz, 2H), 3.39 – 3.32 (m, 2H), 8.27 – 8.18 (m, 2H), 8.14 – 8.06 (m, 2H), 7.72 – 7.60 (m, 4H), 7.53 (t, $J = 7.8$ Hz, 2H) ^{13}C NMR (101 MHz, Methanol- d_4) δ 171.81, 171.68, 170.45, 165.65, 165.36, 133.52, 133.28, 129.98, 129.52, 128.73, 128.32, 101.81, 97.97, 76.42, 71.66, 70.98, 70.02, 69.60, 68.34, 68.02, 67.59, 67.31, 64.69, 64.43, 62.92, 62.54, 53.87, 50.58, 48.36, 48.15, 47.93, 47.72, 47.51, 47.30, 47.08, 19.54, 19.52, 19.45. HRMS m/z calculated for $C_{36}H_{41}N_3O_{23}S_2^{-2}$, 473.5791; Found 473.5793.

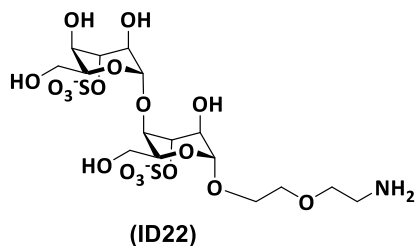
Ethoxy-2-azidoethoxyl-O-((3-O-sulfonato)- $\alpha(1\rightarrow4)$ -L-idopyrnosyl-(3-O-sulfonato))- $\alpha(1\rightarrow4)$ -L-idopyrnoside (21a)



Compound **21a** was obtained by doing ester deprotection reaction of compound **19a** using synthetic procedure of compound **8a** to get 83% yield. 1H NMR (400 MHz, Deuterium Oxide) 4.88 – 4.84 (m, 2H), 4.63 (d, $J = 3.1$ Hz,

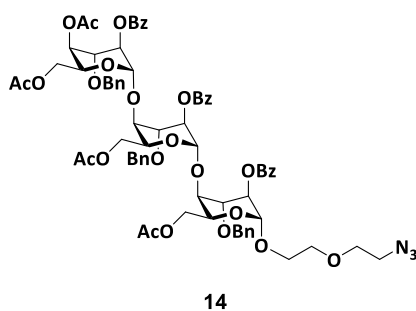
1H), 4.36 (t, $J = 4.1$ Hz, 1H), 4.18 (dt, $J = 17.0, 6.8$ Hz, 2H), 3.98 (d, $J = 3.0$ Hz, 1H), 3.92 (t, $J = 3.0$ Hz, 1H), 3.90 – 3.79 (m, 3H), 3.73 (tdd, $J = 8.4, 6.8, 3.6$ Hz, 7H), 3.67 – 3.59 (m, 2H), 3.42 (t, $J = 4.9$ Hz, 2H) ^{13}C NMR (101 MHz, Deuterium Oxide) δ 102.55, 99.88, 75.78, 73.54, 72.82, 69.62, 69.37, 68.78, 67.24, 66.97, 66.91, 66.66, 66.59, 60.68, 60.50, 50.28. HRMS m/z calculated for $C_{16}H_{27}N_3O_{18}S_2^{-2}$, 306.5371; Found 306.5373.

Ethoxy-2-aminoethoxyl-O-((3-O-sulfonato)- α (1 \rightarrow 4)-L-idopyrnosyl-(3-O-sulfonato))- α (1 \rightarrow 4)-L-idopyrnoside (ID22)



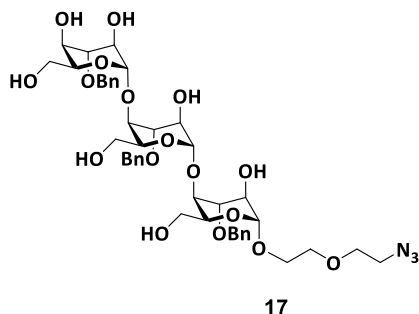
Compound (ID22) was obtained by doing hydrogenolysis reaction of compound 21a using synthetic procedure of compound (ID11) to get 83% yield. ¹H NMR (600 MHz, Deuterium Oxide) 4.90 – 4.78 (m, 2H), 4.63 (d, *J* = 3.1 Hz, 1H), 4.38 – 4.33 (m, 1H), 4.20 (ddd, *J* = 7.2, 5.3, 2.0 Hz, 1H), 4.14 (dd, *J* = 7.3, 5.3 Hz, 1H), 3.99 (d, *J* = 3.2 Hz, 1H), 3.93 – 3.90 (m, 1H), 3.89 – 3.83 (m, 2H), 3.81 – 3.68 (m, 9H), 3.67 – 3.62 (m, 1H), 3.18 – 3.10 (m, 2H)¹³C NMR (151 MHz, Deuterium Oxide) δ 102.52, 99.83, 75.50, 73.45, 72.76, 69.56, 68.78, 68.67, 67.16, 67.04, 66.96, 66.81, 66.63, 66.60, 66.41, 60.71, 60.55, 39.16. HRMS *m/z* calculated for C₁₆H₂₉NO₁₈S₂⁻², 293.5418; Found 293.5419.

Ethoxy-2-azidoethoxyl-O-((4,6-O-diacetyl-2-O-benzoyl-3-O-benzyl)- α (1 \rightarrow 4)-L-idopyrnosyl-(6-O-acetyl-2-O-benzoyl-3-O-benzyl)- α (1 \rightarrow 4)-L-idopyrnosyl-(6-O-acetyl-2-O-benzoyl-3-O-benzyl))- α (1 \rightarrow 4)-L-idopyrnoside (14)



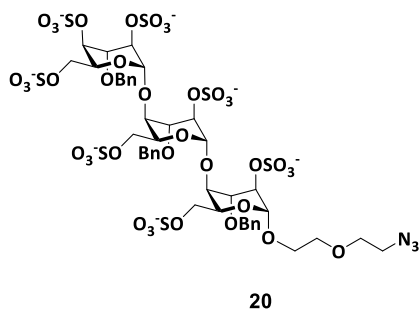
Azido ethoxy ethanol linker glycosylated product 14 was obtained by using synthetic procedure of compound 4 in a 82% yield. ¹H NMR (400 MHz, Chloroform-*d*) 5.36 (dt, *J* = 15.8, 2.7 Hz, 2H), 5.16 – 5.12 (m, 1H), 5.07 – 4.98 (m, 2H), 4.92 – 4.78 (m, 4H), 4.68 (dt, *J* = 13.5, 10.5 Hz, 3H), 4.58 (t, *J* = 2.3 Hz, 1H), 4.53 – 4.25 (m, 5H), 4.17 – 3.99 (m, 3H), 3.99 – 3.77 (m, 5H), 3.76 – 3.46 (m, 7H), 3.21 (ddd, *J* = 5.9, 4.1, 3.0 Hz, 2H), 1.98 (s, 3H), 1.94 (s, 3H), 1.90 (s, 3H), 1.87 (s, 3H), 8.04 – 7.99 (m, 2H), 7.99 – 7.88 (m, 4H), 7.62 – 7.55 (m, 1H), 7.52 – 7.33 (m, 10H), 7.29 (td, *J* = 7.3, 5.4 Hz, 6H), 7.25 – 7.15 (m, 7H)¹³C NMR (101 MHz, Chloroform-*d*) δ 177.47, 170.60, 170.53, 170.51, 169.95, 165.60, 165.38, 165.00, 137.92, 137.51, 137.21, 133.64, 133.36, 133.09, 130.15, 130.00, 129.76, 129.40, 129.32, 129.12, 128.49, 128.42, 128.36, 128.23, 128.20, 128.04, 127.87, 127.78, 127.69, 101.17, 100.65, 98.39, 77.47, 77.34, 77.15, 76.84, 76.73, 76.23, 75.00, 74.47, 72.93, 72.51, 72.38, 72.28, 70.39, 70.29, 70.20, 68.21, 67.73, 67.63, 67.46, 66.69, 65.99, 65.16, 64.10, 62.79, 62.22, 50.73, 31.93, 20.77, 20.75, 20.62, 20.57, 0.04. HRMS *m/z* calculated for C₇₂H₇₂N₃O₂₄Na, 1369.4897, Found 1369.4899.

Ethoxy-2-azidoethoxyl-O-((3-O-benzyl)- α (1 \rightarrow 4)-L-idopyrnosyl-(3-O-benzyl))- α (1 \rightarrow 4)-L-idopyrnosyl-(3-O-benzyl))- α (1 \rightarrow 4)-L-idopyrnoside (17)



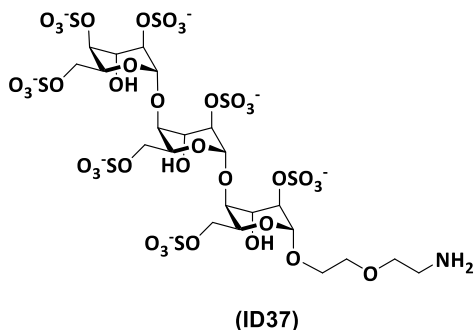
Compound **17** was obtained from esters group deprotection of compound **14** using synthetic procedure of compound **5** to get 88% yield. ¹H NMR (400 MHz, Chloroform-*d*) 4.90 (s, 1H), 4.83 (s, 1H), 4.79 (s, 1H), 4.72 (d, *J* = 11.8 Hz, 1H), 4.62 – 4.49 (m, 6H), 4.43 (d, *J* = 8.5 Hz, 1H), 4.33 (dt, *J* = 15.7, 6.6 Hz, 2H), 4.16 (dd, *J* = 11.7, 5.5 Hz, 2H), 4.01 (d, *J* = 3.8 Hz, 1H), 3.96 – 3.74 (m, 8H), 3.72 – 3.52 (m, 15H), 3.47 (dd, *J* = 12.1, 3.4 Hz, 1H), 3.22 (t, *J* = 5.0 Hz, 2H), 7.38 – 7.26 (m, 15H) ¹³C NMR (101 MHz, Chloroform-*d*) δ 137.08, 128.58, 128.39, 128.34, 128.24, 127.78, 127.56, 103.08, 101.28, 77.28, 74.41, 74.26, 74.07, 73.07, 72.77, 72.62, 71.97, 71.46, 70.39, 70.09, 67.52, 66.73, 66.54, 66.47, 66.29, 64.37, 62.02, 61.05, 50.75. HRMS *m/z* calculated for C₄₃H₅₇N₃O₁₇, 887.3688; Found 887.3691.

Ethoxy-2-azidoethoxyl-O-((2,4,6-O-trisulfonato-3-O-benzyl)- α (1 \rightarrow 4)-L-idopyrnosyl-(2,6-O-disulfonato-3-O-benzyl))- α (1 \rightarrow 4)-L-idopyrnosyl-(2,6-O-disulfonato-3-O-benzyl))- α (1 \rightarrow 4)-L-idopyrnoside (20)



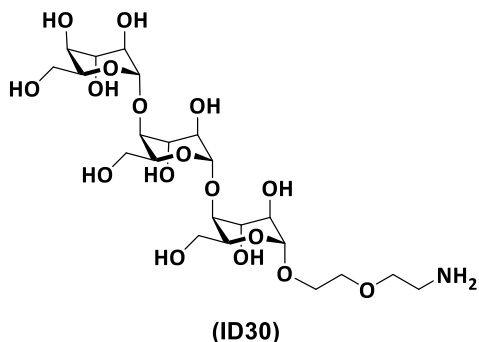
Compound **20** was obtained by performing sulfation reaction of compound **17** using synthetic procedure of compound **6** to get 73% yield. ¹H NMR (600 MHz, Deuterium Oxide) 5.05 (s, 1H), 4.96 (s, 1H), 4.86 (s, 1H), 4.79 – 4.72 (m, 5H), 4.69 – 4.61 (m, 3H), 4.58 – 4.51 (m, 1H), 4.41 – 4.30 (m, 4H), 4.26 (t, *J* = 1.8 Hz, 1H), 4.17 (dd, *J* = 11.6, 8.5 Hz, 1H), 4.14 – 4.06 (m, 6H), 3.98 (dd, *J* = 10.6, 3.4 Hz, 1H), 3.89 – 3.83 (m, 1H), 3.73 – 3.67 (m, 3H), 3.67 – 3.60 (m, 4H), 3.36 – 3.31 (m, 2H), 7.49 – 7.23 (m, 15H) ¹³C NMR (151 MHz, Deuterium Oxide) δ 137.74, 136.96, 128.82, 128.71, 128.65, 128.62, 128.60, 128.54, 128.24, 128.16, 128.06, 100.56, 100.40, 98.43, 75.53, 75.08, 74.41, 73.18, 73.06, 72.37, 71.82, 71.46, 70.91, 70.25, 69.37, 69.22, 67.99, 67.95, 67.69, 67.24, 65.97, 65.73, 64.12, 50.19. HRMS *m/z* calculated for C₄₃H₅₀N₃O₃₈S₇⁻⁷, 205.7165; Found 205.7169.

Ethoxy-2-azidoethoxyl-O-((2,4,6-O-trisulfonato)- α (1 \rightarrow 4)-L-idopyrnosyl-(2,6-O-disulfonato)- α (1 \rightarrow 4)-L-idopyrnosyl-(2,6-O-disulfonato))- α (1 \rightarrow 4)-L-idopyrnoside (ID37)



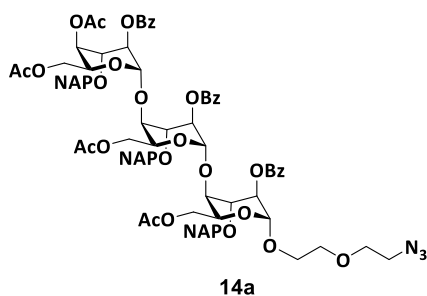
Compound (ID37) was obtained by performing hydrogenolysis reaction of compound **20** using synthetic procedure of compound (ID13) to get 80% yield. ¹H NMR (600 MHz, Deuterium Oxide) 5.16 (dd, *J* = 15.3, 3.8 Hz, 3H), 4.72 (dt, *J* = 9.7, 3.3 Hz, 1H), 4.54 (dtd, *J* = 11.3, 8.0, 6.9, 4.0 Hz, 1H), 4.45 – 4.23 (m, 15H), 4.07 – 3.66 (m, 10H), 3.31 – 3.16 (m, 2H)¹³C NMR (151 MHz, Deuterium Oxide) δ 100.27, 100.06, 98.56, 76.16, 75.87, 74.75, 73.06, 72.70, 72.57, 71.98, 69.62, 68.10, 67.89, 67.79, 67.64, 67.40, 67.36, 67.03, 66.72, 66.23, 66.12, 65.38, 64.23, 39.16. HRMS *m/z* calculated for C₂₂H₃₄NO₃₈S₇⁻, 163.4120, Found 163.4124.

Ethoxy-2-aminoethoxyl-O-((2,3,4,6-anhydro)- α (1 \rightarrow 4)-L-idopyrnosyl-(2,3,6-anhydro))- α (1 \rightarrow 4)-L-idopyrnosyl-(2,3,6-anhydro))- α (1 \rightarrow 4)-L-idopyrnoside (ID30)



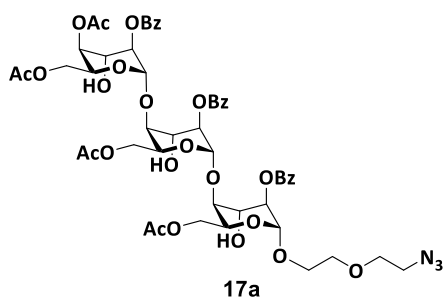
Compound (ID30) was obtained by performing hydrogenolysis reaction of compound **17** using synthetic procedure of compound (ID10) to get 80% yield. ¹H NMR (400 MHz, Deuterium Oxide) 4.76 (t, *J* = 4.6 Hz, 3H), 4.27 (td, *J* = 6.8, 6.3, 3.0 Hz, 1H), 4.15 (ddd, *J* = 7.2, 5.2, 3.6 Hz, 2H), 3.90 (ddd, *J* = 8.7, 6.4, 4.1 Hz, 2H), 3.83 – 3.63 (m, 15H), 3.61 – 3.47 (m, 3H), 3.14 (t, *J* = 5.0 Hz, 2H)¹³C NMR (101 MHz, Deuterium Oxide) δ 101.65, 101.42, 100.37, 77.57, 77.34, 71.29, 70.37, 70.33, 70.13, 70.04, 69.85, 69.69, 69.59, 67.54, 66.35, 59.93, 59.74, 39.06. HRMS *m/z* calculated for C₂₂H₄₁NO₁₇Na, 591.2374; Found 591.2376.

Ethoxy-2-azidoethoxyl-O-((4,6-O-diacetyl-2-O-benzoly-3-O-(2-naphthylmethyl))- α (1 \rightarrow 4)-L-idopyrnosyl-(6-O-acetyl-2-O-benzoly-3-O-(2-naphthylmethyl))- α (1 \rightarrow 4)-L-idopyrnosyl-(6-O-acetyl-2-O-benzoly-3-O-(2-naphthylmethyl))- α (1 \rightarrow 4)-L-idopyrnoside (14a)



Compound **14a** was synthesised by using synthetic procedure of compound **4** in a 75% yield. ^1H NMR (400 MHz, Chloroform-*d*) 5.39 (dt, $J = 8.2, 3.1$ Hz, 2H), 5.22 – 5.15 (m, 1H), 5.06 – 4.92 (m, 5H), 4.91 – 4.75 (m, 4H), 4.66 (t, $J = 2.3$ Hz, 1H), 4.50 (tq, $J = 5.7, 3.3, 2.4$ Hz, 2H), 4.39 (dd, $J = 11.3, 7.2$ Hz, 1H), 4.35 – 4.26 (m, 2H), 4.26 – 4.15 (m, 2H), 4.13 – 4.05 (m, 1H), 4.03 – 3.83 (m, 5H), 3.68 (qd, $J = 6.0, 2.9$ Hz, 3H), 3.65 – 3.51 (m, 4H), 3.13 (dt, $J = 5.9, 3.6$ Hz, 2H), 1.94 (s, 3H), 1.90 – 1.83 (m, 9H), 8.07 – 7.98 (m, 2H), 7.94 – 7.87 (m, 3H), 7.83 (ddd, $J = 8.4, 7.0, 1.5$ Hz, 3H), 7.78 – 7.66 (m, 9H), 7.63 (d, $J = 8.4$ Hz, 1H), 7.61 – 7.54 (m, 2H), 7.49 – 7.34 (m, 12H), 7.19 (td, $J = 7.8, 4.8$ Hz, 4H) ^{13}C NMR (101 MHz, Chloroform-*d*) δ 170.62, 170.57, 170.46, 169.98, 165.59, 165.30, 165.03, 135.39, 134.93, 134.63, 133.66, 133.30, 133.18, 133.16, 133.11, 133.08, 133.02, 132.97, 130.12, 130.04, 129.88, 129.81, 129.42, 129.35, 129.09, 128.67, 128.51, 128.30, 128.28, 128.20, 128.14, 127.90, 127.73, 127.68, 127.65, 127.03, 127.00, 126.60, 126.26, 126.15, 126.10, 125.99, 125.91, 125.88, 125.86, 100.60, 100.28, 98.37, 77.47, 77.35, 77.15, 76.83, 76.49, 75.94, 75.19, 74.76, 73.33, 72.79, 72.62, 72.54, 70.24, 70.20, 68.59, 68.05, 67.82, 67.33, 66.89, 66.29, 65.42, 64.19, 62.84, 62.51, 62.26, 50.70, 20.79, 20.67, 20.58. HRMS m/z calculated for $\text{C}_{84}\text{H}_{83}\text{N}_3\text{O}_{24}\text{Na}$, 1517.5397; Found 1517.5399.

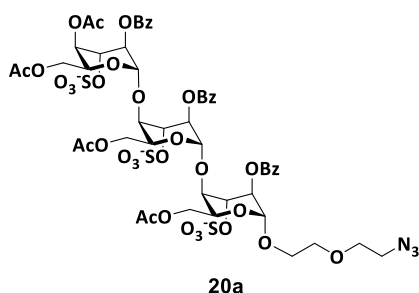
Ethoxy-2-azidoethoxyl-O-((4,6-O-diacetyl-2-O-benzoyl)- $\alpha(1\rightarrow4)$ -L-idopyrnosyl-(6-O-acetyl-2-O-benzoyl))- $\alpha(1\rightarrow4)$ -L-idopyrnosyl-(6-O-acetyl-2-O-benzoyl))- $\alpha(1\rightarrow4)$ -L-idopyrnoside (17a)



Compound **17a** was obtained by doing selective NAP-deprotection reaction of compound **14a** using synthetic procedure of compound **5a** to get 75% yield. ^1H NMR (400 MHz, Chloroform-*d*) 5.19 (dd, $J = 8.6, 5.6$ Hz, 1H), 5.12 (dd, $J = 4.0, 2.2$ Hz, 1H), 5.05 (d, $J = 5.6$ Hz, 1H), 5.02 – 4.96 (m, 2H), 4.91 (t, $J = 1.4$ Hz, 1H), 4.78 (t, $J = 2.8$ Hz, 1H), 4.60 (ddd, $J = 8.8, 3.5, 2.2$ Hz, 1H), 4.41 – 4.22 (m, 5H), 4.19 – 3.98 (m, 8H), 3.93 – 3.83 (m, 1H), 3.77 (t, $J = 3.1$ Hz, 1H), 3.72 – 3.58 (m, 7H), 3.43 (dd, $J = 6.0, 4.3$ Hz, 1H), 3.38 – 3.29 (m, 2H), 2.04 (d, $J = 2.8$ Hz, 3H), 1.98 (d, $J = 5.9$ Hz, 6H), 1.88 (s, 3H), 8.17 – 7.96 (m, 6H), 7.64 – 7.49 (m, 5H),

7.44 (dt, $J = 11.8, 7.8$ Hz, 4H) ^{13}C NMR (101 MHz, Chloroform- d) δ 171.17, 170.76, 170.38, 170.18, 165.54, 165.34, 165.20, 133.67, 133.51, 130.04, 129.88, 129.80, 129.66, 129.25, 129.10, 128.64, 128.51, 128.48, 100.83, 99.67, 98.10, 81.18, 77.39, 77.27, 77.07, 76.88, 76.75, 71.97, 70.68, 70.09, 69.87, 69.24, 68.53, 68.50, 67.61, 66.97, 66.41, 64.84, 64.60, 63.08, 62.18, 61.50, 50.69, 20.71, 20.70, 20.63, 20.47, 0.01. HRMS m/z calculated for $\text{C}_{51}\text{H}_{59}\text{N}_3\text{O}_{24}\text{Na}$, 1097.3488; Found 1097.3490.

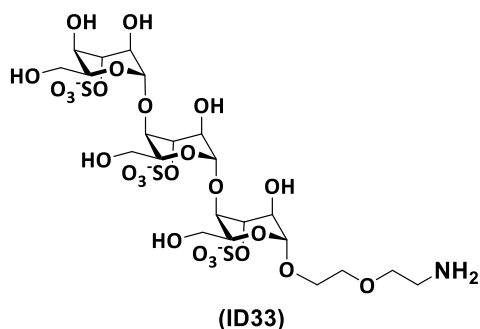
Ethoxy-2-azidoethoxyl-O-((4,6-O-diacetyl-3-O-sulfonato-2-O-benzoyl)- $\alpha(1\rightarrow4)$ -L-idopyrnosyl-(6-O-acetyl-2-3-O-sulfonato-O-benzoyl)- $\alpha(1\rightarrow4)$ -L-idopyrnosyl-(6-O-acetyl-2-3-O-sulfonato-O-benzoyl)- $\alpha(1\rightarrow4)$ -L-idopyrnoside (20a)



Compound **20a** was obtained by doing selective sulfation reaction of compound **17a** using synthetic procedure of compound **6a** to get 75% yield. ^1H NMR (400 MHz, Methanol- d_4) 5.41 (t, $J = 2.4$ Hz, 1H), 5.30 – 5.10 (m, 3H), 4.94 (dt, $J = 8.0, 2.2$ Hz, 3H), 4.83 (d, $J = 1.3$ Hz, 1H),

4.74 – 4.69 (m, 2H), 4.63 – 4.52 (m, 3H), 4.40 – 4.28 (m, 3H), 4.19 (dd, $J = 11.3, 7.5$ Hz, 1H), 4.07 (d, $J = 2.4$ Hz, 1H), 3.90 – 3.51 (m, 9H), 3.28 (t, $J = 4.9$ Hz, 2H), 1.92 (s, 3H), 1.90 (s, 3H), 1.88 (s, 3H), 1.81 (s, 3H), 8.15 – 8.07 (m, 4H), 8.02 – 7.88 (m, 2H), 7.60 – 7.44 (m, 7H), 7.38 (t, $J = 7.8$ Hz, 2H) ^{13}C NMR (101 MHz, Methanol- d_4) δ 172.14, 171.82, 171.43, 170.12, 165.83, 165.61, 165.21, 133.31, 133.14, 129.97, 129.91, 129.70, 129.51, 129.44, 129.38, 128.76, 128.58, 128.21, 101.73, 101.54, 97.79, 78.07, 76.70, 76.29, 72.58, 71.94, 71.11, 70.25, 69.79, 69.56, 68.19, 68.08, 67.62, 67.30, 66.37, 64.77, 64.59, 63.15, 62.77, 62.65, 50.59, 48.26, 48.05, 47.84, 47.62, 47.41, 47.20, 46.99, 19.58, 19.54, 19.46, 19.34. HRMS m/z calculated for $\text{C}_{51}\text{H}_{56}\text{N}_3\text{O}_{33}\text{S}_3^{-3}$, 444.7325; Found 444.7327.

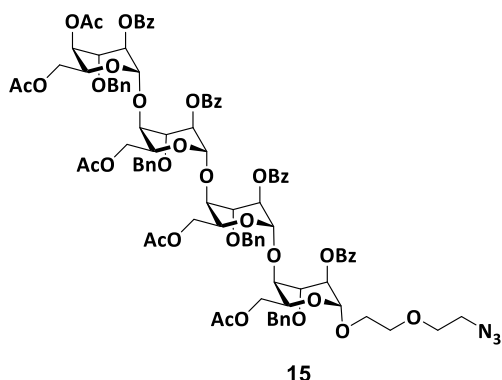
Ethoxy-2-aminoethoxyl-O-((3-O-sulfonato)- $\alpha(1\rightarrow4)$ -L-idopyrnosyl-(3-O-sulfonato)- $\alpha(1\rightarrow4)$ -L-idopyrnosyl-(3-O-sulfonato))- $\alpha(1\rightarrow4)$ -L-idopyrnoside (ID33)



Compound (**ID33**) was obtained by doing hydrogenolysis reaction of compound **20a** using synthetic procedure of compound (**ID11**) to get 83% yield. ^1H NMR (400 MHz, Deuterium Oxide) 4.83 (d,

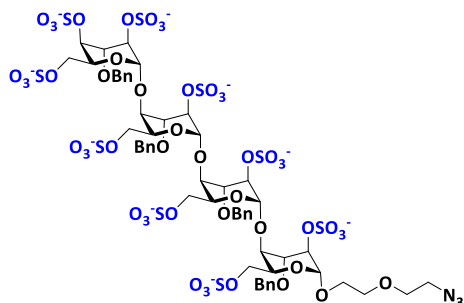
$J = 2.2$ Hz, 3H), 4.59 (s, 1H), 4.55 – 4.47 (m, 1H), 4.35 – 4.21 (m, 2H), 4.18 – 4.04 (m, 2H), 4.01 – 3.92 (m, 3H), 3.89 – 3.80 (m, 4H), 3.80 – 3.54 (m, 18H), 3.12 – 3.04 (m, 2H) ^{13}C NMR (101 MHz, Deuterium Oxide) δ 102.56, 102.22, 99.94, 75.72, 73.53, 72.90, 72.69, 72.28, 69.63, 68.87, 67.27, 67.13, 66.89, 66.73, 66.67, 66.56, 66.33, 60.74, 60.61, 60.03, 39.24. HRMS m/z calculated for $\text{C}_{22}\text{H}_{36}\text{NO}_2\text{S}_3^{-3}$, 276.0287; Found 276.0289.

Ethoxy-2-azidoethoxyl-O-((4,6-O-diacetyl-2-O-benzoyl-3-O-benzyl)- α (1 \rightarrow 4)-L-idopyrnosyl-(6-O-acetyl-2-O-benzoyl-3-O-benzyl)- α (1 \rightarrow 4)-L-idopyrnosyl-(6-O-acetyl-2-O-benzoyl-3-O-benzyl)- α (1 \rightarrow 4)-L-idopyrnosyl-(6-O-acetyl-2-O-benzoyl-3-O-benzyl)- α (1 \rightarrow 4)-L-idopyrnoside (15)



Compound **15** was synthesised by using synthetic procedure of compound **4** in a 75% yield. ^1H NMR (400 MHz, Chloroform-*d*) 5.34 – 5.23 (m, 3H), 5.13 (d, $J = 2.5$ Hz, 1H), 5.03 – 4.95 (m, 2H), 4.93 – 4.75 (m, 6H), 4.71 – 4.60 (m, 4H), 4.57 (t, $J = 2.4$ Hz, 1H), 4.49 – 4.38 (m, 2H), 4.38 – 4.24 (m, 4H), 4.14 – 3.96 (m, 6H), 3.96 – 3.88 (m, 1H), 3.88 – 3.76 (m, 4H), 3.72 – 3.51 (m, 7H), 3.48 (t, $J = 3.6$ Hz, 1H), 3.19 (dt, $J = 6.0, 4.0$ Hz, 2H), 1.98 (s, 3H), 1.94 (s, 3H), 1.88 (s, 3H), 1.85 (s, 3H), 1.79 (s, 3H), 8.05 – 7.99 (m, 2H), 7.95 (ddd, $J = 8.5, 3.6, 1.3$ Hz, 4H), 7.92 – 7.85 (m, 2H), 7.63 – 7.55 (m, 1H), 7.51 – 7.41 (m, 8H), 7.36 (ddd, $J = 7.8, 6.7, 1.7$ Hz, 3H), 7.32 (p, $J = 1.5$ Hz, 3H), 7.30 – 7.27 (m, 4H), 7.27 – 7.26 (m, 3H), 7.25 – 7.20 (m, 6H), 7.20 – 7.14 (m, 4H) ^{13}C NMR (101 MHz, Chloroform-*d*) δ 170.50, 137.93, 137.53, 137.18, 133.62, 133.34, 133.08, 130.12, 130.06, 129.97, 129.75, 129.41, 129.29, 128.47, 128.41, 128.34, 128.32, 128.30, 128.25, 128.22, 128.17, 128.09, 128.02, 127.85, 127.80, 127.71, 127.65, 101.00, 100.64, 100.28, 98.35, 76.56, 76.16, 75.91, 74.96, 74.53, 72.91, 72.78, 72.45, 72.38, 72.28, 70.27, 70.17, 68.19, 67.72, 67.64, 67.50, 66.78, 66.04, 65.15, 64.16, 62.71, 62.17, 62.11, 50.72, 20.76, 20.74, 20.61, 20.53, 20.50. HRMS m/z calculated for $\text{C}_{94}\text{H}_{99}\text{N}_3\text{O}_{31}\text{Na}$, 1766.6296; Found 1766.6299.

Ethoxy-2-azidoethoxyl-O-((2,4,6-O-trisulfonato-3-O-benzyl)- α (1 \rightarrow 4)-L-idopyrnosyl-(2,6-O-disulfonato-3-O-benzyl)- α (1 \rightarrow 4)-L-idopyrnosyl-(2,6-O-disulfonato-3-O-benzyl))- α (1 \rightarrow 4)-L-idopyrnosyl-(2,6-O-disulfonato-3-O-benzyl))- α (1 \rightarrow 4)-L-idopyrnoside (21)

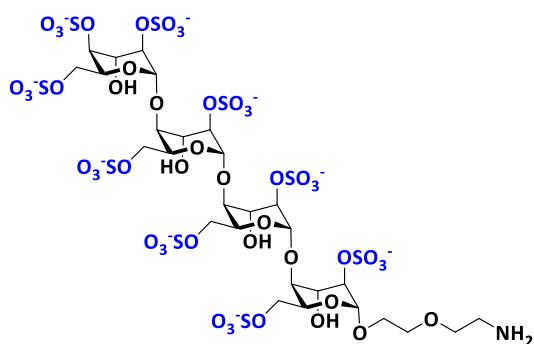


21

Compound **21** was obtained by performing sulfation reaction of compound **18** using synthetic procedure of compound **6** to get 62% yield. ¹H NMR (600 MHz, Deuterium Oxide) 5.08 (s, 1H), 5.01 (d, *J* = 11.5 Hz, 1H), 4.91 (s, 2H), 4.81 – 4.72 (m, 7H), 4.65 (s, 1H), 4.63 – 4.49 (m, 2H), 4.45 – 4.33 (m, 5H), 4.31 (s, 1H),

4.27 – 4.20 (m, 1H), 4.20 – 4.11 (m, 6H), 4.06 (d, *J* = 10.4 Hz, 3H), 4.03 – 3.94 (m, 1H), 3.90 (d, *J* = 10.6 Hz, 1H), 3.74 (d, *J* = 11.7 Hz, 3H), 3.70 (dd, *J* = 2.2, 1.3 Hz, 2H), 3.68 – 3.63 (m, 3H), 3.59 (s, 1H), 3.37 – 3.32 (m, 2H), 7.51 – 7.44 (m, 5H), 7.44 – 7.29 (m, 15H) ¹³C NMR (151 MHz, Deuterium Oxide) δ 137.68, 137.65, 137.61, 136.95, 128.66, 128.62, 128.60, 128.24, 128.11, 100.50, 100.41, 74.31, 73.86, 73.15, 73.02, 72.55, 71.45, 70.96, 70.29, 69.39, 69.29, 68.00, 65.85, 65.41, 55.51, 50.22, 50.17. HRMS *m/z* calculated for C₅₆H₆₄N₃O₄₉S₉⁻⁹, 205.5572; Found 205.5575.

Ethoxy-2-aminoethoxyl-O-((2,4,6-O-trisulfonato)- α (1 \rightarrow 4)-L-idopyrnosyl-(2,6-O-disulfonato)- α (1 \rightarrow 4)-L-idopyrnosyl-(2,6-O-disulfonato))- α (1 \rightarrow 4)-L-idopyrnosyl-(2,6-O-disulfonato))- α (1 \rightarrow 4)-L-idopyrnoside (ID49)



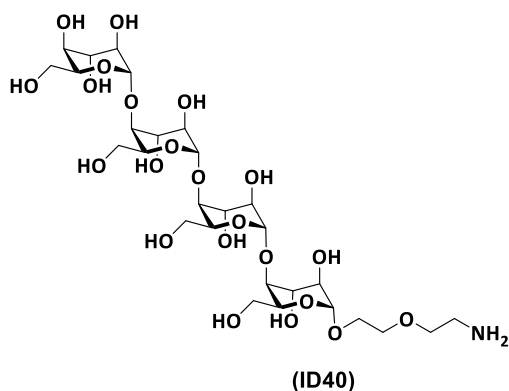
(ID49)

Compound (**ID49**) was obtained by doing hydrogenolysis reaction of compound **21** using synthetic procedure of compound (**ID13**) to get 83% yield. ¹H NMR (600 MHz, Deuterium Oxide) 5.07 (d, *J* = 10.6 Hz, 4H), 4.63 (t, *J* = 7.6 Hz, 2H), 4.50 – 4.40 (m, 1H), 4.34 – 4.15 (m,

17H), 3.86 (qd, *J* = 12.1, 10.8, 5.8 Hz, 5H), 3.77 – 3.68 (m, 5H), 3.15 (t, *J* = 5.1 Hz, 2H) ¹³C NMR (151 MHz, Deuterium Oxide) δ 100.35, 99.98, 98.56, 76.15, 75.92, 75.80, 74.92, 73.40, 72.70, 72.65, 71.88, 69.64, 68.13, 67.65, 67.52, 67.38, 67.00, 66.52, 66.22, 66.11,

65.66, 65.17, 64.20, 39.17. HRMS m/z calculated for $C_{28}H_{42}NO_{49}S_9^{-9}$, 162.6485; Found 162.6487.

Ethoxy-2-aminoethoxyl-O-((2,3,4,6-anhydro)- α (1 \rightarrow 4)-L-idopyrnosyl-(2,3,6-anhydro))- α (1 \rightarrow 4)-L-idopyrnosyl-(2,3,6-anhydro))- α (1 \rightarrow 4)-L-idopyrnosyl-(2,3,6-anhydro))- α (1 \rightarrow 4)-L-idopyrnoside (ID40)



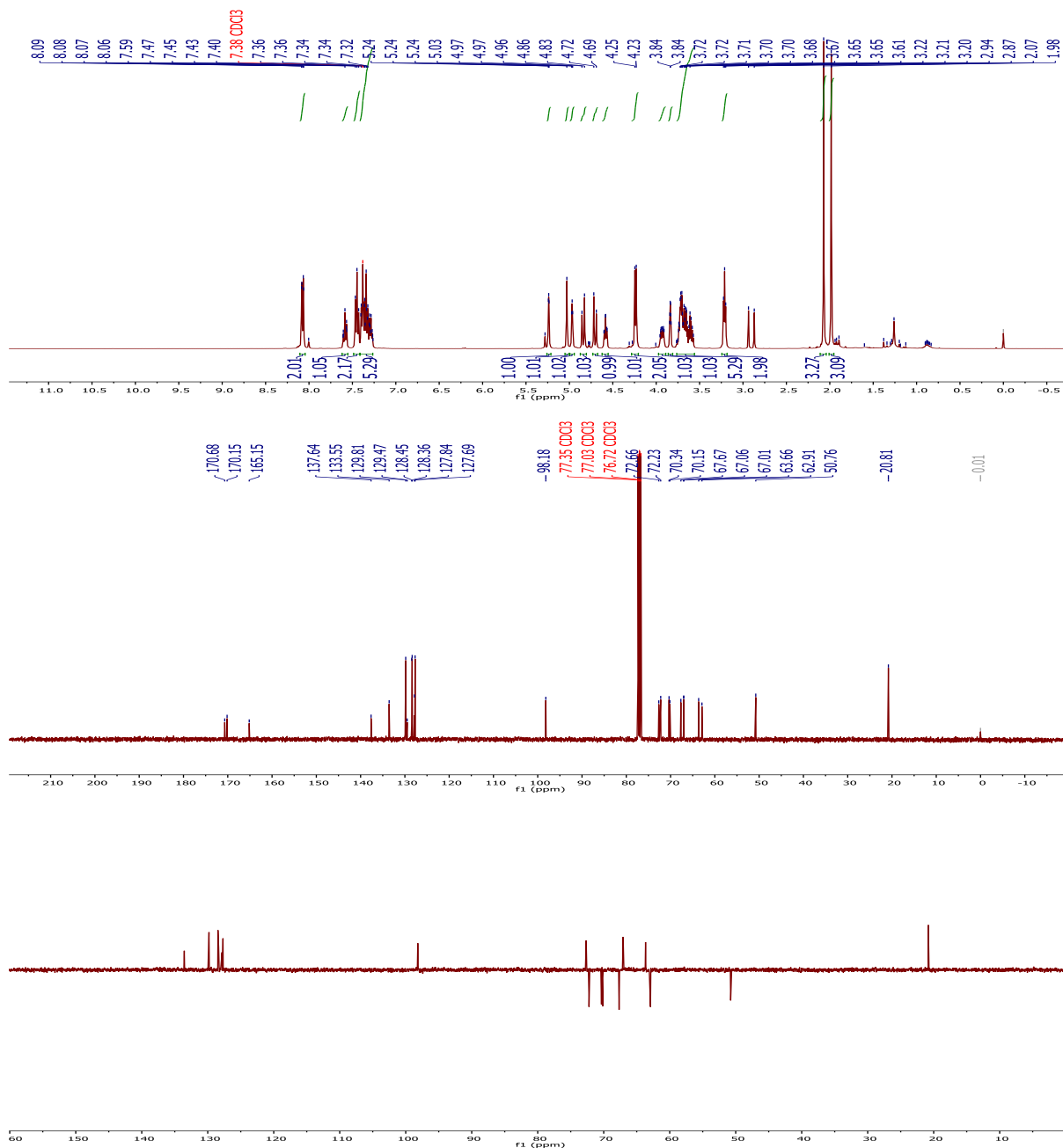
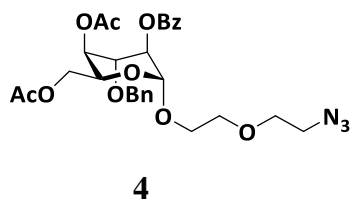
Compound (ID40) was obtained by doing hydrogenolysis reaction of compound **18** using synthetic procedure of compound (ID10) to get 83% yield. ¹H NMR (600 MHz, Deuterium Oxide) 4.85 – 4.73 (m, 4H), 4.26 (dt, $J = 7.5, 3.9$ Hz, 2H), 4.15 (tt, $J = 7.9, 4.1$ Hz, 2H), 3.90 (dt, $J = 17.7, 5.6$ Hz, 4H), 3.73 (dddt, $J = 38.7, 29.0, 17.9, 5.5$ Hz, 21H), 3.62 – 3.47 (m, 5H), 3.13 (t, $J = 5.1$ Hz, 2H) ¹³C NMR (151 MHz, Deuterium Oxide) δ 101.66, 101.40, 100.35, 77.44, 77.31, 71.23, 70.30, 70.09, 69.97, 69.78, 69.68, 69.63, 69.57, 67.52, 66.34, 59.95, 59.91, 59.73, 39.04. HRMS m/z calculated for $C_{28}H_{51}NO_{22}Na$, 753.2903; Found 753.2905.

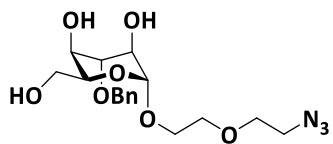
5.5 Reference

1. Varki, A.; Cummings, R. D.; Esko, J. D.; et al., Editors. *Essentials of Glycobiology*
2. Westling, C.; Lindahl, U. Location of N-Unsubstituted Glucosamine Residues in Heparan Sulfate. *J. Biol. Chem.* **2002**, 277 (51), 49247-49255.
3. Capila, I.; Linhardt, R. J. Heparin-Protein Interactions. *Angew. Chem., Int. Ed.* **2002**, 41 (3), 390-412.
4. Fisher, J.; Linder, A. Heparin-Binding Protein: A Key Player in the Pathophysiology of Organ Dysfunction in Sepsis. *J. Intern. Med.* **2017**, 281 (6), 562-574.

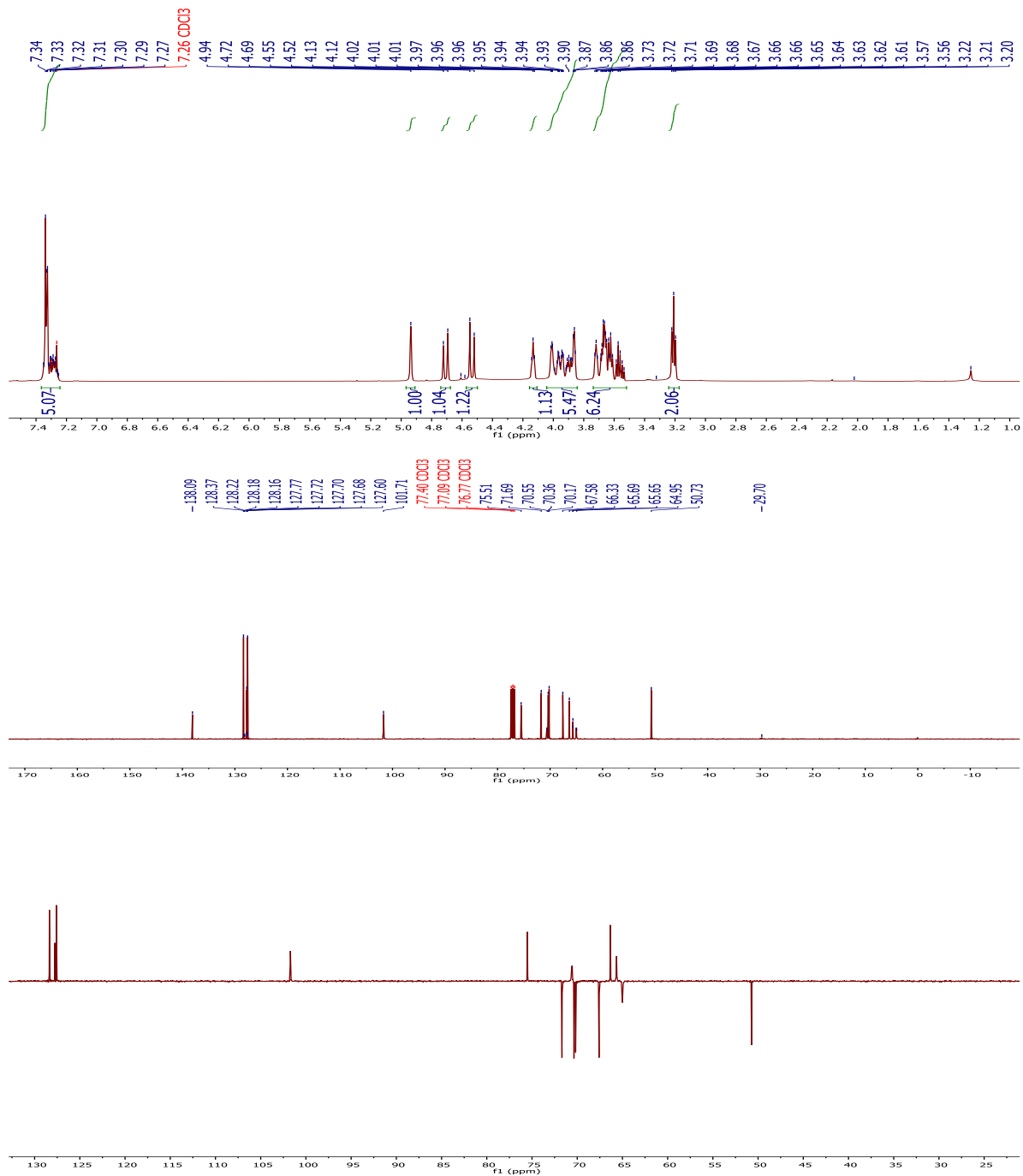
5. Noti, C.; Seeberger, P. H. Chemical Approaches to Define the Structure-Activity Relationship of Heparin-Like Glycosaminoglycans. *Chem. Biol.***2005**, *12* (7), 731-756.
6. Xu, D.; Arnold, K.; Liu, J. Using Structurally Defined Oligosaccharides to Understand the Interactions Between Proteins and Heparan Sulfate. *Curr. Opin. Struct. Biol.***2018**, *50*, 155-161.
7. Arungundram, S.; Al-Mafraji, K.; Asong, J.; Leach, F. E., III; Amster, I. J.; Venot, A.; Turnbull, J. E.; Boons, G. J. Modular Synthesis of Heparan Sulfate Oligosaccharides for Structure–Activity Relationship Studies. *J. Am. Chem. Soc.***2009**, *131* (47), 17394-17405.
8. Zhang, J.; Liang, L.; Yang, W.; Ramadan, S.; Baryal, K.; Huo, C. X.; Bernard, J. J.; Liu, J.; Hsieh-Wilson, L.; Zhang, F.; Linhardt, R. J. Expedient Synthesis of a Library of Heparan Sulfate-Like “Head-to-Tail” Linked Multimers for Structure and Activity Relationship Studies. *Angew. Chem., Int. Ed.***2022**, *61* (48), e202209730.
9. Abdelfadiel, E. I.; Gunta, R.; Villuri, B. K.; Afosah, D. K.; Sankaranarayanan, N. V.; Desai, U. R. Designing Smaller, Synthetic, Functional Mimetics of Sulfated Glycosaminoglycans as Allosteric Modulators of Coagulation Factors. *J. Med. Chem.***2023**, *66* (7), 4503-4531.
10. Shanthamurthy, C. D.; Leviatan Ben-Arye, S.; Kumar, N. V.; Yehuda, S.; Amon, R.; Woods, R. J.; Padler-Karavani, V.; Kikkeri, R. Heparan Sulfate Mimetics Differentially Affect Homologous Chemokines and Attenuate Cancer Development. *J. Med. Chem.***2021**, *64* (6), 3367-3380.
11. Chhabra, M.; Shanthamurthy, C. D.; Kumar, N. V.; Mardhekar, S.; Vishweshwara, S. S.; Wimmer, N.; Modhiran, N.; Watterson, D.; Amarilla, A. A.; Cha, J. S.; Beckett, J. R.; De Voss, J. J.; Kayal, Y.; Vlodaysky, I.; Dorsett, L. R.; Smith, R. A. A.; Gandhi, N. S.; Kikkeri, R.; Ferro, V.; Amphiphilic Heparinoids as Potent Antiviral Agents Against SARS-CoV-2. *J. Med. Chem.***2024**, *67* (16)

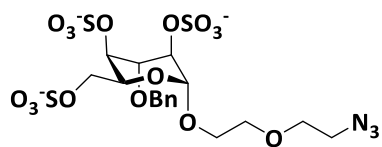
5.6 NMR :



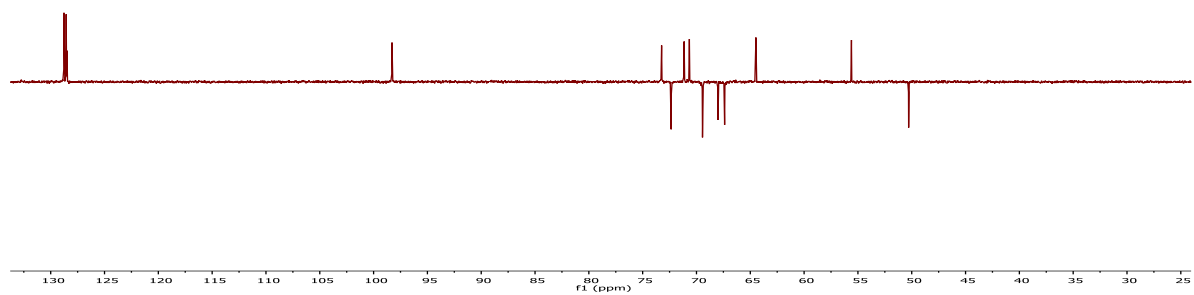
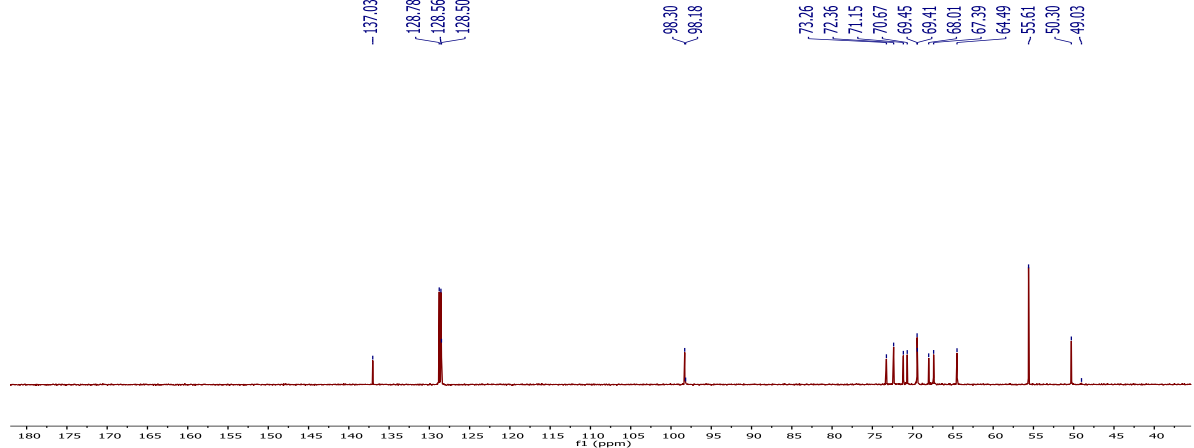
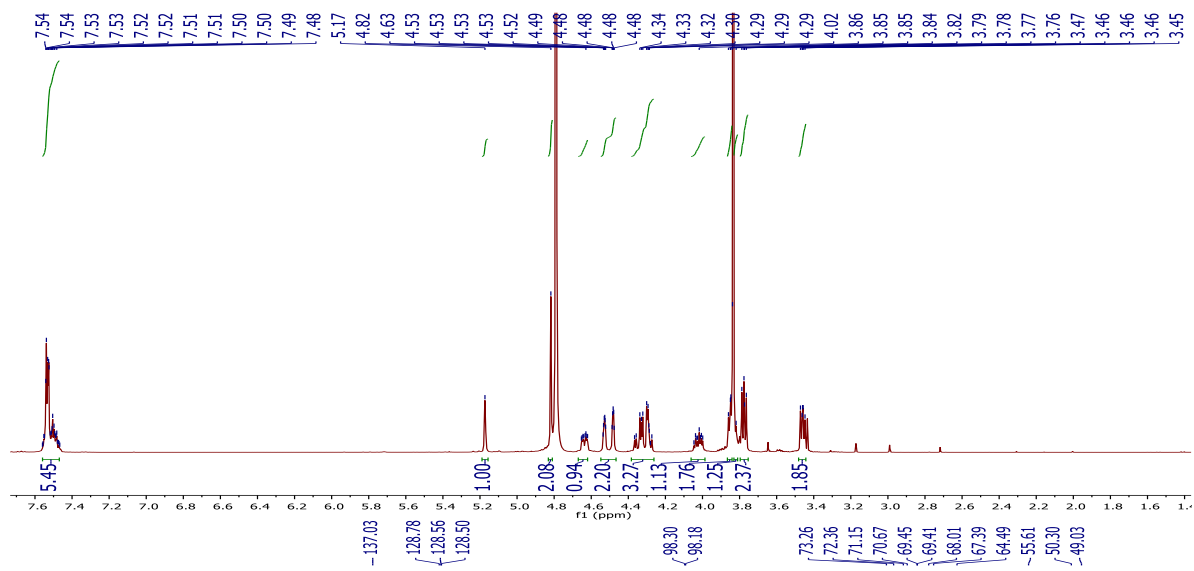


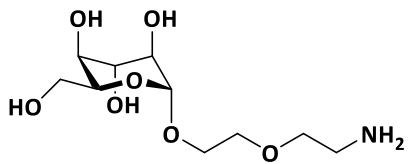
5



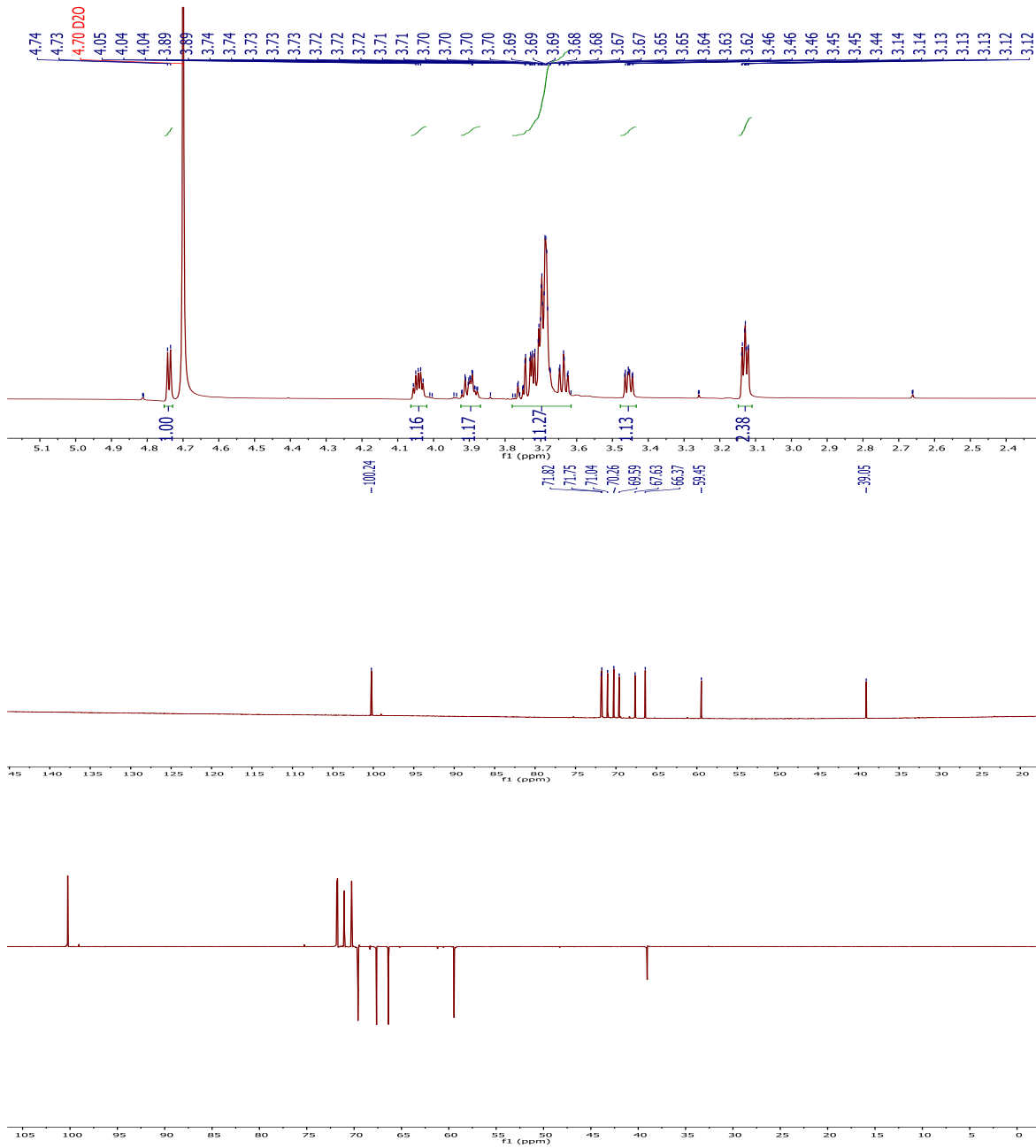


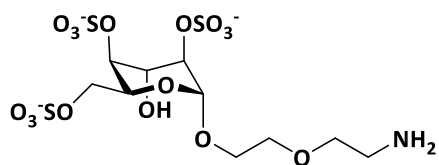
6



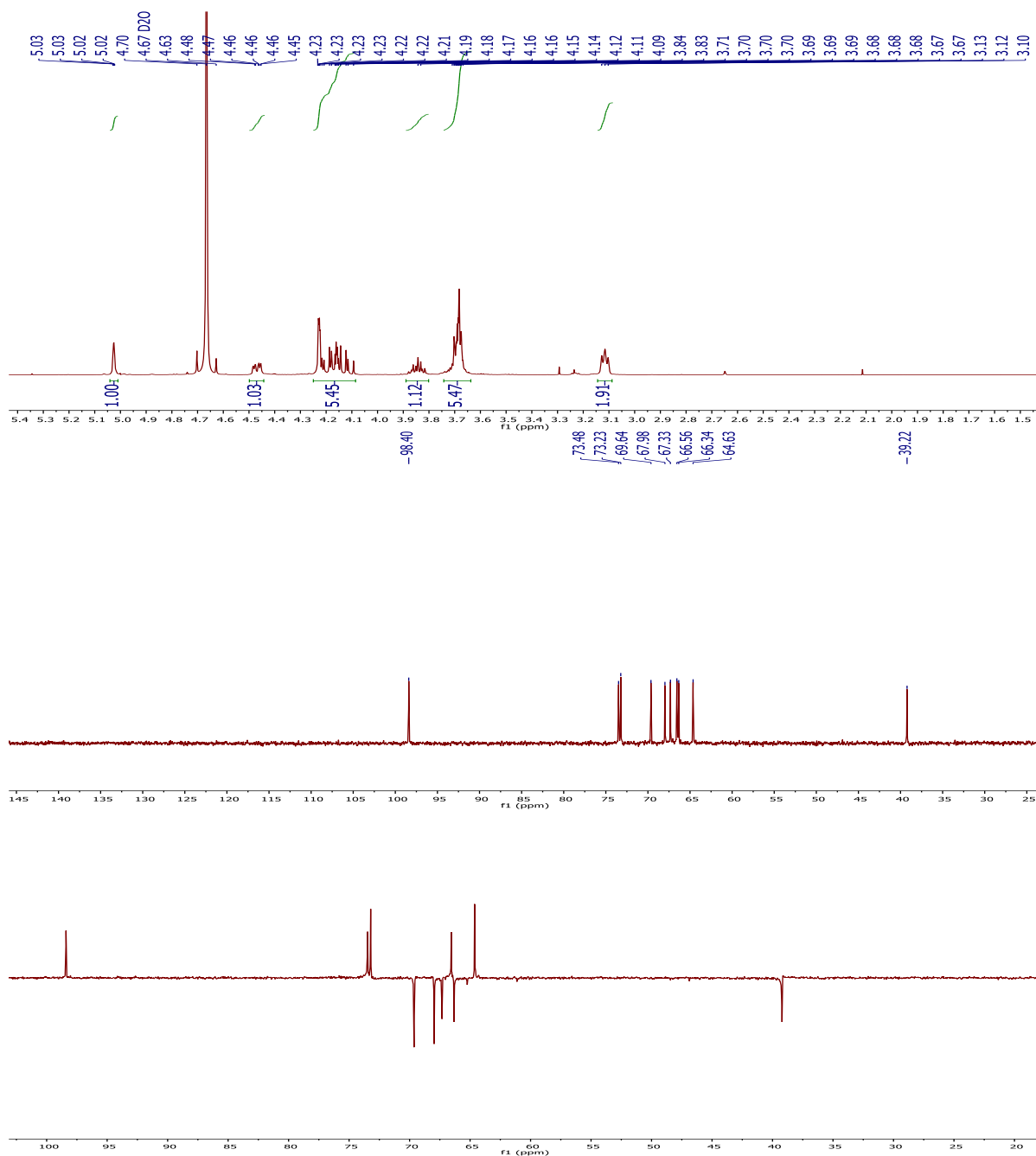


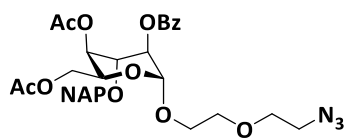
(ID10)



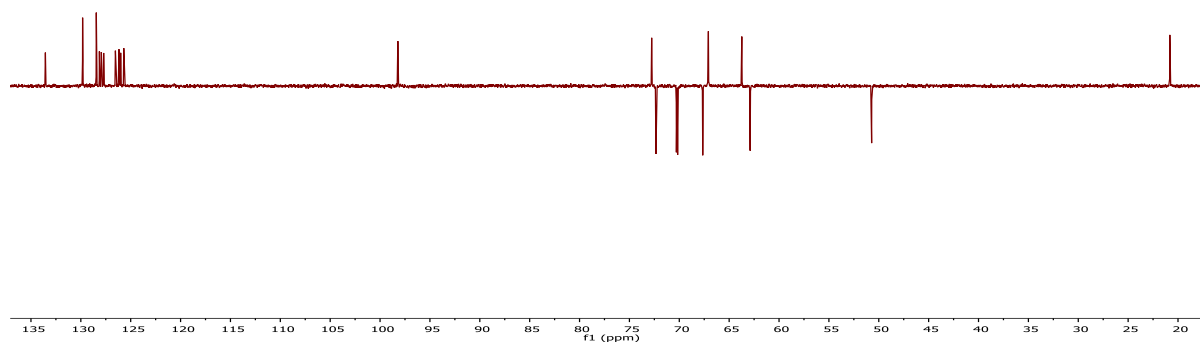
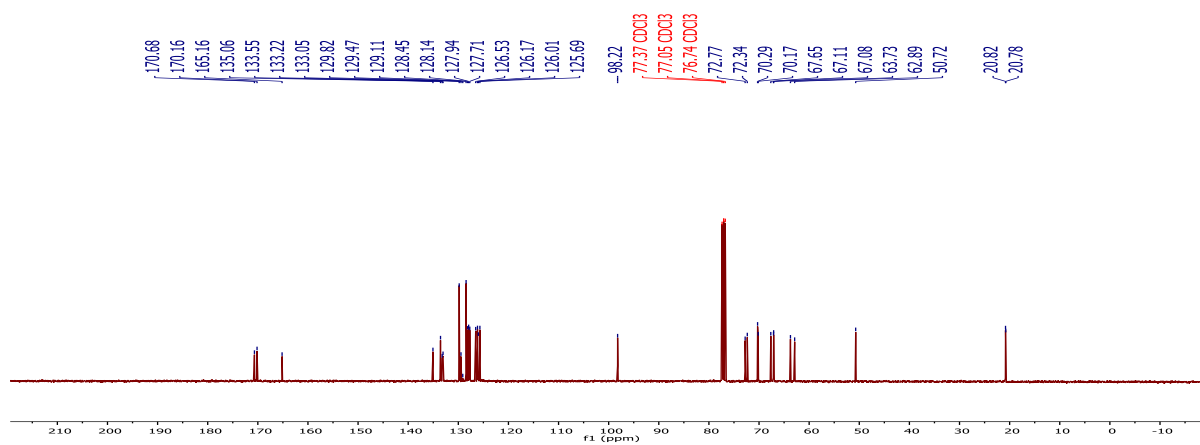
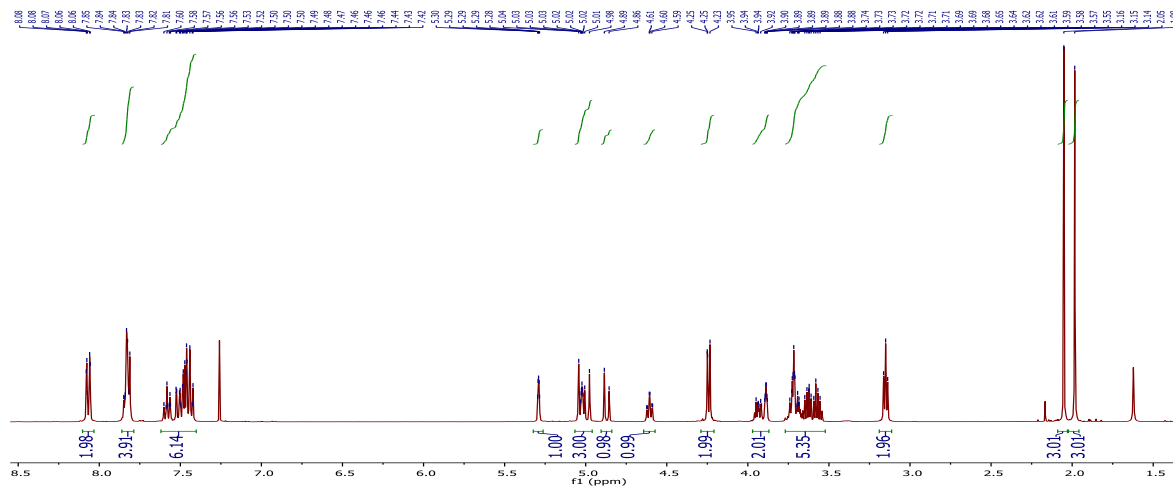


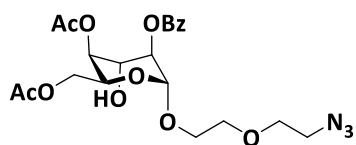
(ID13)



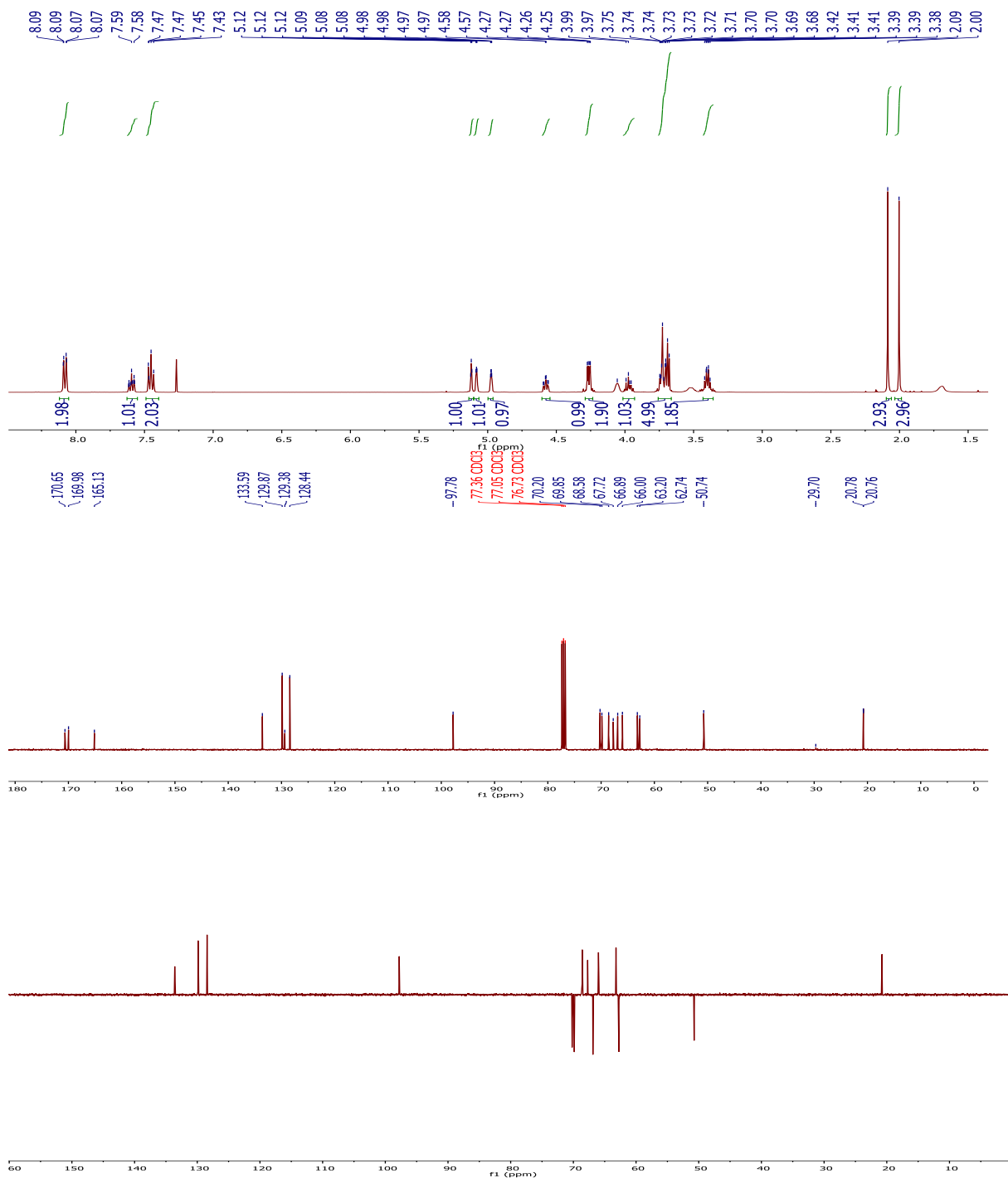


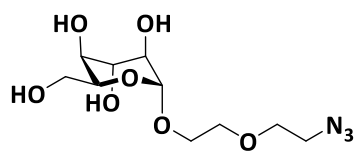
4a



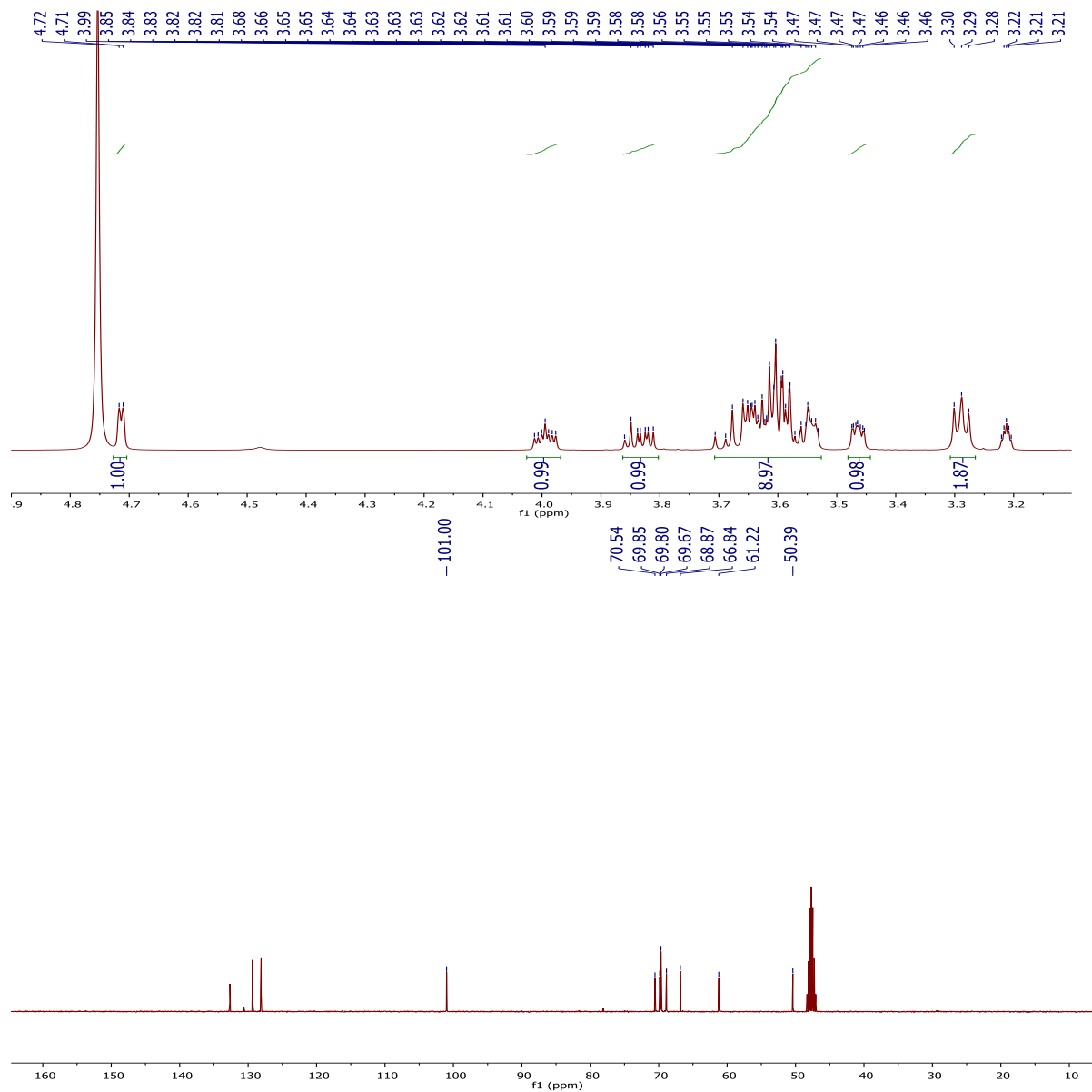


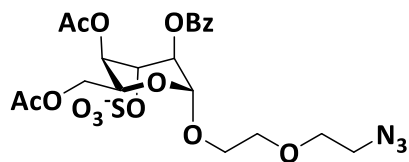
5a



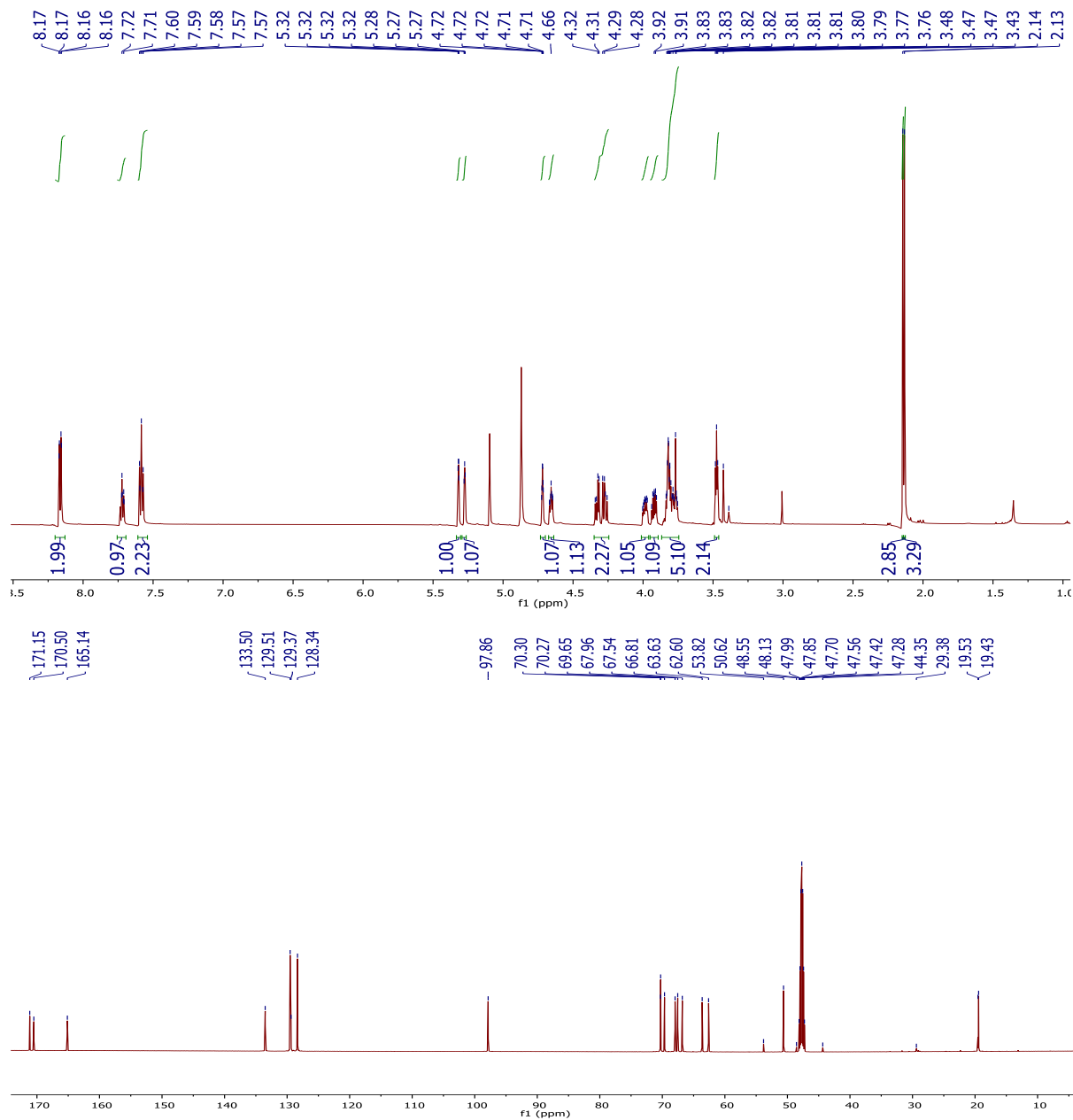


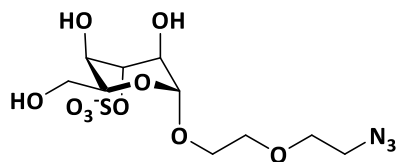
6a



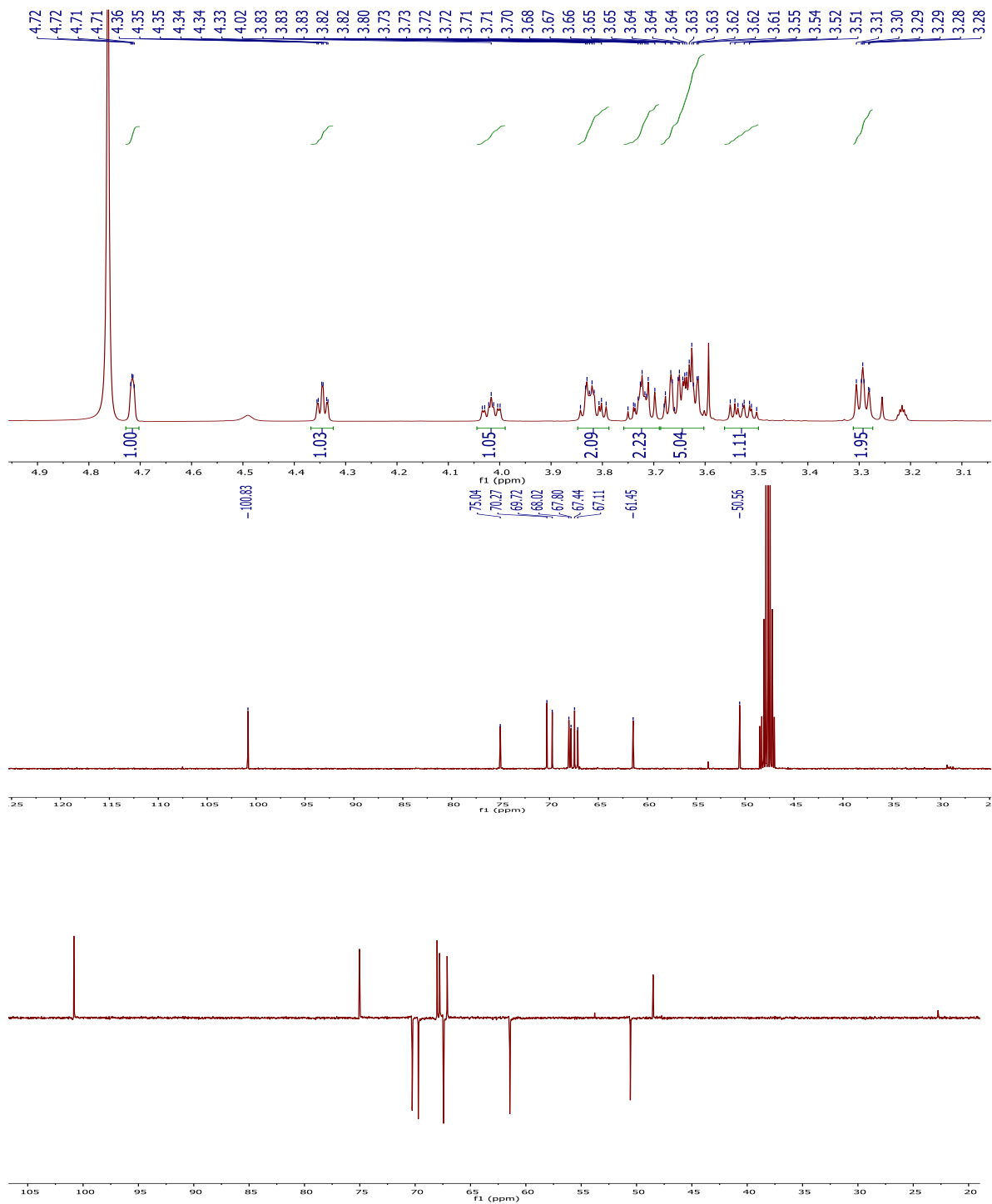


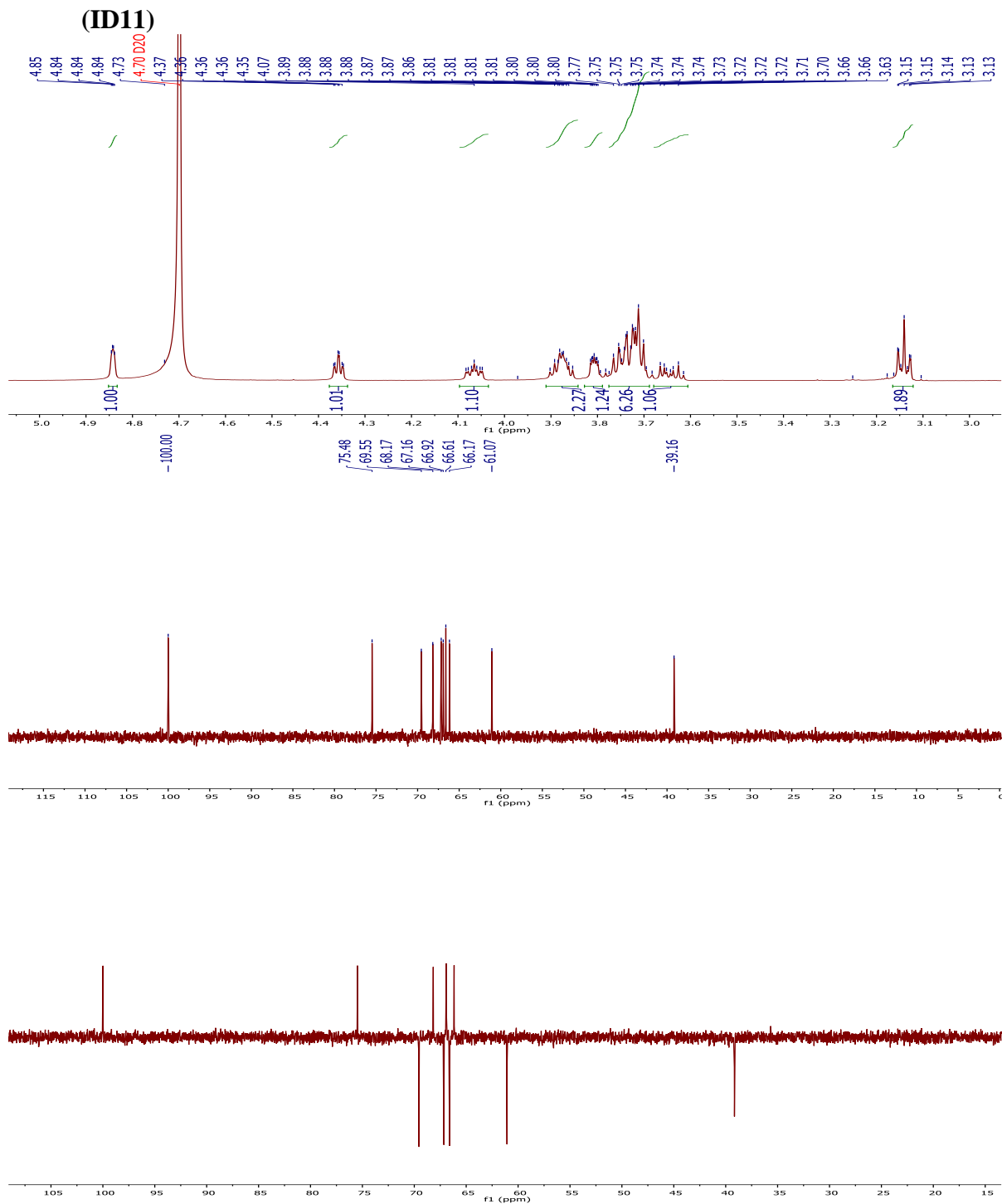
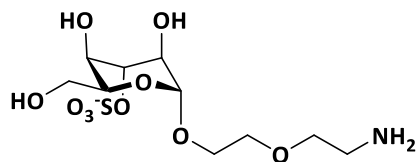
8a

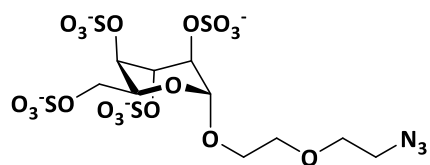




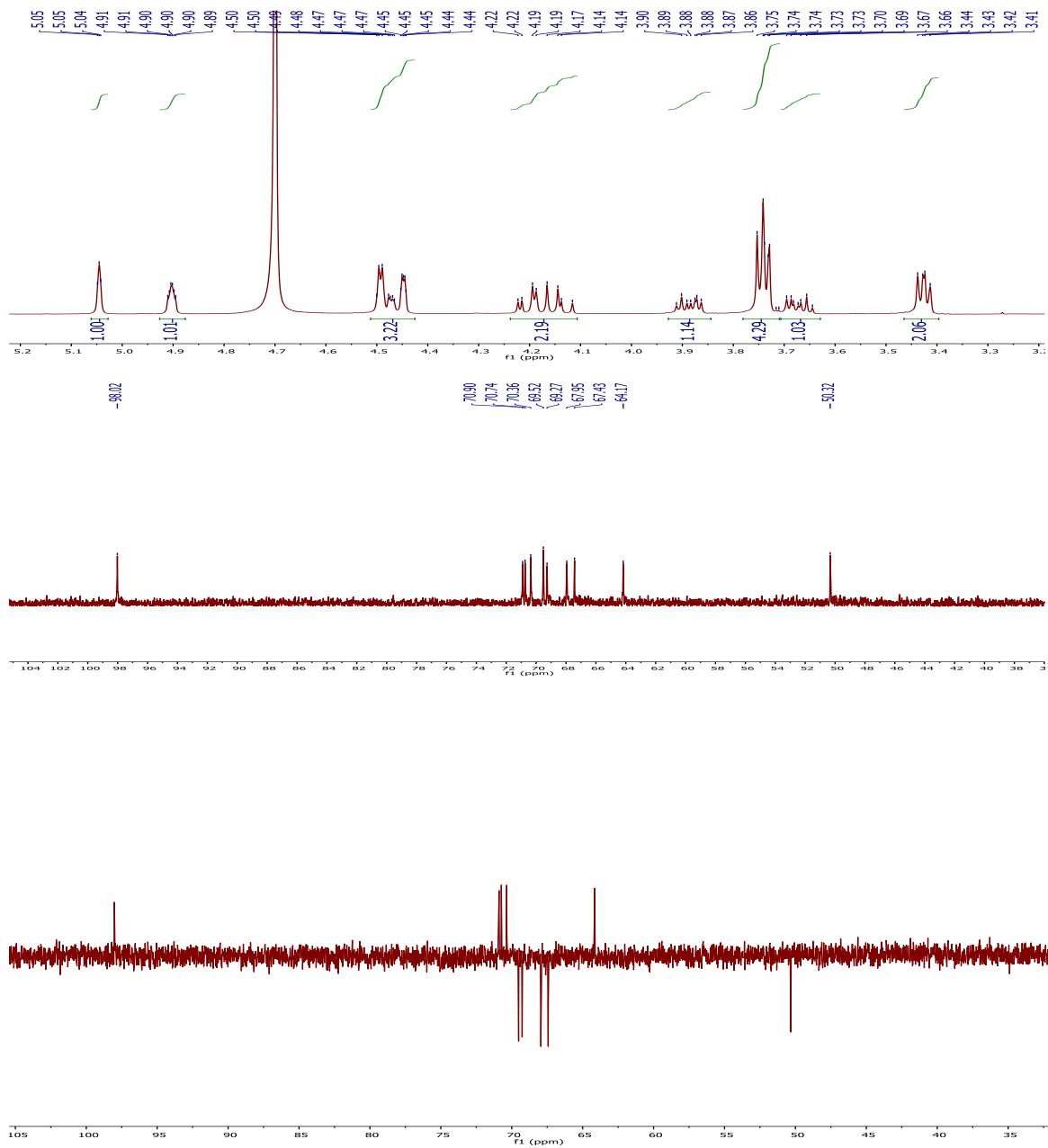
9a

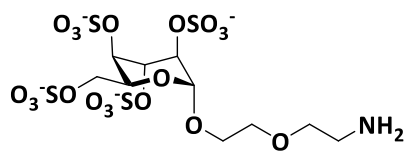




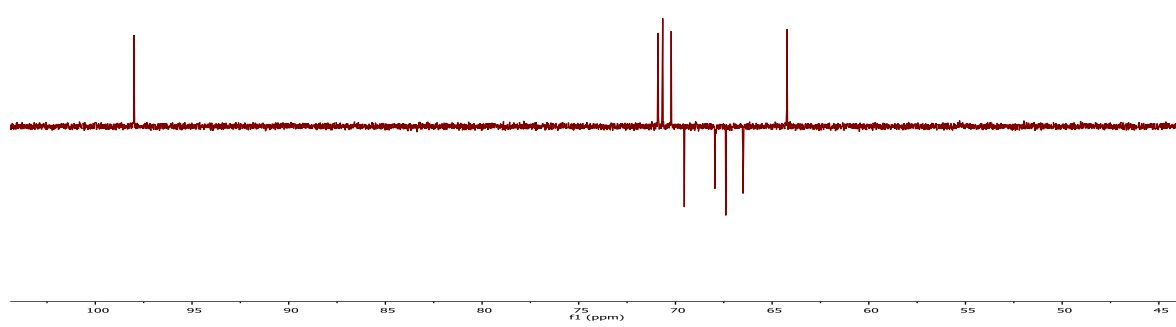
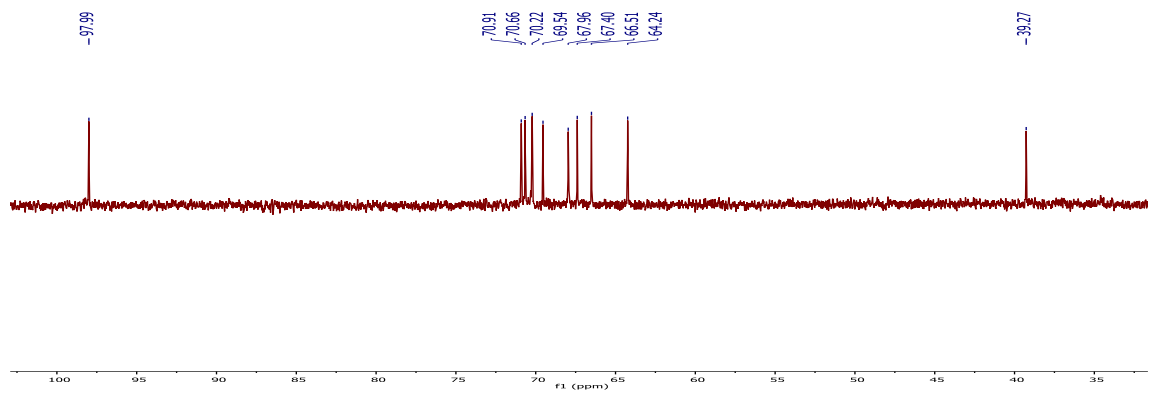
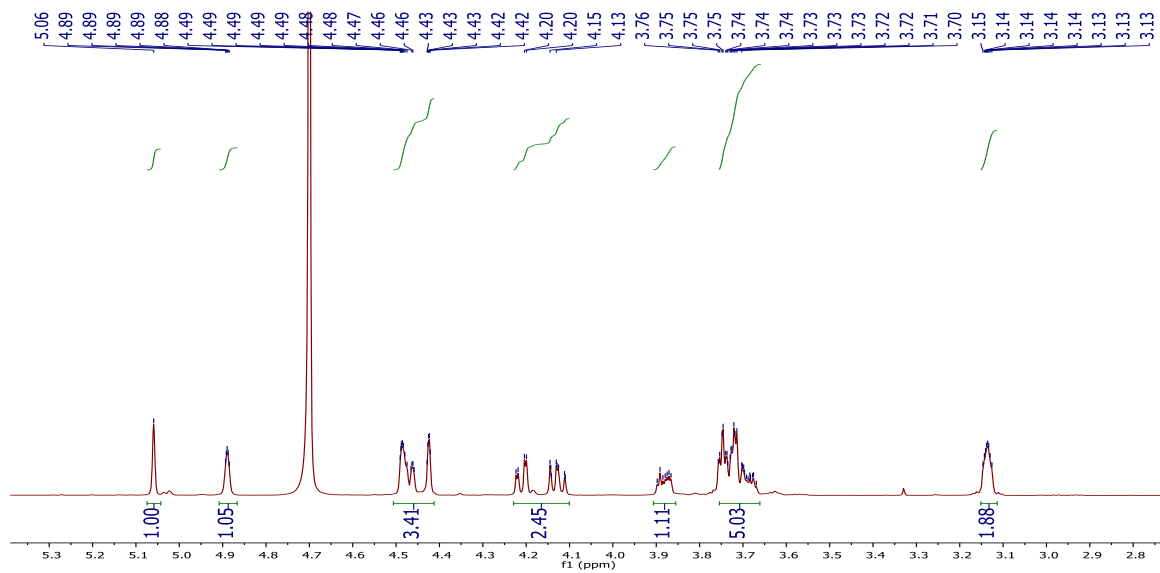


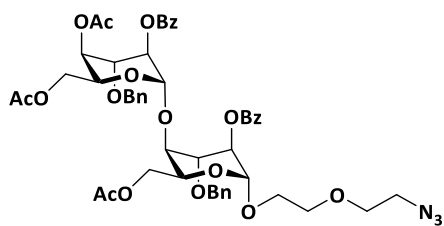
7a



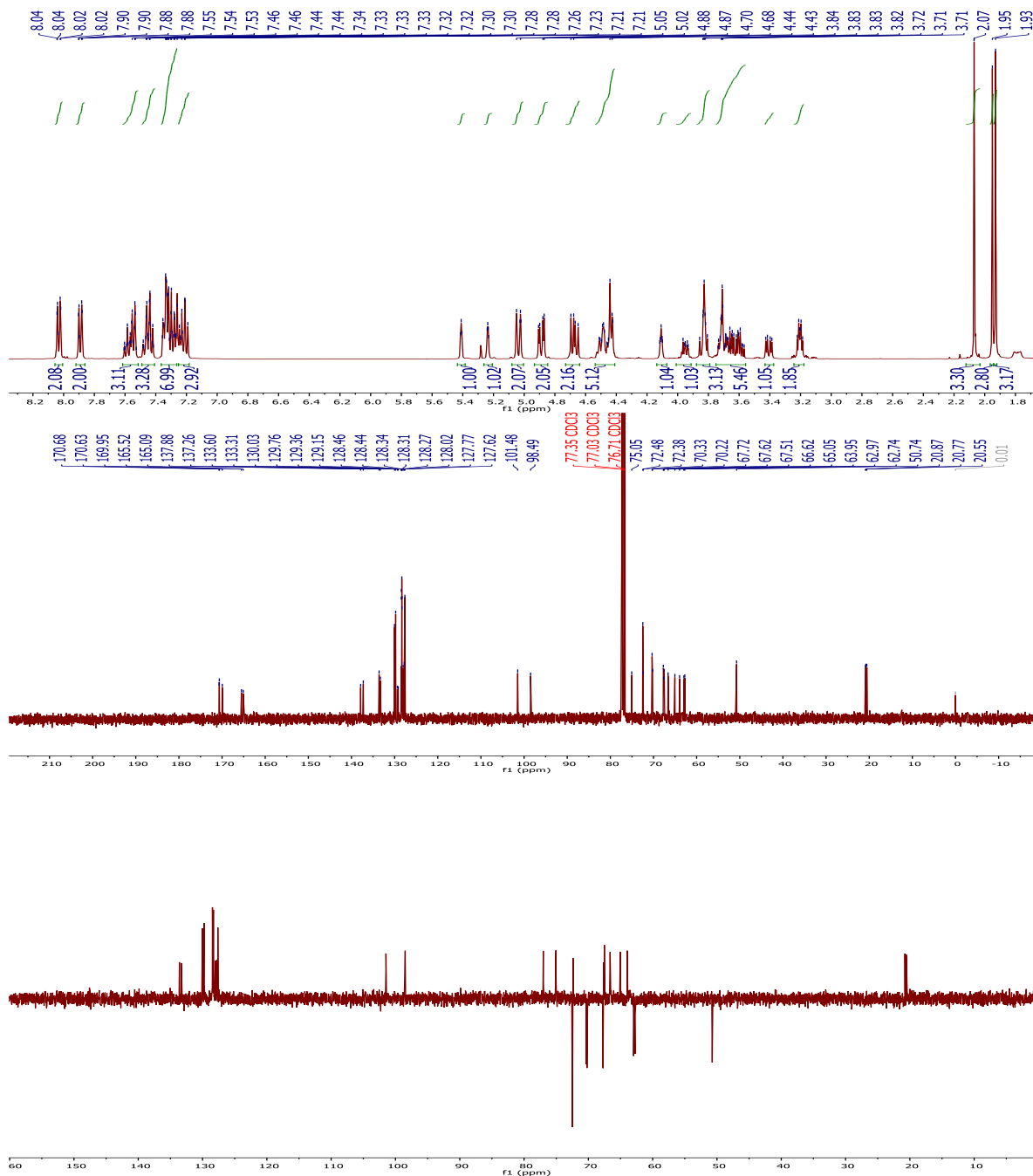


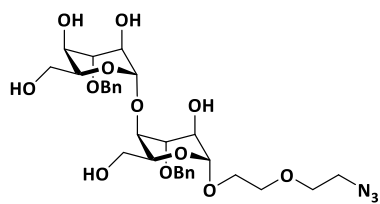
(ID14)



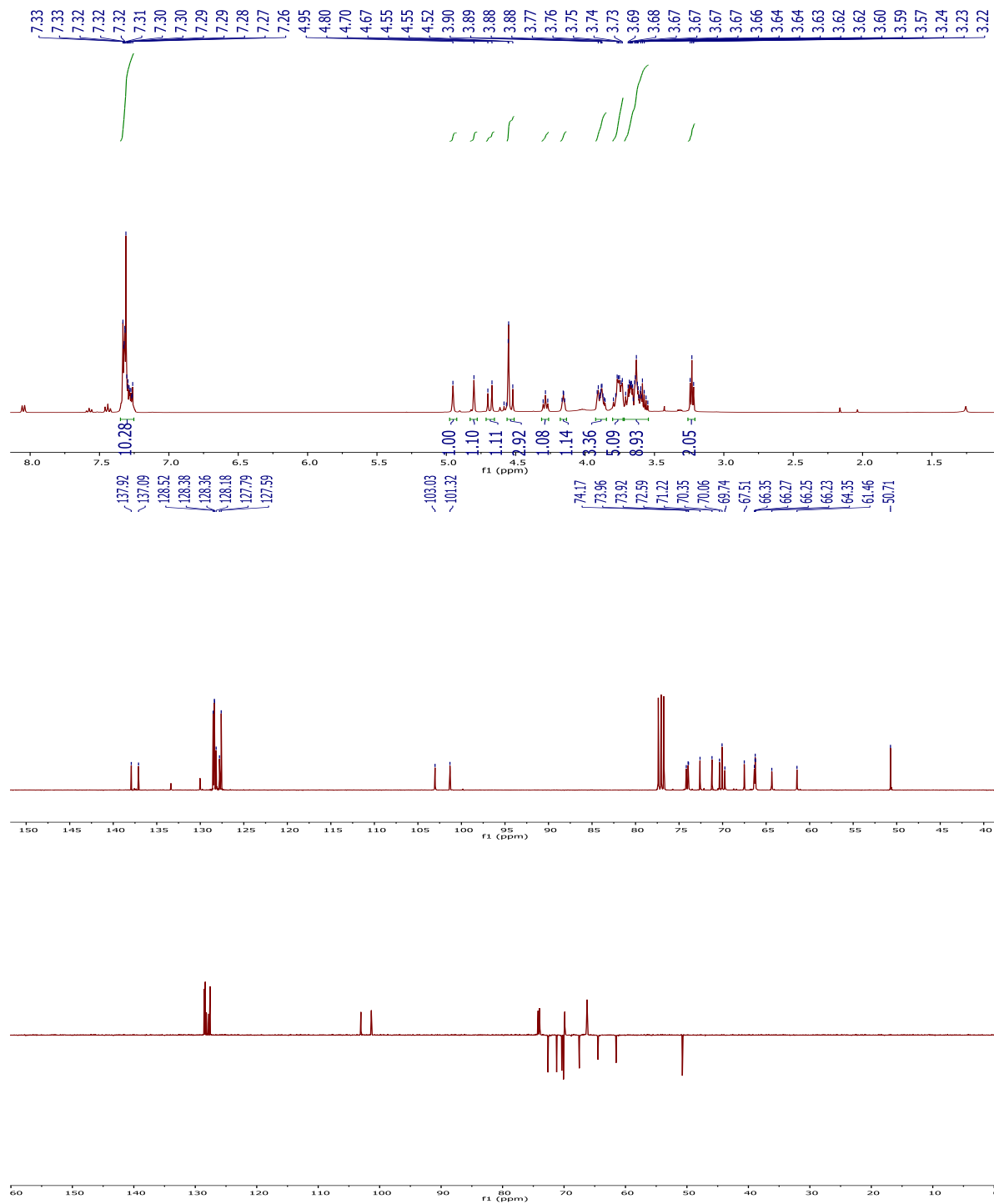


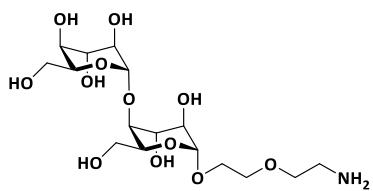
13



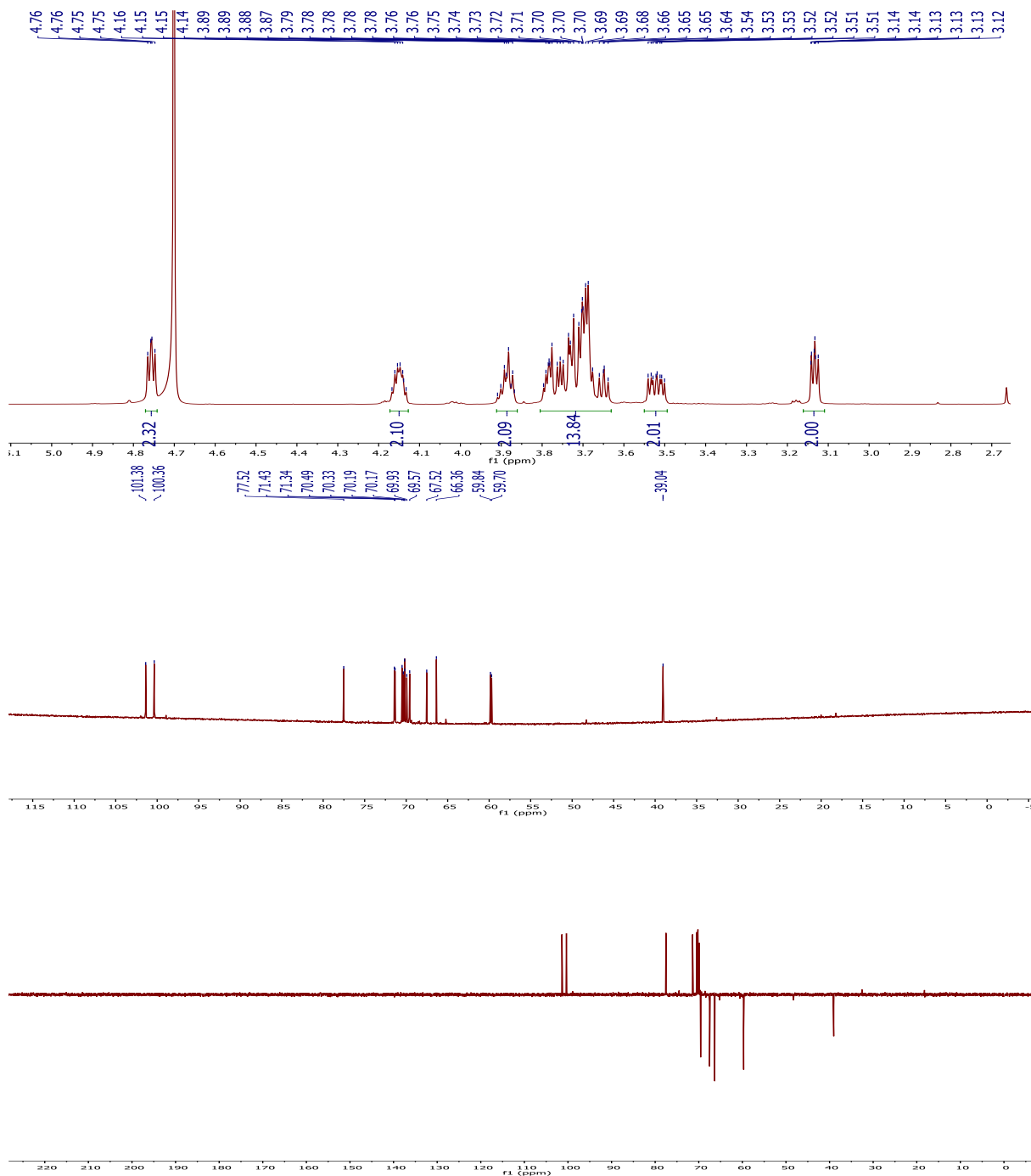


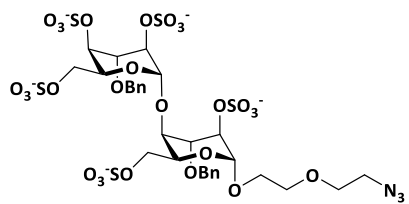
13



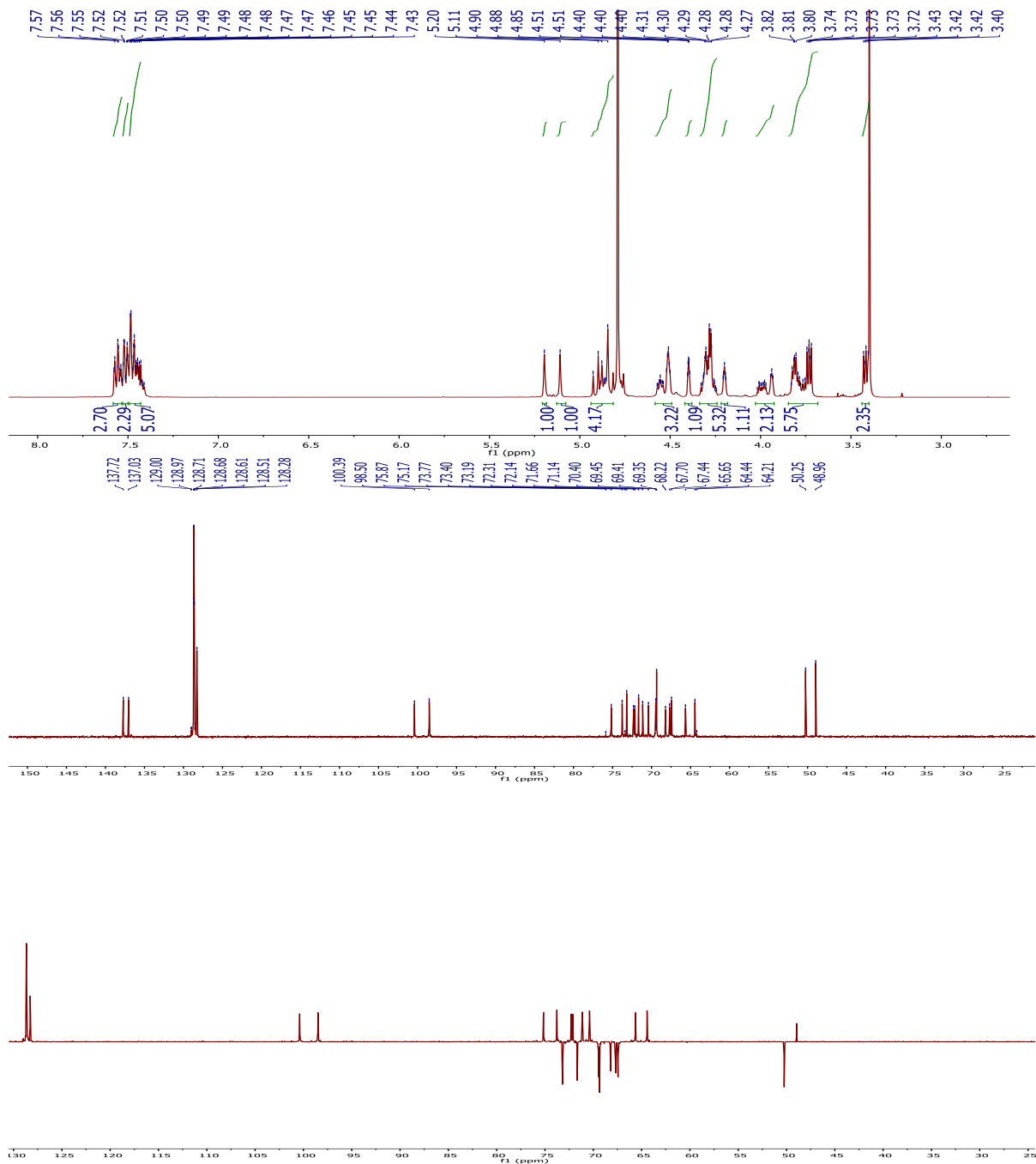


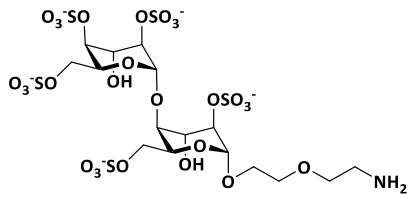
(ID20)



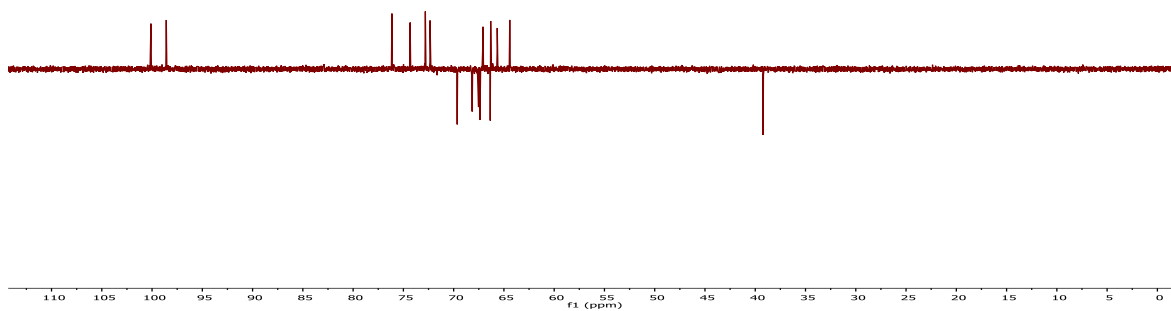
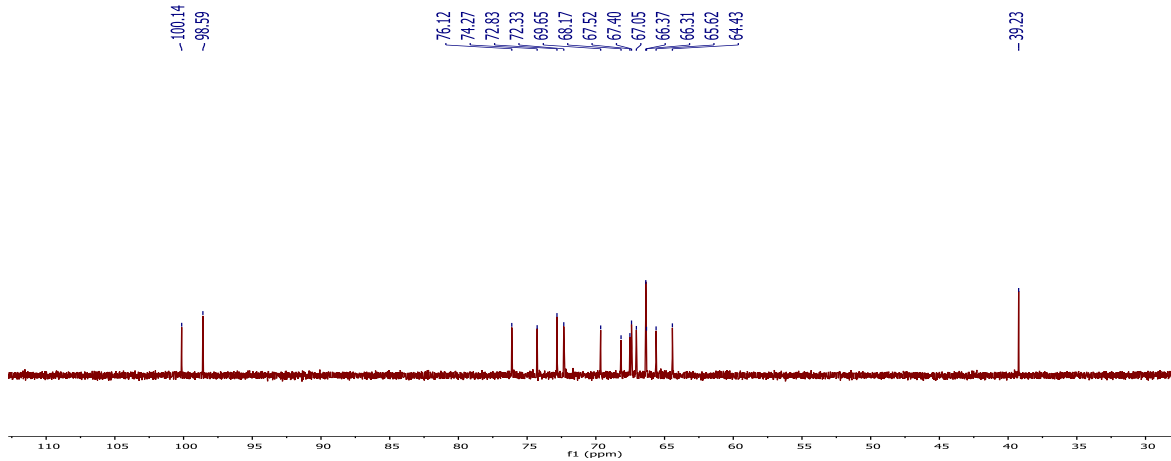
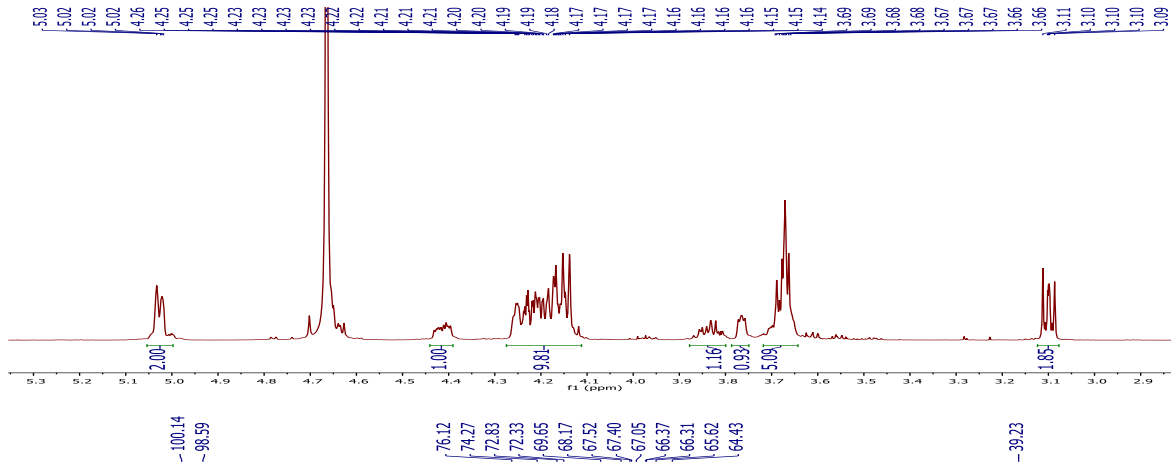


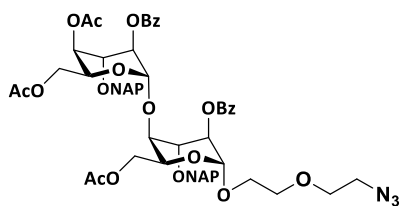
19



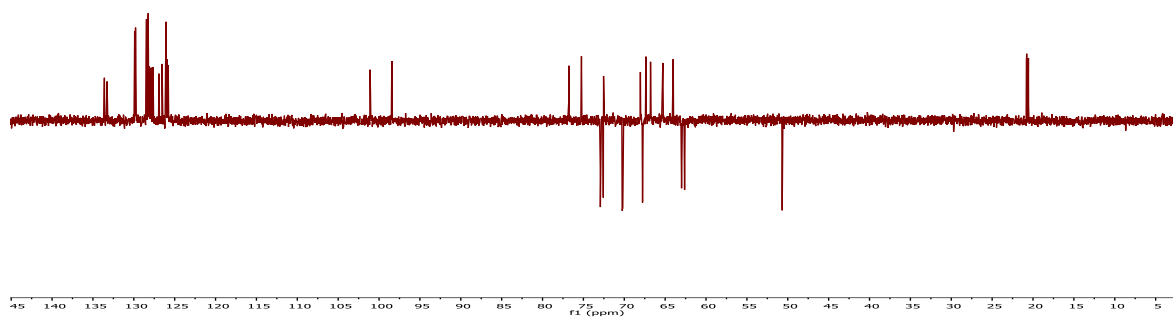
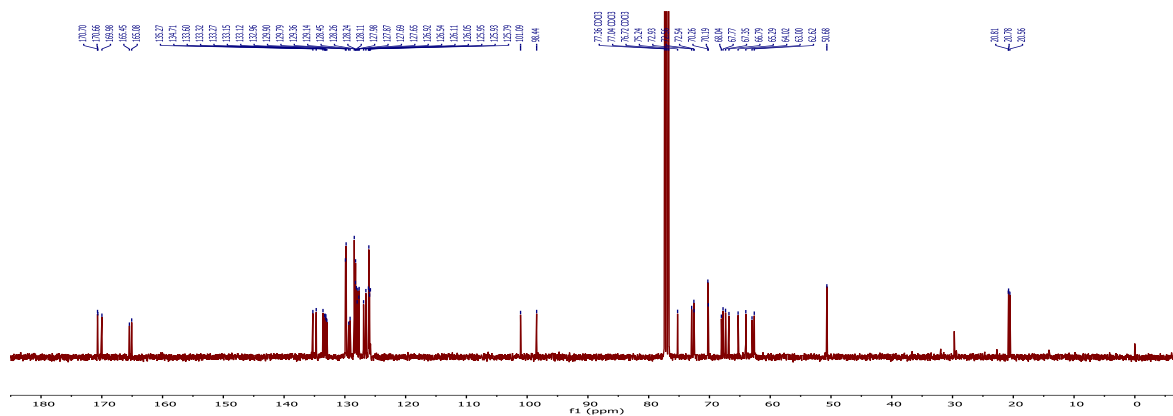
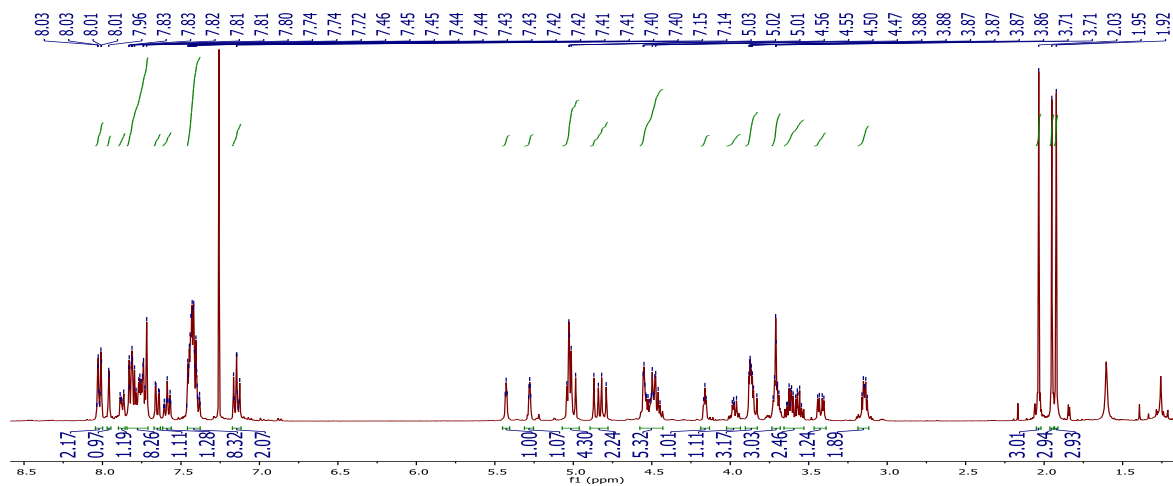


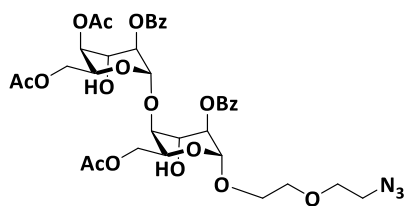
(ID25)



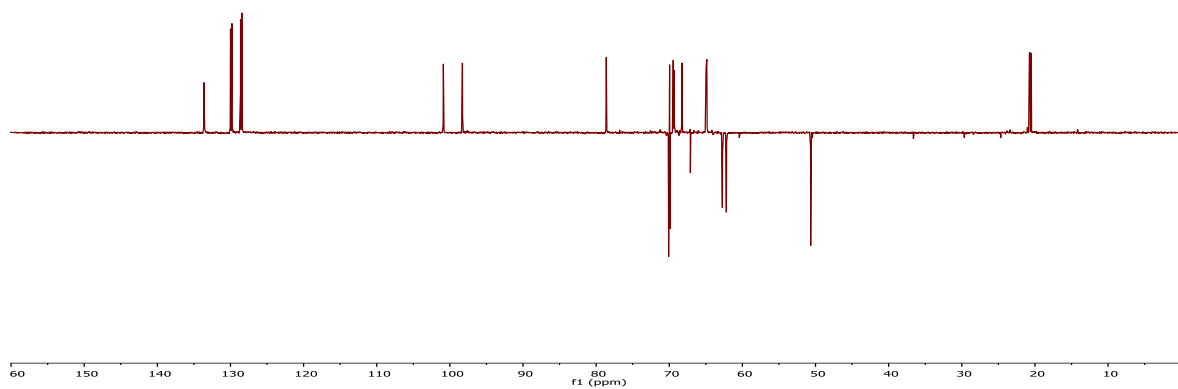
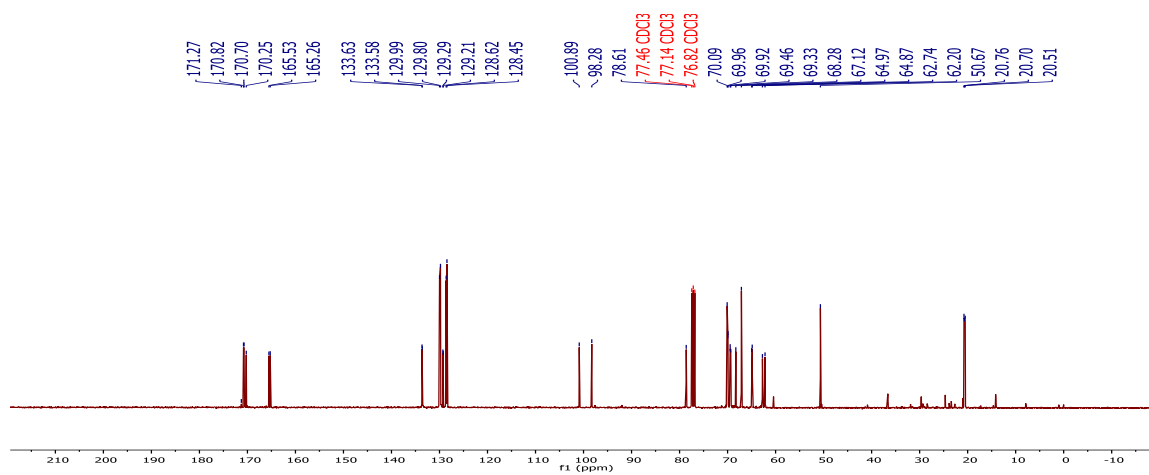
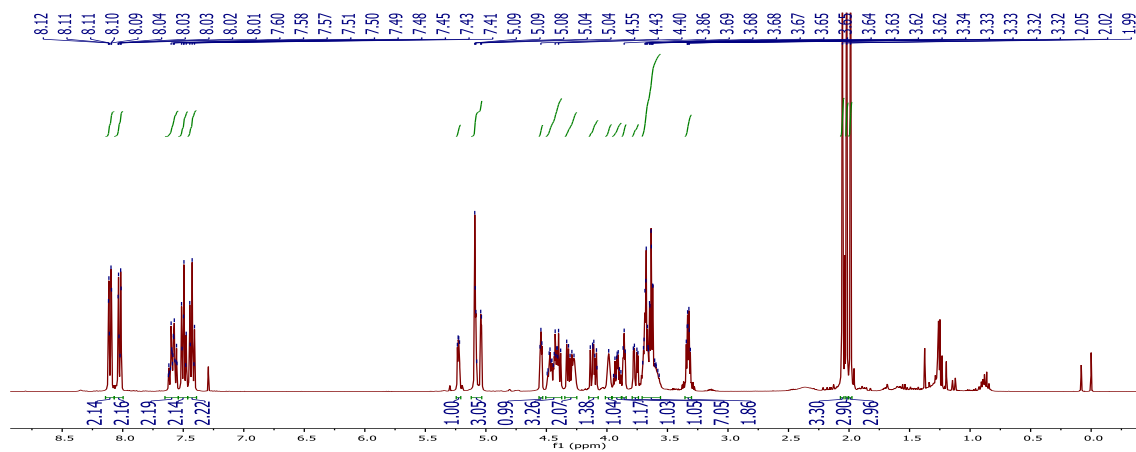


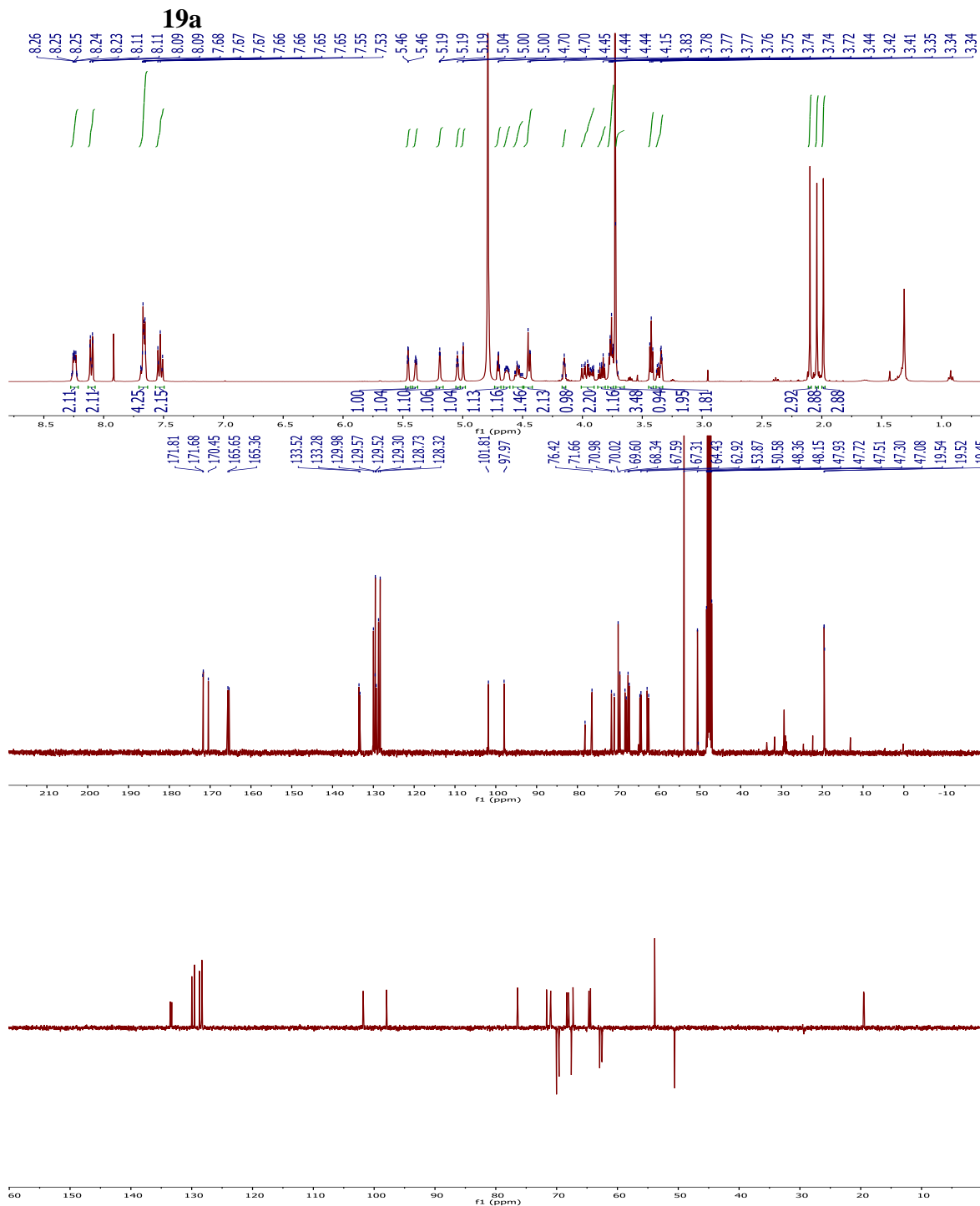
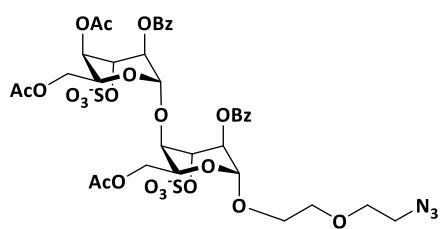
13a

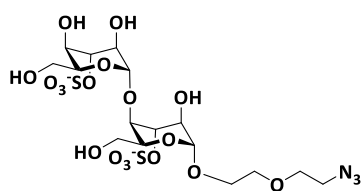




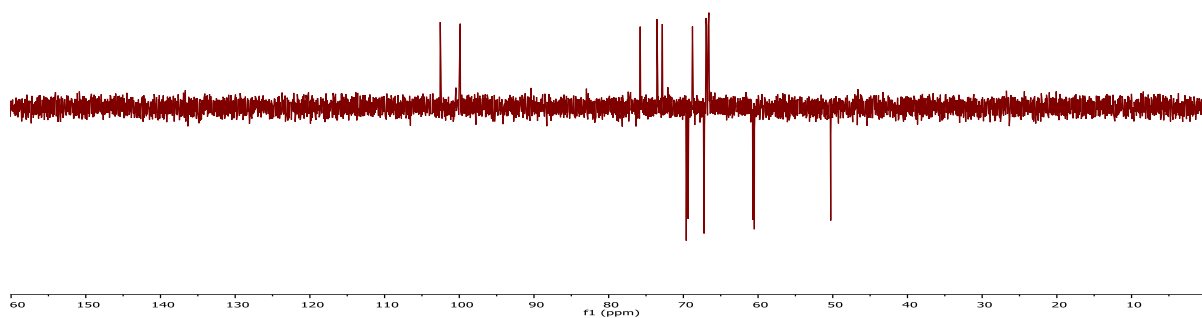
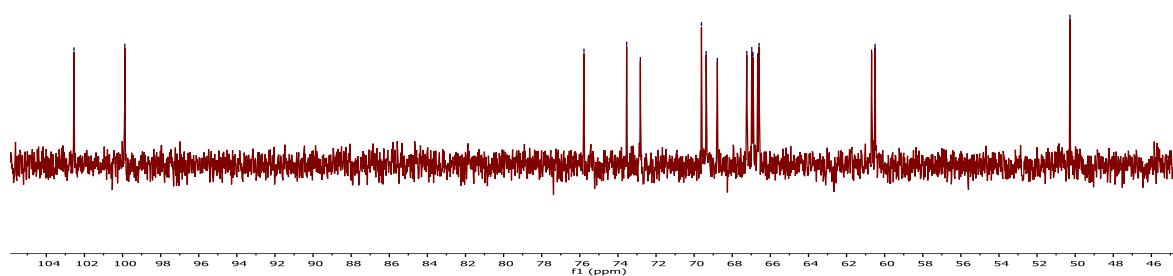
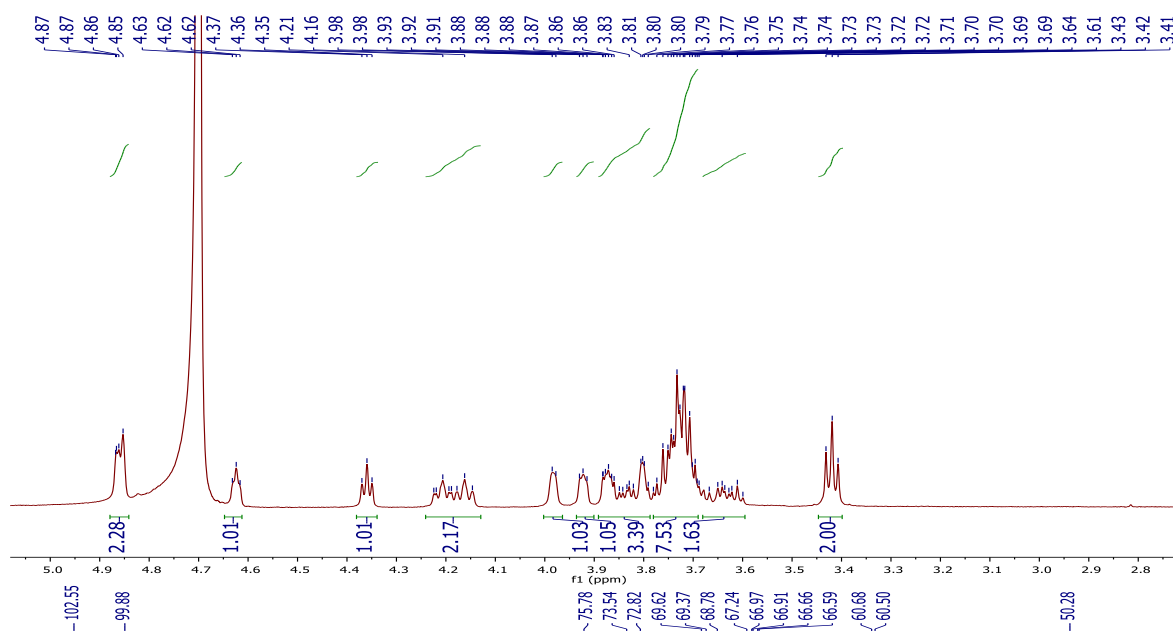
16a

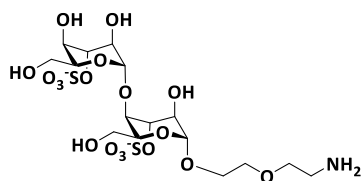




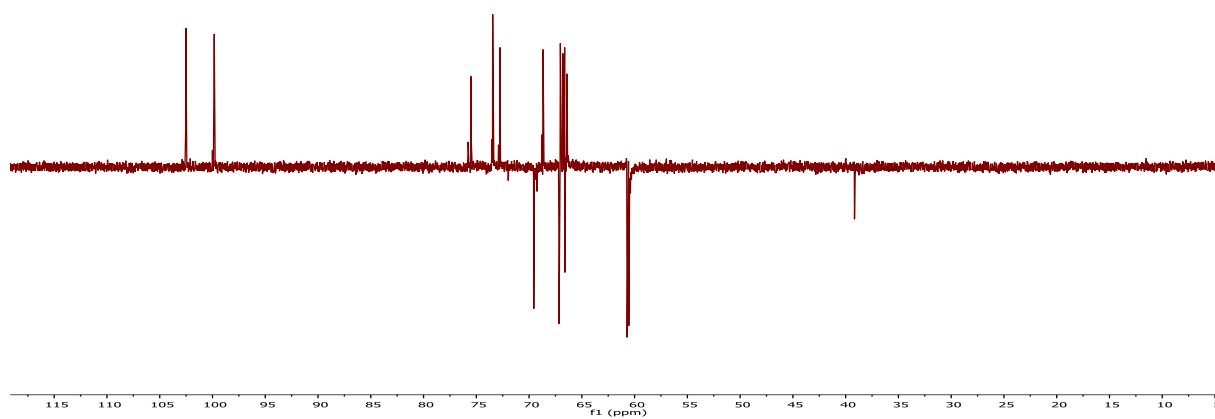
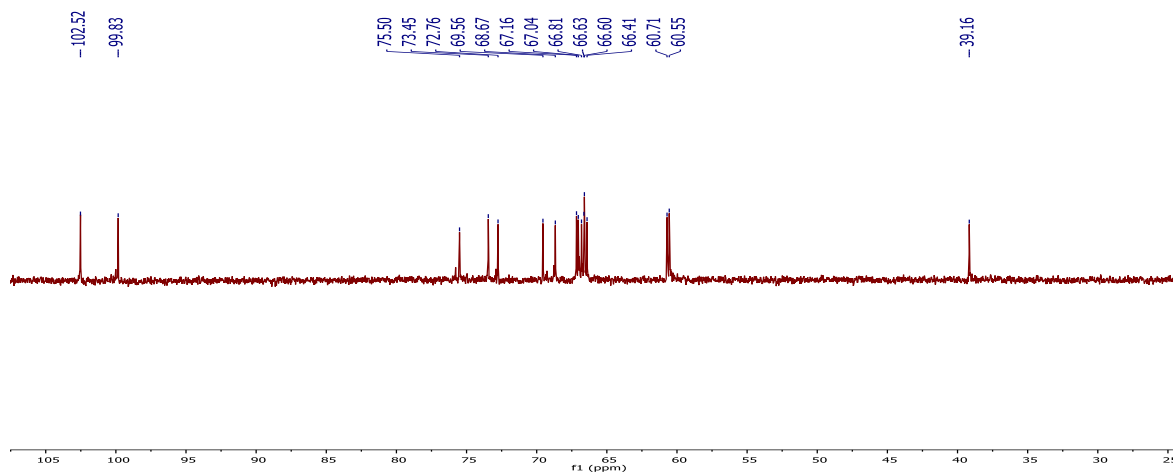
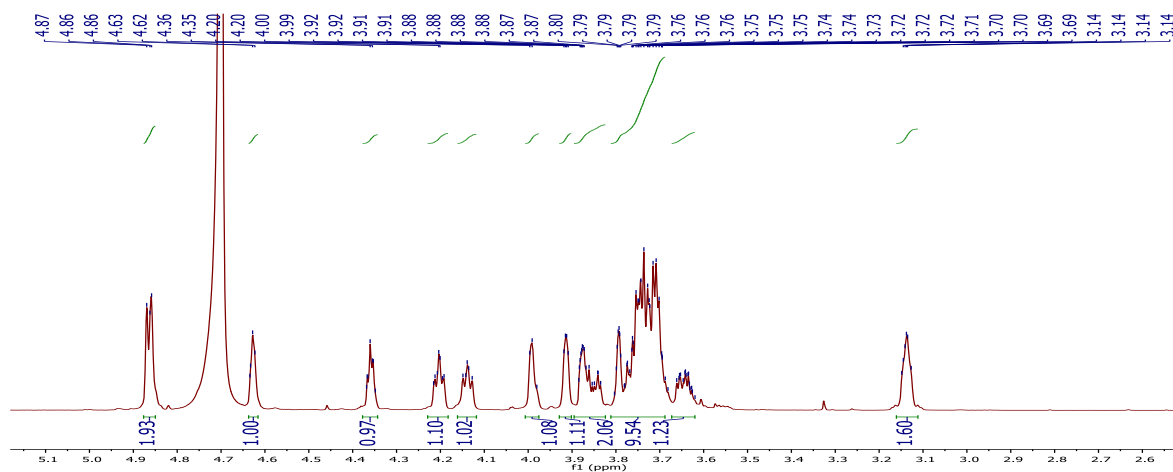


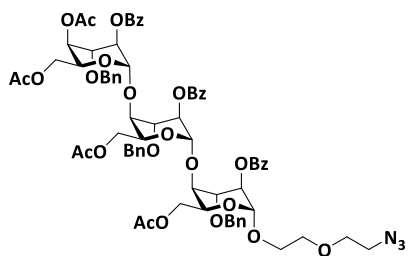
21a



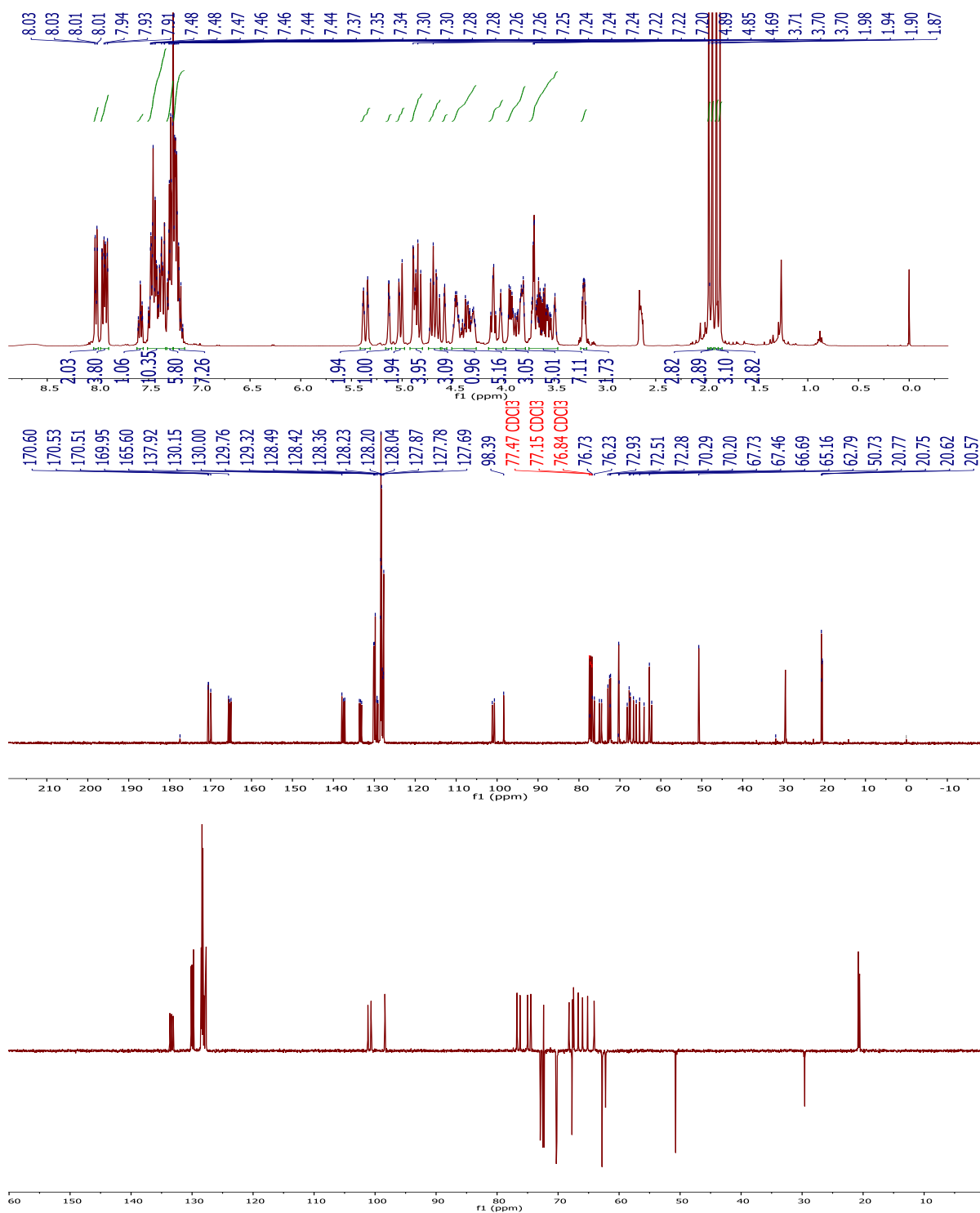


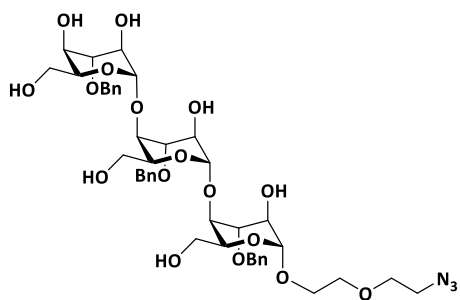
(ID22)



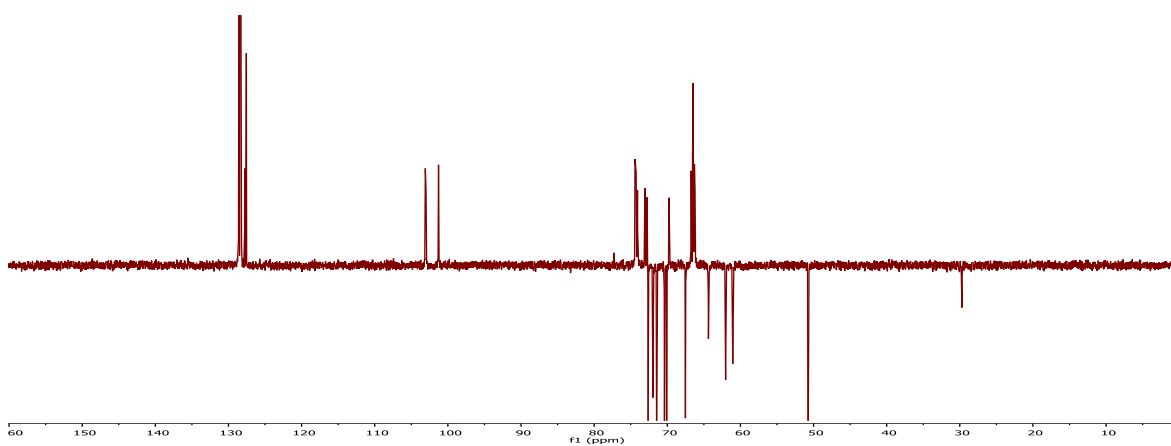
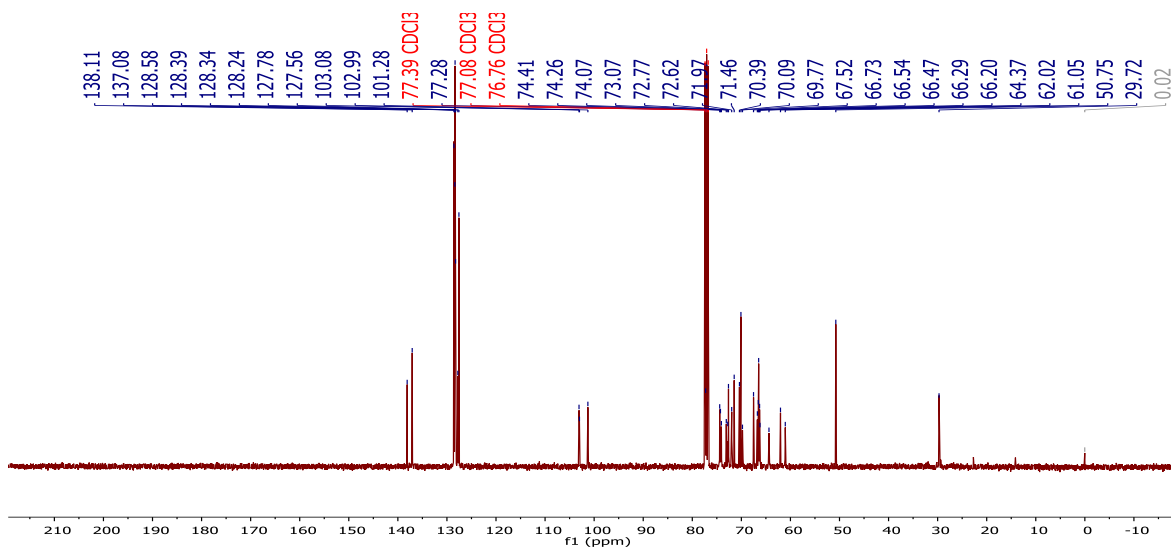
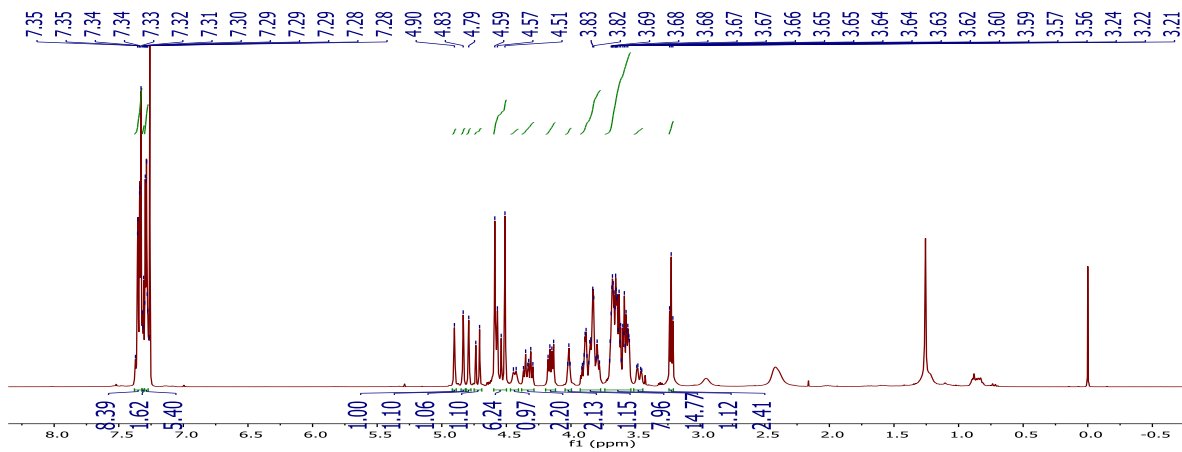


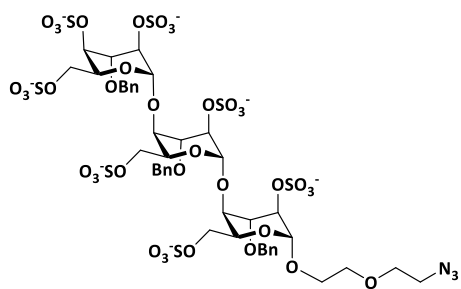
14



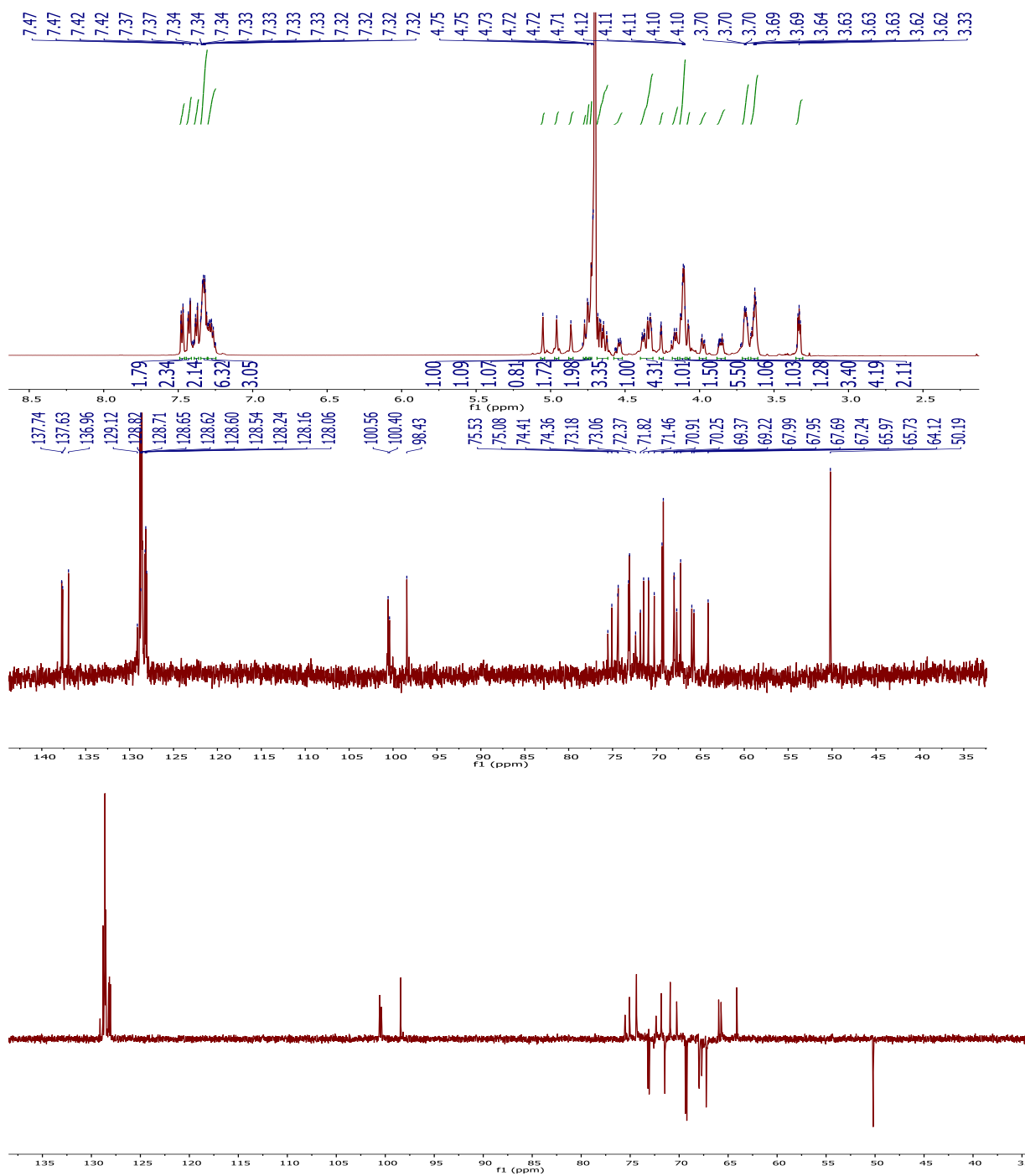


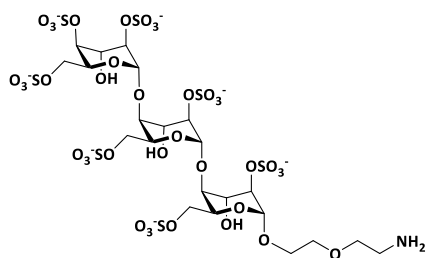
17



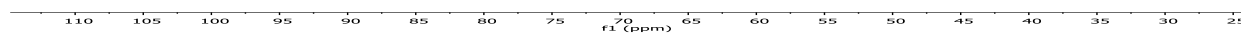
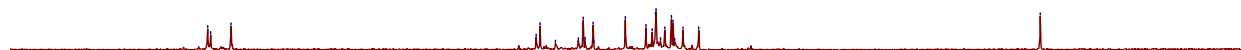
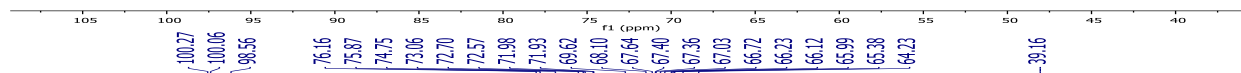
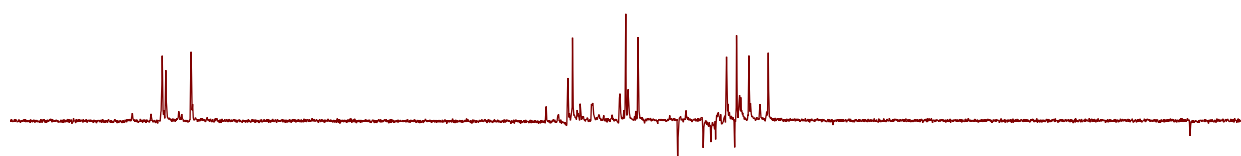
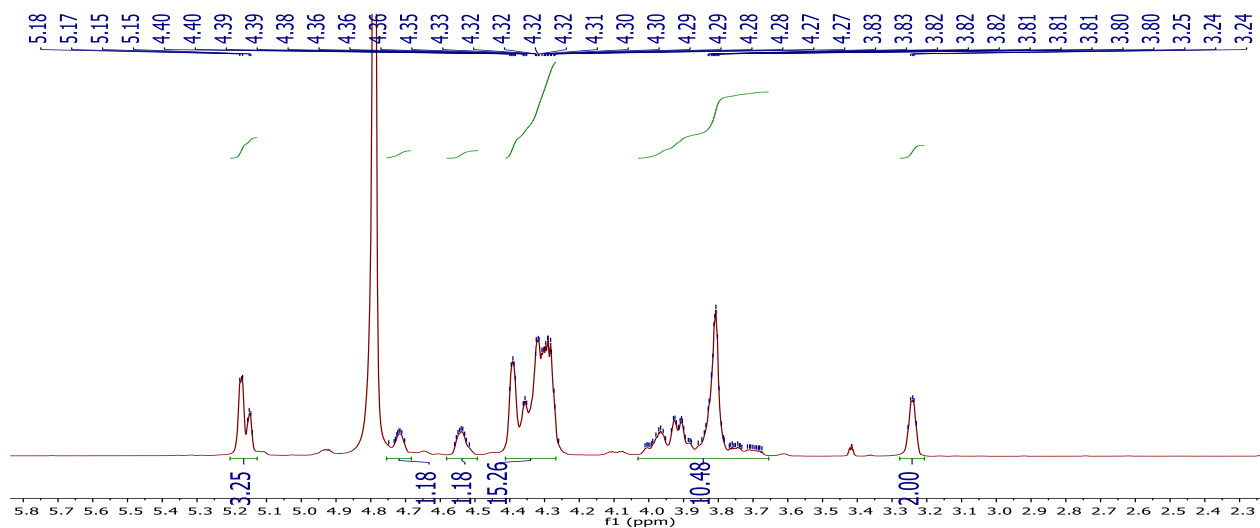


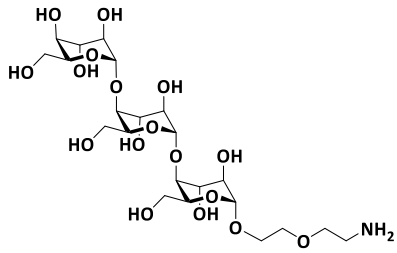
20



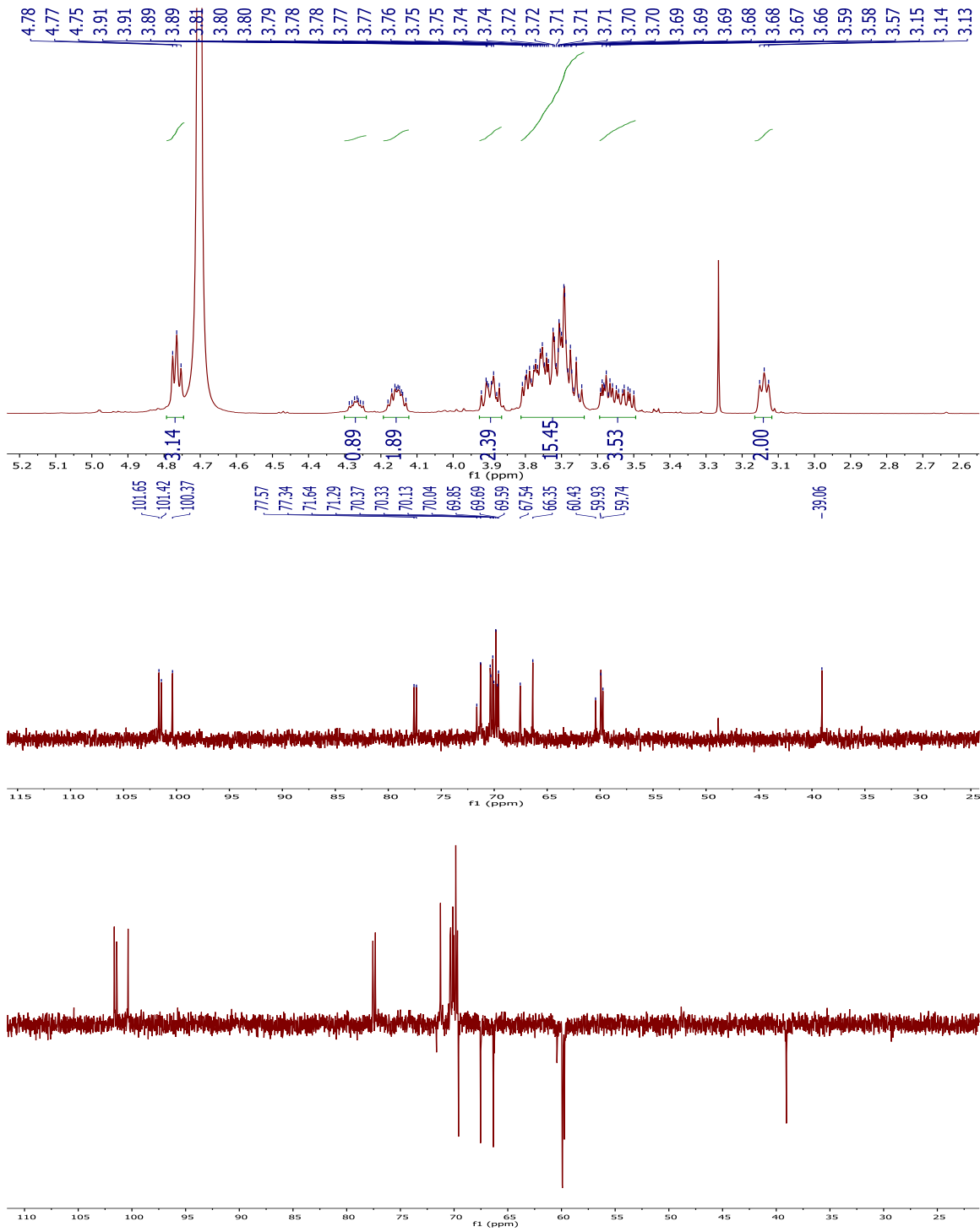


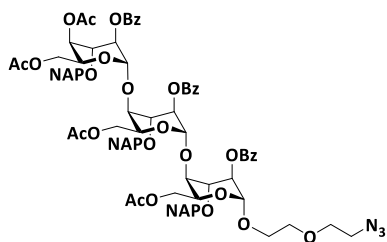
(ID37)



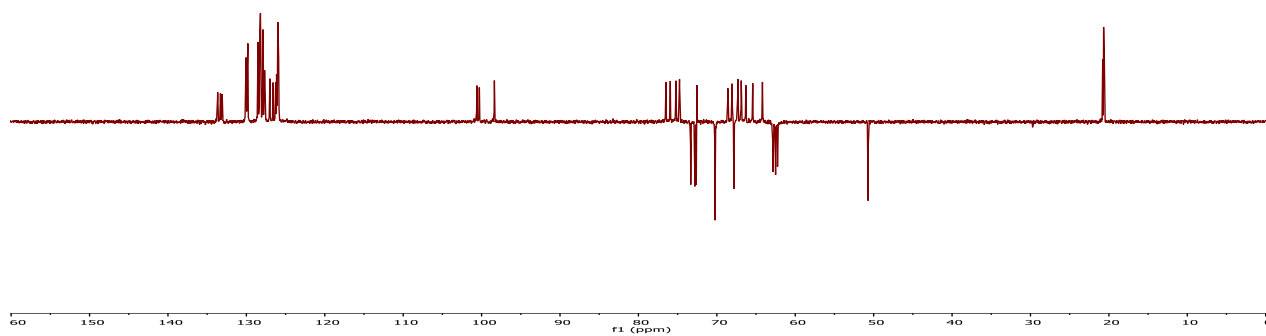
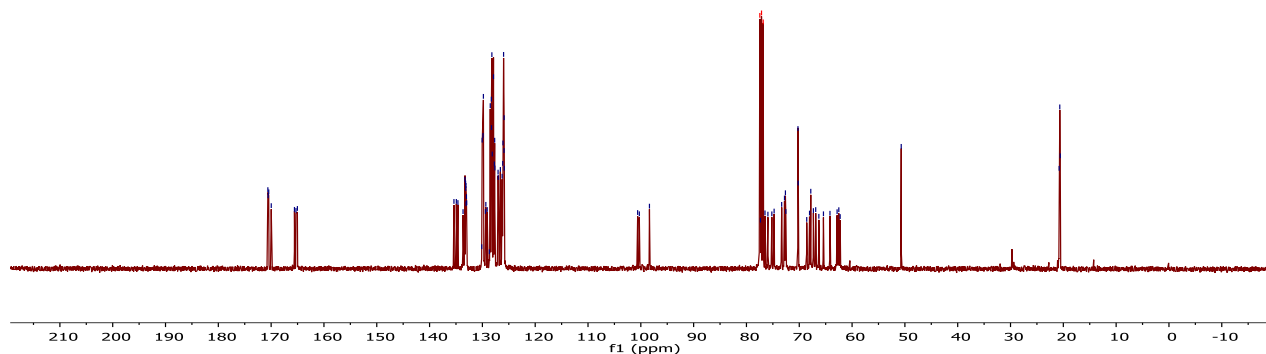
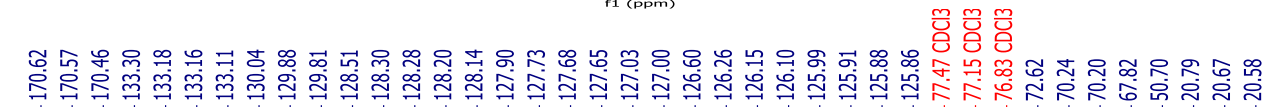
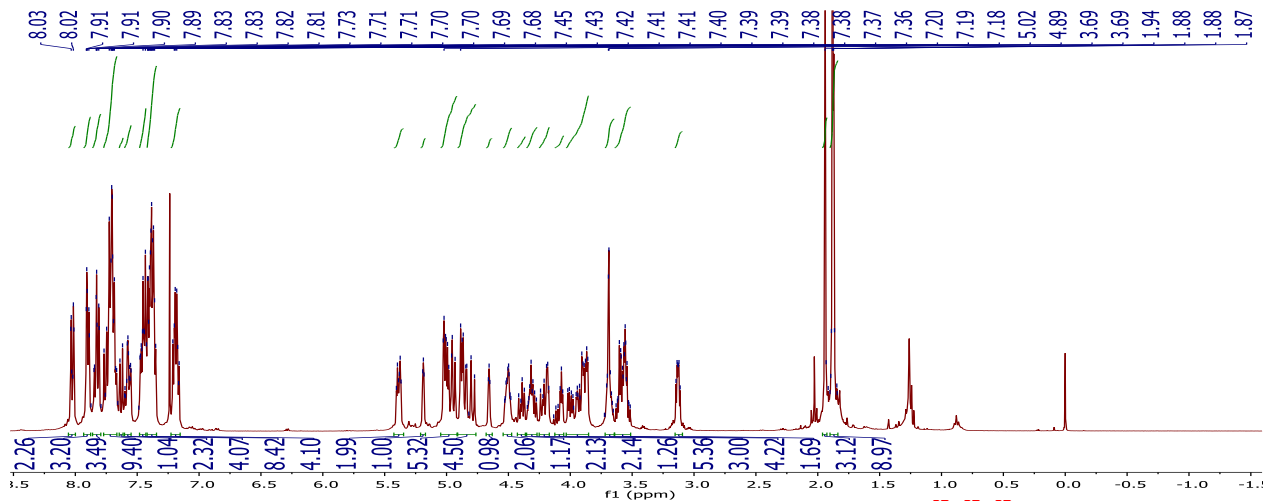


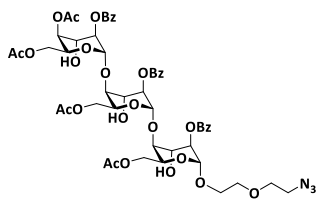
(ID30)



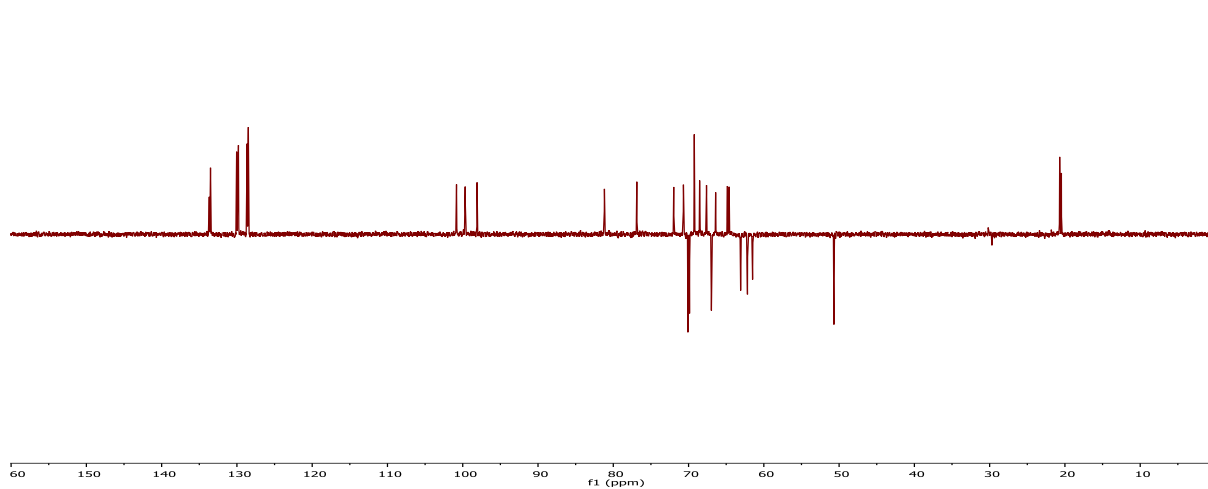
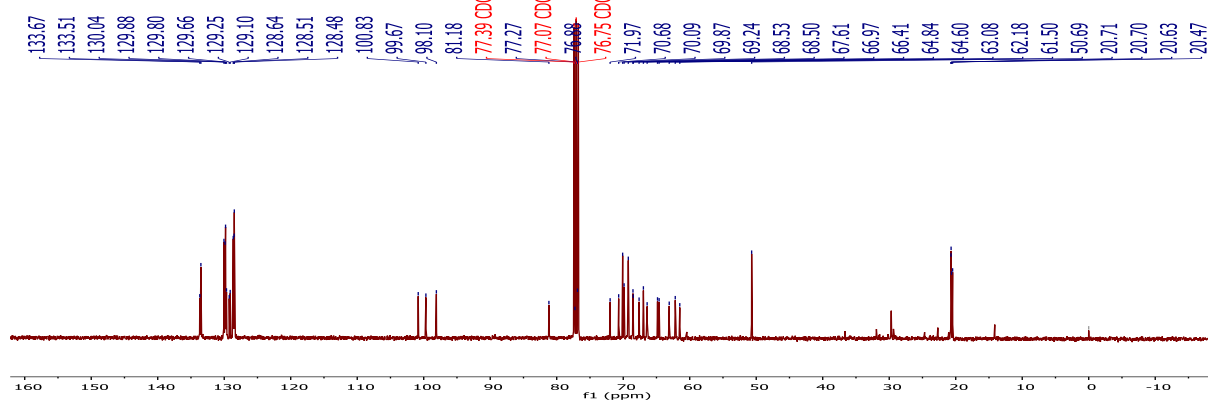
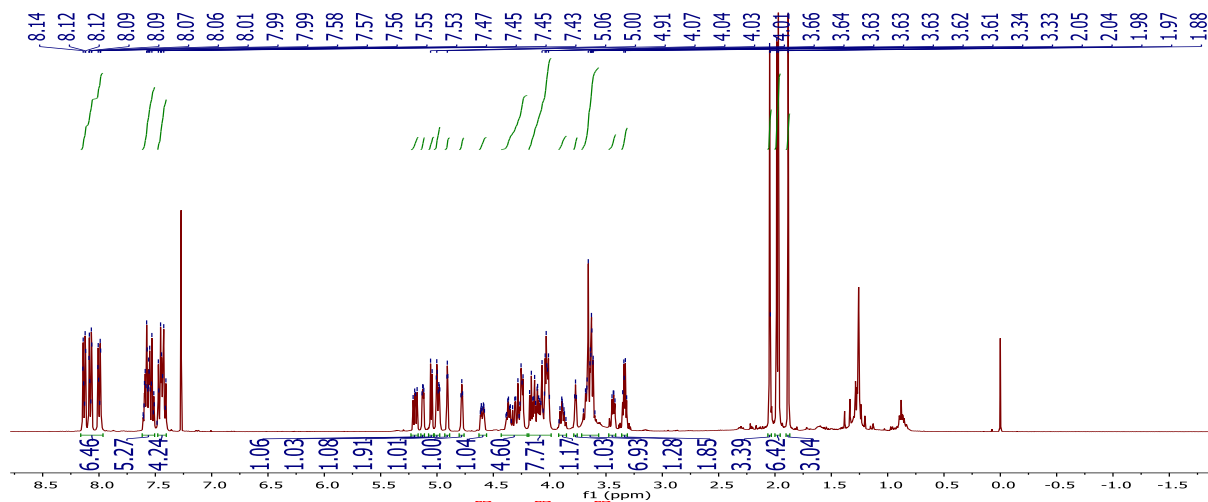


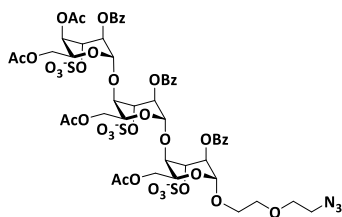
14a



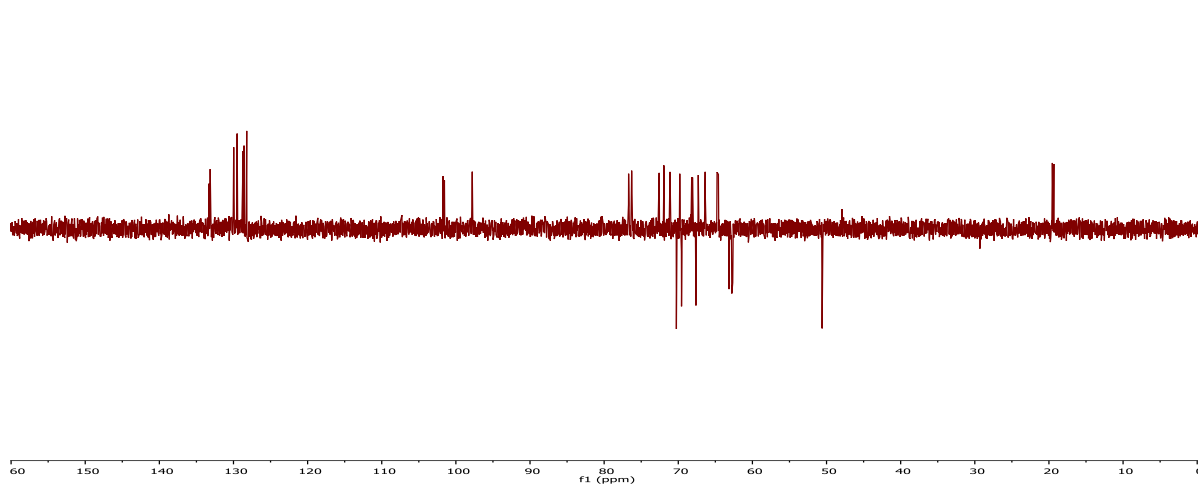
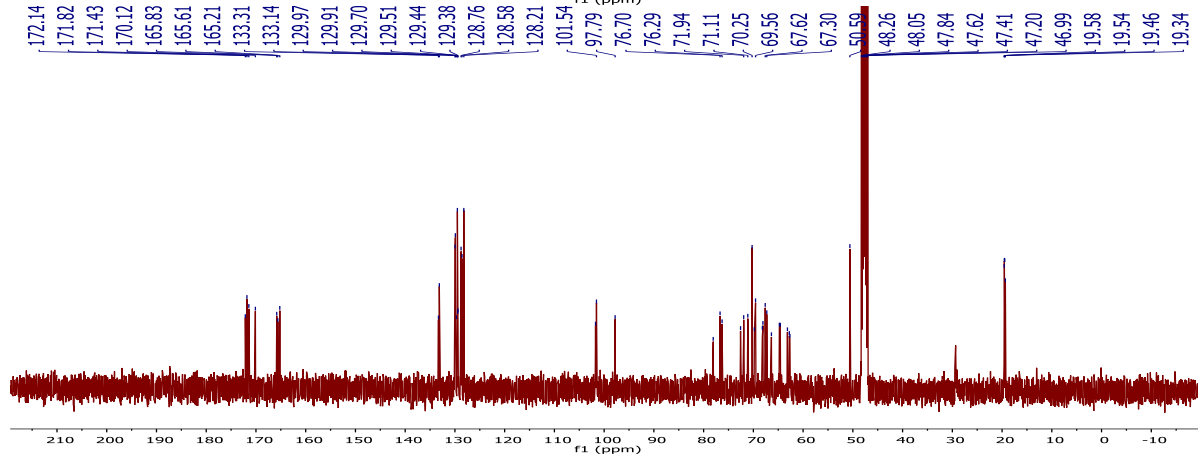
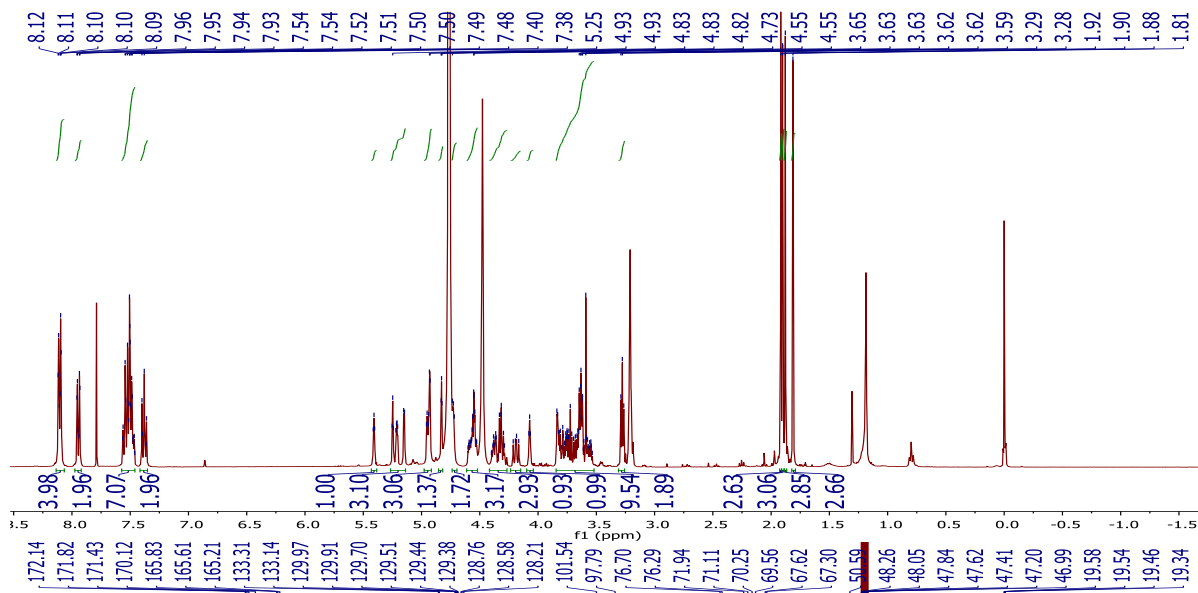


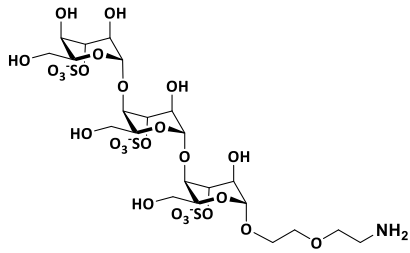
17a



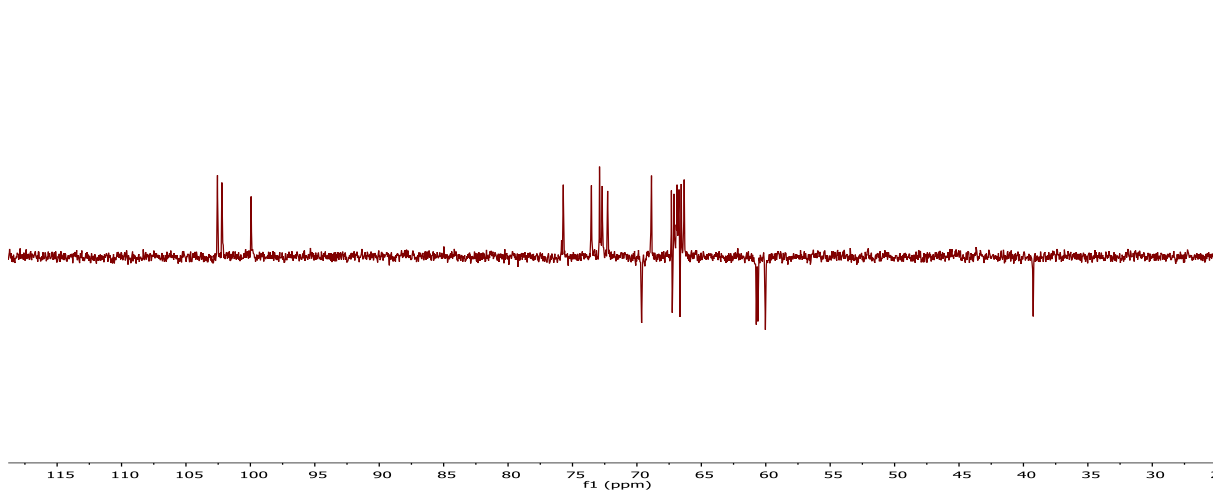
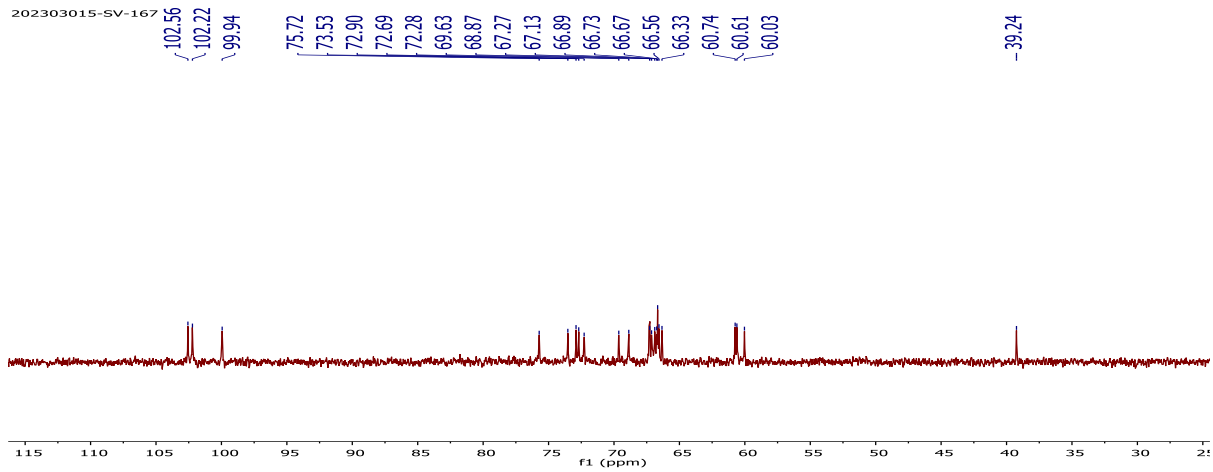
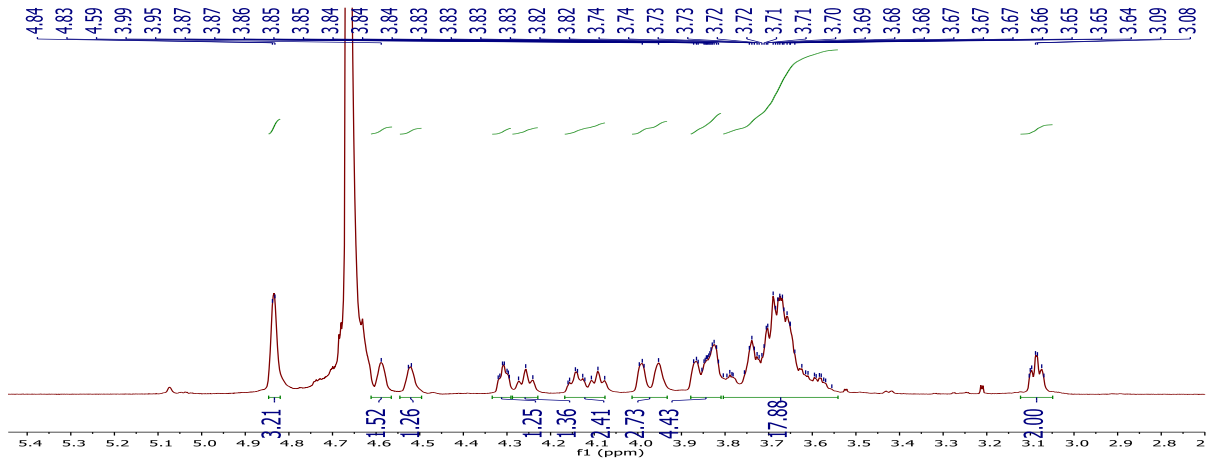


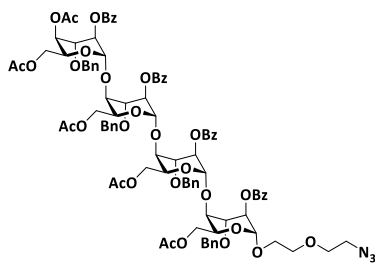
20a



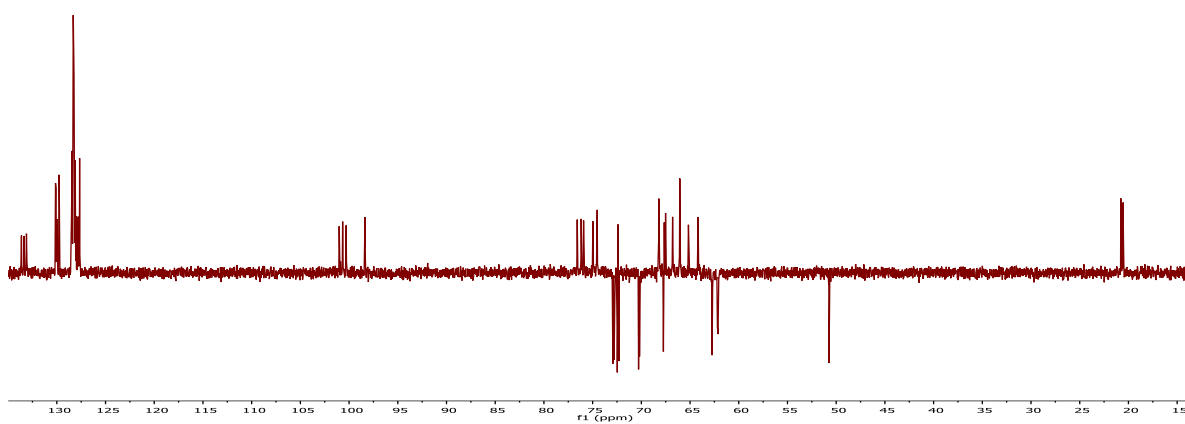
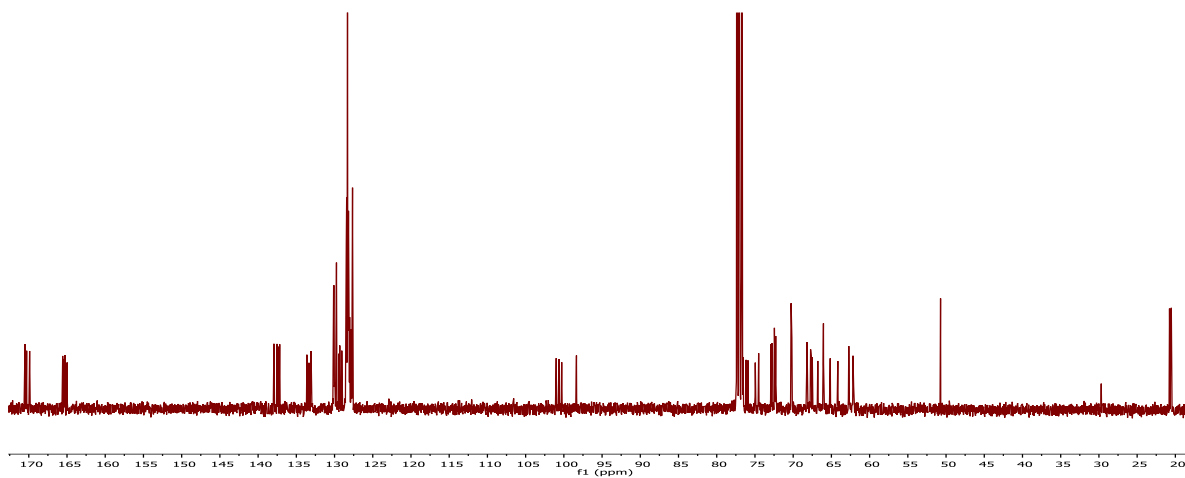
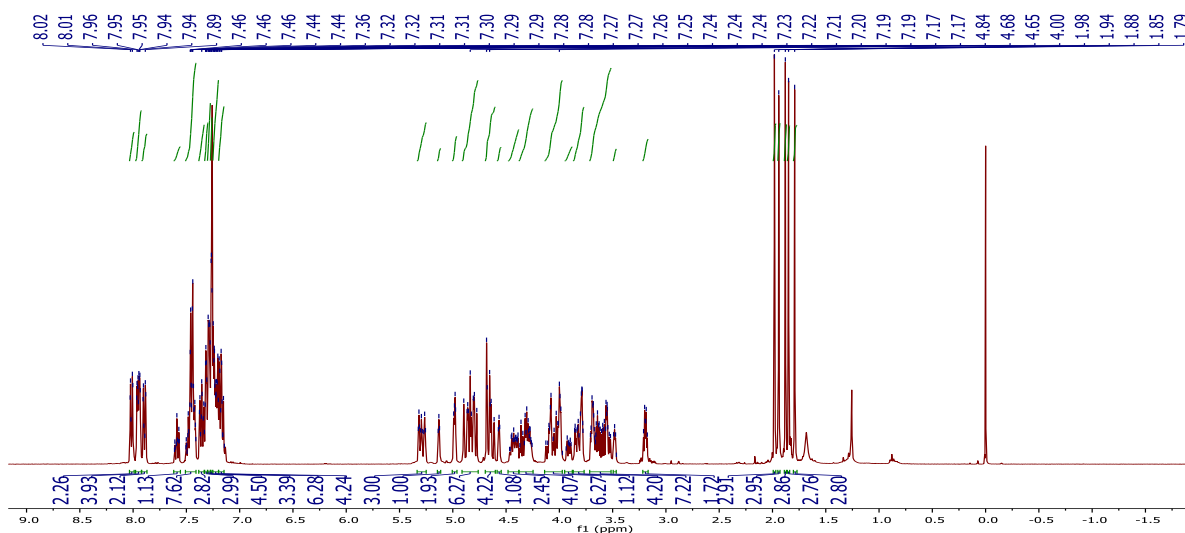


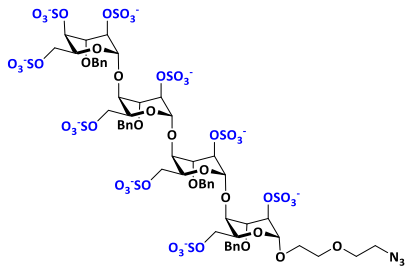
(ID33)



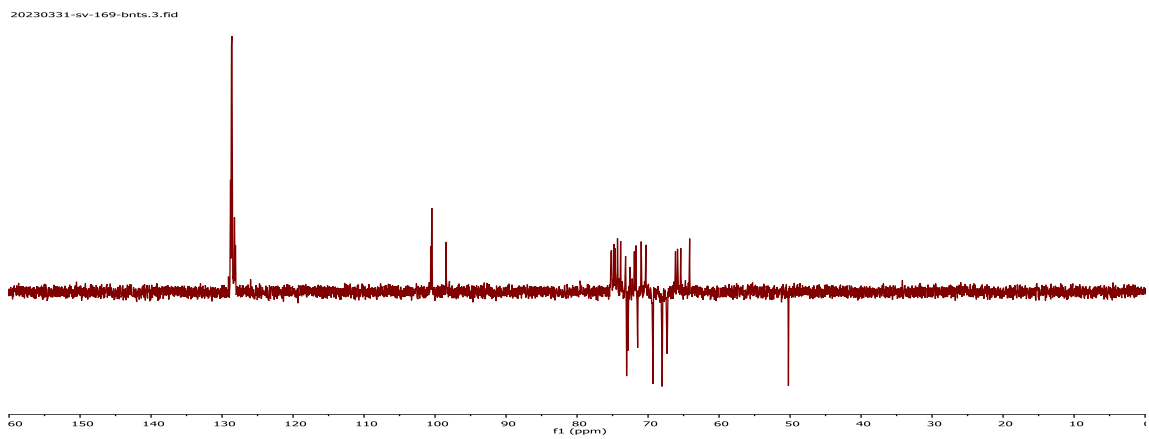
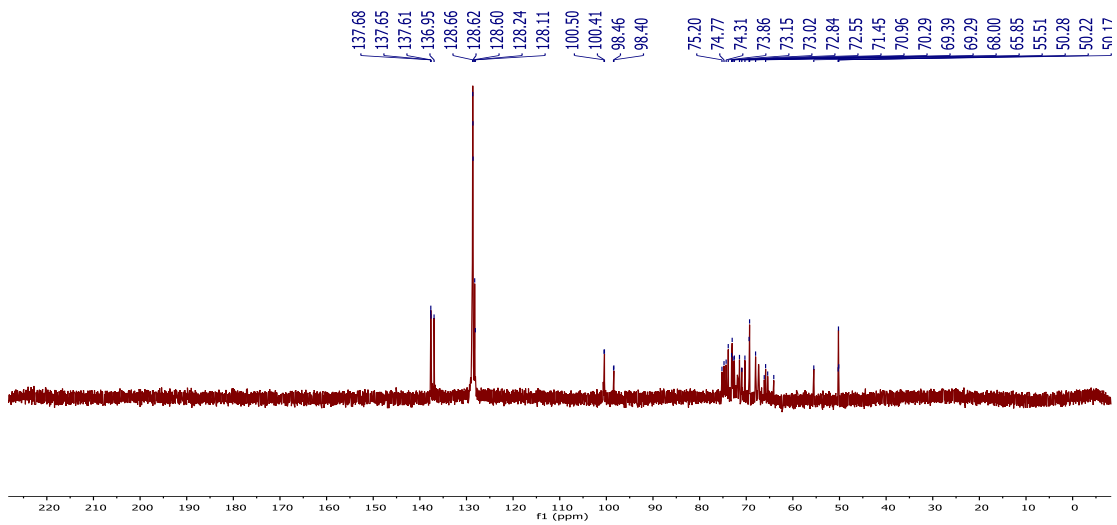
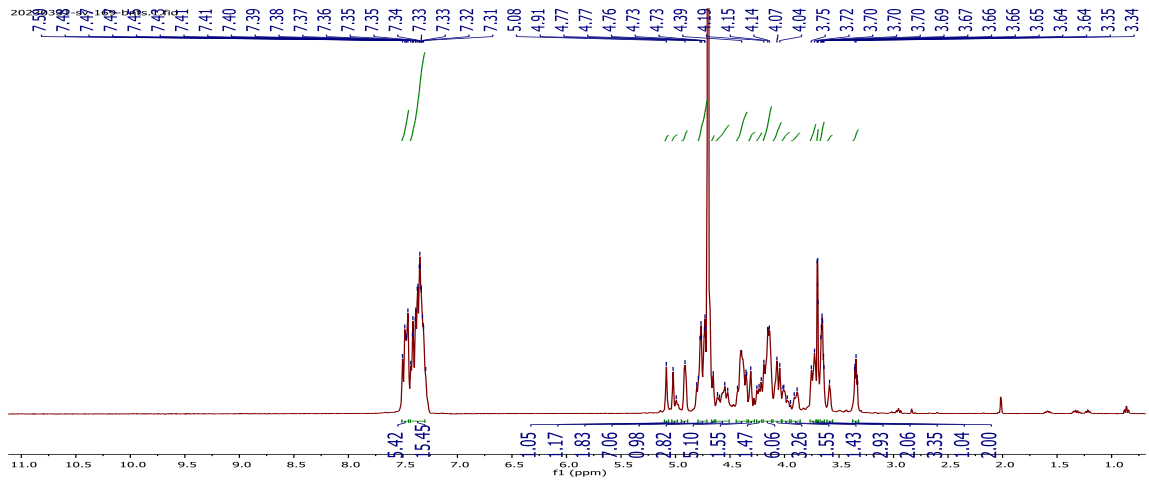


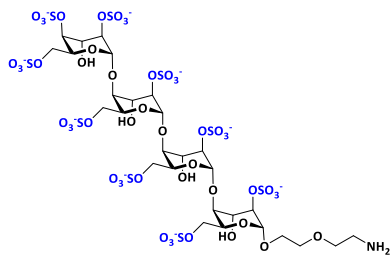
15



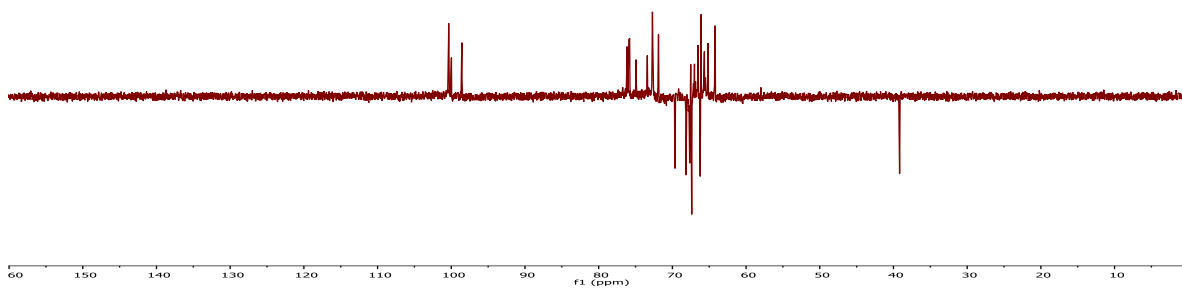
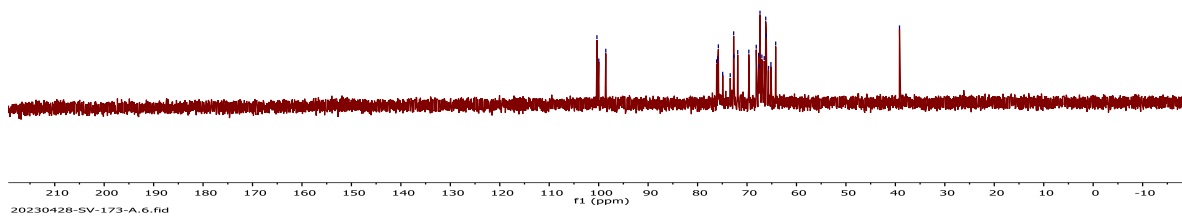
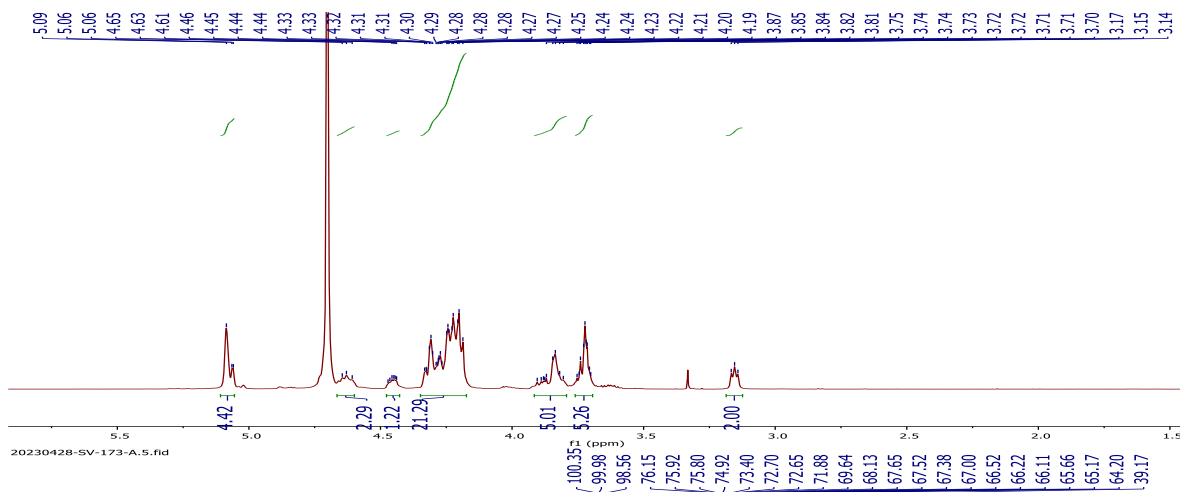


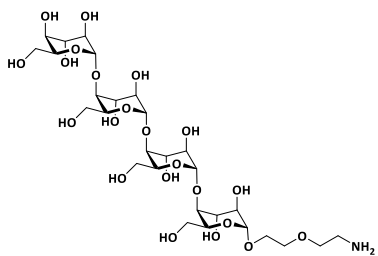
21



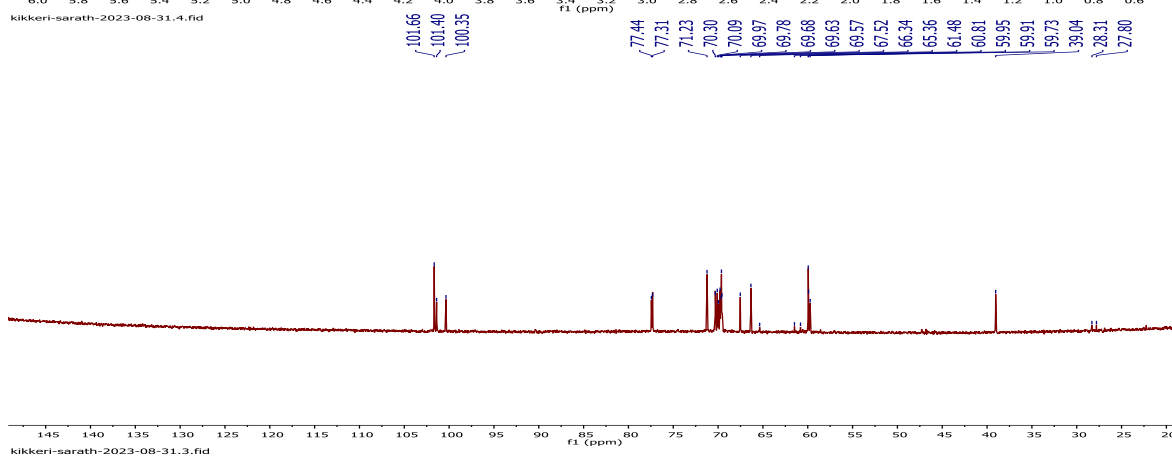
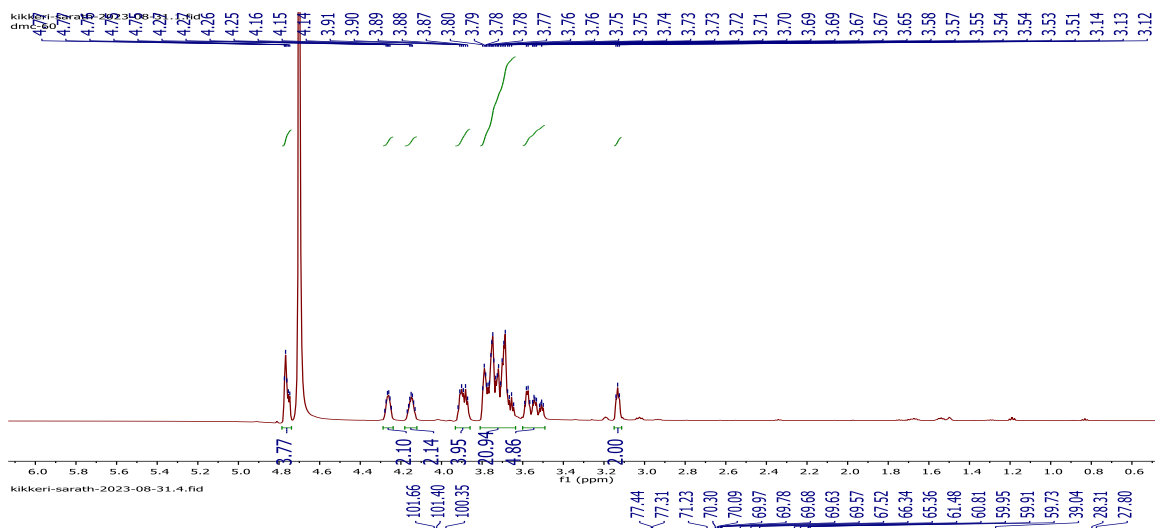


(ID49)





(ID40)



List of Publications

1. Mohit Chhabra.; Chethan D. Shanthamurthy.; Nanjundaswamy Vijendra Kumar.; Sandhya Mardhekar.; **Sharath S. Vishweshwara.**; Norbert Wimmer.; Naphak Modhiran.; Daniel Watterson.; Alberto. A Amarilla.; Jonathan S. Cha.; James R. Beckett.; James J. De Voss.; Yasmin Kayal.; Israel Vlodavsky.; Lauren R. Dorsett, Raymond A A Smith, Neha S. Gandhi, Raghavendra Kikkeri, Vito Ferro.; Amphiphilic Heparinoids as Potent Antiviral Agents Against SARS-CoV-2. *J. Med. Chem.* (Accepted 2024)
2. **Sharath S. Vishweshwara***; Preeti Ravindra Bhoge, Saurabh Anand, Rakesh Raigwali, Sinivas Vinod Saladi, Raghavendra Kikkeri.; Immunogenic Heparinoid Elicit Neutralizing Antibody Against Native Heparan Sulfate with Biomarker and Therapeutic Applications (*Manuscript Submitted*) (*Equal contribution)
3. **Sharath S. Vishweshwara***; Saurabh Anand, Preeti Ravindra Bhoge, Sinivas Vinod Saladi, Raghavendra Kikkeri.; Heparan Sulfate Neoproteoglycan Promotes Lysosome Targeting Degradation of Amyloid- β . (*Under Revision*) (*Equal contribution)
4. **Sharath S. Vishweshwara**; Shani Ben-Arye, Vered Padler-Karavani, Raghavendra Kikkeri.; Modulations of Growth Factors and Chemokines Specificity of Heparan Sulfate Mimetics Through Charge Diversity (*Manuscript Under Preparation*)